NASA MEMO 5-25-59W VOL. 2

NASA MEMORANDUM

1958 NASA/USAF SPACE PROBES

(ABLE-1)

FINAL REPORT

VOLUME 2. PAYLOAD AND EXPERIMENTS

By Space Technology Laboratories, Inc.
Los Angeles 45, Calif.

NATIONAL AERONAUTICS AND SPACE ADMINISTRATION
WASHINGTON
June 1959

1958 NASA/USAF SPACE PROBES

(ABLE-1)

FINAL REPORT

VOLUME 2. PAYLOAD AND EXPERIMENTS

Prepared for Air Force Ballistic Missile Division
Headquarters ARDC
Under Contract AF 04(647)-205

18 February 1959

SPACE TECHNOLOGY LABORATORIES, INC.
P.O. Box 95001
Los Angeles 45, California

Page intentionally left blank

CONTENTS

Page intentionally left blank

ILLUSTRATIONS

ILLUSTRATIONS (Continued)

ILLUSTRATIONS (Continued)

ILLUSTRATIONS (Continued)

ILLUSTRATIONS (Continued)

Page intentionally left blank

TABLES

2.0 PAYLOAD

2.1 Introduction

The Able-1 payload was created more by evolution than by specification, and normal development series sequences could not be observed due to rigid time pressures. (Section 2.1.4 presents a developmental history of the payload configuration.) In the early study phases, flexible interfaces were established between the trajectory, weight, propulsion capabilities, payload experiment list, telemetry requirements, dynamics, total electrical life, and other parameters, in order to proceed with design and fabrication on an expedited basis.

An attempt was made to keep these parameters as static as practical. Each separate problem was then approached as rapidly as possible and problem areas were flexibly designed to allow concomitant incorporation of alternate concepts as specific problems were resolved.

In formulating the final payload design it was necessary that the satellite launch weight be some maximum value that would still allow a high probability of success. Within the weight limits the satellite was to gather the greatest amount of data from the widest variety of experiments, and its electrical system was to have the maximum possible life. At the same time, weight considerations demanded that subminiaturization and multipower devices be employed to the greatest possible extent, without loss of circuit power efficiency or reliability. Operational reliability was the only factor that could compromise weight limitations. Other considerations that influenced the design were; (1) the ambient thermal properties of the vehicle, (2) dynamic stability, (3) experimental environment, and (4) the ability to quickly make prelaunch emergency repairs and calibration checks.

2.1.1 Dynamic Stability

Three steps taken to ensure dynamic stability of the vehicle in inertial space were: (1) the payload weight was distributed in a manner which provided suitable moments of inertia; (2) a spin of approximately two revolutions per second was imparted to the payload; and (3) a damper ring was used to damp out precessional motions. Although the necessity for such dynamic stability

arose basically from the need for directional control of the vehicle during the firing of the third and fourth stages and the vernier rockets, some of the scientific instruments also required spin. (See Section 3.26 for a detailed discussion of spin stabilization.)

The scientific instruments placing the most stringent requirements on dynamic stability were the television systems, both the NOTS system and the STL TV scanner. Both of these systems depended on the payload spin motion to generate a circular scan about the vehicle axis, as well as the vehicle motion in its trajectory to cause a parallel displacement from one circular scan to the next. A precessional motion of the vehicle figure axis about the total angular momentum vector would result in circular scan lines which were no longer parallel. If this lack of parallelism became sufficiently great, it would be extremely difficult, if not impossible, to process the received data into a picture. For reasonable processing, the maximum variation of the figure axis in space is an angle equal to one-half of the angular size of the scanning spot. For both the STL and the NOTS system, this angle is one-quarter of a degree. For larger precessional angles, there will be areas of the object approaching a spot diameter in size which will not be properly sampled. When the precessional angle exceeds the spot size, there will be areas which are completely missed; the relation of one scanning line to the next will become very complicated until a point is reached at which too much information is missing from the picture or at which it is impossible to process the received data without having additional information from the payload.

Since the magnetometer records the EMF generated as a coil within the payload rotates through the external magnetic field, this instrument is completely dependent upon the vehicle spin for its function. The magnetometer is also sensitive to relatively large precessional motions, since such motions imply that the coil cuts across the field at varying angles as the figure axis precesses about the total angular momentum vector. In addition, the comparison of the magnetometer data with the theoretical geomagnetic field is affected by precessional motions, (as well as by any errors in the establishment of the total angular momentum vector in inertial space), since the comparison with the theory depends upon the ability to compute the component of the theoretical

field in the plane perpendicular to the payload spin axis. In all cases, however, the sensitivity of the magnetometer experiment to payload precessional motions is less than the corresponding sensitivity to the TV systems. For example, a precessional angle of four degrees will produce an error of about one per cent in the magnetometer reading. This is considerably less than the errors due to other sources.

2.1.2 Temperature Control

Temperature control of the payload was effected by proper selection of the ratio of solar absorptivity to long wave length emissivity of the surface material. Since the payload was nonspherical, the projected area intercepting solar energy varied with the sun look-angle. The curve of projected area as a function of sun look-angle was nonlinear so that at certain sun angles the amount of solar energy intercepted--and consequently the payload mean temperature--was quite sensitive to changes in attitude angle. At other sun look-angles the intercepted area was relatively insensitive to changes in angle. Because of the rotation of the earth-moon system around the sun, the look-angle changed about 1 degree per day during flight, or about 10 degrees for the expected useful life of the flight. This resulted in temperature changes well within allowable limits even at the most sensitive region of the curves of intercepted area as a function of sun look-angle. Since the trajectory changed to accommodate rotation of the moon around the earth, the look-angle changed by 13 degrees (nominally), giving a total possible range of about 39 degrees over the four possible launch dats, plus perhaps an additional 10 degrees during flight. If the range of angles expected to occur for any given month's flight happened to fall in the least sensitive region of the curve, the resulting temperature changes fell well within the design limits. If, however, the possible angles for a given month fell in a more sensitive region of the curve, the resulting temperature changes would have not been tolerable, necessitating changes in the absorptivity-to-emissivity ratio to keep the temperature within design limits. In fact, if the expected temperatures for a given month fall within the most sensitive region of the curve, as in October, it is necessary to provide a different absorptivity-to-emissivity ratio for each of the four possible launch dates.

Operational requirements made it quite possible that the payload prepared for a given launch date would have to be readied within a relatively few hours for the next launch date. Such rapid changes of absorptivity-to-emissivity ratio were achieved by the addition or removal of paint tapes of the proper area, to yield the desired mean value of the ratio for the new launch date. Figure 2-1 shows the two such paint patterns.

2.1.3 Experimental Environment

Because the magnetometer experiment was intended to measure the magnetic fields existing in space around the payload, any magnetic materials or magnetized objects which might distort the observed field are highly undesirable. It was therefore necessary to keep the mass of such materials to an irreducible minimum, and to place the magnetometer coil as far as possible from those magnetic materials which must be included in the payload.

In addition, to comply with antenna requirements, it was necessary to introduce a series of radial conductors to provide a ground plane for the antennas.

2.1.4 Developmental History

This section concerns itself with the evolution of the final physical configuration of the vehicle rather than the electronic development. It is followed by a description of the final configuration for the three Able-1 flights.

On about April 15, it was decided that the payload should consist of a flat disc containing the necessary electronics attached at the center of gravity of the retrorocket. This is illustrated in Figure 2-2. The Thiokol TX8 rocket had been selected as suitable and mechanization of the payload on this tentative concept was proceeding. Physical details were established as follows:

Electronics weight	20 pounds
Container weight	2.65 pounds
Container diameter	22.00 inches
Container over-all thickness	3.50 inches
Vehicle spin rate	2 to 3 cps
Internal ambient temperature	25°C ±5°C

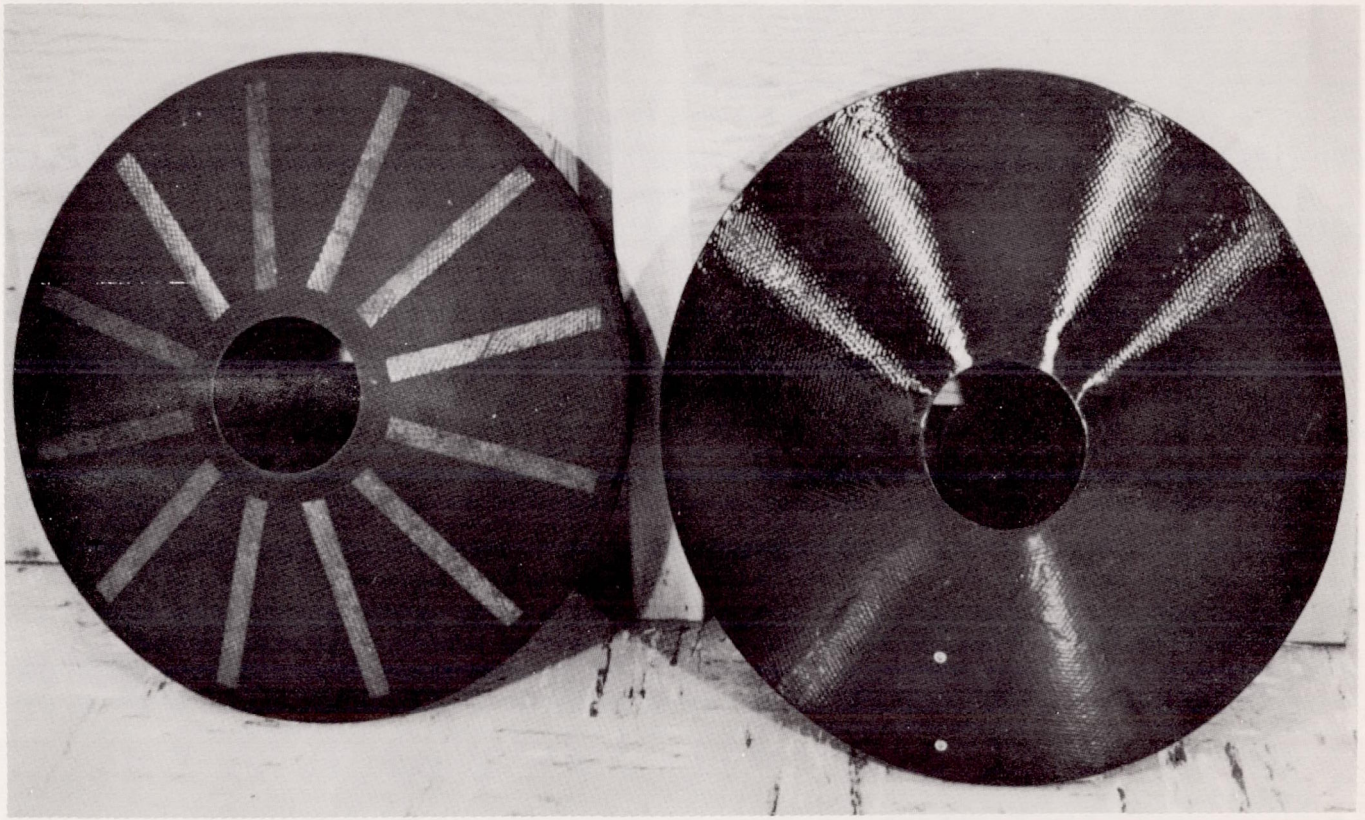

Figure 2-1. Two Paint Patterns for Temperature Control.

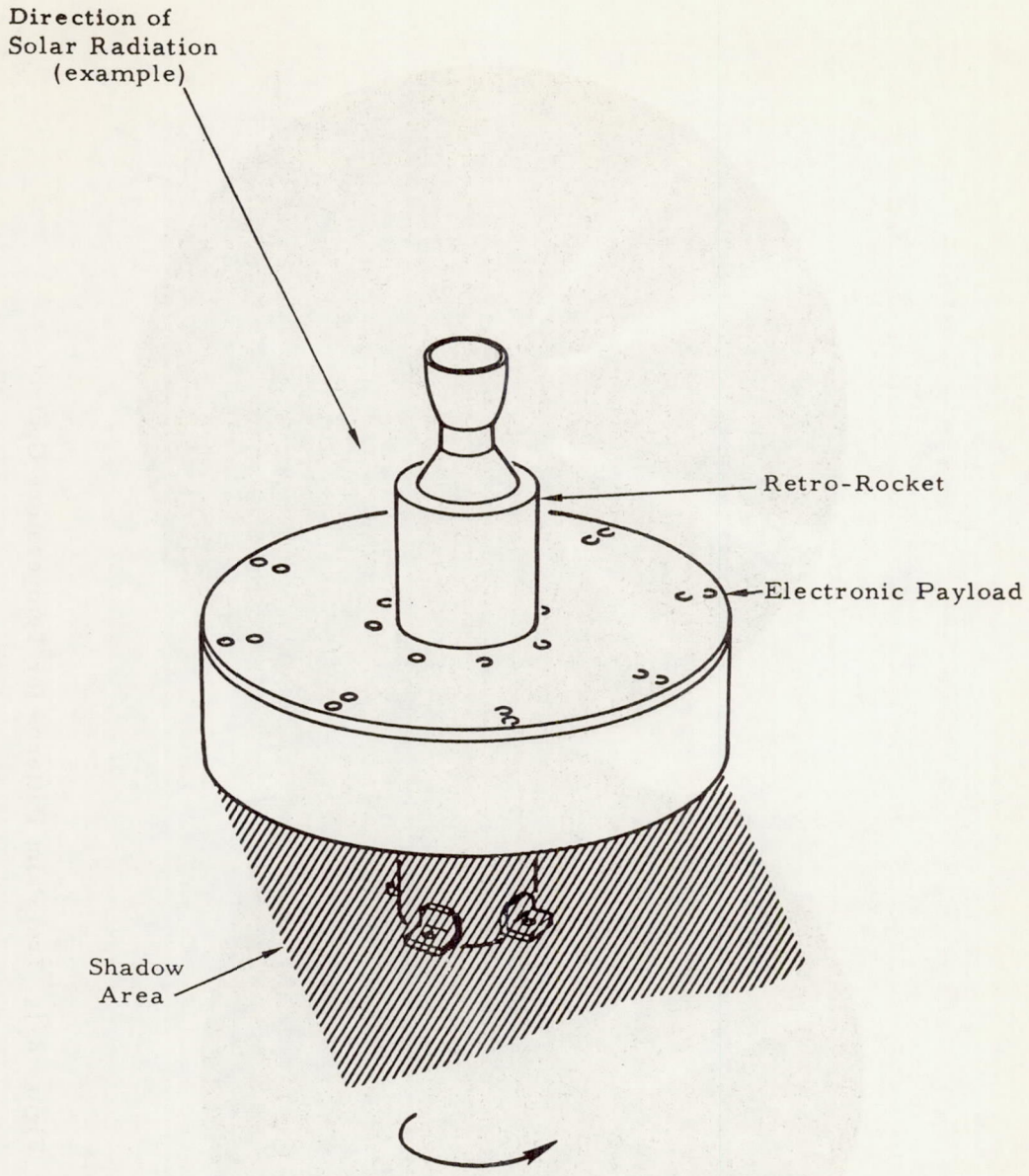

Figure 2-2. Able-1 Payload, Preliminary Version No. 1 on 15 April 1958.

The circular electronics container was to be fabricated of 0.250-inch thick fiberglas epoxy honeycomb. It would be rather transparent to solar radiation. The cover, as shown, would be removable for access to internal equipment. The electronics would be internally arranged to locate items with highest weight volume ratio on the outer periphery to achieve a suitable pitch to roll moment ratio for spin stability.

Studies of the thermal ambient properties of this configuration established that the approach was not suitable. It was shown that the area of the rocket normally exposed to solar radiation would have a very high ambient temperature and conversely that the area totally in shadow would be extremely cold. The electronic equipment internal to honeycomb structure would likewise be affected.

On about 16 May the concept was changed to one similar to that illustrated in Figure 2-3. It was believed that at least for the August launch the trajectory was suitable to allow minimum shadowing of the rocket surface.

The electronic container honeycomb material was still suitable. The physical shape was a torus of 22-inches outer diameter, 3.5-inches thick in the axial direction, and about a 3-inch cross section radially attached to the rocket with four interconnecting ribs permanently fastened to the rocket shell at the center of gravity.

It appeared that this concept would satisfy thermal requirements for the specific payload attitudes, with respect to inertial space, for the August launch. However, on succeeding launch months the solar attitude was different and the preliminary feeling was that a new design concept was necessary at least after August, obviously not a desirable situation.

On about 23 May, a decision was made to enclose the electronics and rocket in a single spherical envelope. A spherical shape was necessary to create a constant solar intercept area regardless of the attitude of the vehicle.

The design was worked out and volume adjustments were made. The new concept as shown in Figure 2-4 was a 22-inch diameter cylinder, 6 inches high on the rocket center of gravity blending into the rocket extremities by conical surfaces. The material would continue to be fiberglas honeycomb.

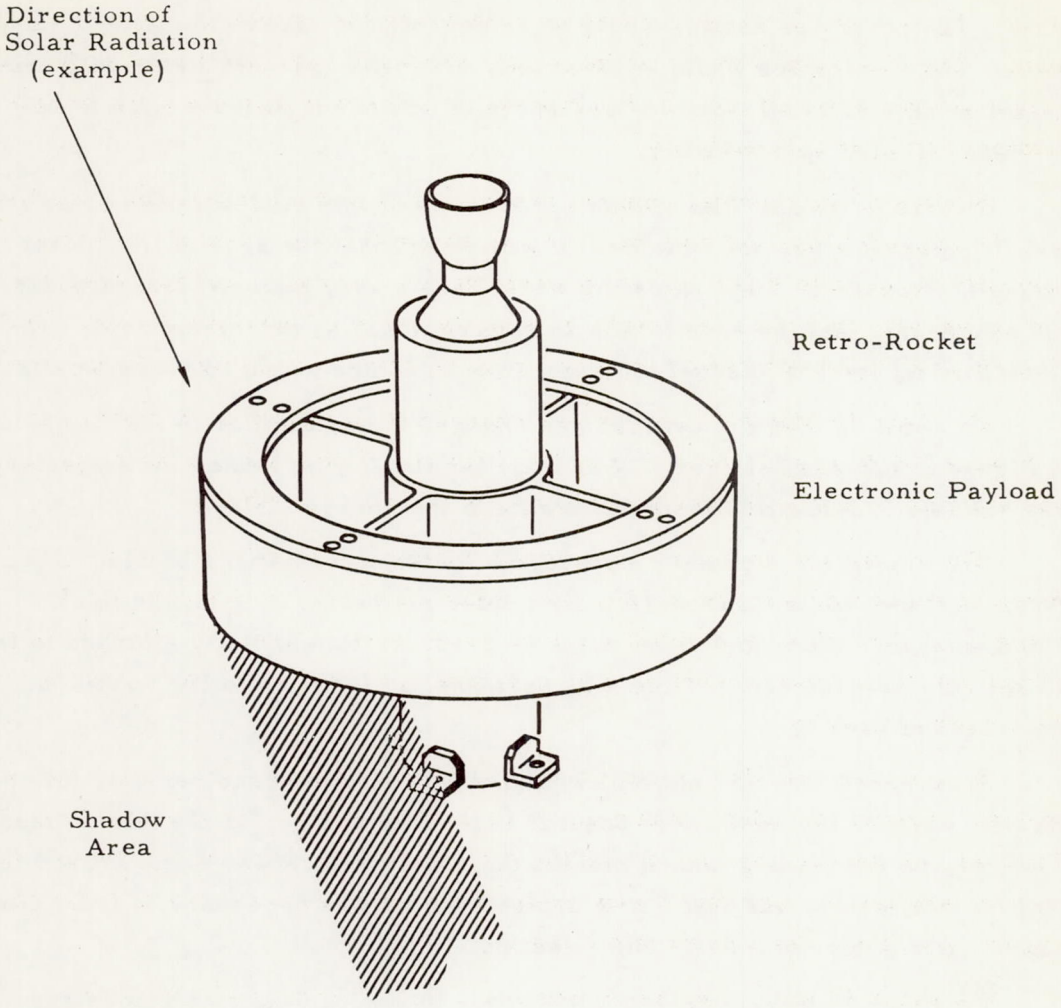

Figure 2-3. Able-1 Payload, Preliminary Version No. 2 on 16 May 1958.

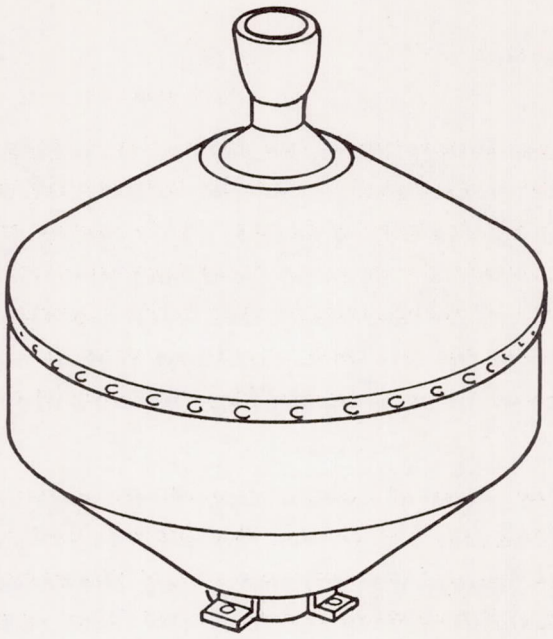

Figure 2-4. Able-1 Payload, Preliminary Version No. 3 on 23 May 1958.

Tentative estimated weight breakdown:

Electronics	22.5 pounds
Container	4.0
Stage 3/4 interface	1.5
	28.05 pounds

In another area, separation of the payload from Stage III was being accomplished by an electrical signal in parallel with the third stage ignition circuit into a five minute delay timing device. This means of separation created an electrical interface problem that could contribute to malfunction and possibly cause attitude shift when interconnecting wires were separated. On about 15 June, it was decided to eliminate the interface wires and provide a lanyard pull activation for the timer which would be released by jettisoning of the aerodynamic fairing.

On about 5 June, several modifications to the existing philosophy were determined. Further analysis had showed that pitch to roll moment ratios were not satisfactory and the payload with present weight allowance was not dynamically stable. Propulsion capabilities were redetermined, leading to the conclusion that the total payload weight could be increased to about 75 pounds. The requirements for maximum angular momentum necessitated installation of all the available weight at as large a radius as possible, normal to the rocket center of gravity.

At the same time, propulsion performance figures showed that some velocity correction was necessary after Stage 3 burnout. It was decided to attach several small vernier rockets to the payload to be fired by a command receiver link from the launch point after precise velocity determination was made by doppler link.

On about 10 June, a more detailed analysis of the thermal behavior of the double-wall plastic structure housing the Able-1 payload had been completed. It was established that the double cone plastic structure using a honeycomb-type fabrication with a 10-mil thick fiberglas-epoxy resin facing was acceptable. Some modification of the equilibrium temperatures could be achieved by the use of an external paint pattern not yet completely defined.

Solar transmission through the external surface of the package (except, of course, for the paint just referred to) must not be impeded by an antenna surface. It was important, therefore, that the antenna and associated parasitic elements be placed on the inside surfaces. Furthermore, the complete payload inner surface was to be painted black. All metal to be placed on this painted surface including the backside of the antenna and parasitic elements were also to be painted black. The effects of the micrometeorite microphone diaphragm were not serious if the area affected was limited to an estimated 58 square inches.

The inside surface on which the antenna was placed was to operate at temperatures in the range of 100° to 160°F. If flights took place at times when the look-angle to the sun was such that the cone containing the antenna was shielded from the sun, then the antenna temperature would be between 0° and 40°F. In general, the temperatures were to range from a maximum on the outer surface on the sun side of about 90° F to a minimum on the outer surface on the shadowed side of about -80°F.

It was thought necessary to provide reflecting surfaces, for example, aluminum foil, on the two ends of the rocket. The foil around the nozzle was, of course, to be blown off on firing.

After an exhaustive dynamic analysis was completed on 23 June, the final payload configuration was determined. The analysis disclosed that the original 22-inch diameter was unstable as the result of unsatisfactory pitch-roll moment ratio partially due to vernier rocket location. It was decided to maintain the same style payload but to increase the diameter to 29 inches. All vehicles launched were built this way. The unsatisfactory feature of this approach was that the solar intercept area was not constant. The 29-inch diameter subtended an intercept area substantially larger with axial sun angles than when sun angles approached the payload equatorial area. It was determined that all other requirements being constant, the thermal properties could be tailored for individual launch dates. (Figure 2-5)

Table 2-1 provides a detailed weight analysis of the final payload configuration for all three Able-1 flights.

Figures 2-6, 2-7 and 2-8 show the final payload configurations for all three flights.

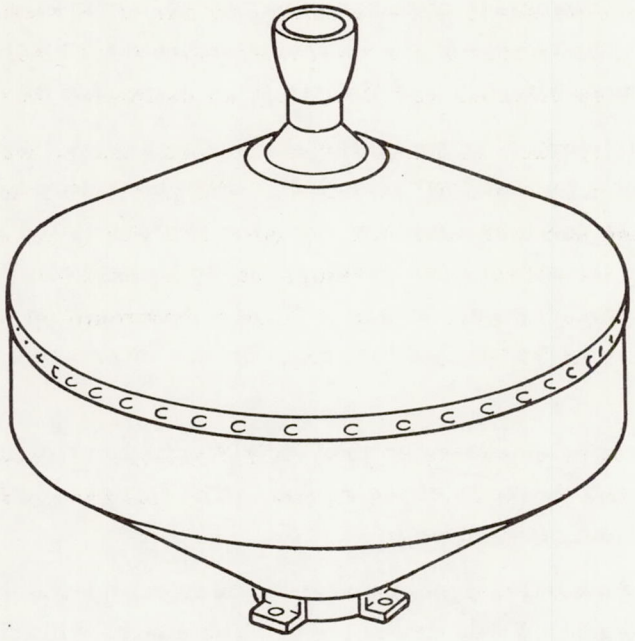

Figure 2-5. Able-1 Payload, Final Version on 23 June 1958.

Table 2-1. Weight Analysis for Pioneer Payloads

Item	Pioneer "O" (Aug) (weight/lb)	Pioneer I (Oct) (weight/lb)	Pioneer II (Nov) (weight/lb)
Command Receiver	5.60	5.65	5.91
Cosmic Ray Detector	--	--	5.96
Ion Chamber	--	1.10	1.10
TV (with lens system)(including power supply)	8.38 (NOTS)	8.53 (NOTS)	3.18
Micrometeorite System	1.06	0.46	0.46
Magnetometer System	2.32	0.97	0.97
VCO	0.94	0.94	1.09
VCO Filters	0.34	0.49	0.58
VCO Multiplexers	0.24	0.24	0.45
Transmitter (300 mw)	0.90	0.92	0.92
Transmitter (100 mw)	--	--	0.20
Antenna Filter - Diplexer	1.16	1.16	0.92
Antenna Stubs	0.20	0.16	0.16
	21.14	20.62	21.90
Batteries - Main Transmitters (3) 5.2 V	5.39	5.39	5.39
Battery - Receiver Relay	--	0.28	0.28
Battery - 100 kw Transmitter	--	--	1.24
Battery - Transistor	1.76	1.60	1.60
Battery - Rocket Ignition	0.50	0.50	0.56
	7.65	7.77	9.07
Payload Structure, Lower (with ground plane)	6.59	8.76	5.94
Payload Cover (with loop antenna)	2.00		2.19
Timer - 2.5 Day	0.50	0.50	--
Damper Ring	0.56	0.56	0.56
Cable harness, Antenna, Coax, Balance Weights, Brackets, Clamps and Misc.	1.66	2.48	3.34
	11.31	12.30	12.03
Verniers and Interface (3-4) Retrorocket	43.7	43.7	44.3
Payload Lift-off Total	83.8	84.39	87.3

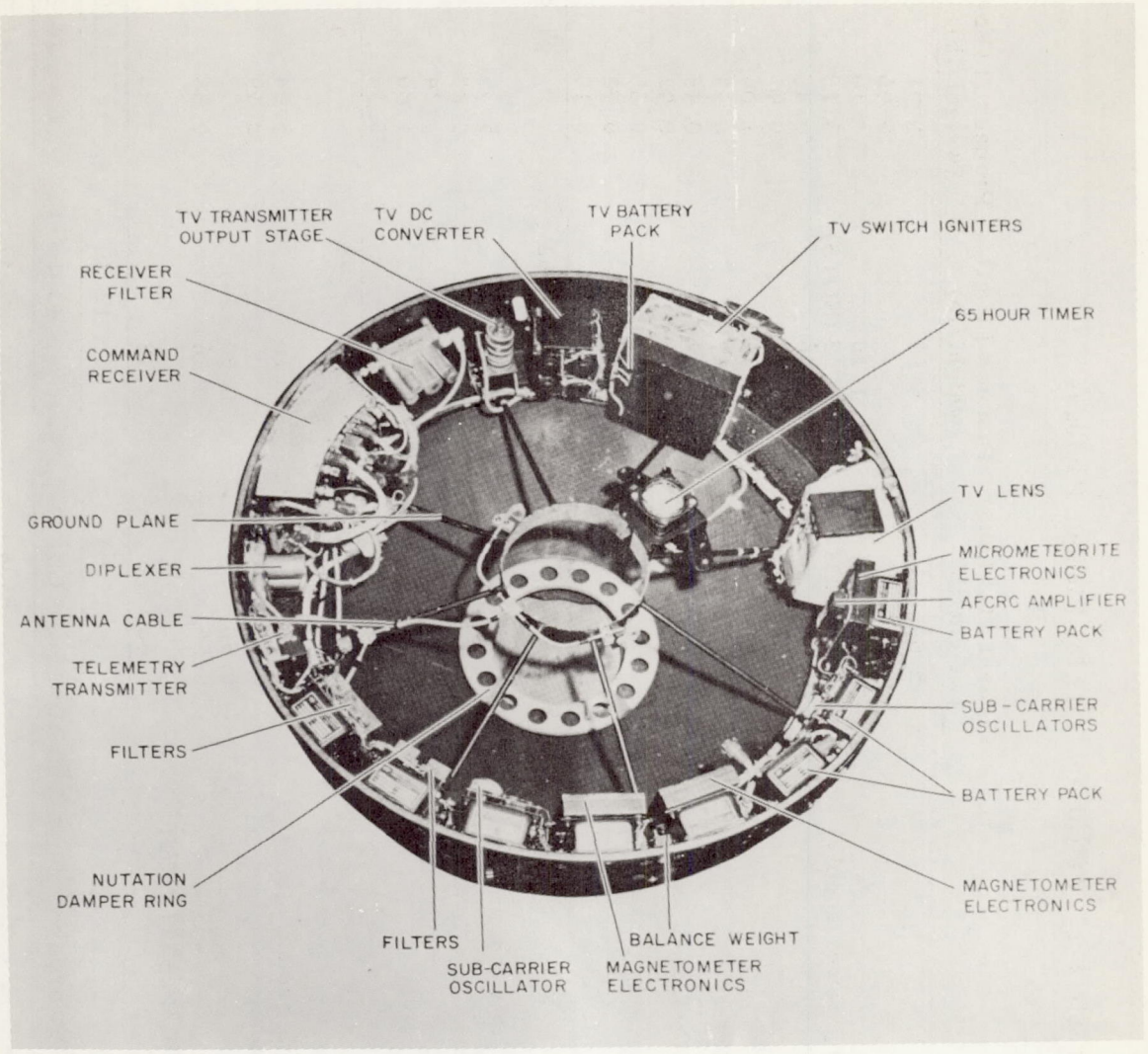

Figure 2-6. Payload Configuration for Flight One.

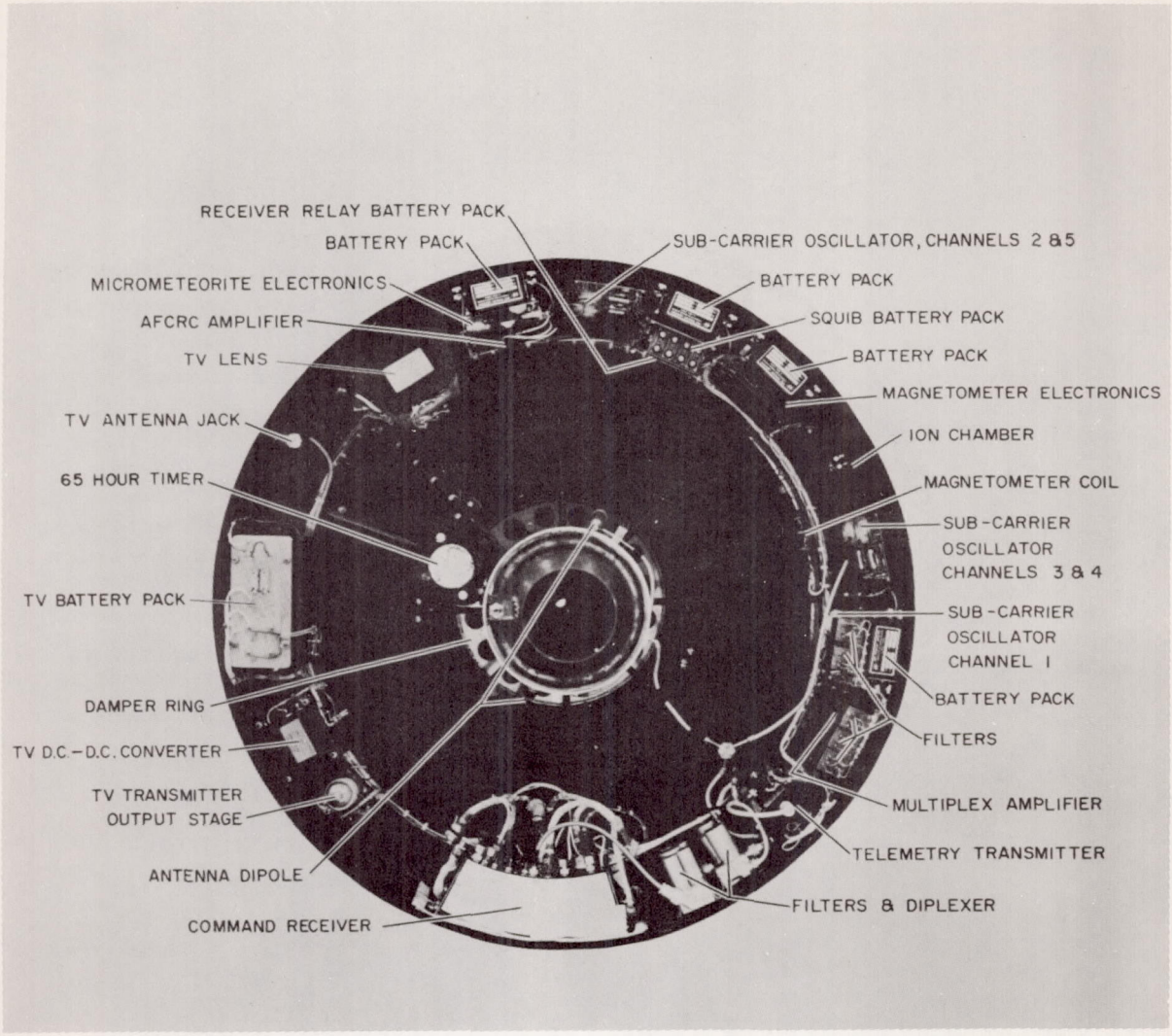

Figure 2-7. Payload Configuration for Flight Two.

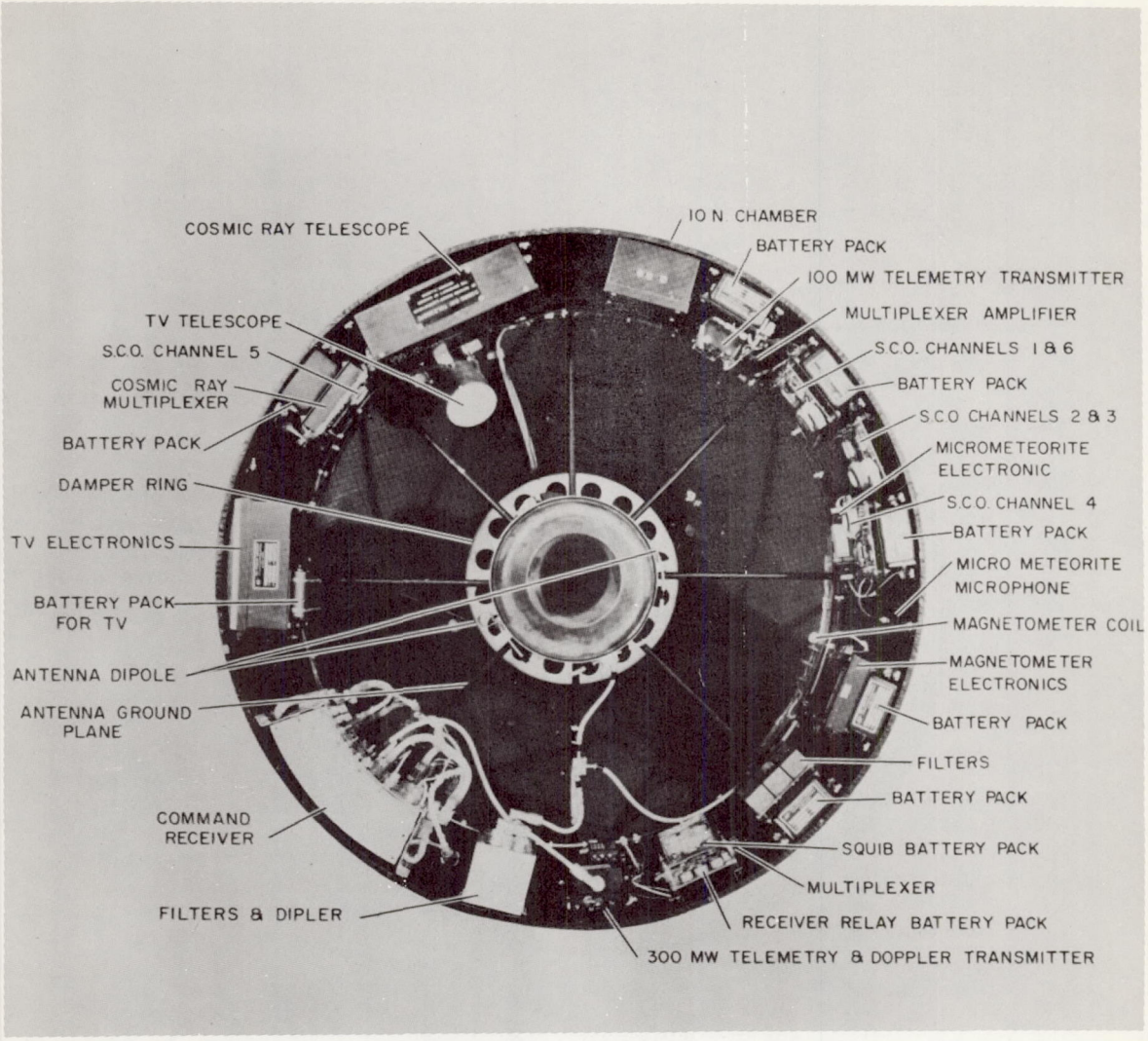

Figure 2-8. Payload Configuration for Flight Three.

2.1.5 Detailed Physical Requirement for the August Launch

The physical requirements for the August launch are used as a representative example of the requirements for all three Able-1 launches. For August, two different external surface coatings were needed, the first required for launch on August 17, 18, or 19 and the second for launch on 20 August. The change in coating from the first condition to the second was to be achieved as follows.

Two payload tops (the part of the package at the nozzle end) were to be prepared in advance, with the proper paint configuration on each. Between the 19 August launch time and the 20 August launch time, the first top would replace the second. The loop antenna mounted to the inside surface of the top was to be changed simultaneously. A simple disconnect was provided for the coaxial cable for this antenna. Screw holes for fastening the top were jig-located. The remainder of the payload surface was to be changed in place by adding strips of colored plastic in the form of pressure sensitive tape in thin strips, to be placed at regular intervals on the cylindrical and cold conical surfaces. It was thought that moderate care in placing the strips would suffice. Preparation of the tops required a laboratory operation done in advance. An alternate possibility was to spray-paint the package, exclusive of the top, in place on the launch stand. In view of the difficult working conditions, the short time available for repainting, the relatively long drying time of the suitable paints, especially in a humid atmosphere, and resultant interference with others working on the payload, this alternate possibility was abandoned.

The finished package surface had to be treated with utmost care. Clean gloves were to be worn by persons handling the package; and, if possible, it was to be handled only at the corners and by the mounting structure. Fingerprints and small amounts of oil and grease could significantly alter the radiation characteristics of the surface.

Two micrometeorite impact plates were needed, one with bare aluminum on both sides for the launch dates of 17-18 August, the other with black anodized aluminum on both sides for launch on 19-20 August.

For the 17-18 August launch dates, the cases containing temperature sensitivity batteries were to be partly insulated from the relatively cold cylindrical surface by slipping aluminum foil in the spaces between the inside surface

of the plastic cylindrical section and the back side of the battery cases. Foil was to be as large as practicable, that is, as large as could be slipped in between mounting screws. The screw heads on the outside package surface were to be left bright and uncoated. For the 19-20 August launch dates, these aluminum foil pieces were to be removed and the screw heads painted black.

The rocket nozzle exterior was to be completely covered with aluminum foil, shiny side out, with a foil-covered plastic disc to cover the nozzle opening. The opposite end of the rocket was to be covered with aluminum foil as completely as possible. The unjettisoned Stage 3/4 interface structure was to be polished, electroplated nickle.

The fourth stage rocket case was to be wrapped with aluminum foil which could have a paint configuration on it. This foil was to be held on loosely with wires.

2.2 Experiments

To the maximum extent possible, within the weight and power restrictions, experiments were designed to obtain scientific measurements of the environment in cislunar space. A magnetometer experiment was devised to measure the earth's and the moon's magnetic fields. The flux and approximate energy spectrum of micrometeorites was measured. Two facsimile television systems, a Naval Ordnance Test Station design on the first flights and an STL system on the last, were included. Internal payload temperature was measured. To measure radiation in space, an ion chamber was installed in Flight 2. For Flight 3 this experiment was augmented by a University of Chicago proportional counter.

2.2.1 Ion Chamber

Analysis of Explorer-series data has indicated the existence of a high flux of penetrating radiation surrounding the earth. This radiation varies both in intensity and energy with spatial position. Little is known of the energy spectrum and species of radiation present. Even the existence of the high flux of penetrating radiation was totally unanticipated, and theories that may account for such a flux are now being formulated.

The distribution of radiation has been determined directly to 2200 km by Explorer IV, and by inference to higher altitudes. For example, the only conceivable mechanism that can be used to account for the high flux is trapping of the radiation by the earth's magnetic field. This field is confined to altitudes of a few earth radii, and it is reasonable to assume that a direct correlation exists between the magnetic field vector and cosmic radiation intensity. Explorer IV measurements at 2200 km indicate a radiation radial gradient near the equator which is equivalent to a factor of two increase in the radiation flux per 100-km increase in altitude. Extension of the observed radiation flux at 2200 km, to one earth radius yields the astronomical value of approximately one million roentgen per hour. Such considerations served as a guide in determining the range of radiation to which the ion chamber is sensitive.

An ion chamber measures the number of ion pairs produced in the volume of the chamber.

a. Units Used to Measure Radiation

In this section several units of radiation will be defined and discussed:

Roentgen: A unit of flux that represents the quantity of X or gamma radiation which is effective in producing 1 esu of ions of either sign (including all secondaries) in 1 cm^3 of dry air at S.T.P.

In general the quantity of ionization is a complicated function of the ionized material. The energy of the incident radiation, the geometry and density of the mass surrounding the ionization detector. In particular for high energy gamma rays most of the energy of the photon is lost in pair production

rather than ionization, and it becomes exceedingly difficult to fulfill the requirements of the basic definition of the roentgen. Because of these difficulties the roentgen has been abandoned as a general unit of flux (it may still be used as such for X or gamma rays in air with energies of 0.08-2.5 Kev) and an alternative definition called Roentgen Equivalent Physical has been adopted.

REP (Roentgen Equivalent Physical): This definition is based on the fact that an average energy of 32.5 ev must be expended to produce an ion pair in air. Thus, to produce 1 esu requires 5.24×10^{13} ev or 83 ergs of energy. The REP is thus defined as any type of radiation which will result in the absorption in a substance of interest 83 ergs per gm. Recently this unit has been superceded by the Rad.*

Because biological damage depends on specific ionization as well as the total dose received by a living organism, two other units are of particular interest. These are REM (Roentgen Equivalent Man) and RBE (Relative Biological Effectiveness). The REM is defined as the amount of ionizing radiation, which when absorbed by living tissue, produces an effect biologically equivalent to 1 roentgen of gamma radiation at 400 Kev. The RBE is the ratio of specific ionization of a given particle to the specific ionization of 400 Kev gamma rays. (i.e., for 400 Kev gamma rays RBE = 1 whereas for protons RBE $\cong$ 5, Alphas RBE $\cong$ 10). Note that:

$$(\text{REP}) = (\text{RBE})\,(\text{REM})$$

b. The Environment

In order to properly analyze the results of experiments performed with ionization chambers it is necessary to consider the response of the chamber to a wide variety of particles, and energies. Besides the response to primary cosmic rays, the chamber will respond to secondary mesons, protons, beta particle and gamma rays. These secondaries result from interaction of

---

* Rad: Unit of absorbed radiation dose equivalent to an energy deposition of 100 ergs/gm.

the primary particles with the walls of the chamber and with the material surrounding the ion chamber. High energy primary radiation may cause shower cascades (spallation reactions or stars) so that the number of secondaries produced by a single primary may be as high as 50 penetrating particles. The ionization due to such a shower may be increased by a factor of 50, when compared to the ionization due to the original primary. It thus becomes clear that the ion chamber can at most yield a qualitative idea of the nature of the radiation present in outer space. Probably only a versatile spectrometer could give a quantitative measure of the kinds of particles and their energy distributions. However, problems of weight, power, complexity, and, in particular, problems relating to the environment of space prohibited the use of such a device on the Able-1 flights. Therefore, since the ion chamber yields a direct measure of the number of REM in the region where the chamber is located, it is most suitable for determining the biological damage which a living organism might undergo if it were situated in the payload.

c. Theory

Ionization is the principal mechanism of energy dissipation for changed particles. For heavy particles of velocity V, the amount of energy lost per unit path length, when traversing a material containing N atoms/cm^3 is

$$-\left(\frac{dE}{dx}\right)_{ion} = \frac{4\pi z^2 e^4 N}{V^2 m_o}\left[\ln\frac{2V^2 m_o}{\bar{I}(1-\beta^2)} - \beta^2\right]$$

where $\bar{I}$ is the average ionization potential of the electrons in the absorber.

$$\bar{I} \cong (13.5Z) \times 1.6 \times 10^{-12} \text{ ergs}$$

Note that the energy loss varies inversely as the mass and directly as the charge squared. For electrons the corresponding equation is

$$-\left(\frac{dE}{dx}\right)_{ion} = \frac{2\pi e^4 N}{V^2 m_o}\left[\ln\frac{V^2 m_o T}{2\bar{I}^2(1-\beta^2)} - \ln 2\,(2\sqrt{1-\beta^2} - 1 + \beta^2) + 1 - \beta^2\right]$$

where T is the kinetic energy of the electron.

Making use of these equations, the energy loss by ionization in air has been tabulated by Curran.* From these values it is possible to determine the number of particles that must strike the ionization chamber per unit time in order to give rise to a reading of 1 roentgen/hour. The following assumptions are made:

(1) The energy loss in air given in mev/gm/cm^2 is approximately the same as the energy loss in argon given in mev/gm/cm^2

(2) The amount of energy required to ionize an argon atom is 26 ev and this value is independent of energy.

(3) The pressure in the chamber is approximately 1 atmosphere.

(4) The mean distance traversed by each particle is approximately 5 cm.

Table 2-2. Number of Particles per Second† Which Must Strike the Chamber per Unit Time to Give Rise to a Radiation Rate of 1 Roentgen/Hour.

Energy ev	Electrons	Energy ev	Protons	Energy ev	Mesons	Energy ev	Alphas
10^4	10^4						
10^5	5.45×10^4						
10^6	12×10^4	10^6	0.66×10^3	0.117×10^6	0.66×10^3	4×10^6	0.165×10^3
10^7	10.2×10^4	10^7	0.425×10^4	0.117×10^7	0.425×10^4	4×10^7	0.106×10^4
10^8	8.1×10^4	10^8	2.64×10^4	0.117×10^8	2.64×10^4	4×10^8	0.66×10^4
10^9	7.2×10^4	10^9	8.7×10^4	0.117×10^9	8.7×10^4	4×10^9	2.17×10^4
10^{10}	5.75×10^4	10^{10}	8.7×10^4	0.117×10^{10}	8.7×10^4	4×10^{10}	2.17×10^4

†Assuming the ionization chamber is filled to a pressure of one atmosphere.

The range of the various species in the walls of the chamber also imposes a limitation on the sensitivity of the detector. Only electrons of energy greater than 1 mev have a range which is sufficient to penetrate the chamber

*Curran, S.C. "Luminenscence and the Scintillation Counter," Academic Press, Inc., p. 24, New York.

wall. Similarly protons must have an energy of 5 mev and alphas 200 mev in order to penetrate. It is interesting to note that if all the radiation were due to electrons, it would be possible to deduce the number of electrons striking the chamber per unit time. For example, if the energy of the electrons were greater than 1 mev, then approximately 10^5 electrons/sec would have to strike the chamber to produce an intensity of 1 roentgen/hour.

One of the most useful quantities which may be deduced from ionization rates is the average specific ionization. For this purpose, it is necessary to know the omnidirectional intensity. The average specific ionization is defined by $\overline{\sigma} = I/J_o$. $\overline{\sigma}$ is usually measured in ion pair per centimeter. I is the ionization produced in a sphere of unit area filled to 1 atmosphere gas pressure. J_o is the number of particles crossing the sphere of unit area per unit time. J_o, the omnidirectional intensity, is related to the count rate observed in any detector by

$$AJ = R$$

where A is the average projected area of the detector, taken over all possible orientations in space. For a convex body, A is related to the total surface area, S, by*

$$d\overline{A} = \frac{1}{4\pi}\int_{\omega}\left[\int\left|d\vec{\sigma} \cdot \eta\right|\right] d\omega$$

A knowledge of the average specific ionization of a particle may, to some extent, lead to an identification of the particle.

d. Description

The ionization chamber, designed by J. A. Van Allen, State University of Iowa, consisted of an aluminum-walled vessel filled with spectroscopically pure argon to a pressure of 200 lb/in.^{2} at 20°C. Volume of the chamber was 43 cm^3 and the areal density of the walls was 400 gm/cm^2. Some of the chambers utilized in the experiment were filled to a somewhat smaller pressure. In the interior of the chamber, a wire is coaxial with the cylindrical

*Vonk, V., Nature, Vol. 162, p. 330, August 1948.

wall. This wire is insulated from the walls of the chamber and an electric potential of approximately 100 volts is placed across the chamber. The effect of this potential is to sweep out the ions and electrons which are formed in the stopping process for penetrating radiation. (Figure 2.9.)

The current from the ion chamber was then applied to the input of an electrometer tube circuit. The input circuit for the electrometer was essentially the same as that used for the CsI scintillation count-rate meter in the Explorer IV series.* For the second flight, the current range of the input circuit was approximately 10^7 (that is, from 10^{-11} to 10^{-4} ampere was measurable by the circuit). On Flight 3 the range was decreased so as to cover four decades within the band of the telemeter. Any higher intensity radiation would have been within the guard band between channels 1 and 2. It was decided that there was little chance that the radiation level would exceed the band-edge values.

A schematic diagram of the ion chamber electrometer tube and in-flight calibrate circuits is shown in Figure 2-10. The ion chamber is an Anton Type 706 radiation detector whose case is biased 90 volts negative with respect to the center electrode. The 90-volt supply consists of four Burgess Type-Y15 22.5-volt batteries connected in series and to the chamber through the nonlinear input attenuator consisting of resistors to R_1, R_2, and R_3 and Zener diodes Z_1 and Z_2.

The nonlinear input attenuator serves to extend the useful dynamic range of the instrument as illustrated in the calibration curve shown in Figure 2-11. As current into this network increases, the resistance of the Zener diodes decreases exponentially to shunt part of the current away from the resistance divider. The Zener diodes are Texas Instruments Type-653C4 selected for a maximum reverse current of 2×10^{-11} ampere with one volt applied. Using a Raytheon Type-5886 electrometer tube, selected for a maximum grid current of 10^{-12} ampere, radiation levels as low as one-half roentgen/hour can be measured.

---

* Van Allen, J. A., C. E. McIlwain, and G. H. Ludwig, "Radiation Observations with Satellite 1958 Epsilon," (preprint of an article to be published in the Journal of Geophysical Research).

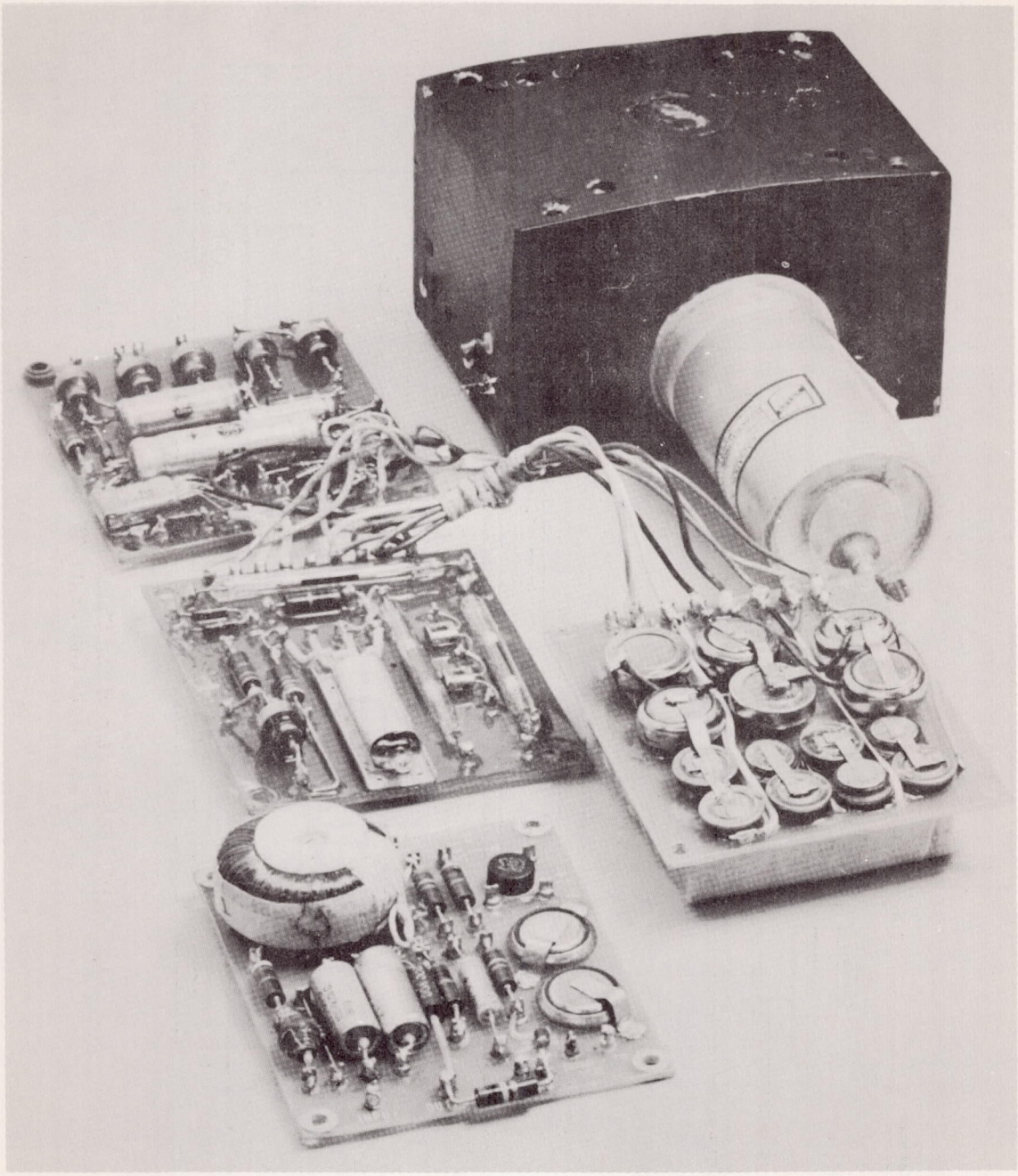

Figure 2-9. Ionization Chamber. Shown above is the ion chamber and associated electronic circuitry. In the upper right-hand corner is the in-flight calibration multivibrator. Just below, is the electronic amplifier: at the bottom of the photo is the subcarrier oscillator and to the left is the battery pack.

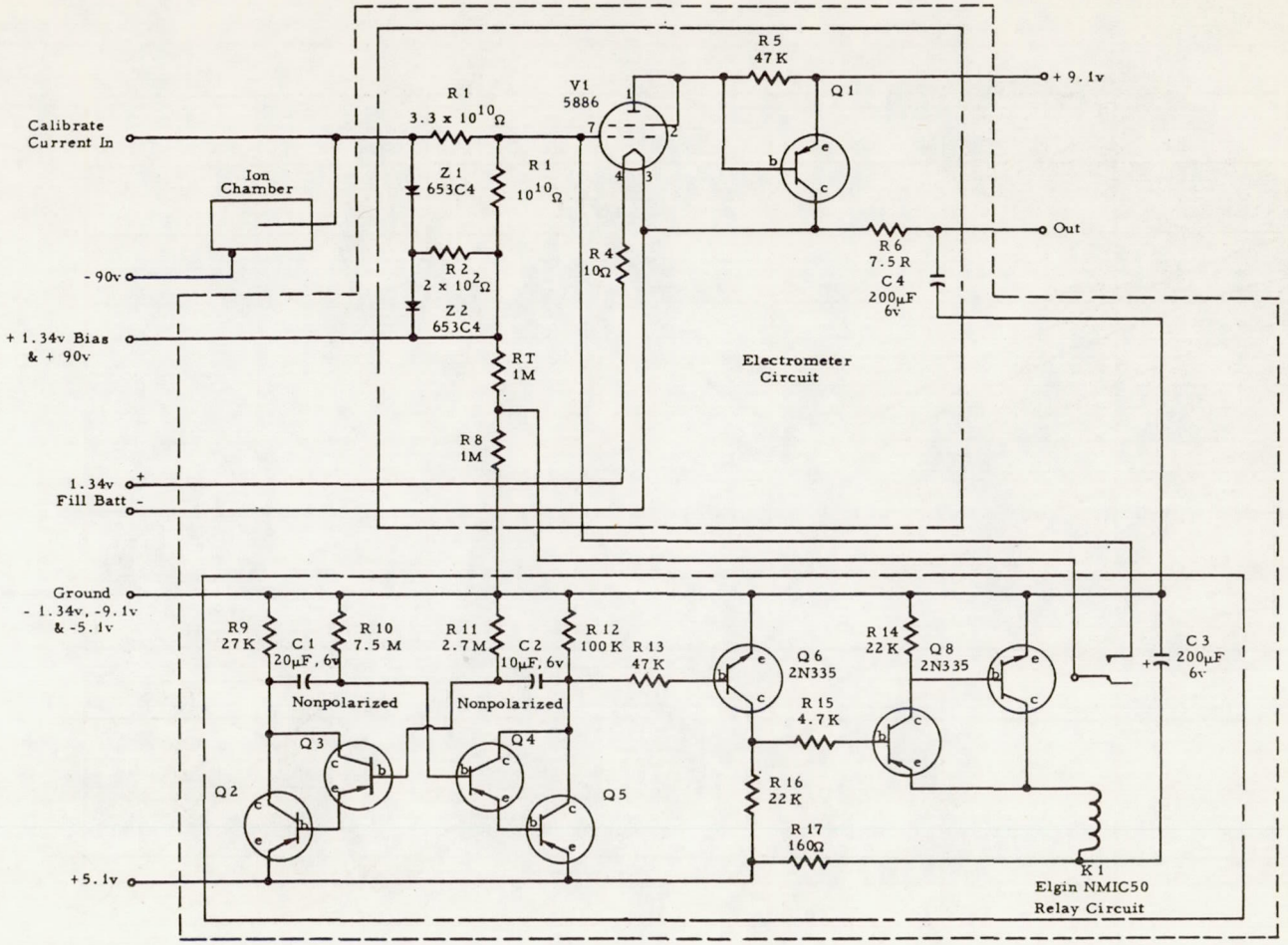

Fig. 2-10. Schematic of Ion Chamber Electrometer Tube and In-Flight Calibrate Circuits

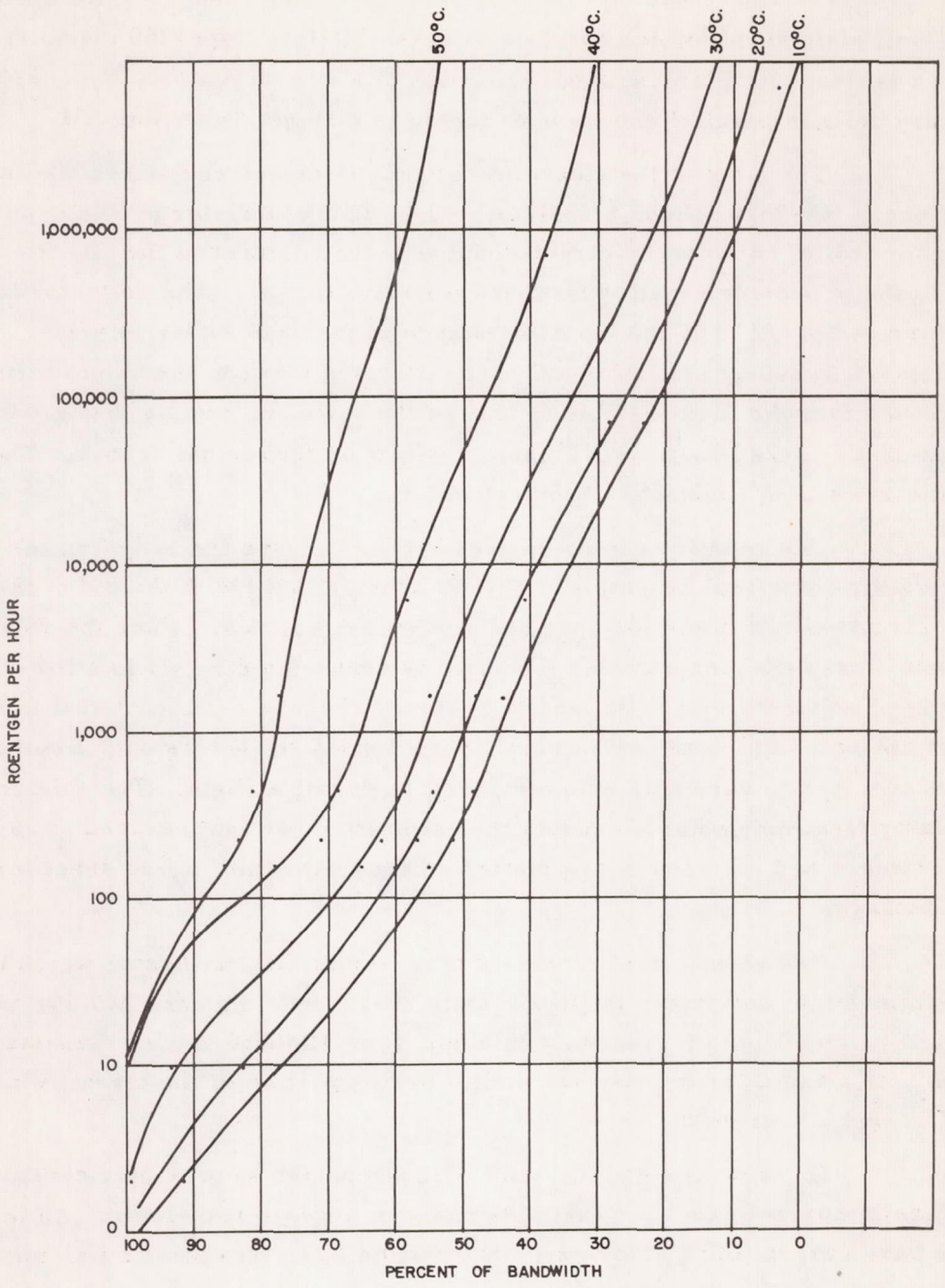

Figure 2-11. Ionization Chamber Calibration Curves

The Type #5886 electrometer tube is triode-connected and uses a 9.1-volt plate supply which consists of seven Mallory Type-400 mercury cells in series. Its filament supply consists of a pair of Mallory Type-630 mercury cells in parallel and its bias supply is a single Type-400 cell.

The plate of the electrometer tube is direct-coupled to the base of a Hughes HA-7510 silicon transistor, Q_1. This transistor provides current gain and its collector is direct-coupled to the filament of the electrometer tube to provide negative feedback for stabilization. The collector load is comprised of R_6 and the input resistance of the channel 1 subcarrier oscillator. A 200-μf capacitor, C_4, is connected between the output terminal and ground to make it impossible to change the output so rapidly that ground station phase-locked-loop discriminators might be thrown out of lock. The output circuit time constant is 1.5 seconds.

The need for direct-coupled circuits makes the use of an in-flight calibrated signal desirable. This is accomplished with the aid of the relay circuit shown in the ion chamber schematic diagram. When the relay contacts close, the electrometer tube grid is connected directly to a low-resistance voltage divider (R_7 and R_8) across the bias cell, such that 0.67 volt is applied. The bias cell is very lightly loaded so that its output voltage can be assumed to vary only with temperature during a flight. The subcarrier oscillator frequency obtained during the calibrate mode is measured at various temperatures and the results are plotted on the calibration curve sheet for each package.

The relay circuit consists of a stable multivibrator which has an asymmetrical duty cycle (approximately 20-seconds high and 200-seconds low) and an amplifier which drives an Elgin Type-NMIC50 relay. Transistors Q_2, Q_3, Q_4, and Q_5 comprise the multivibrator portion of the circuit while Q_6, Q_7, and Q_8 drive the relay.

Q_2 and Q_3 and Q_4 and Q_5 are paired to provide a considerable increase in current gain over that obtainable in a single transistor. An increase in the base current of Q_3, for example, results in an increase in its emitter

current, and likewise the base current of Q_2, of approximately β times the change in Q_3 base current. Consequently, the collector current of Q_2 is increased by approximately β^2 times the original base current change.

Q_6 is an isolating common emitter amplifier and Q_7 and Q_8 form another bootstrap circuit which operates similarly to Q_2 and Q_3 described above. A 200-μf capacitor, C_3 is connected from the relay coil to ground. This serves the function of applying the full 5.1-volt supply voltage to the relay coil and transistors Q_7 and Q_8 for pull-in. As the capacitor discharges, relay coil current is supplied from the battery through R_{17} and battery drain is reduced below that which would be required if it had to supply the pull-in current as well as the holding current.

The battery supply for the relay circuit consists of four Type-630 cells in series. It has been established that the Type-630 cells were too heavily loaded to last for the required battery-life when operated at temperatures approaching 0°C. Consequently, in future units, all of the Type-630 cells will be replaced with the larger capacity Type-640 cells for increased life at low temperatures. The Type-630 cells were used in this flight as the relay circuit supply and for the electrometer tube filament supply.

e. Calibration of Pioneer I

Calibration of the chamber and associated circuitry was accomplished in two steps.

First, the ionization chamber was disconnected from the circuit and a known current was fed into the system. Graphs of current input versus SCO output for various temperatures are shown in Figure 2-12. The chamber and circuits were then taken to the cobalt-60 bomb located at the Radiology Department of the UCLA Medical Center. Under the supervision of Dr. M. Greenfield, ionization chambers were irradiated with known doses and SCO outputs recorded. The following calibration data were obtained for the chamber which was flown.

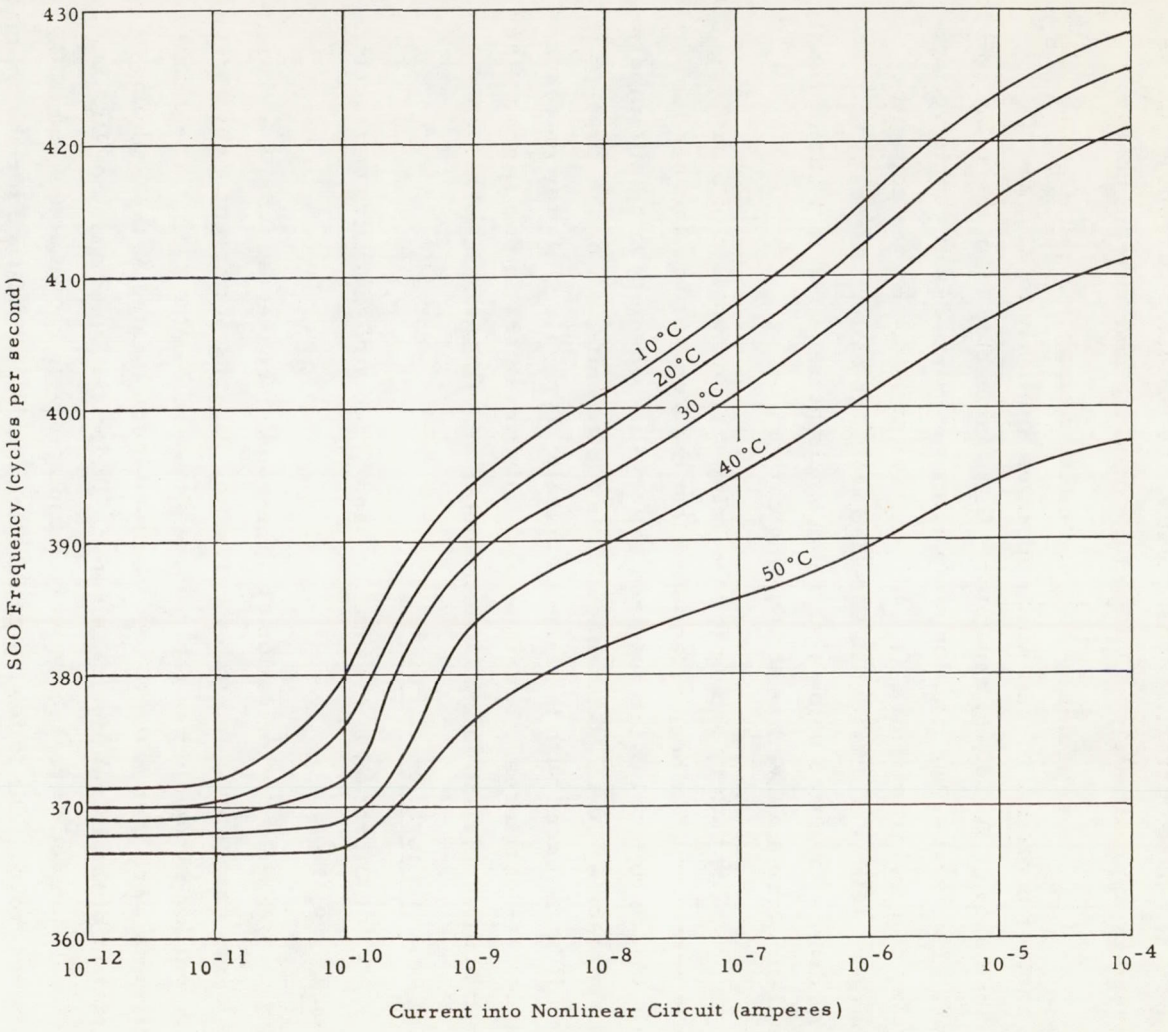

Figure 2-12. Ion Chamber Calibration with Temperature as Parameter.

Table 2.3. Calibration Data for Ion Chamber.

Radiation Dose	SCO Output	Corresponding Current Input	Empirical Calibration Current for 1 R/hour Input
10	379	1.7×10^{-10}	1.7×10^{-11}
150	392+	2.05×10^{-9}	1.37×10^{-11}
220	394	4×10^{-9}	1.82×10^{-11}
420	396	6.8×10^{-9}	1.62×10^{-11}
1820	400	2.6×10^{-8}	1.43×10^{-11}
6120	403+	10^{-7}	1.63×10^{-11}

Room temperature - 23°C
Potential on chamber - 90 volts
Average empirical calibration - 1 R/hour = $(1.6 \pm 0.05) \times 10^{-11}$ amp

Utilizing this data in conjunction with the data in Figure 2.12, an empirical calibration curve was devised. Figure 2-13 represents the empirical calibration curve deduced from Figure 2-12 and Table 2-3. This calibration indicates that an output current of $(1.6 \pm 0.05)\ 10^{-11}$ amperes was produced by a radiation level of one roentgen per hour. However, a post flight estimate of the sensitivity, based on the mass of argon and the energy formation of an ion pair, yielded a value of 8.9×10^{-11} amperes per roentgen per hour. It was found that recombination, diffusion, and wall effects did not subtract significantly from this estimated sensitivity. Hence, this discrepancy between the calculated sensitivity and the empirical one was interpreted to mean that the ion chamber had leaked in the period between filling and calibration. The discrepancy disappears if one assumes that the pressure in the chamber, at the time of empirical calibration, was only 2.42 atmospheres.

Next, an estimate was made of the pressure in the chamber at the time of launch. Anton Electronic Laboratories reported that the chamber had been filled to 13.6 atmospheres on 10 September 1958. Calibration took place on 2 October 1958 and yielded a sensitivity that corresponded to a calculated pressure of only 2.42 atmospheres. If the gauge pressure had

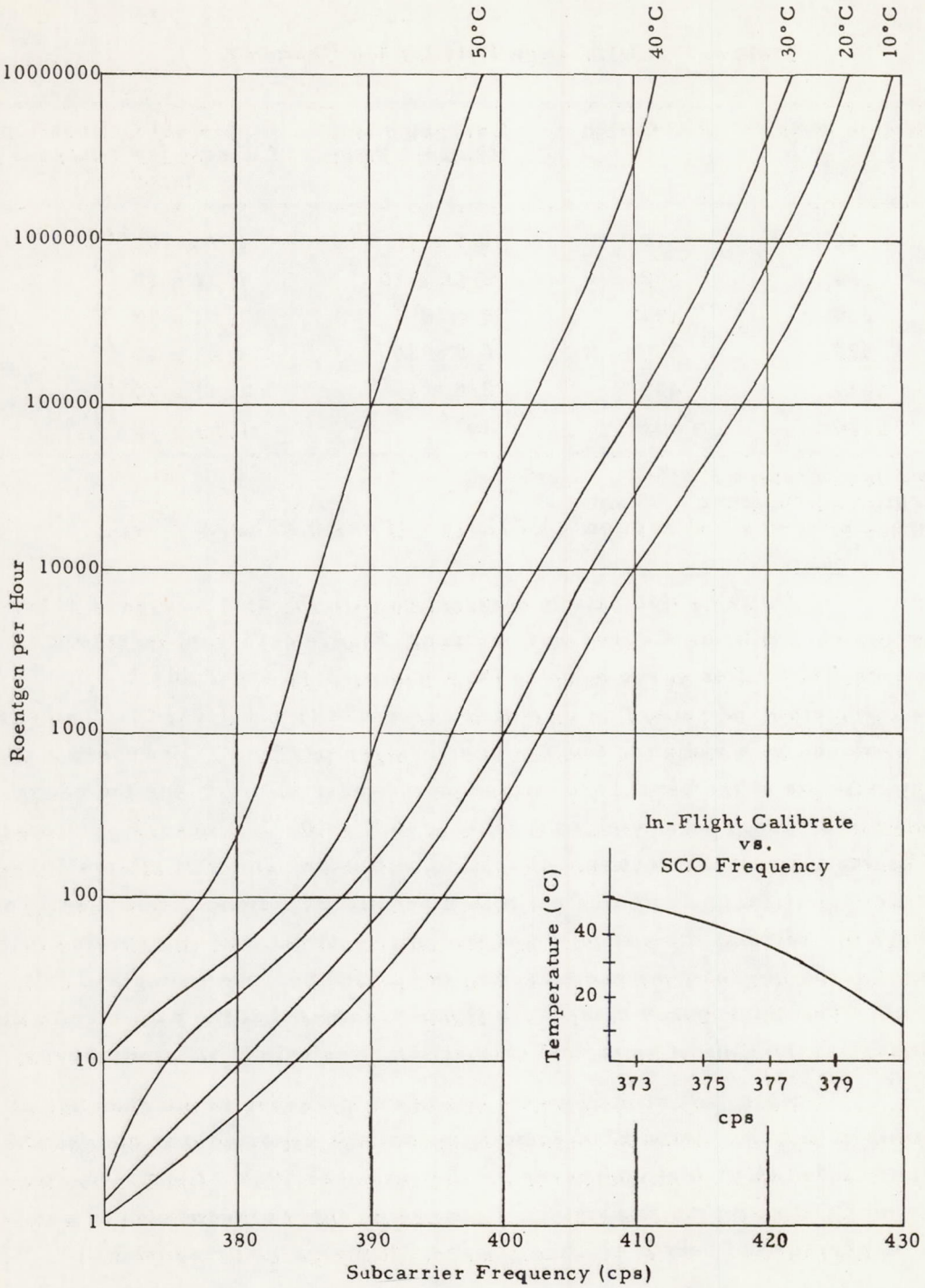

Figure 2-13. Ionization Chamber Empirical Calibration Curves.

decreased exponentially, the time constant, according to these data, would have been 10 days. If it is assumed, also, that the leak aperture and the leak time constant did not change, calculations indicate that the pressure in the chamber just before launch on 11 October 1958 would have been 1.58 atmospheres. This calculation implies that the sensitivity of the chamber had been reduced, from the empirically determined value, by a factor of 1.5 at the time of launch.

Post flight evaluation of the observed radiation levels and a more quantitative analysis of the error inherent in the experiment led to an improvement in the calibration curve and the data reduction procedure. The observation that the peak ionization intensity striking the chamber was approximately 10 roentgen per hour made it necessary to replot an expanded and more accurate version of the foot of the curve in Figure 2-13. Figure 2-14 shows the expanded calibration curve with the detailed dependance of the radiation level on temperature.

f. Evaluation of Errors

Several errors, arising from the data collection system, were considered:

(1) The frequency output of the voltage controlled subcarrier oscillator in the vehicle was determined empirically as a function of the input voltage. (This voltage is a measure of either radiation level or calibration level.) The output frequency was found to be stable to within ± 1.5 cycles per second or ± 2.5 per cent of the subcarrier bandwidth.

(2) The next step in the collection of data involved the reconversion of the received subcarrier frequency to the Sanborn reading. The error introduced by this portion of the system was found, by calibration, as follows: A frequency, known to ± 1 cps, was fed into this portion of the equipment over a period of 2 days. A total of 15 readings was taken.

(3) The standard deviation for these readings was found to be approximately 0.75 cps or 1.20 per cent of bandwidth.

(4) The standard deviation in the frequency determination then was found to be approximately 2 cps or 3.4 per cent of bandwidth.

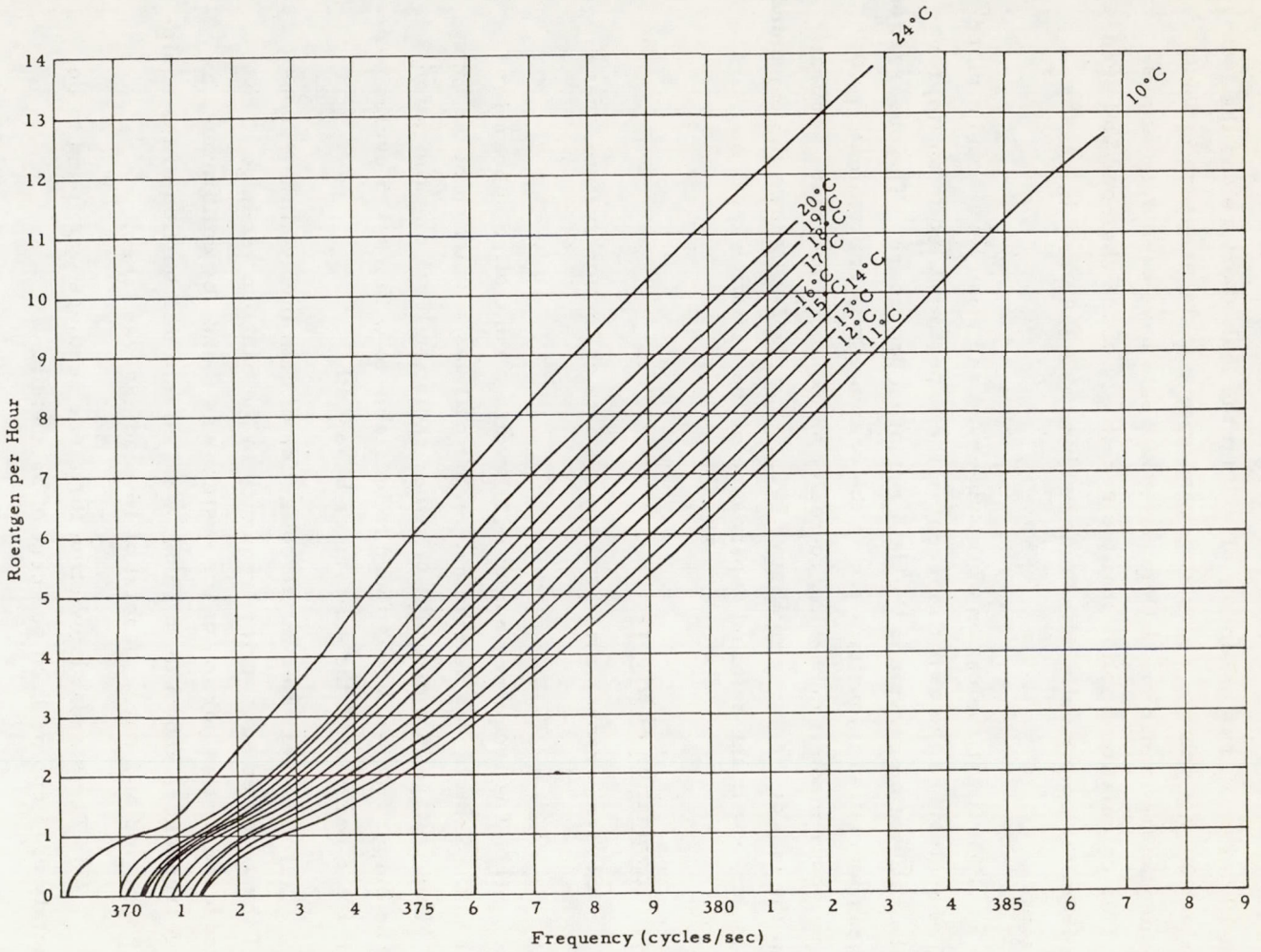

Figure 2-14. Expanded Pioneer I Calibration Curve.

(5) The relationship between radiation level and subcarrier frequency was found to vary with temperature. For this reason an in-flight calibration pulse was transmitted from the vehicle. The subcarrier frequency corresponding to the in-flight calibration voltage varied with temperature. This frequency versus temperature relationship was determined empirically to within 1 cps or 1.6 per cent of bandwidth. The standard deviation in the determination of temperature from the in-flight calibration pulse was then 2.6 cps or 3.3 per cent of bandwidth. The corresponding error in the temperature reading was approximately 10°C.

g. Pioneer I Data Reduction

The results shown in Figure 2-15 were obtained during the first 4 hours of flight. The radiation levels plotted in this figure are based on the assumption that the sensitivity of the chamber had been reduced by a factor of 1.5 with respect to the sensitivity determined by the empirical calibration. The question of the effect of the leak on the sensitivity of the chamber during these 4 hours was also considered. (See subsection e.) Based on the calculated leak rate and assuming the chamber to be in vacuum, the calculated fractional change in pressure is 1.01. Such a change would produce a negligible change in the sensitivity of the chamber.

Two different methods for data reduction were evaluated with respect to reliability. In the first method the in-flight calibration frequency was used as the reference; and the frequency difference between the in-flight calibration and the signal was looked upon as the value determining the radiation level. In the second method only the temperature dependance of the response was taken into consideration. The in-flight calibration was looked upon as a temperature sensor similar to the more accurate vehicle temperature sensor of channel 3 which was located elsewhere on the vehicle. Once the temperature was known the calibration curve which corresponds to that temperature (see Figure 2-12) was used to determine the radiation intensity.

Ordinarily the first data reduction method would be more accurate than the second, since in using the difference between the signal level

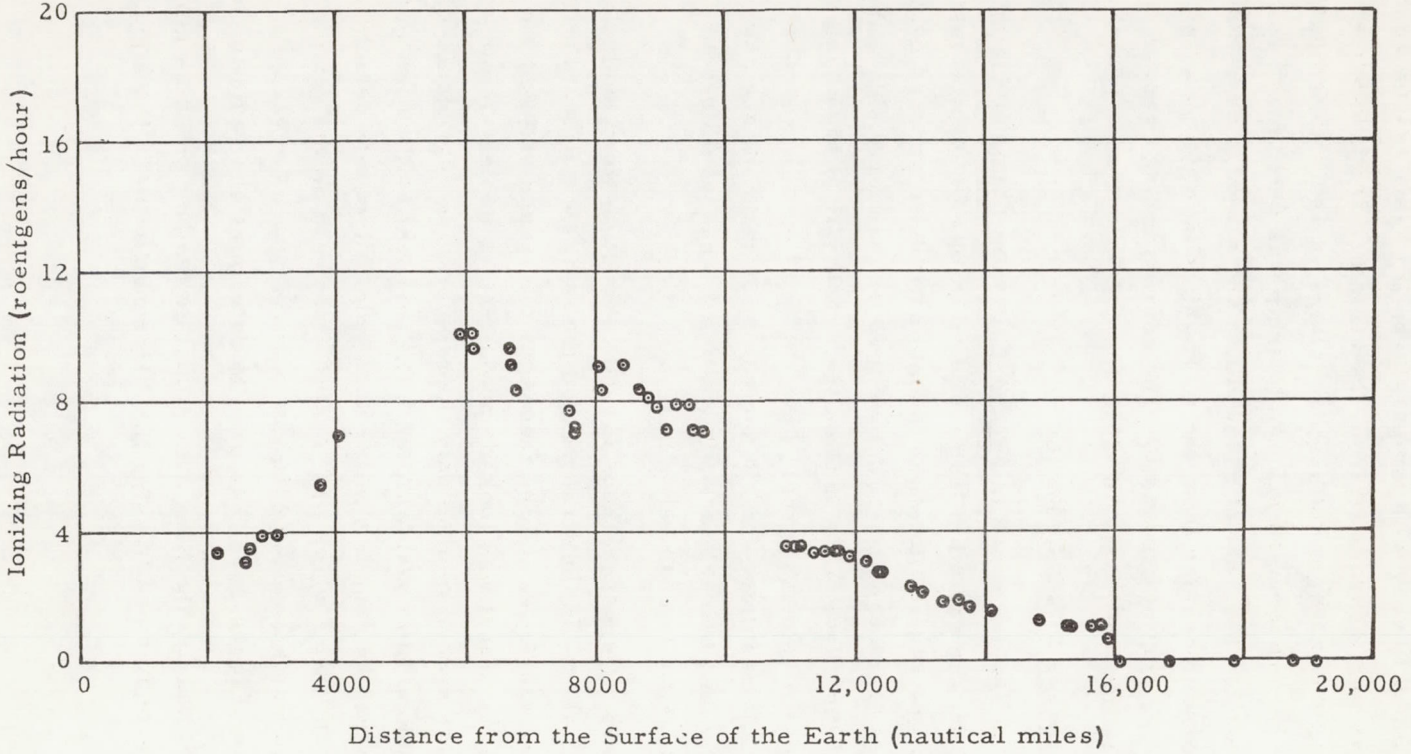

Figure 2-15. Pioneer I Ionizing Radiation Versus Distance from the Surface of the Earth.

and in-flight calibration as a measure of the radiation level we compensate for a possible drift in the electrometer amplifier. For this flight, however, the second method was decided upon as most accurate for the following reasons.

(1) During calibration the in-flight calibration was accurate to ± 1 cycle/sec. This leads to a temperature uncertainty of 10°C according to the insert in Figure 2-12. In view of the extreme temperature dependance of response of the electrometer amplifier such a large temperature uncertainty leads to immense error flags on the data points.

(2) A more accurate temperature sensor was located elsewhere in the vehicle. It was thus possible to determine the vehicle temperature by two independent methods. In all cases the temperature determined by the more accurate vehicle temperature sensor was in agreement with the temperature as determined by the in-flight calibration when the uncertainty in the in-flight calibration was taken into consideration. If the assumption that channel 3 temperature sensor also determines the temperature of the ion chamber package then the radiation could be determined with much greater accuracy. The data shown in Figure 2-15 were determined by use of channel 3 temperature sensor for evaluating the temperature dependence of the circuit. If the maximum temperature variation, consistent with the in-flight calibration is taken into account, then the uncertainty in the radiation level increases by almost 50 per cent. Figure 2-16 shows the resulting error flags when this uncertainty is added to the instrumented errors in the observation. These error flags represent the maximum conceivable uncertainty in the data.

h. Analysis of Pioneer I Ionization Data

Analysis of the observed data indicates that the following deductions may be made:

(1) The radiation level rises to a peak and then drops to a very low level as the altitude increases. This represents the first experimental verification of the existence of a confined radiation zone of the type postulated by Van Allen, et al*.

---

*Van Allen, J. A., G. H. Ludwig, E. C. Ray and C. E. McIlwain, "IGY Satellite Report Series", Number 3, National Academy of Sciences, National Research Council, Washington 25, D. C., 1 May 1958.

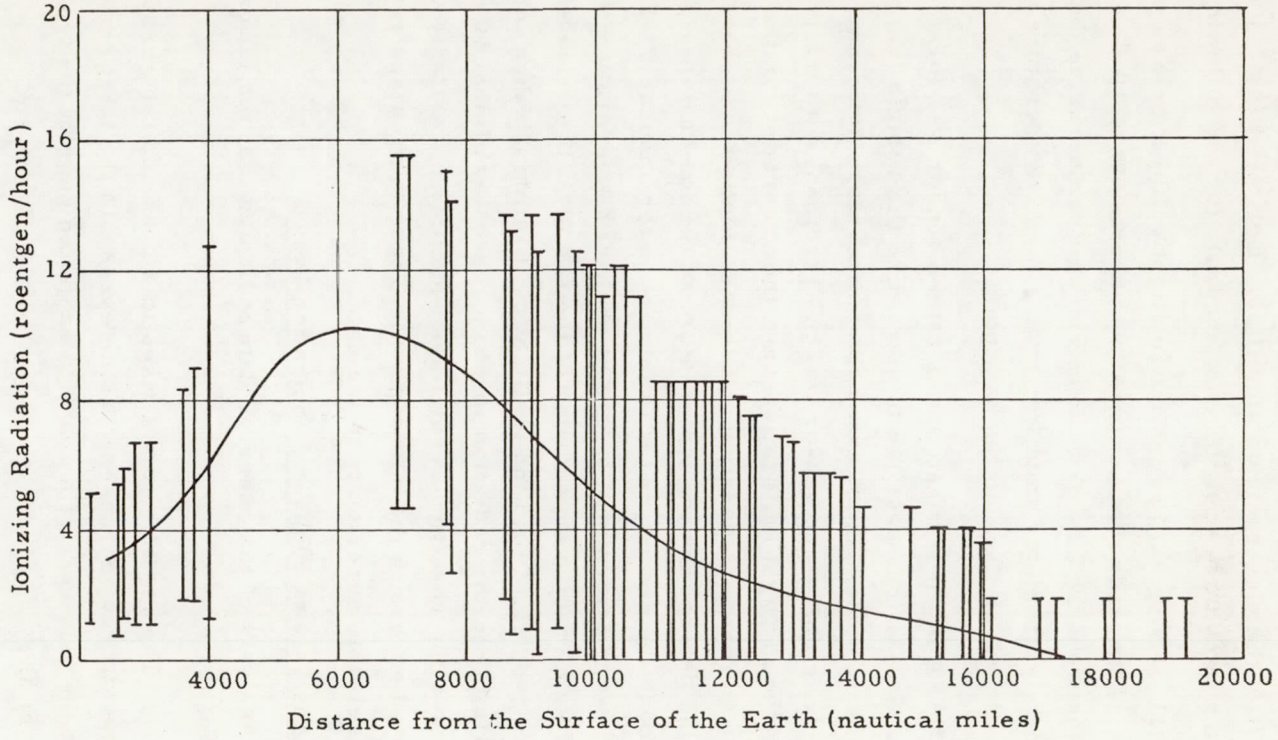

Figure 2-16. Pioneer I, Ionizing Radiation vs. Distance from the Surface of the Earth.

(2) In the altitudes ranging from approximately 4000 to 24,000 km, the radiation level is in excess of 2 roentgens per hour. This result yields a quantitative measure of the depth of the radiation belt in the region of 20°N latitude.

(3) In the vicinity of 20°N latitude, the peak of the radiation belt occurs at an altitude of 10,000 ± 2000 km.

(4) The maximum radiation level observed is 10 roentgens per hour. Considering the uncertainty in the chamber pressure, it is possible that this value is too low by 60 per cent.

i. Calibration and Analysis of Pioneer II Ionization Data

The apparatus used in Pioneer II was essentially the same as that used in Pioneer I. The major changes were a reduction of the temperature sensitivity of the circuits by a careful choice of circuit components, and a reduction in the range of values of ionization to which the circuit was sensitive. A calibration curve of the circuit is shown in Figure 2-17.

Ion chamber data were received during the first half-hour of flight. The measured radiation levels are plotted versus altitude in kilometers in Figure 2-18. The declination and longitude of the vehicles position are given for each data point.

The significance of the information on ionizing radiation which was gathered during the brief life of Pioneer II lies in the fact that it clearly indicates an increase of such radiation with decreasing north latitudes. At the apogee of the orbit, in the altitude range of 1470-1520 km, the vehicle traversed 7° of latitude from 30°N to 23°N latitude. Thus, for essentially constant altitude the variation of ionization with latitude was observed. Figure 2-19 shows the variation of ionization with latitude when the chamber was located in the 50-km range, between 1470-1520 km altitude. Since these data show the radiation increasing greatly near the geomagnetic equator, it appears that the trapping of the particles follows a pattern similar to the earth's measured geomagnetic field. (See Section 2.2.2 subsection b) for a summary of results relating to both radiation experiments.)

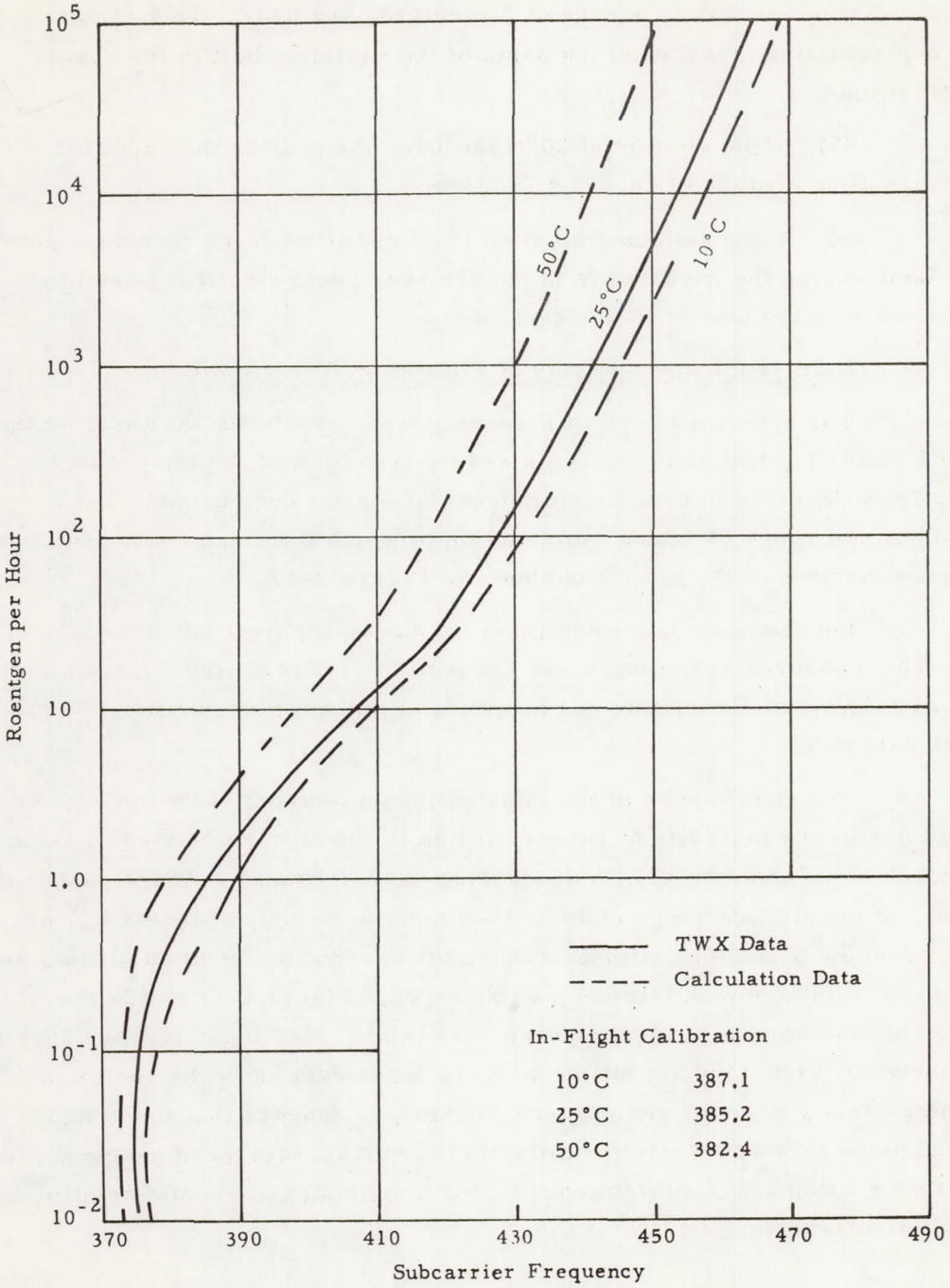

Figure 2-17. Revised Ion Chamber Calibration.

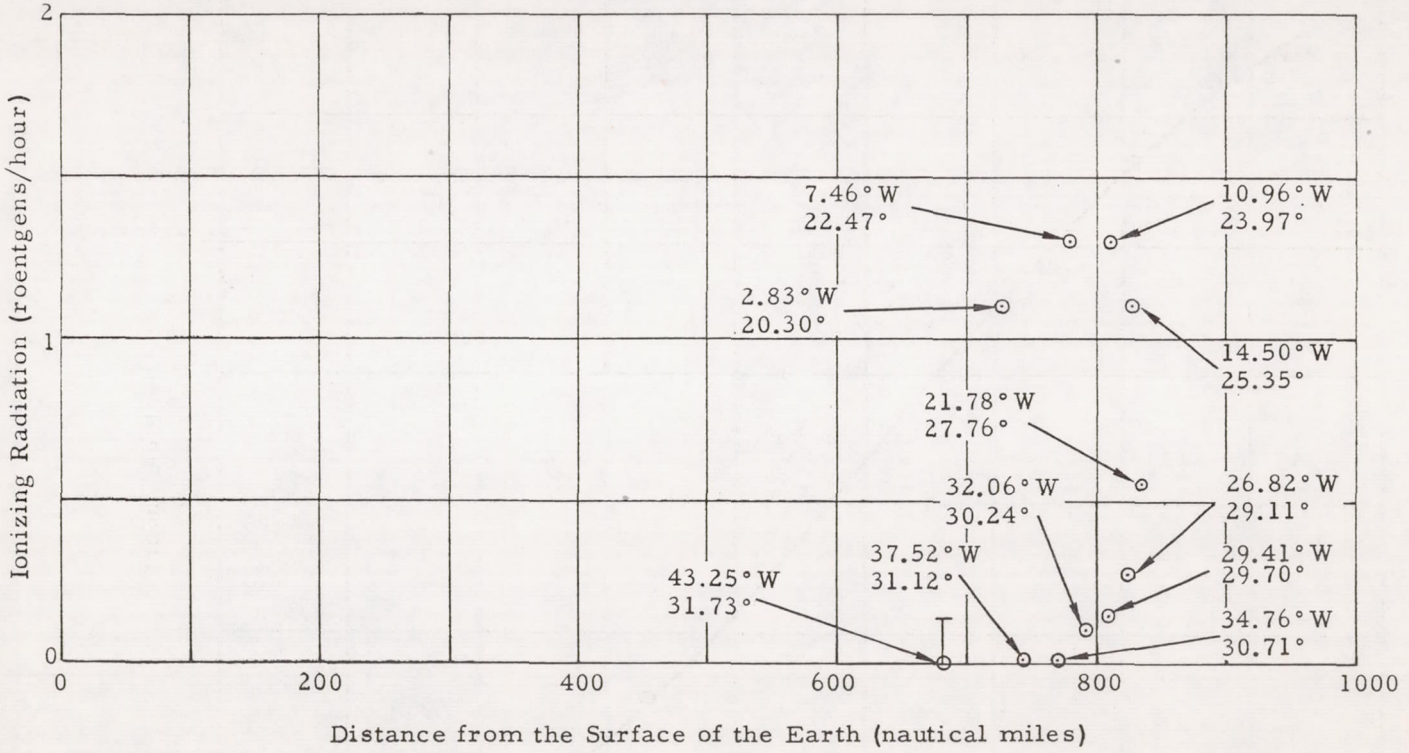

Figure 2-18. Pioneer II Ionizing Radiation Versus Distance from the Surface of the Earth Including Longitudes and North Latitudes.

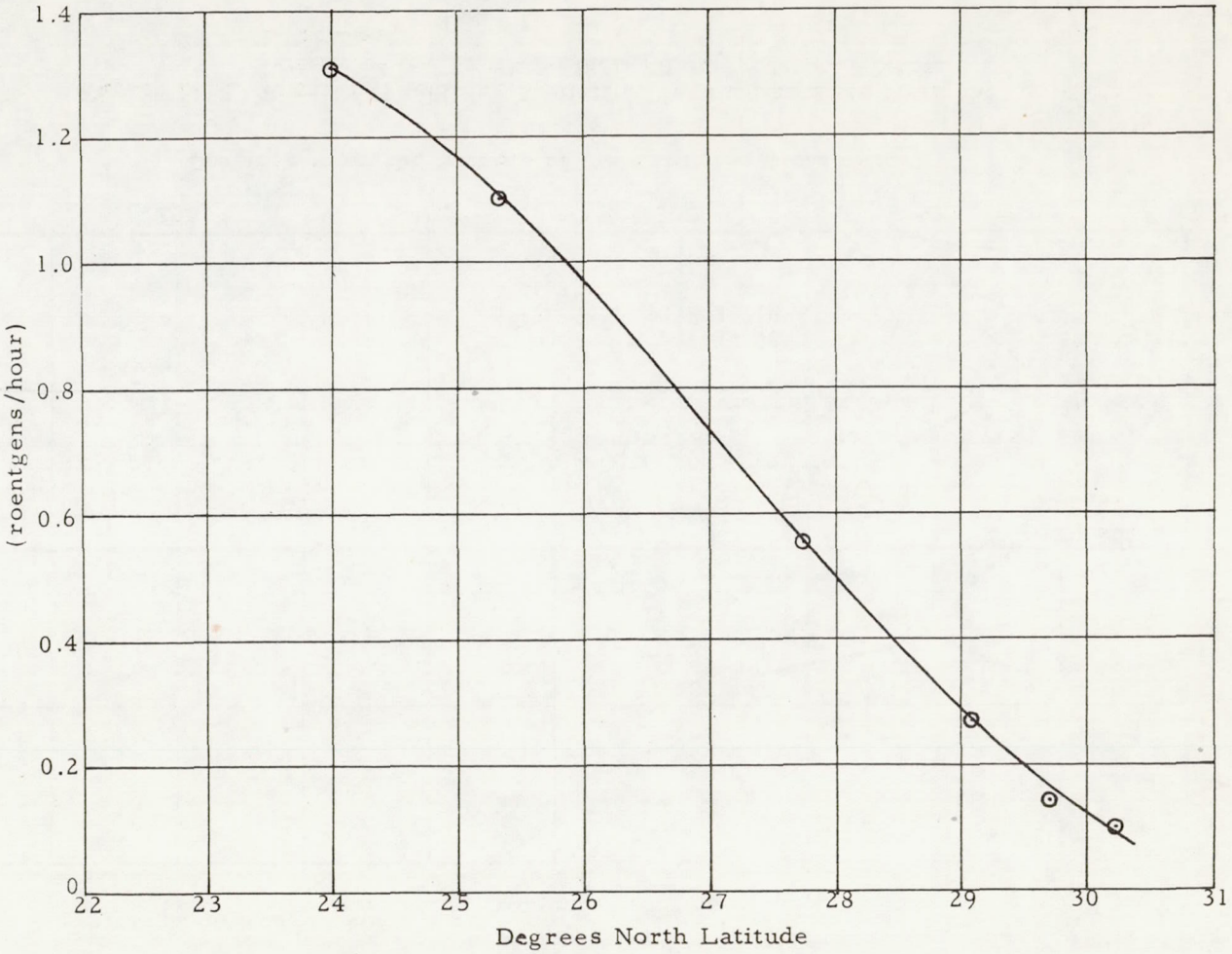

Figure 2-19. Ionization Versus Latitude at an Altitude of 1500 ±25 km.

2.2.2 Proportional Counter Telescope

a. Description of the Experiment

Over the past few years, a long term variation in the over-all cosmic ray level has been noticed. The change, amounting to as much as a factor of two, correlates well with solar activity. This solar activity is believed to produce pronounced changes in the interplanetary magnetic fields. A heliocentric or geocentric disordered magnetic field may serve as an energy-dependent diffusion barrier to incoming cosmic radiation.

As a means of testing the disordered field hypothesis and the extent of such a field about the earth, a proportional counter telescope was proposed to ARPA by the University of Chicago. Upon the subsequent direction of ARPA (the Able-1 program was then under its direction) such an experiment was constructed for inclusion in the third firing (Pioneer II). The inclusion of this equipment, which weighed 6.07 pounds, necessitated the removal of other equipment of at least this weight. The only other sensor which contributed weight of this order was the NOTS television system (8.5 pounds), and the decision was made not to include it in the Pioneer II. It is well to note here that the total remaining sensor weight including three experiments came to about 2.5 pounds.

The proportional counter consisted of a 1-cm tube, 2 inches in length, surrounded by 6 others of the same size in a concentric arrangement about the center tube. These counters were filled to 60-cm pressure with a mixture of 40 percent methane and 60 percent argon, yielding with associated amplifiers a resolving time of 1 microsecond. The center wires were 1 mil tungsten and the counter walls 1 gm/cm^2 brass. The whole assembly was contained in a lead shield of thickness 5 gm/cm^2 (Figure 2-20).

The center counter was connected to a pulse amplifier, in turn feeding a scaler chain. The other counters were connected in two triples to identical amplifiers. In addition to the single events counted by the center tube, triple events ocurring in the center tube and any two others diametrically opposed were counted by having the three outputs connected to a triple coincidence circuit which was in turn connected to a scaler chain. The

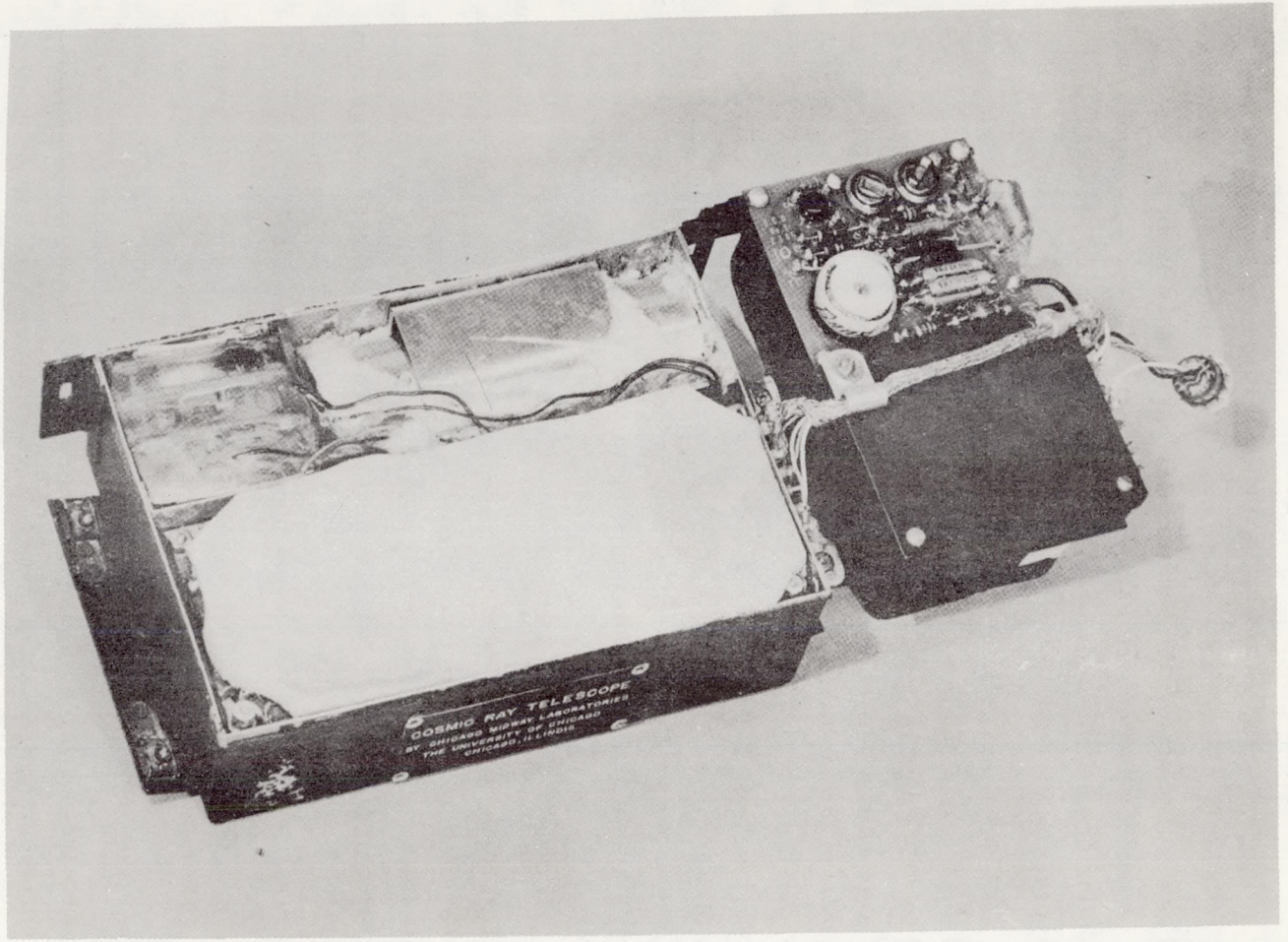

Figure 2-20. Proportional Counter Telescope.

scalers were serial binary, the singles channel being scaled down 2^{15} and the triples by 2^{11}. The trigger threshold was 1 millivolt at amplifier input.

The counters were gamma sensitive although the low photo-electric conversion efficiency in the counter walls tended to reduce the sensitivity. The triple coincidence channel had a relatively narrow solid angle for a coincidence (though the acceptance solid angle is almost 4π stearadians), and the gamma coincidence rate was further reduced because of the high scattering cross-section for gammas. The shielding corresponded to the stoppage of a 50 mev electron in the case of nominal incidence.

It was planned to observe the single rates and triples coincidence rates as a function of radial distance from the earth and thus to obtain data on whether the existing minimum on the earth (due to the present solar activity maximum) changes and whether the counting rate increases and approaches a plateau characteristic of the cosmic ray level during inactive solar years.

The equipment was intended to be kept as isotropic in response as possible, the singles and triples events allowing some separation in range. The triple coincidence circuit was introduced some time after the initial design had begun to serve as an adjunct to the ion chamber experiment and thus help map the radial distribution in the high flux about the earth. By utilizing such a triple channel, the expected counting rate could be held to a tolerable level and not block the scalers.

Figure 2-21 shows the observed triples rate as a function of altitude. As the vehicle approached the equator the triples counting rate became so high that the telemetry could no longer respond. No data was obtained from the singles channel predominantly because the telemetry did not seem to lock on this frequency; however, the count rate might have been so high, for example, that it was not possible for the telemetry to lock on a single frequency. It is interesting to note that the ionization chamber data, used in conjunction with the count rate from the University of Chicago may be used for the purpose of making deductions about

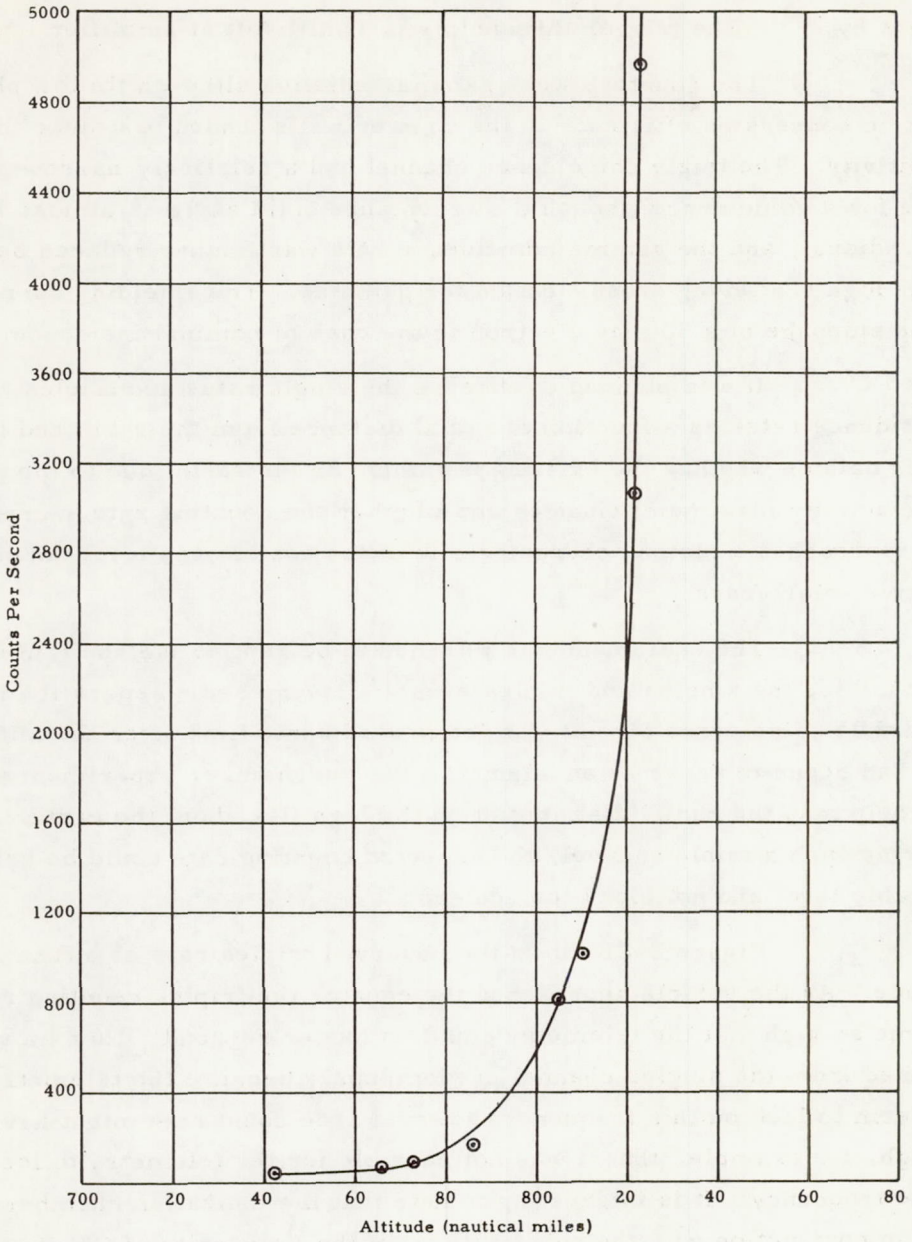

Figure 2-21. University of Chicago Proportional Counter Telescope Triples Rate.

(1) average specific ionization of the particles,

(2) the species of particles present,

(3) the energy of the particles,

(4) the trapping mechanism,

(5) the geomagnetic field.

b. Conclusions to be Drawn from Pioneer I and II Cosmic Ray Experiments

Conclusions may be drawn from the direct observations with the ion chamber and the proportional counter telescope. Much of the reduced data from these observations has already been presented in graphic form.

The conclusions can be outlined briefly as follows:

(1) The first experimental verification of the existence of a confined radiation zone of the type postulated by Van Allen, et al* was made.

(2) In the altitudes ranging from approximately 2000 to 13,000 nautical miles, the radiation level is in excess of 2 roentgens per hour. This result yields a quantitative measure of the depth of the radiation belt in the region of 30°N latitude.

(3) In the vicinity of 20°N latitude, the peak of the radiation belt occurs at an altitude of 6000 ±1000 nautical miles.

(4) The maximum radiation level observed is 10 roentgens per hour; however, because there was an uncertainty in the chamber pressure, it is possible that this value is too low by 60 per cent.

(5) A pronounced latitude effect is observed at an altitude of 1500 km. At 25°N latitude the radiation gradient is 0.2 roentgen per hour per degree change in latitude.

*Van Allen, J.A., G.H. Ludwig, E.C. Ray, and E.C. McIlwain, "IGY Satellite Report Series," Number 3, National Academy of Sciences, National Research Council, Washington 25, D.C., 1 May 1958.

(6) The count rate, as observed from the University of Chicago count rate telescope, increased in a manner similar to the increase in ionization. The average specific ionization was calculated from the omnidirectional intensity and the ionization level. The ratio of average specific ionization to minimum average specific ionization was found to be greater than 3. Considering the fact that electrons of less than 1 mev cannot penetrate the walls of the ionization chamber, this high specific ionization could not be produced by high energy electrons alone, but would require an admixture of electrons and protons.

2.2.3 Micrometeorite Detector

a. Introduction

It is of considerable scientific interest to observe micrometeorites at distances such that the earth does not block off nearly half the heavens, and where the influence of the earth's gravitational field is considerably reduced. The micrometeorite experiment was essentially an attempt to make an initial survey of the number density and the rough momentum spectrum of micrometeorite particles at altitudes far above regions in which previous measurements had been made. A probe in orbit about the moon gives an opportunity to observe micrometeorite particles in a different gravitational field, and also a chance to study the effect of the moon in blocking the passage of particles from various directions in space.

In addition to statistics concerning the number of micrometeorites observed as a function of time and of vehicle position in space, it is of great interest to establish the characteristics of the individual particles. The Pioneer payloads contained a two-level detection system capable of separating the observed impacts into two classes which depend upon the momentum of the particle, a first step in measuring the momentum spectrum of the micrometeorites.

Early in the Able-1 program, the Air Force Cambridge Research Center was requested to assist in a micrometeorite experiment; the Geophysical Directorate of that organization had an extensive background in the field of micrometeorite research and had developed equipment which was applicable to the lunar probe program. AFCRC supplied the microphones for the detector, and the amplifier. In addition, it lent valuable assistance in the calibration of the micrometeorite system. The logic circuit was developed by STL.

b. Description

Airborne components of the micrometeorite detection system consisted of: (1) a detector (diaphragm and microphone), (2) a bandpass amplifier, and (3) two logic circuits (each with a trigger, flip-flop, and emitter follower). (See Figure 2-22.) The outputs of the logic circuits were fed to the subcarrier oscillators of the telemetry system.

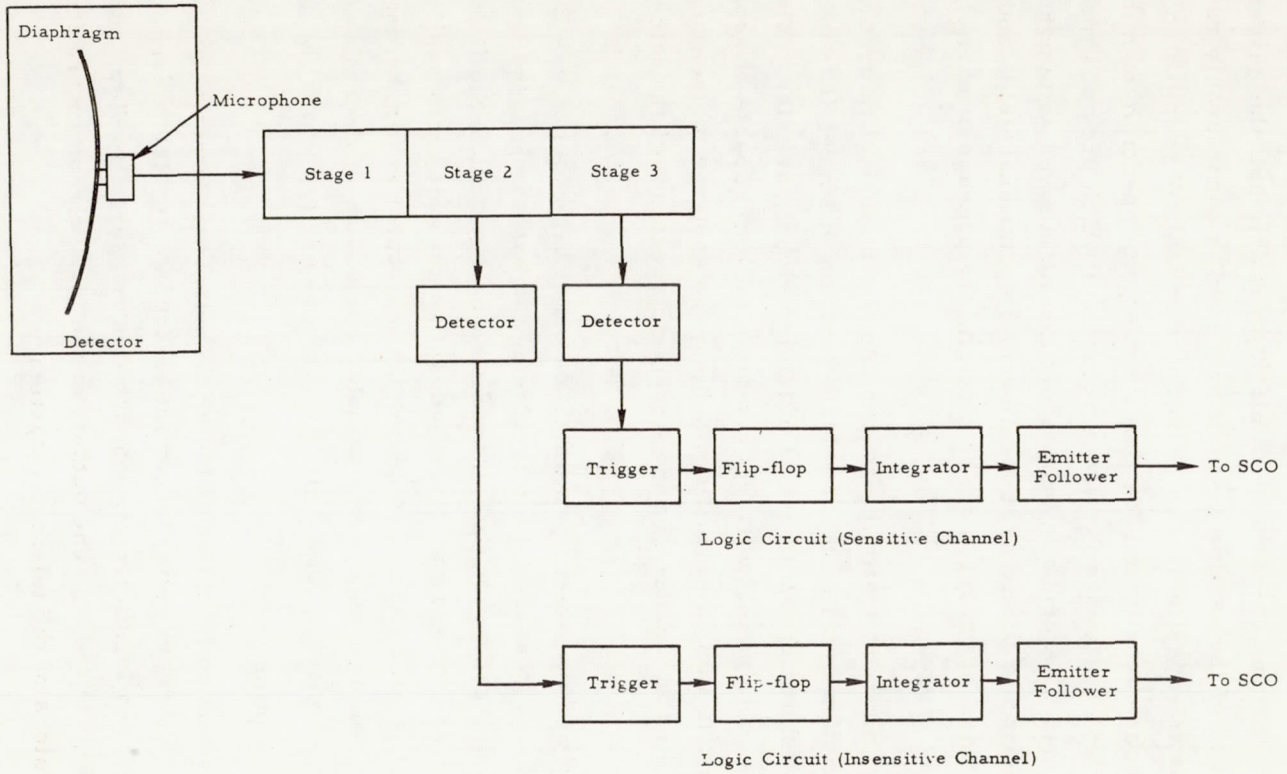

Figure 2-22. AFCRC Micrometeorite Amplifier.

A micrometeorite striking the diaphragm generated an acoustic pulse which traveled through the diaphragm to the microphone. The microphone contained a piezoelectric crystal which rings at 100 kc under the influence of the acoustic pulse. The envelope decay time was approximately 3 milliseconds. The 100-kc signal was amplified in the bandpass amplifier and detected. The amplifier had three stages of gain; the output of all three stages drove the first logic circuit (sensitive channel), whereas the output from only two stages drove the second logic circuit (insensitive channel).

In either logic circuit, the input pulse (a replica of the 100-kc ringing envelope) was presented to a trigger. When the input pulse was greater than the trigger threshold, a sharp output pulse was generated. This pulse is used to change the state of the flip-flop (bistable multivibrator). The integrator was employed to reduce the rate of change of output voltage for later ease of data reduction. An emitter follower was employed to decouple the subcarrier oscillator from the logic circuit and to provide a low-impedance output.

When a small micrometeorite impacted on the diaphragm, a pulse existed at the output of two amplifier stages, but was too small to trigger the logic-circuit (insensitive channel). The same pulse existed also at the output of the third amplifier stage, but of larger voltage. When a sufficiently large micrometeorite impacted on the diaphragm, both logic circuits were triggered.

The diaphragm was made of aluminum (7075-ST6) painted black on the side toward the vehicle and polished on the outer face. It was 5 inches wide by 12 inches long, the long direction curved (14.5-inch radius) to conform to the payload shell. It was mounted equatorially on the vehicle with six rubber grommets. The purpose of the grommets was to provide a large acoustic mismatch at the connection to the vehicle.

The microphone was a piezoelectric type, designed and constructed by AFCRC. The crystal, made by Brush for AFCRC, is capable of operation from 0° to $+500^{\circ}$F and had a natural resonant frequency near 100 kc. The units are illustrated in Figure 2-23. The microphone was attached to the diaphragm with Eccobond Solder 56-C (a conductive epoxy with high shear strength) and a bracket.

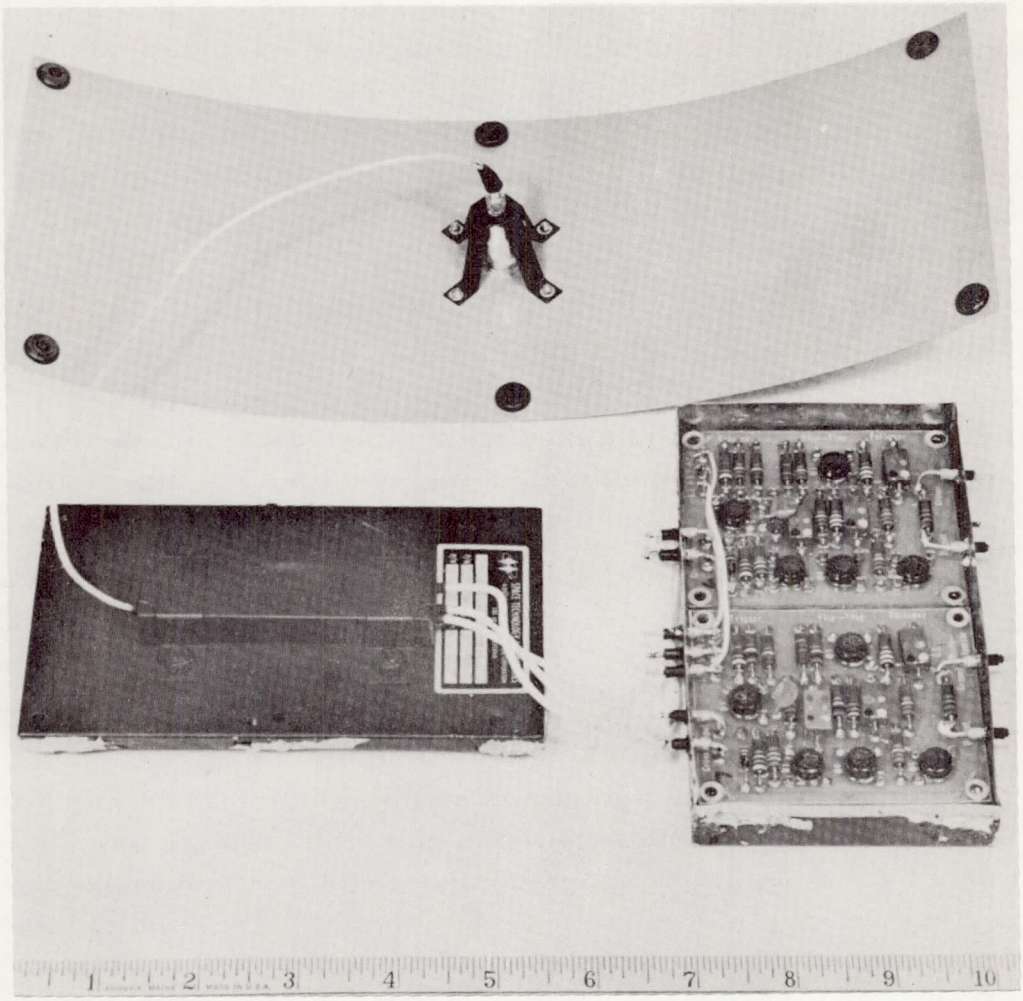

Figure 2-23. Micrometeorite Experimental Apparatus

The amplifier, designed and constructed by AFCRC, had a 90-db gain at center frequency. Three conventional transformer-coupled stages are employed, each with a 30-db gain. The bandwidth was approximately 10 kc centered at the nominal 100-kc crystal ringing frequency. The amplifier mounted inside the payload shell on the can containing the logic circuits.

The logic circuits, both sensitive and insensitive in each channel, were identical. Each logic circuit produced an output which changed back and forth between two levels when an input voltage of arbitrary shape was applied and when the peak input level was greater than the trigger threshold. The change of output voltage from one level to the other was exponential, governed by the time constant (1 second) in the integrator.

A schematic of the logic circuit is shown in Figure 2-24. Each circuit was constructed on an epoxy board 3 by 2-1/2 inches. The two circuits were mounted side by side in a brass shield can, and this can was attached to the inside of the payload shell. The purpose of the shield was to minimize r-f interference.

The operation of the electronic circuits (amplifier and logic circuits) was unaffected by temperature from 0^{o} to 80^{o}C; i.e., amplifier gain, trigger threshold, and output voltage were independent of temperature over this range.

c. Calibration

The micrometeorite system is momentum sensitive, i.e., the output of the amplifier is proportional to the mass times the velocity of the impacting particle. Calibration was accomplished by dropping small glass spheres onto the diaphragm from a height of about an inch. The mass of the glass sphere was determined by measuring, under a microscope, the sphere radius, calculating the volume and multiplying by the density. Particles of 5 to 500 micrograms were used.

The velocity of the spheres at impact was determined by allowing them to bounce on the diaphragm. Until the impact momentum was smaller than detectable, each bounce would produce a change of state of the flip-flop.

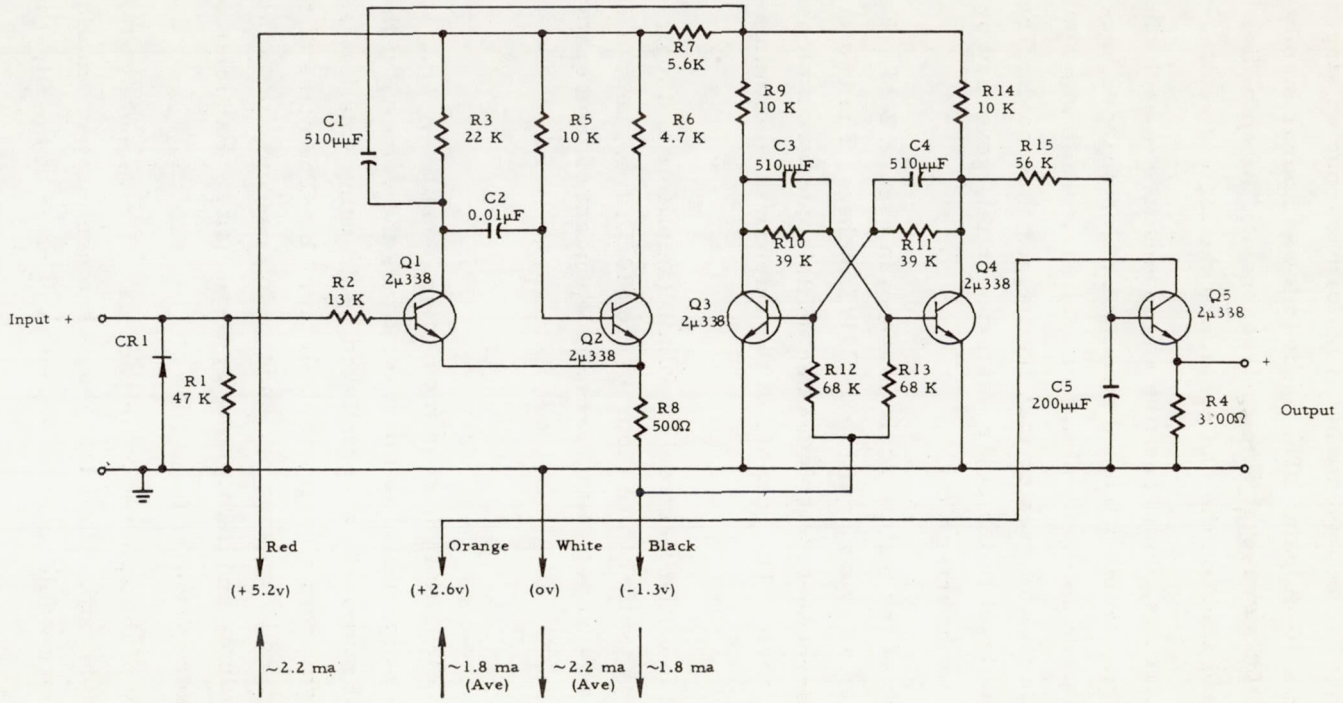

2. For assembly see drawing 60000903.
1. All resistors are Y_2W 10%

NOTE: (Unless otherwise specified.)

Figure 2-24. Micrometeorite Logic Circuit.

By measuring the period (T) from the previous change of state, the velocity (V) at an impact could be calculated:

$$V = \frac{g\,T}{2}$$

The impact momentum of the bounce associated with the last recorded change of state was somewhat greater than the system threshold. The next bounce, showing no change of state of the flip-flop, was below system threshold. By dropping many spheres, the large statistical sample provided a fair estimate of the momentum threshold.

The procedure outlined above was employed independently by STL and AFCRC personnel with close agreement of results. In addition, AFCRC dropped smaller and smaller beads from an accurately determined height to locate the system threshold; again, these results agreed with the other calibrations. The final momentum threshold were found to be (in gram-cm/sec):

Momentum Threshold

Over MIC	Average over diaphragm	Channel
6×10^{-5}	15×10^{-5}	Sensitive
250×10^{-5}	530×10^{-5}	Insensitive

Early in the Able-1 program, the validity of using relatively heavy particles at low velocities to calibrate the system was questioned. Both AFCRC and STL have investigated this problem, however, and have independently validated the calibration method for velocities up to a km/sec.

A further check on the system was to determine the relative sensitivity of various portions of the diaphragm. The sensitivity directly over the microphone was about three to four times the average sensitivity over the entire diaphragm area.

d. Results

A surprising result of the Pioneer I flight was the paucity of impacts from interplanetary matter. The actual recorded strikes are shown in Figure 2-25 for the low momentum channel (No. 5) and in Figure 2-26 the single count observed on the high level subcarrier (No. 4). Since the area of the diaphragm was 0.0381 square meter and the number of low momentum strikes was 11 for the first nine hours, the mean flux over this time becomes 9×10^{-3} m^{-2} sec^{-1} in the momentum range of 3×10^{-4} to 10^{-2} gram-cm/sec. The number of counts is sufficiently small so that detailed statistics are somewhat irrelevant. A general trend can be conjectured from the data, however, that the flux seems to decrease away from the earth. The other pertinent comment is that only one count was observed in the momentum class above 10^{-2} gram-cm/sec, so that only a very general statement can be made to the effect that the flux does appear to grow with decrease in momentum.

On Pioneer II the results appear considerably different. Here the sampling is quite different in that the time interval was very short and the flux high. On the Malabar record at approximately 650 nautical miles altitude a strike occurred followed by three others within the following one minute of flight. The next receiver locked signal occurred at an altitude of 775 nautical miles. For the next one minute, 16 strikes were made indicating a burst of flux density 6.1 m^{-2} sec^{-1}. In the ensuing short intervals of Manchester recording, no strikes were recorded. In the event that the count rate on Pioneer II is borne out by future experiments, the existence of an electromagnetic and/or a geogravitational containment of meteoritic debris about the earth is suggested.

During the flight of Pioneer I, the vehicle was exposed to the Epsilon Arietid shower radiant. This would imply that the effective area of the sensitive diaphragm would have to be considered to determine the effective area for this direction. Such a calculation would be meaningful only for meteors above about 10^{th} magnitude. Since this size particle would register only on channel 4 (high momentum) and only one count was observed, questions of flux anisotropy are meaningless.

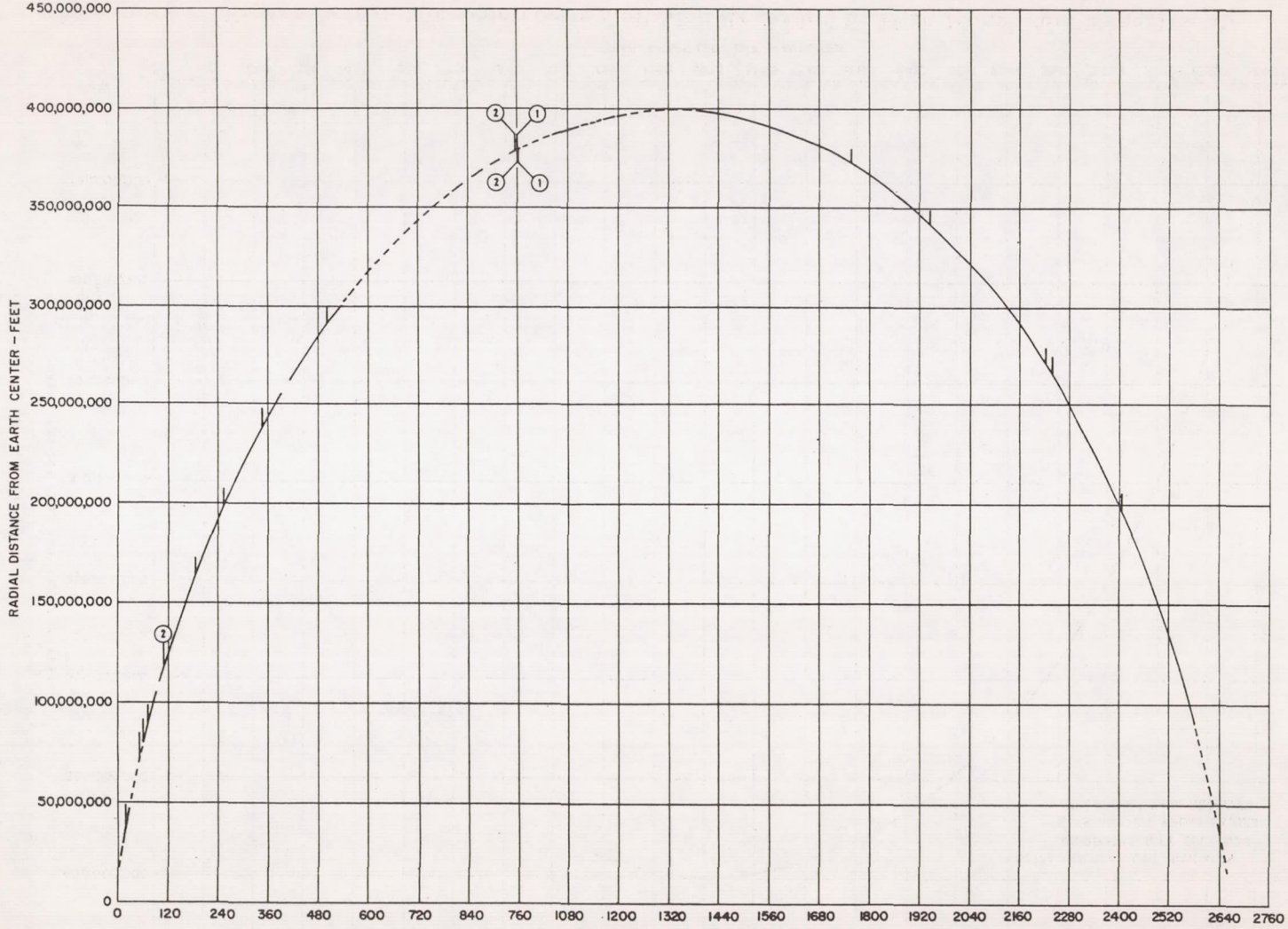

Figure 2-25. Micrometeorite Collisions Recorded by Low Momentum Experiment.

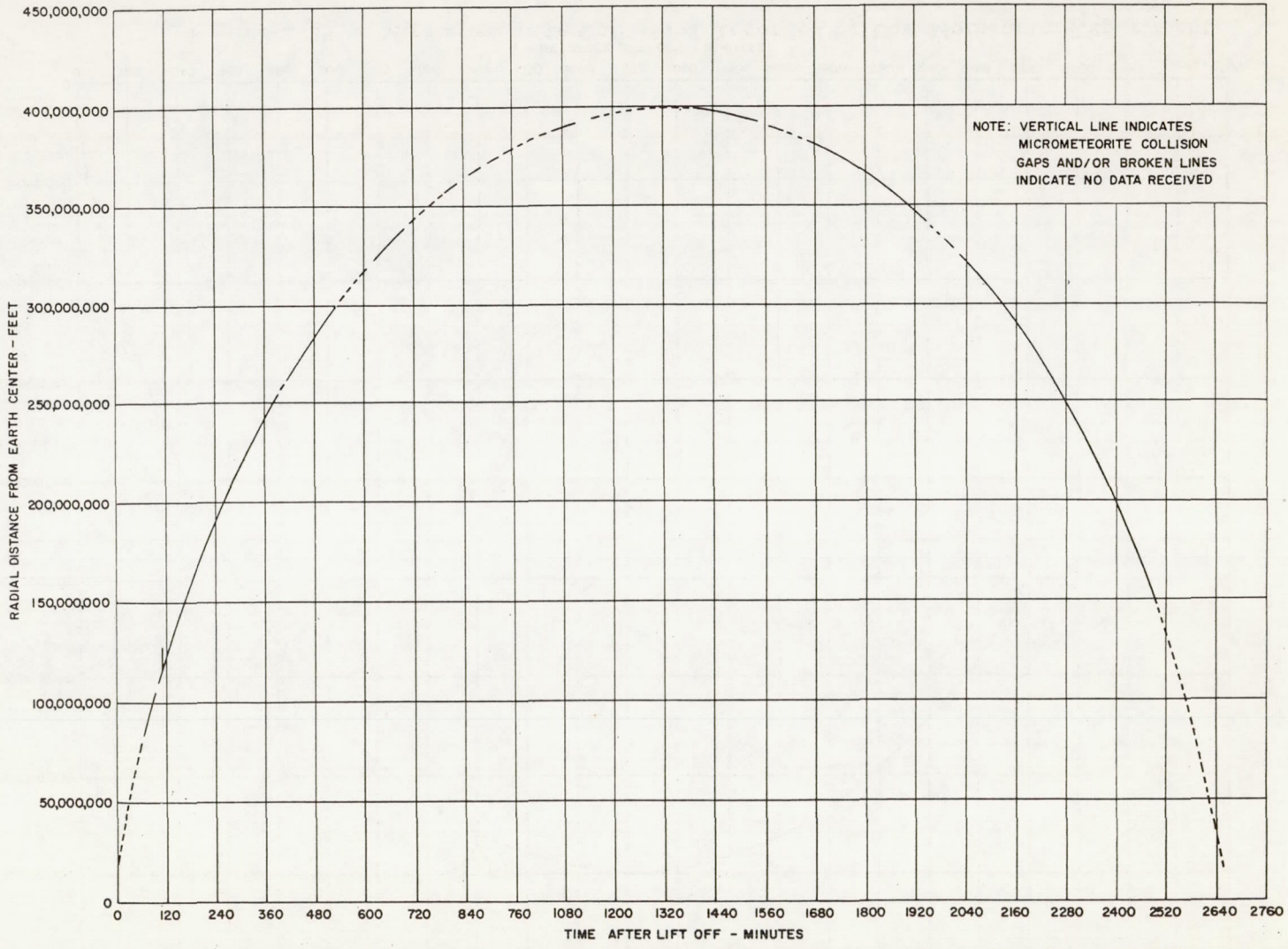

Figure 2-26. Micrometeorite Collision Recorded by High Momentum Experiment.

Some estimate of the density of matter can be made for interplanetary space by considering the mean velocity as 4×10^4 m/sec. Then the particle density in the low momentum range becomes of the order of $10^{-7}/m^3$.

2.2.4 Magnetometer

a. Introduction

Theoretical considerations have led to considerable interest in the outer fringes of the earth's magnetic field and to the type of boundary, if any, that exists between the geomagnetic field and the field attributed to the solar corona.

On the basis of current theory it is hypothesized that the geomagnetic field terminates at perhaps 5 to 10 earth radii depending upon the state of interplanetary magnetic activity. The termination is expected to be relatively abrupt (on the astronomical scale), and such an interface might produce hydromagnetic turbulence resulting in the generation of hydromagnetic waves propagating into the atmosphere.

The magnitude of the interplanetary field has been variously estimated to lie between 1 and 1000 micro-oersteds* depending on the state of solar activity. Evidence exists that the field strength fluctuates and that the orientation is nonconstant. It is important to obtain data on both the magitude and the orientation of the field.

The existence of a lunar magnetic field is undetermined. Considerations of mass density imply that a field such as the earth possesses would be unlikely. Based upon the dipole moment per unit volume of the earth, one might expect a surface value for a lunar field not to exceed the order of a few millioersted. If dynamomechanisms are in effect on the moon any estimate of the external field strength would be assumptive. Because the existence of a field is uncertain, it is best to make a survey experiment with the maximum sensitivity limited by the interplanetary field which might occlude the measurement of a selenocentric magnetic field.

The design of a magnetometer experiment is based upon the ultimate sensitivity desired, the dynamic range, and the transient response. The optimizations of these characteristics are not mutually compatible. It was decided that the extended range should be the prime consideration,

---

* Although the gauss is commonly used as the unit in this context, the proper unit for magnetic intensity, H, is the oersted. In the emu system 1 oersted = 1 gauss numerically.

together with a minimum sensitivity of at least 6 micro-oersted. This would reduce the chance that the field would lie outside the range of the equipment during the most significant part of the flight. The transient response is important in the study of the fluctuation, in magnitude and direction of the field, but for the initial survey it had to be partially sacrificed in order to obtain the maximum dynamic range.

b. System Description

The magnetometer consists of a search coil and a nonlinear amplifier which provides an appropriate signal to the telemetry channel.

The search coil consists of about 30,000 turns of number 40 copper wire wound on a coil form through which a μ-metal core is passed. The coil is shown in Figure 2-27, together with the amplifier and subcarrier oscillator (SCO). In this figure, the μ-metal coil is shown in its original straight form. Upon installation in the vehicle, the coil is placed with the core lying along the circumference of the inner surface of the payload package in a plane perpendicular to the figure axis, and the core is bent to conform to the shape of the mounting surface. As the coil rotates with the vehicle, it experiences a change in flux through the coil as the aspect of the coil with respect to magnetic field changes during the rotation. The geometry for the apparatus is indicated in Figure 2-28 where X Y Z is an inertial reference centered in the vehicle and X' Y' Z' is a rotating frame fixed in the vehicle. In a uniform and time-invariant magnetic field, the change in flux produces a sinusoidal voltage whose amplitude is proportional to the magnitude of the normal component of the magnetic field, that is, the magnitude of the component of the magnetic field in the plane perpendicular to the vehicle spin axis. In a time-varying magnetic field, the pure sinusoidal voltage has superimposed on it a voltage produced by the changes in flux arising from the time variations in the field.

The magnitude of the magnetic field at the surface of the earth is 0.25 to 0.7 oersted, depending on the location of the point of observation. The magnitude of the field decreases roughly as the one-third power of the distance to the vehicle measured in units of the earth's radius. The field may therefore decrease to values as low as a micro-oersted over the region

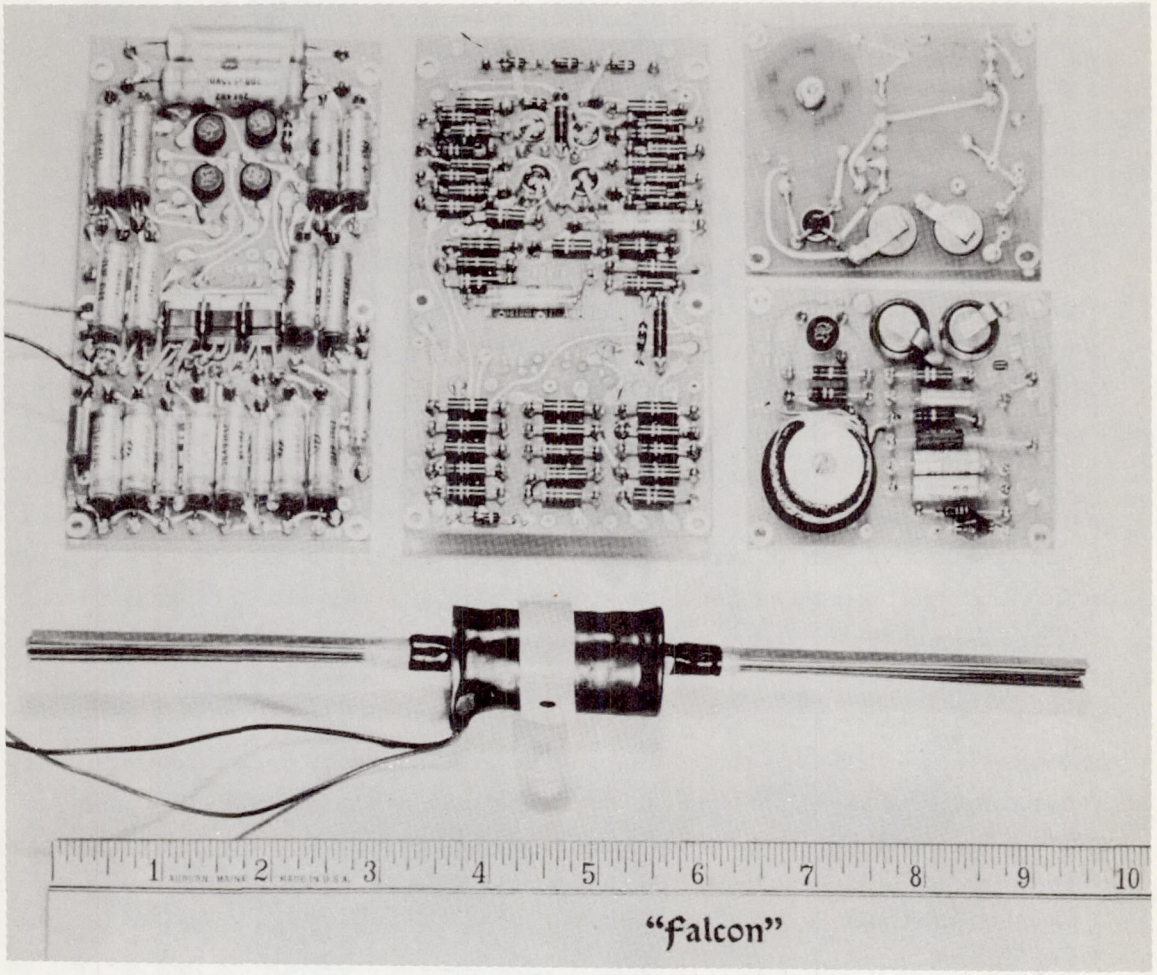

Figure 2-27. Magnetometer. Shown above is a front and back view of the magnetometer amplifier and the subcarrier oscillator. A search coil is also shown.

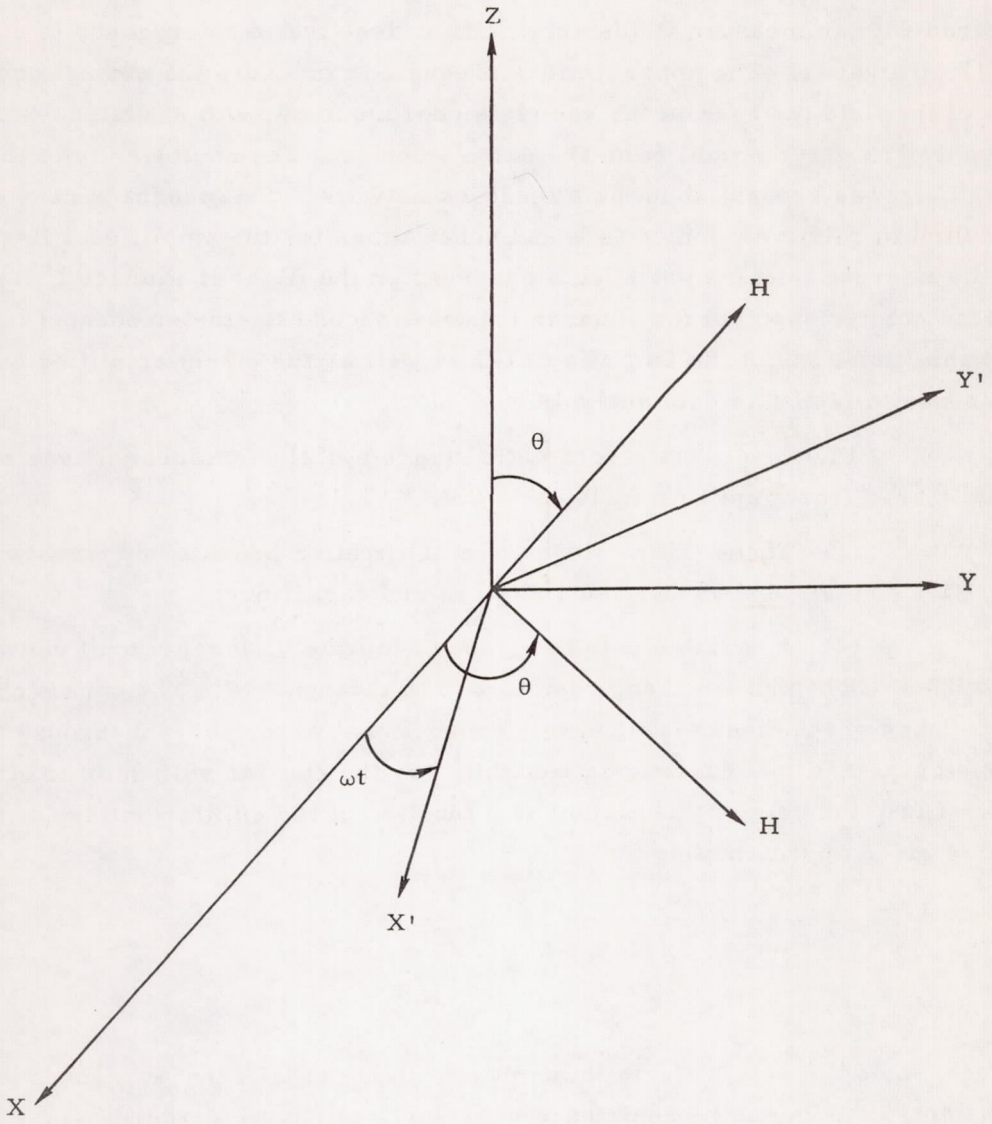

Figure 2-28. The magnetometer frame $X'Y'Z$ referred to an inertial set XYZ. The spin axis of the vehicle is colinear with Z and the search coil is mounted in the plane $X'Y'$ thus measuring $H_{\perp}$.

interest. Since such an enormous dynamic range is clearly impractical for a linear amplifier, the magnetometer amplifier was made nonlinear. The resulting nonlinear amplifier covered a range of about three decades. This instrument can measure fields varying from less than 6 microgauss to a value of 12 milligauss. The upper limit is adequate to measure the normal component of the field (as seen in the vehicle's coordinate system) at distances of roughly 1.5 earth's radii from the earth's center. The nonlinearity of the amplifier was brought about by a feedback network. This feedback network resulted in relatively long attack and decay times for the amplifier. Because of the interesting transient effects observed on the flight of Pioneer I, the magnetometer supplied for Pioneer II used a second telemeter channel to transmit the variations of the amplifier AGC as well as the direct amplifier output. This was to facilitate data analysis.

Figure 2-29 is a schematic diagram of the nonlinear magnetometer amplifier. This amplifier contains:

(1) Three initial stages of amplification provided by transistors Q1, Q2, and Q3, and associated resistors and capacitors;

(2) A variable gain (or, more accurately, loss) circuit consisting of diodes CR1 and CR2 and resistors R15 through R19. The dynamic impedance of the diodes is inversely proportional to the current through the resistors, and this current is controlled by the emitter voltage of transistor Q7. Thus, the gain of this circuit is a function of the emitter voltage of Q7, and is given approximately by

$$A \approx \frac{K_1}{C + I_R^2}$$

where A is the gain, I_R is the emitter voltage of Q7, and K and C are constants determined by resistance values, diode characteristics, and source and load impedances. For small values of I_R the gain is constant, while for large values of I_R it is inversely proportional to the square of I_R.

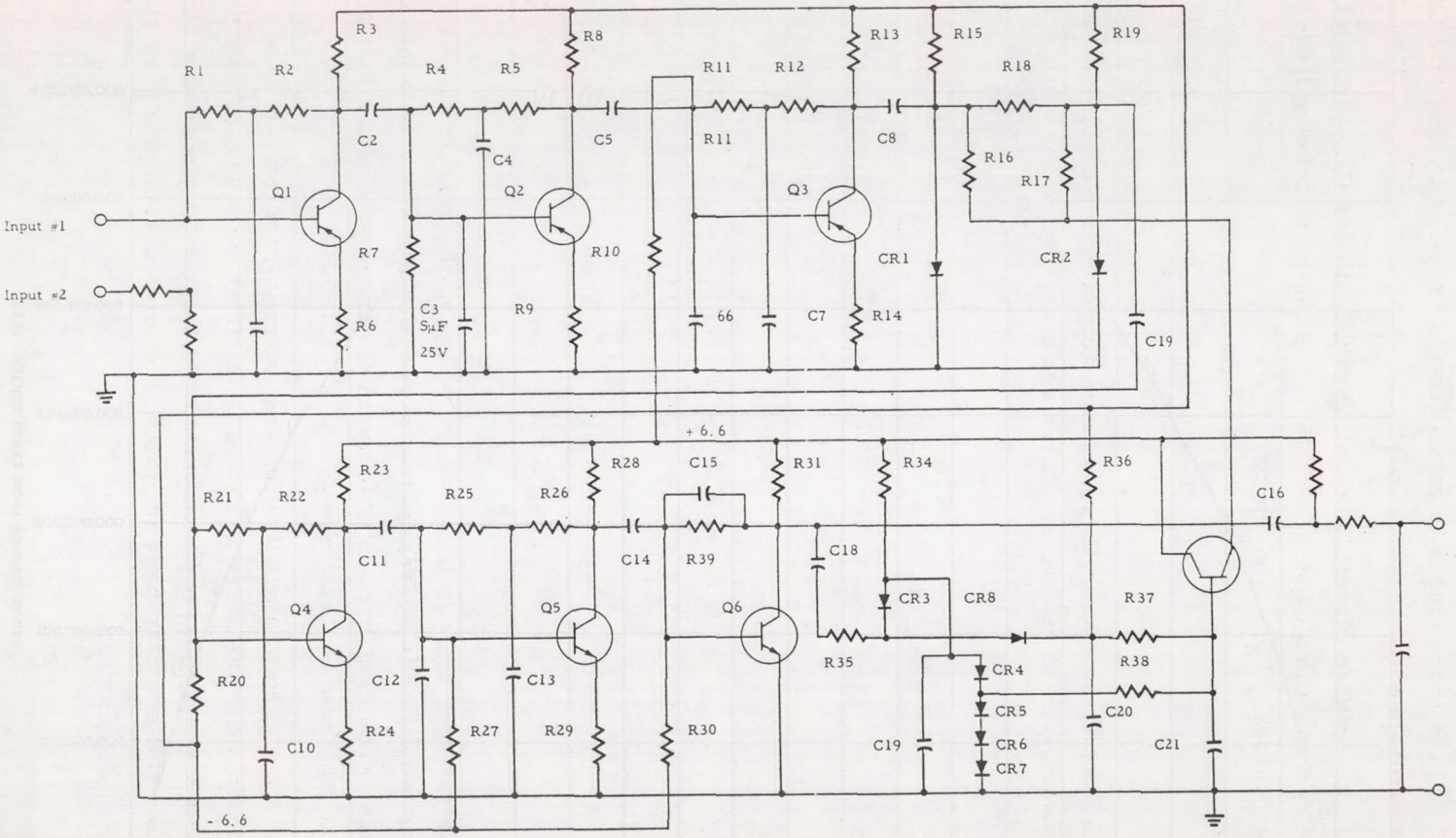

Figure 2-29. Nonlinear Magnetometer Amplifier

(3) Three more stages of amplification provided by Q4, Q5, Q6, and associated components;

(4) A rectifier circuit, consisting of Q7, diodes CR3 through CR8, and associated resistors and capacitors. If I_o is the rms output voltage, the rectifier output voltage, I_R, is given by

$$I_R = K_2 I_o$$

where K_2 is a circuit constant. If I_1 is rms amplifier input voltage, and K_3 is the combined gain of the two amplifier sections, the output voltage is given by

$$I_o = \frac{K_1 K_3}{C + I_R^2} I_1$$

which gives

$$C I_o + K_2 I_o^3 = K_1 K_3 I_1$$

and for $K_2 I_o^3 >> C I_o$,

$$I_o \approx K I_1^{1/3}$$

where K is determined by K_1, K_2, and K_3. Thus, the rms output voltage of the nonlinear amplifier is approximately proportional to the cube root of the input voltage. The measured input-output characteristics of the unit used in the second attempted moon shot are given in Table 2-4.

All six stages of amplification are essentially identical. Low-noise PNP germanium transistors are used in the first three stages, while NPN silicon transistors are used elsewhere because of their superior temperature characteristics. Collector-to-base feedback is used to obtain good bias stability.

Table 2-4. Amplifier Calibration.

Output Volume (Peak-to-Peak)
Millivolts

Temperature	50°F	75°F	100°F
Amplifier	A	A	A
Input (p-p)			
4 microvolts	200	200	200
8	--	400	--
16	550	540	520
32	--	600	--
64	650	680	650
128	--	780	--
256	880	900	900
512	1020	1040	1040
1 millivolt	--	1200	--
2	1450	1500	1500
4	--	1850	--
8	2500	2400	2450
16	--	3000	--
32	2800	3000	3000
64	--	--	--

This feedback is removed at signal frequencies by capacitors in the feedback network, which together with the coupling capacitors between stages, determine the low-frequency cutoff. Bypass capacitors between stages determine the high-frequency cutoff. C15 also limits the high-frequency response by providing more feedback at high frequencies. Resistors R32 and R33 influence the bias and sensitivity of the subcarrier oscillator load. Diodes CR3 and CR8 form a peak-to-peak reading device, or rectifier. Q7 is an emitter follower which avoids loading of the rectifier. Capacitors C19 and C20 are part of a low-pass filter, which prevents the feedback from causing oscillations. Diodes CR4, CR5, CR6, and CR7, with CR19 form a bias voltage supply for the rectifier circuit. Diodes are used in the supply to compensate for changes with temperature of CR1, CR2, CR3, CR8 and Q7.

Because of the long time constant associated with the capacitors C20 and C21, the response of the amplifier to changes of input signal level is quite sluggish. If the input signal level is suddenly increased from zero to a value sufficient to saturate the amplifier, the gain of the amplifier will require about 15 seconds to fall to its final value. If the input signal level is suddenly reduced from saturation value to zero, the amplifier gain will require about 75 seconds to increase to its final value. The time constant is thus a function of the direction of signal change. It is also a function of both initial and final signal levels.

Table 2-5. Amplifier Specifications.

Noise:	<4 microvolts = <6 microgauss
Bandwidth:	1.5 cps to 2.5 cps (3db)
Temperature:	tested between 50°F and 100°F
Gain:	50,000 feedback
Useful Range:	<3 decades - <6 microgauss to 12 milligauss
Input-output Characteristics:	See Table 2-4
Time Constant:	1. increasing signal - 15 seconds 2. decreasing signal - 75 seconds

c. Calibration Procedure

Laboratory calibration of the magnetometer consisted of two steps. The first established the relationship between the open circuit output voltage of the magnetometer coil and the ambient magnetic field. Step two consisted of applying a series of 2 cps notes of different peak-to-peak voltages to a simulated magnetometer coil and then observing the frequency swing of a subcarrier oscillator. Knowing the input voltage relation to SCO frequency swing and to the magnetic field, the relationship between the transmitted VCO frequency swing and magnetic field was determined.

The experimental setup for the "spin" calibration of the magnetometer coil is sketched below.

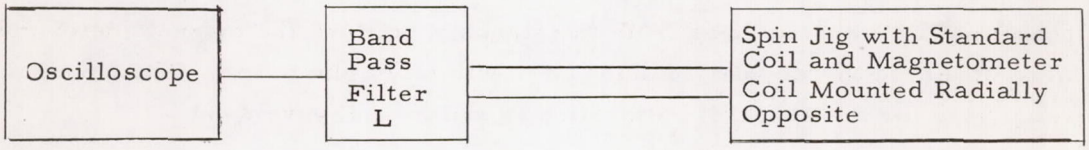

The magnetometer coil constant $K_c \equiv E/B$, where E is the open circuit output voltage of the magnetometer coil and B is the ambient magnetic field. In the actual calibration B is determined by observing the peak-to-peak open circuit voltage of a standard coil whose effective area and number of turns is known. The measured emf, E_1, induced in the standard coil due to the 2 cps rotation in field B is given by

$$LE_1 = 4\pi BAN \times 10^{-8}$$

where L is insertion loss of the filter defined as the ratio of input to output voltage, B is the field in gauss, A is the effective area of the standard coil in cm^2 and N is the number of turns (ω is included in the factor 4). Thus

$$K_c = \frac{E}{B} = \frac{E_2}{E_1} \times 4\pi AN \times 10^{-8} \frac{\text{volts}}{\text{gauss}}$$

as a function of the ratio of the open circuit voltages E_1 and E_2. These outputs, E_1 and E_2 are determined in terms of the deflection they display on an oscilloscope. Multiplying this ratio by the constant $8\pi AN\,10^{-8}$ yields the magnetometer coil constant K_c, in volts (peak-to-peak)/gauss.

It is clear that the ambient field does not enter explicitly into the calculation. It is important, however, since the area in which the calibration was done had sources of time-varying field-gradients as well as a slight steady-state gradient. Hence, it was desirable, in an effort to reduce error, that the error-contributing factors be made a small percentage of the quantity to be measured. In order to do this, it was necessary to orient the spin coil rotation plane so that dB/dt was maximized. This was accomplished by aligning the spin jig axis parallel to the magnetic field of the earth by adjusting for a minimum voltage output. The spin axis was then rotated 90 degrees. The peak-to-peak 2 cps voltages from the standard coil and the magnetometer coil were observed thereby determining K_c with minimum error. The physical setup used for the spin coil calibration is shown in Figure 2-30.

The magnetometer system was calibrated "statically" by determining the frequency shift of the SCO for each input voltage to the magnetometer amplifier. The magnetometer amplifier worked into the simulated flight load shown in Figure 2-31. The calibration input voltage to the magnetometer amplifier was varied by changing the value of R_1. Know R_1 and R_2 in kilohms the exact value of e_1, the open circuit voltage to the magnetometer amplifier, is then determined by the following relationship,

$$e_1 = \left(\frac{10}{11}\right) \frac{\left(\frac{R_1(11)}{R_1 + 11}\right)}{\left(\frac{R_1(11)}{R_1 + 11}\right) + R_2}$$

If e_1, the corresponding peak-to-peak frequency swing of the SCO, and the "static" coil constant K_c are known, B versus SCO peak-to-peak frequency swing can be determined since B is given by the following relation

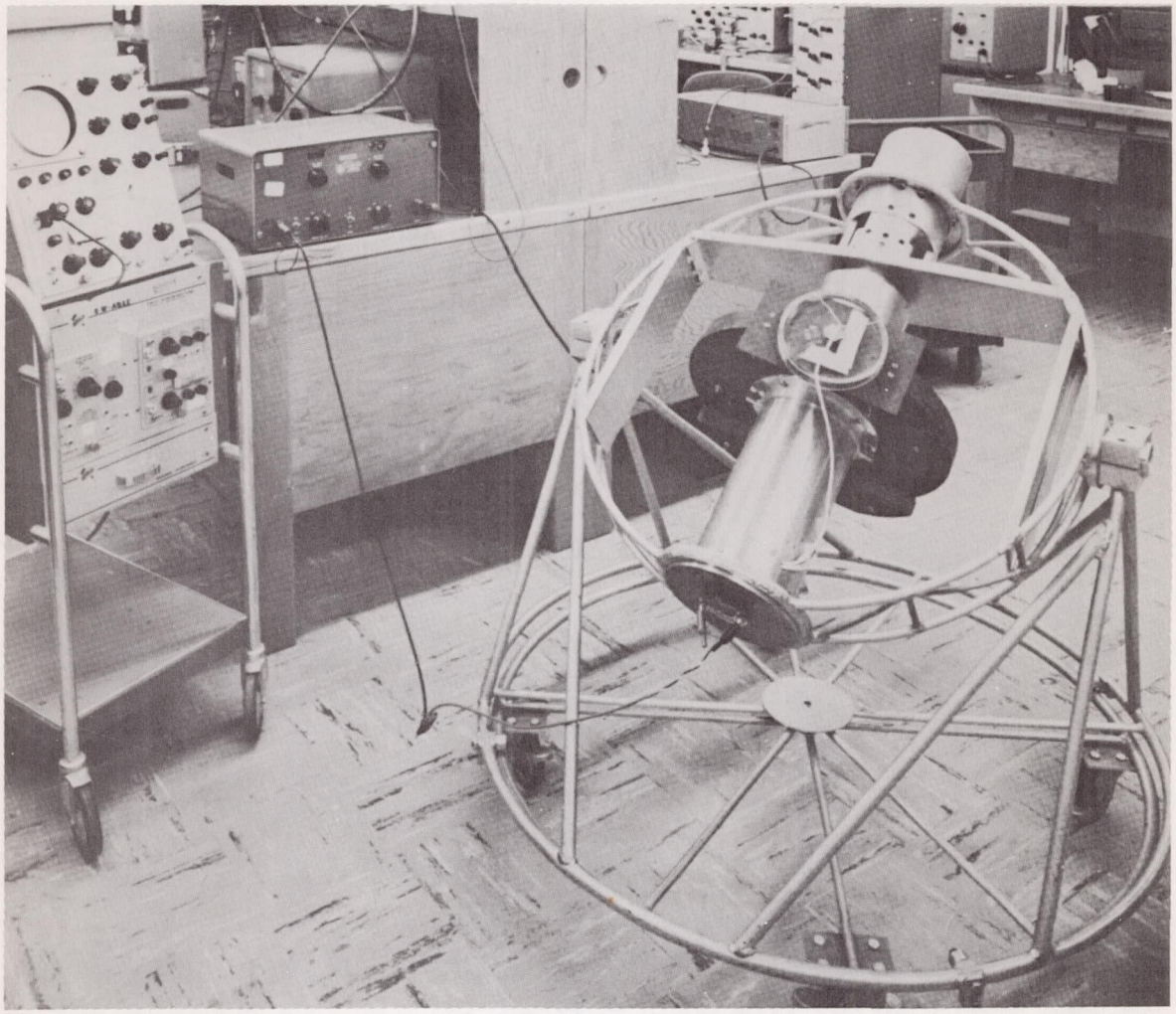

Figure 2-30. Magnetometer Calibration Apparatus

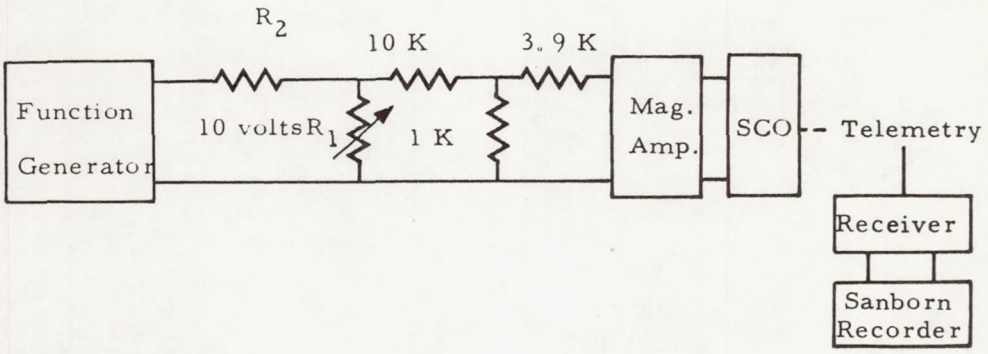

Figure 2-31. "Static" Calibration Setup.

$$B = \left(\frac{1}{K_c}\right) e_1$$

Figures 2-32 and 2-33 graphically show the magnetic field B in gauss versus the peak-to-peak frequency swing and peak-to-peak per cent of full bandwidth devaition. The data from which these graphs were plotted were taken at 70°F; however, they are a good approximation over a range from 35° to 100°F (see Table 2-6). Also, it should be noted that these curves are for a payload rotation frequency of 2 cps. The amplifier frequency response is shown in Figure 2-34.

It was found, during preliminary claibration, that the 60 cycle pickup being fed into the amplifier through the pickup coil was shifting the frequency of the SCO by about 5 cps. To eliminate this calibration error a simulated resistive load, shown in Figure 2-31, was designed for the input to the magnetometer amplifier. The inductive effect of the coil is negligible at 2 cps The SCO frequency shifts were transmitted to the receiver by the flight transmitter to eliminate the errors brought about by the capacitive effects of a shielded cable from the SCO to the discriminator. These procedures enable one to simulate the actual in-flight environment of the magnetometer.

Estimated Calibration Errors

Step	Source	Amount (per cent)
1	Standard coil parameters	2.0
	Waveform distortion	0.36
	Oscilloscope	1.0
2	Oscilloscope reading	1.0
3	Oscilloscope reading	1.0
	Sanborn tape recording	2.0
Total	System calibration error	3.4

$$R^2 = \sum_1^n \gamma_i^2$$

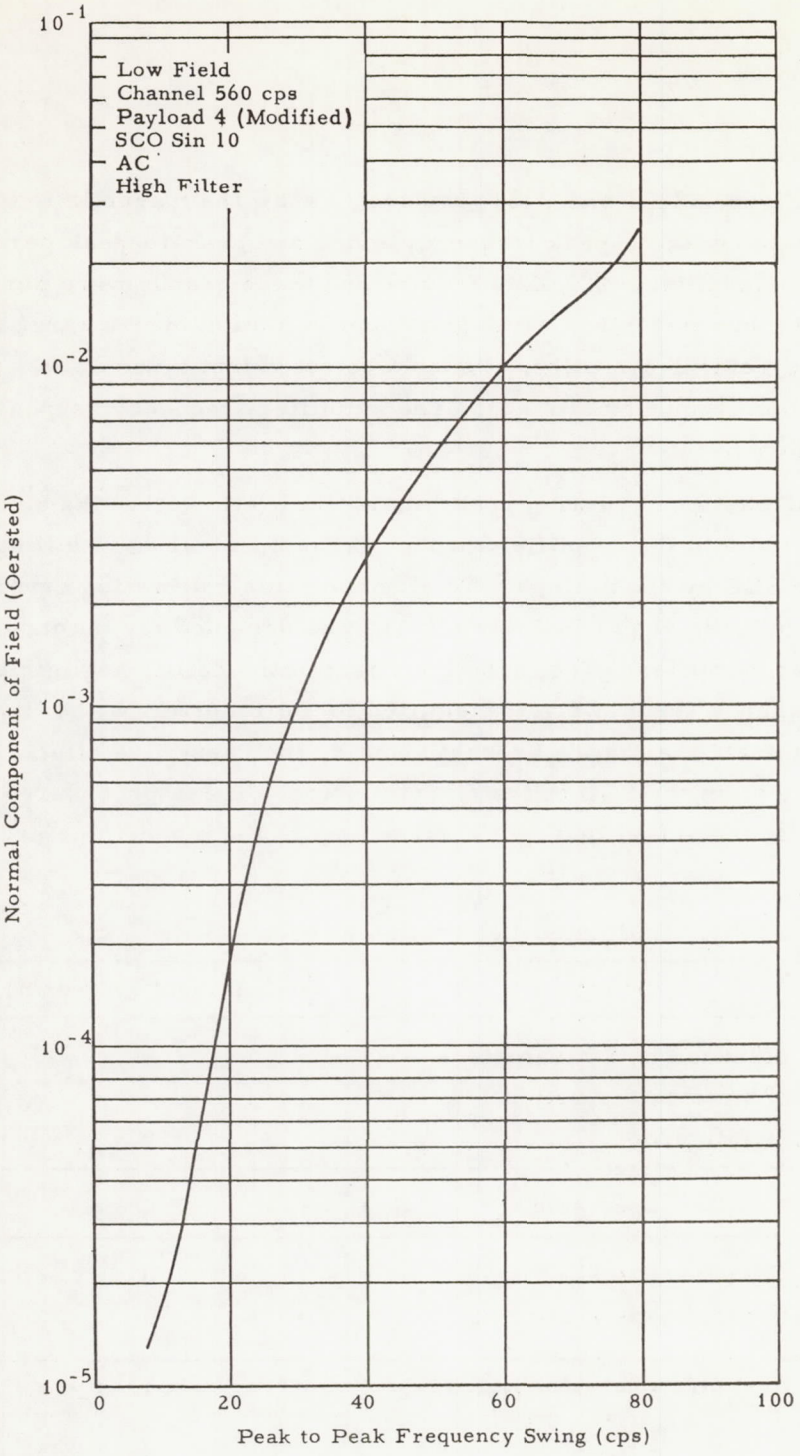

Figure 2-32. Field vs Frequency Swing of Subcarrier.

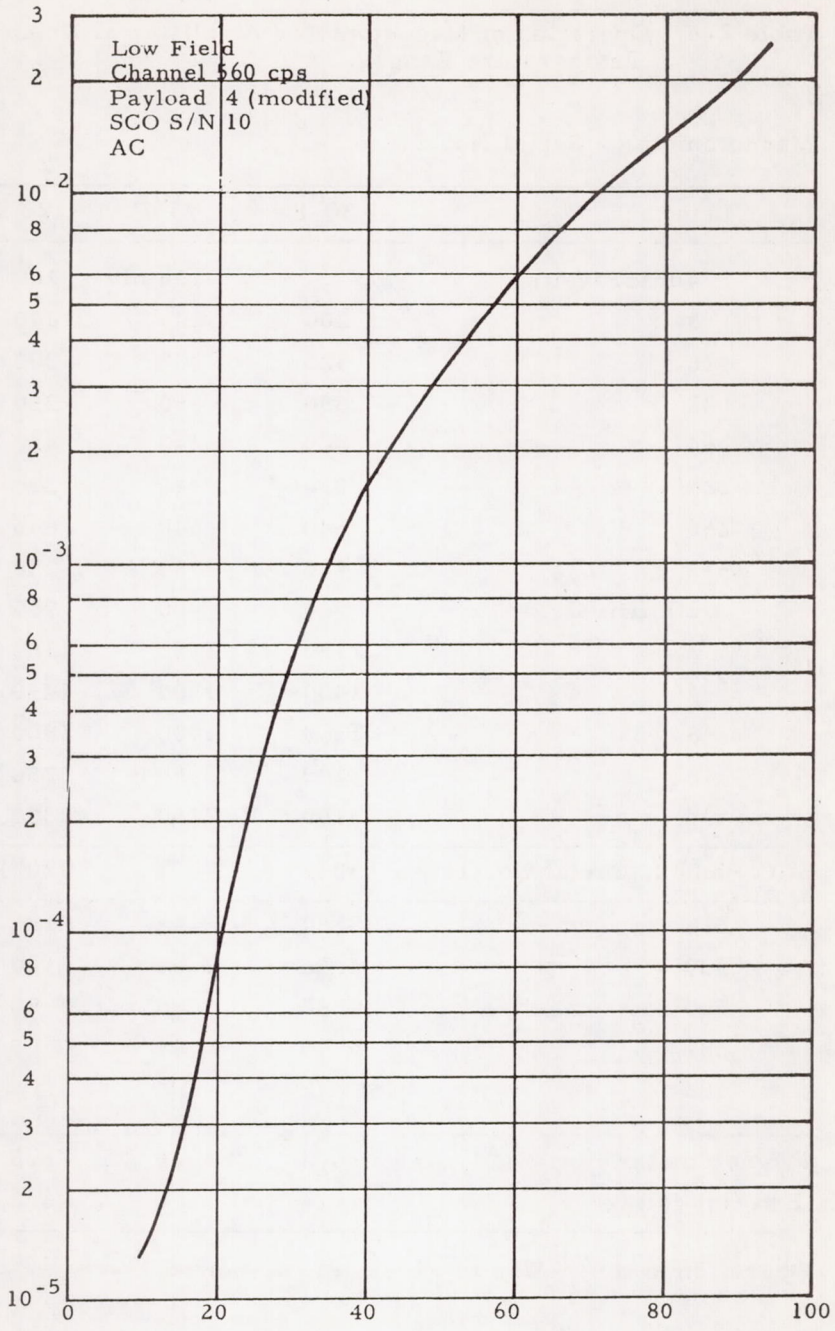

Figure 2-33. Field vs Percent Bandwidth Deviates for Magnetometer Calibration.

Table 2-6. Operation of Magnetometer Amplifier at Extended Temperature Ranges.

Magnetometer - Serial No. 11

Input	30°F	75°F	120°F
4 microvolts		125 mv	100
8	200	200	200
16	325	300	300
32	380	350	350
64	440	440	420
128	550	540	530
256	640	640	640
512	780	780	780
1 millivolt	900	900	900
2	1150	1150	1150
4	1400	1500	1450
8	1800	1900	1800
16	2100	2250	2250
32	2100	2250	2300
SCO Band 2, Serial No. 11	**30°F**	**75°F**	**120°F**
518 cps	3.50	3.45	3.40
539	2.56	2.60	2.60
560	1.80	1.80	1.80
581	0.96	0.95	0.95
602	(601)OV	OV	OV
Magnetometer	+6.4	+6.6	+6.6
Battery Voltage	-6.4	-6.6	-6.6

Operation at 30°. Was in excess of two hours.

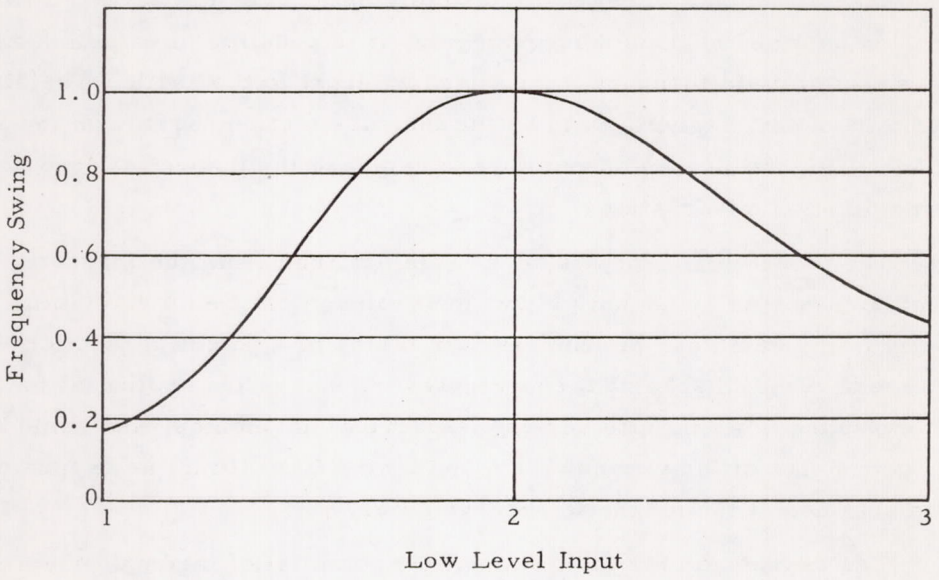

Figure 2-34. Amplifier Frequency Response.

d. Results

The data obtained from the magnetometer are exceedingly complex and are being statistically analyzed. Both quiescent field and transient effects have been observed. A computer program described below has been utilized to determine deviations from a theoretical model. An adjustment of the transmitter modulation deviation in the field resulted in a change in calibration increasing the estimated error of the quiescent field values obtained.

Observations of the earth's magnetic field are commonly made at a large number of magnetic observatories distributed over the earth. From the information obtained at these observatories, it is possible to establish a model for the magnetic field throughout the space external to the earth. The direct observations of the magnetic field by the instrumentation carried on the Pioneer I and II flights give an opportunity to compare the theoretical predictions with experimental observations.

The theoretical analysis of the data obtained from the magnetic observatories begins by assuming that the geomagnetic field originating internally in the earth can be expressed in terms of a potential function V, which is expressed in spherical coordinates r, θ, λ. This potential function is then expanded in an infinite series of spherical harmonics, and some number of the coefficients of the expansion are determined by fitting the expansion to the data obtained at the magnetic observatories.*

The expression for the geomagnetic potential of internal origin is given by

$$V = a \sum_{n=1}^{\infty} \sum_{m=o}^{m=n} \left(\frac{a}{r}\right)^{n+1} \left(g_n^m \cos m\lambda + h_n^m \sin m\lambda\right) P_n^m(\theta)$$

where a is the radius of the earth, r is the radial distance from the center of the earth, θ is the colatitude, λ is the longitude, $P_n^m(\theta)$ is a spherical

*Chapman, S. and J. Bartels, Geomagnetism, Vol. 2, Oxford, Clarendon Press, 1940

harmonic function of Schmidt of degree n and order m, and g_n^m and h_n^m, called the Gauss coefficients, are the coefficients to be determined in the process of fitting the expansion to the observations. For comparison with the Pioneer data, only the first eight Gauss coefficients were used. This corresponds to taking the two terms for V involving n = 1 and n = 2. The values of the Gauss coefficients, given by Vestine and Lange* for the 1945 epoch, are presented in Table 2-7.

Table 2-7. Gauss Coefficients for the 1945 Epoch.

Coefficient	g_1^0	g_1^1	h_1^1	g_2^0	g_2^1	h_2^1	g_2^2	h_2^2
Value	-3057	-211	+581	-127	+296	-166	+164	+54

The geomagnetic field B may be found by taking the negative gradient of V. The result gives the earth's main field of internal origin at any desired point in space external to the earth. The inclusion of higher degree terms in the expansion of V would not contribute significantly to the present work, since such contributions (which are small, at best) decrease rapidly with altitude, and are insignificant in the present experimental conditions.

To compare the theoretical experimental values of the magnetic field, it is necessary to compute the predicted magnitude of the geomagnetic field component lying in the plane perpendicular to the vehicle spin axis. The needed computation was carried out as part of the calculation of nominal trajectories. The program contains a routine to determine the three components of the gradient of the geomagnetic potential corresponding to the instantaneous vehicle position. Since this operation gives the three components of the magnetic field vector B, and since the directions of the spin vector are also contained in

* Vestine, E. H. and I. Lange, as quoted by E. H. Vestine, J. Geophys. Res., Vol. 58, No. 2, pp. 127-145, June 1953.

the trajectory program, it is a simple matter to compute the quantity $B_{\perp}$, which is the component perpendicular to the vehicle spin axis. Thus, the nominal trajectory print-out for each interval of time includes the value of $B_{\perp}$ predicted from the spherical harmonic expansion.

As seen in Figure 2-35, the general trend of the field follows that, obtained by the theoretical analysis; some scatter does exist at the latter set of values. This is primarily a result of two effects: (1) the large dynamic range of the magnetometer amplifier tends to increase the absolute error, and (2) fluctuations in the data complicate the determination of the mean. (A computer program is being carried on to perform a complete statistical analysis.) An estimate of errors is included in Table 2-8. The deviation of the field at 10 to 12 earth radii appears to have a real basis.

Table 2-8. Error Sources and Their Maximum Deviation.

1.	Sanborn calibration input frequency	±0.2 per cent of band
2.	Sanborn accuracy of reading	±1 per cent of band
3.	Sanborn drift	±3 per cent of band
4.	Telemetry	±5 per cent of band
5.	Vehicle axis orientation	±3 per cent of band
6.	Calibration uncertainty	±5 per cent of band
7.	Laboratory calibration error	±3.4 per cent of band

The errors quoted above are the maximum errors observed from a limited amount of data. Since a statistical distribution is not available to enable one to determine a standard deviation, the error is being overestimated by calling these maximum errors the standard deviation.

The deviation of the value of $H_{\perp}$ from that based upon the model described can be attributed to several different effects, there being an error in the assignment of the position of the geomagnetic pole (for extreme

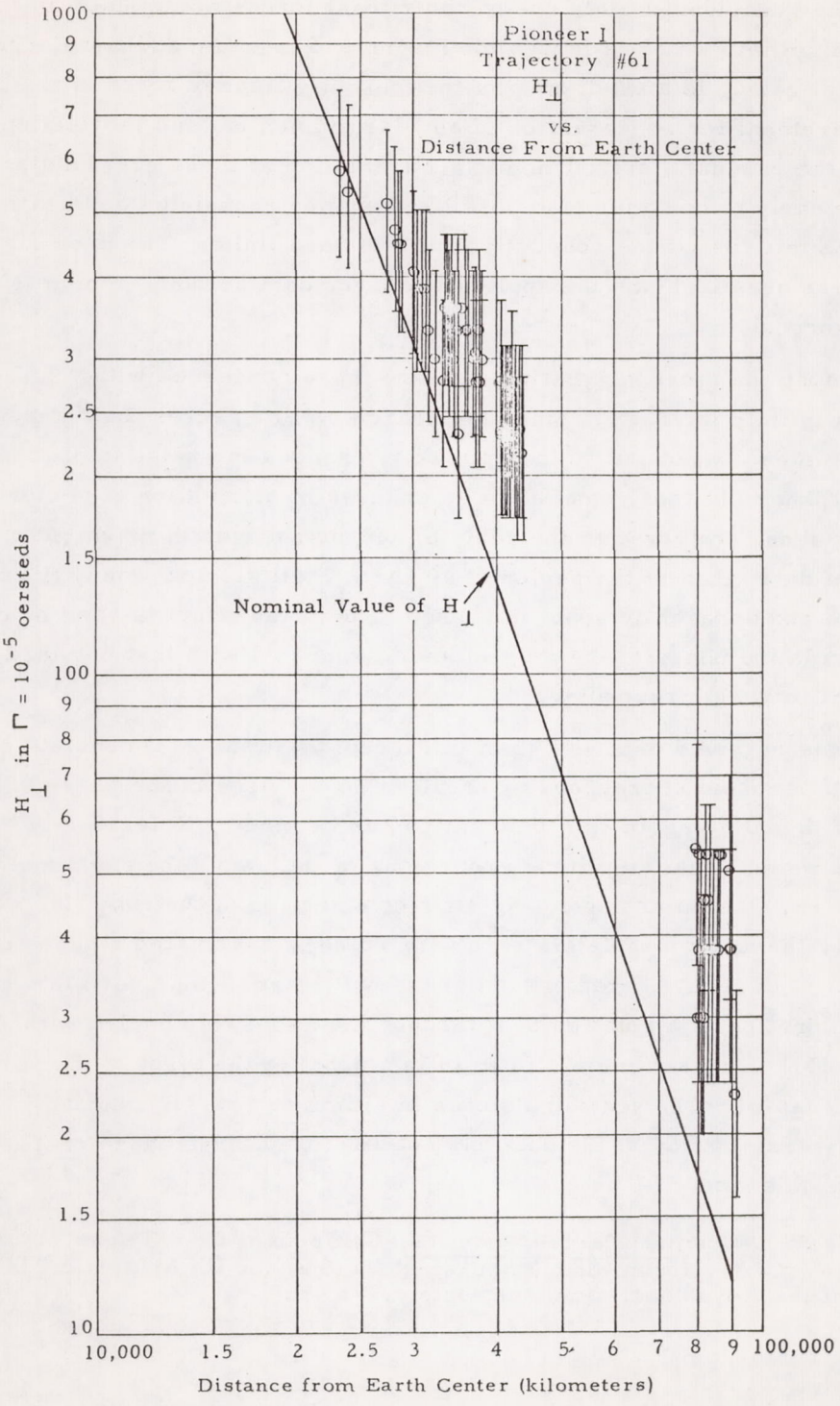

Figure 2-35. $H_\perp$ Component of Magnetic Field in Oersteds vs Distance from Center of Earth (Pioneer I).

altitudes), circulating currents, or an increased energy density per unit volume of the geomagnetic field due to centrifugal forces acting upon an ionized medium into which is frozen the magnetic field. An additional effect, not yet investigated, is a winding up of the magnetic lines of force occasioned by the requirement for conservation of angular momentum and isorotation.* Because of the unusual electrodynamic state existing at these great distances it is not too early to consider also possible dynamomechanisms and heating of the gas by Ohmic loss if the conductivity is assumed finite. The deep significance of these questions and the application of the data at hand to them is being pursued vigorously.

Among the most interesting data are those concerned with fluctuations in field intensity. Since the search coil measures the component of magnetic intensity normal to the spin axis, changes in signal amplitude divorced of phase changes, can be due to changes in orientation of vector β in the polar sense (referred to the vehicle) and/or changes in magnitude. Over two hours of data taken in the region of 10 earth radii disclose many fluctuations in amplitude and apparently some in phase. The latter effect is seen by comparing the relative phase of the magnetometer sinusoid with that obtained from the r-f signal strength recording.

Some received data as shown in Figures 2-36 and 2-37 consists of the spin rate sinusoid corresponding to $H_{\perp}$. Comparison of the phase of $H_{\perp}$ with the r-f signal strength spin modulation can be made. Referring to Figure 2-38 we note that amplitude excursions of $H_{\perp}$ would be explained by changes if H, the polar angle, θ, or a combination of the two. In Figure 2-36, the arrows isolate a zero with which is associated a phase change (rotation of ϕ) of about π radians. Because of the amplitude zero this appears to be a combination of a rotation of H through the apin axis coupled with a change in H. The asymmetric form of the signal to the right of the zero would imply fast ($\tau < 1/2$ second) changes in either or both H and θ. Preliminary examination of the data has not disclosed large phase changes occurring in this time.

---

* Dungey, J.W., Cosmic Electrodynamics, Cambridge Univ. Press, (1958) p. 65. Ferraro, V.C.A., Nonuniform Rotation of the Sun and its Magnetic Field. Notices of the Royal Astronomical Society, 97, 958.

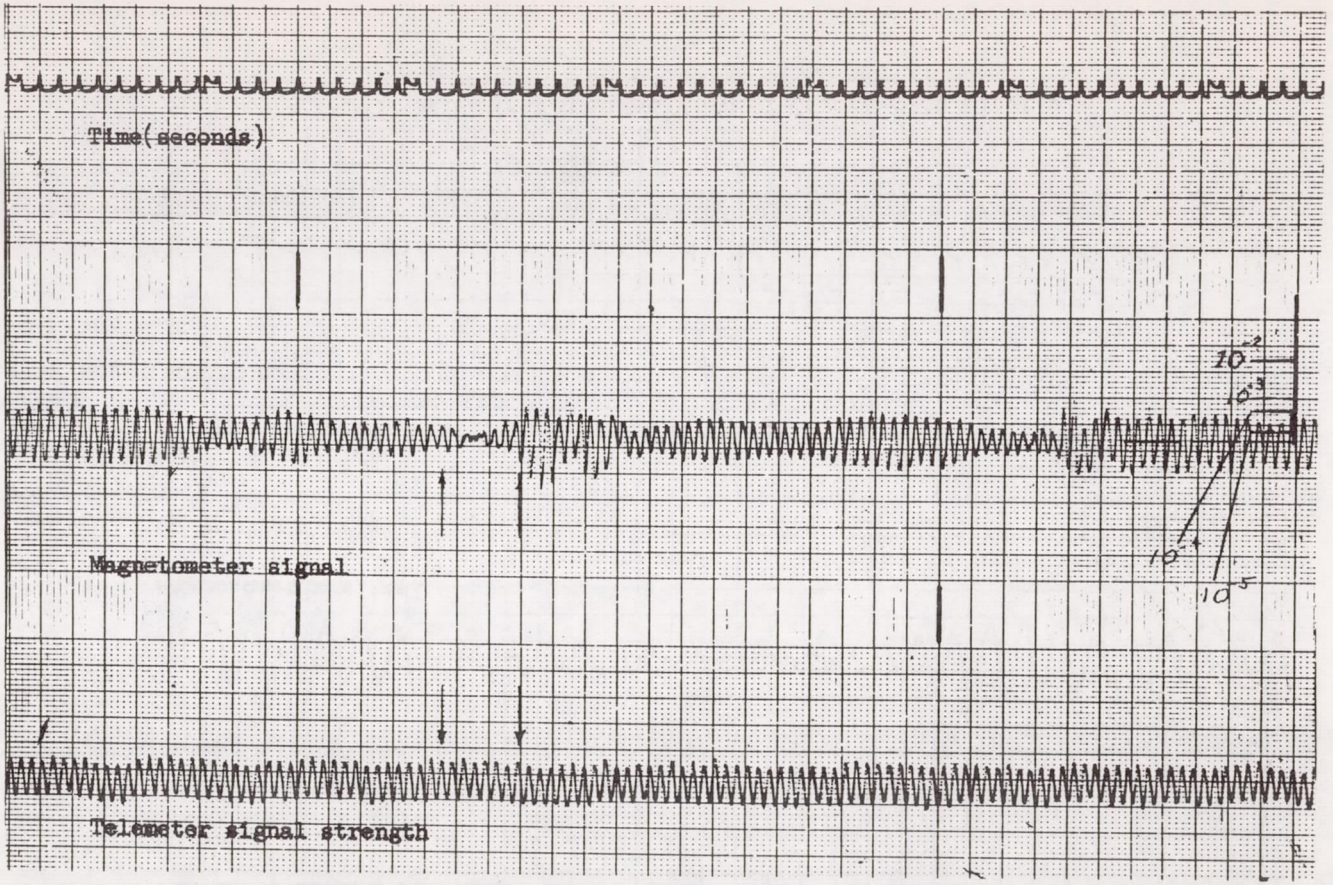

Figure 2-36. A typical magnetometer recording showing a signal zero associated with large phase-change (between arrows), signal oscillations, and rapid changes in signal level. The magnetometer note shows a characteristic spin rate. Time is shown on the upper trace and the telemeter r-f signal strength shown below, so as to serve as a phase reference for the magnetometer. The scale for the magnetic field is indicated at the right-hand side, the units being oersted (emu). This record represents the signal at approximately 47,000 nautical miles from the earth's surface.

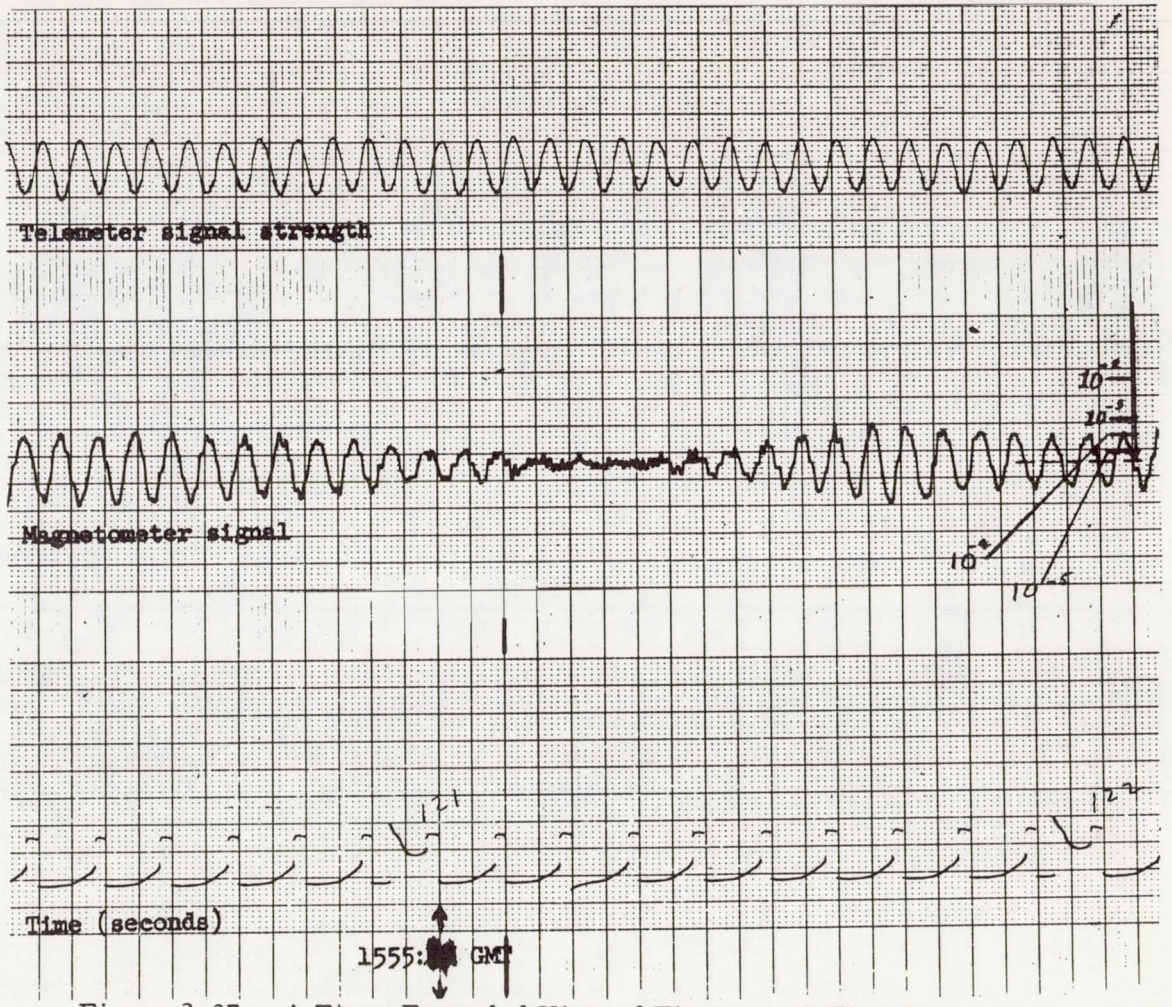

Figure 2-37. A Time-Expanded View of Figure 2-36 Clearly Showing A Phase Change of About π radians.

Figure 2-37 is a more compressed version of some data in the region of 10 to 12 earth radii. The amplitude excursions are accentuated by the amplifier gain characteristics and thus the time fluctuations, if real, are not as extreme as shown. The removal of amplifier effects from the data is planned as a part of the computer program.

The generation of hydromagnetic waves at the geomagnetic field termination due to a magnetic instability associated with a coronal wind had been proposed.*, ** Periodic variations in amplitude are seen in Figure 2-36. The periods are typical for the region centered at about 10 earth radii. The day of the firing (11 October 1958) was extremely quiet magnetically. A proton magnetometer at Palo Alto disclosed surface fluctuations of 10^{-6} gauss rms.# Extrapolation of these values to about 10 earth radii would yield wave amplitudes consistent with those obtained.*** It has been suggested that 10 earth radii represent a suitable geomagnetic-field-coronal-wind interface for a quite day, though the region of instability sampled by Pioneer I may be broader than that suggested by Simpson.## A further flight will be necessary to determine the boundaries of the observed phenomena, if, in fact, an outer boundary exists. The possibility that some of the fluctuations represent the injection of interplanetary gas is being explored. Detailed interpretation of the available data is pending the statistical analysis.

Some of the amplitude discontinuities in the data appear to occur in times limited by amplifier response. These would be attributable to compressional waves. Sudden phase changes associated with the above amplitude discontinuities may enable longitudinal and transverse waves to be sorted out since Alfvén waves would be expected to show an abrupt phase discontinuity.

---

* Biermann, L., Observatory, Vol. 77, p. 109 (1957).

** Hoyle, F., Phys. Rev., Vol. 104, p. 269 (1956).

*** Dessler, A.J., Jour. of Geophysical Research, Vol. 64, p. 507 (1958).

\# We are indebted to A.J. Dessler for this data.

\## Simpson, J.A., private communication.

The following conclusions can now be drawn:

(1) Rotations of the magnetic intensity vector, through both large and small angles, appear. At least some of those associated with large angular excursions have characteristic times of the order of 10 seconds.

(2) Almost periodic oscillations in amplitude occur (sometimes accompanied by rotational changes) having lifetimes of 2 to 5 cycles and periods of the order of 10 seconds. (Figure 2-38).

(3) The steady component of H, at 10 to 12 radii, has a magnitude several times that predicted by an eccentric dipole, thus suggesting the need for investigation of centrifugal instabilities in the terminal field, a possible modification of the present geomagnetic pole at extreme altitudes* or currents.

*R. A. Helliwell has pointed out that very low-frequency Whistler-mode propagation would suggest a slight change in latitude of the geomagnetic pole.

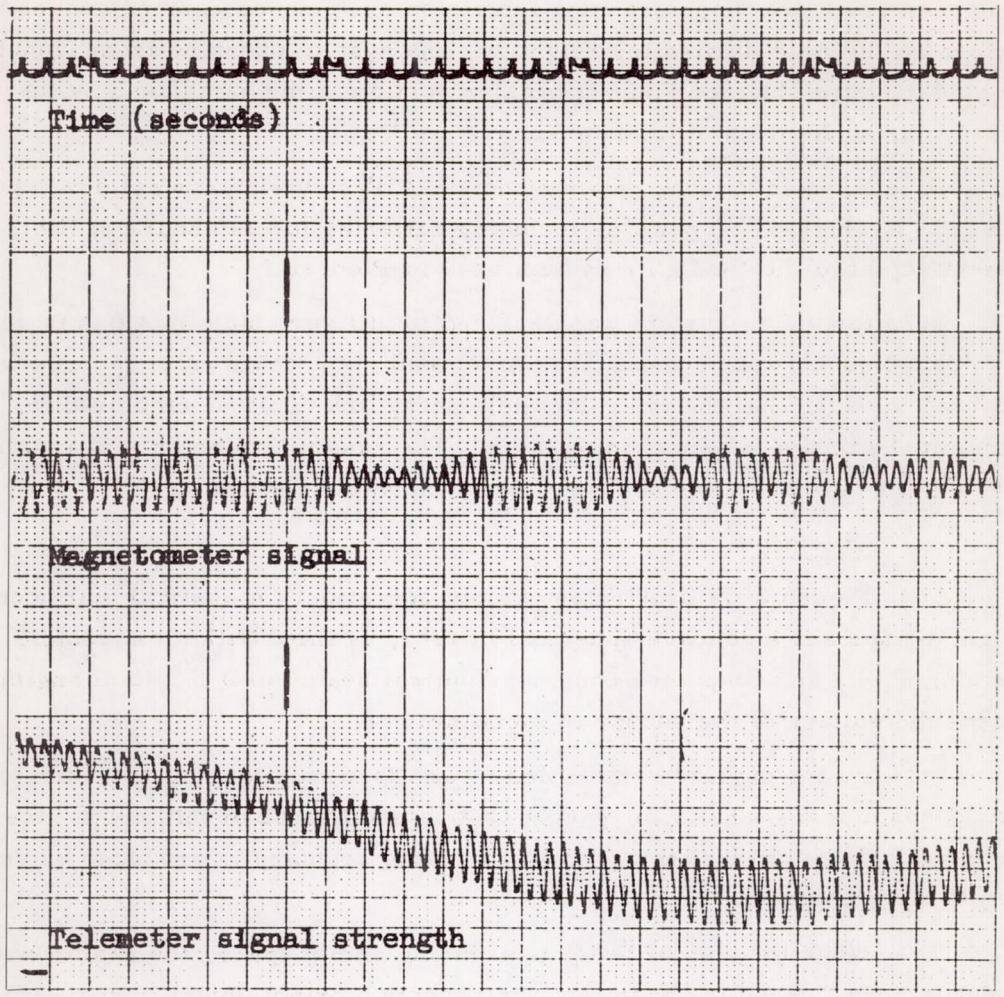

Figure 2-38. Almost Periodic Variations In The Value of $H_{\perp}$.

2.2.5 STL Television System (Pioneer II)

An earth and moon scanning television system was carried aboard the payload on the Able-1 missile, Flight 3. The system operated from launch, but no data were obtained since the major portion of the earth seen by the vehicle during its flight was in darkness.

The Pioneer II lunar payload contained a television system developed by STL. It weighed 3.0 pounds, including batteries for 240 hours of life. This system replaced the NOTS TV system used in Pioneer I.

The television system was designed to utilize vehicle motions to accomplish both line and frame scanning. A nominal output bandwidth of 1 cps was provided in order that the Microlock telemetry link could be employed to transmit the image information to earth. The system had an optical resolution of 0.5°; a single scan line contained 126 resolvable elements.

a. Operation

Figure 2-39 illustrates system operation. An optical unit, containing a light sensor and a concave spherical mirror, is fixed within the vehicle. Light arriving within an acceptance cone, or "optical beam" of 0.5° (total angle) causes the voltage of the sensor to increase.

As the payload rotates and moves forward along its trajectory, the optical beam scans a helix in space. Over a small area of this helix, line scanning is produced by vehicle spin and frame scanning is produced by vehicle motion along the trajectory.

When the optical beam is scanning empty space, the photosensor output is zero. When the beam scan intersects a bright object in space, such as the earth or moon, the photosensor output voltage at any instant is proportional to the average brightness of the spot on the object seen by the optical beam at this instant. As the beam travels across the surface of the planet during each spin revolution, a video waveform is generated. The electrical bandwidth required to transmit this video signal is about 1 kc.

The electronic circuitry of the television system is employed to reduce the bandwidth required to transmit the video signal. Bandwidth reduction is accomplished in a manner explained below.

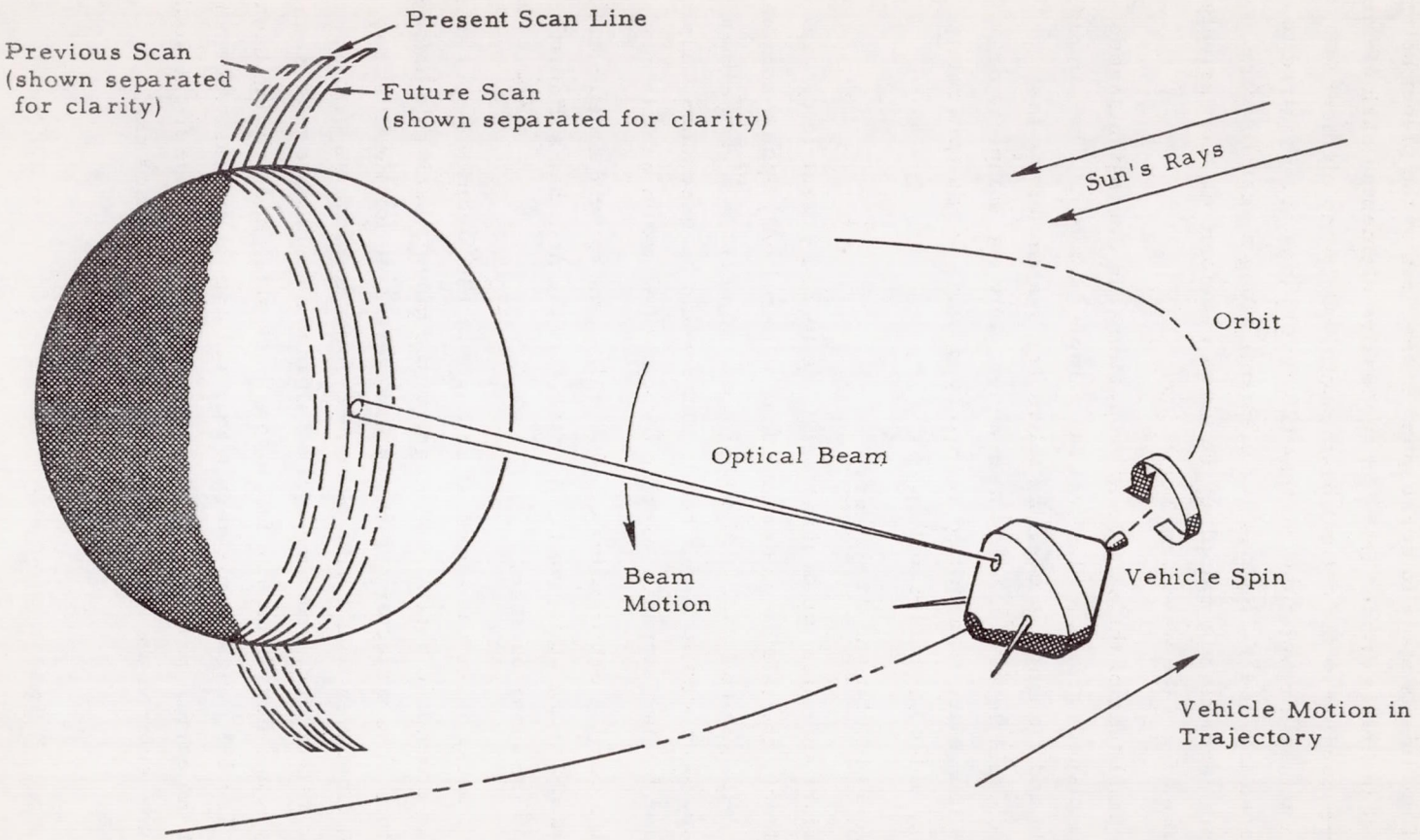

Figure 2-39. Illustration of TV System Operation

A 64° segment of each 360° scan line is chosen for transmission. The beginning of the line is made to correspond to the limb of the planet being scanned. Each scan line is divided into 128 successive elements, each element about 0.5°, corresponding to the optical beam width. Only one element is sampled during each spin revolution, so that 128 revolutions are required to obtain a single scan line (64°). Successive elements along a scan line are obtained each spin revolution by sampling the video waveform at successively more delayed times from the waveform beginning.

The amplitude of the sample is proportional to the instantaneous brightness of the planet surface at the time the sample is taken. The sample amplitude is held and transmitted over the telemetry system during the remainder of each spin revolution. In this manner, only two samples, or elements, of the image are transmitted each second (for a 2-rps spin rate), which reduces the video bandwidth to 1 cps.

b. Effects of Orbit and Trajectory

A priori specification of lunar orbit radius and eccentricity was not possible. Hence, the television design could be based only upon a nominal circular orbit. With an orbit radius of 4000 miles, adjacent 0.5° scan lines would not overlap. For smaller orbit radii, there would be unscanned strips between lines; and for larger radii, overlap of scan lines would be obtained.

With a vehicle orbit radius of 4000 miles, the moon diameter subtends an angle of about 30° at the optics unit. A resolvable element has a diameter of about 25 miles on the lunar surface.

The optical beam was aimed at an angle of 135° from the spin axis (nozzle end) in an attempt to obtain two images of the moon's back side before battery exhaustion. The trajectory is shown in Figure 2-40 for the first day firing date. The first view would have occurred, for a nominal trajectory, about the time of retrofiring, and a view of a half moon would have been seen. The second view would have been of a full moon, back side, had orbiting been accomplished. The 135° angle between spin axis and optical axis also permitted an early view of the earth, half illuminated. At no time during the flight would the sun's rays have entered the 0.5° acceptance cone of the optics unit.

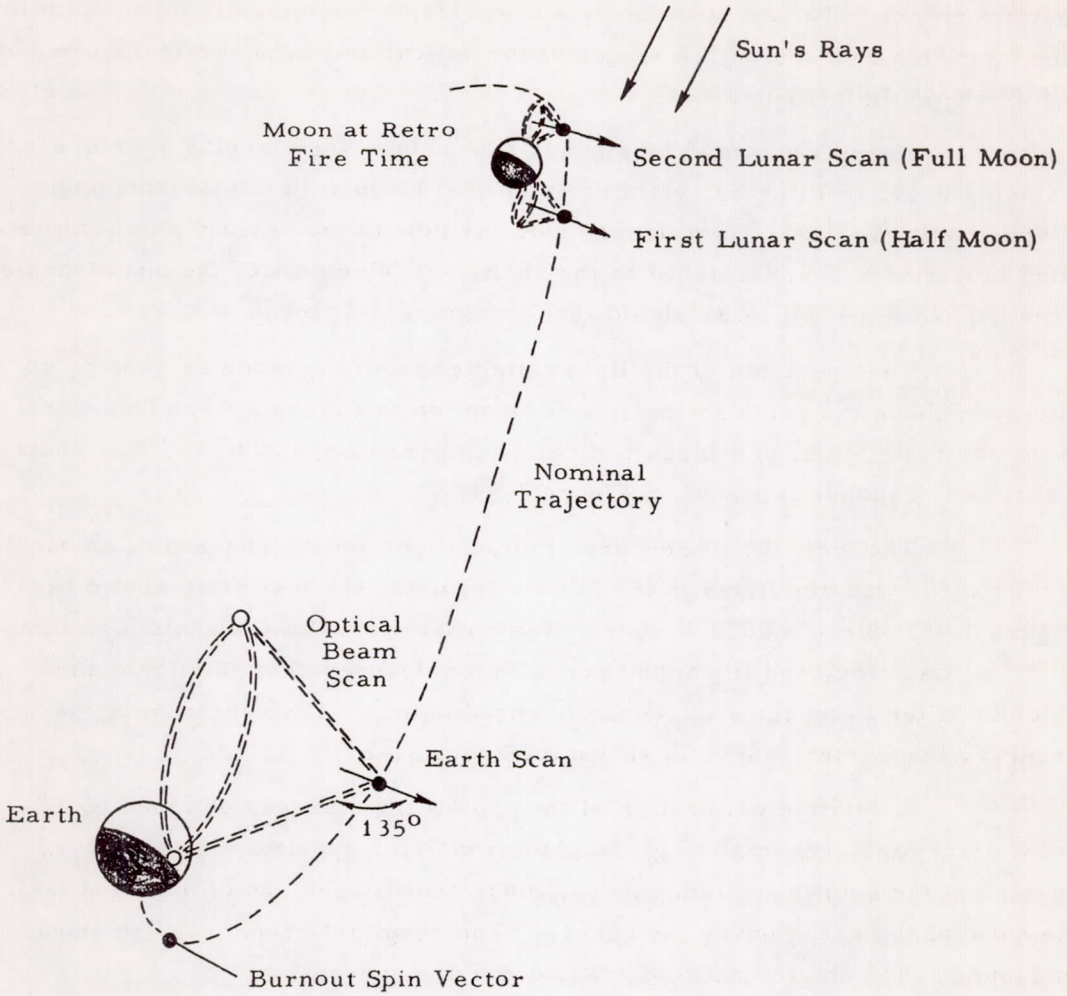

Figure 2-40. Sketch of Trajectory and Viewing Possibilities.

c. Optical System

The optics consisted of a spherical concave mirror located at one end of an aluminum tube. Light was focused on an aperture stop mounted in the center of the tube near the opening. Behind the aperture was located a phototransistor. The aperture and phototransistor were rigidly mounted to the tube by means of a spider. A sketch of the optical unit is shown in Figure 2-41 and a schematic in Figure 2-42.

The mirror focal length was 2.5 inches, the circular aperture diameter 0.576 millimeter, yielding an optical beam with a total cone angle of approximately 0.5°. Two flanges held the tube to the payload shell, and a third mounting bracket fastened to the shelf. All elements of the phototransistor were bypassed and all leads shielded to minimize r-f pickup.

The spectrum of the light reflected from the moon as seen by an observer above the earth's atmosphere is shown in Figure 2-43. This curve is approximately that of a black body at a temperature of 6000°K. The phototransistor response is shown in Figure 2-44.

The optical unit response to moonlight, in the absence of an atmosphere, was simulated in the laboratory using the test setup shown in Figure 2-45. Since a 6000°K source was not available, a GE photoflood lamp (3000°K) was employed in conjunction with a 2-1/2 per cent solution cupric chloride filter 2-cm thick to reduce infrared output. The spectrum of the resulting laboratory source is shown in Figure 2-46.

A relative calibration of the phototransistor was obtained by multiplying (and renormalizing) the phototransistor spectral response curve by each of the source-system curves, moon and filtered photoflood, and taking the ratio of the areas under the curves. The resultant responses are shown in Figure 2-47, and the ratio of areas under the curves is

$$\rho_1 = \frac{\text{Response of transistor to moonlight}}{\text{Response of transistor to filtered photoflood}} = \frac{2.32}{0.41}$$

An absolute calibration was obtained using a spot brightness (SB) meter. Since this meter has a spectral response consistent with the optical definition of spot brightness, one can relate the brightness of the laboratory

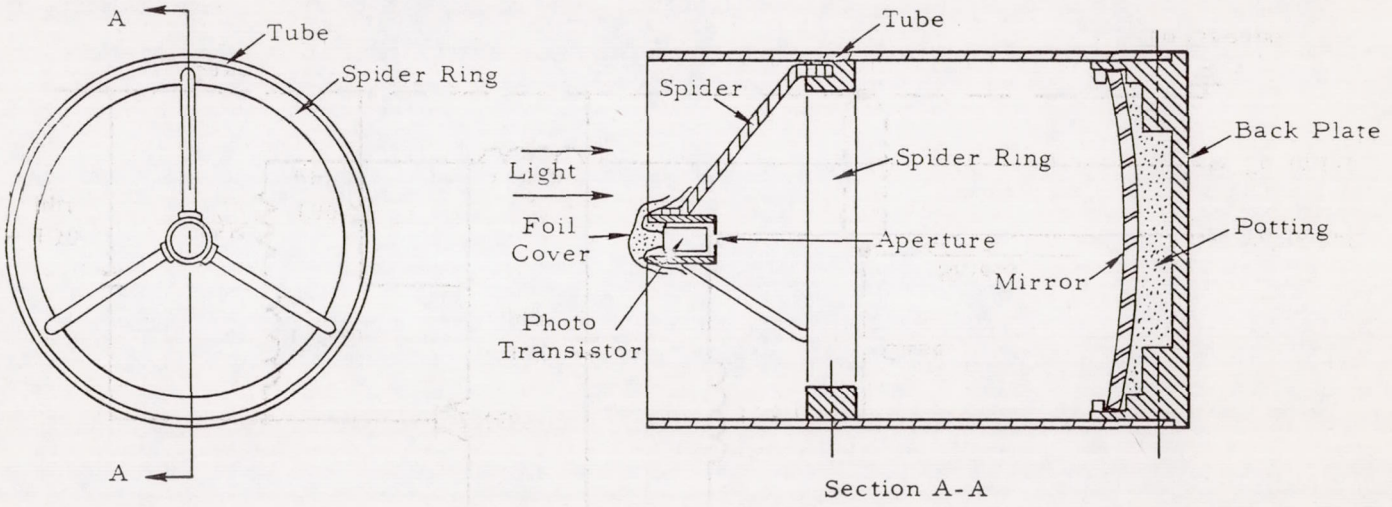

Figure 2-41. Sketch of Optical Unit Assembly.

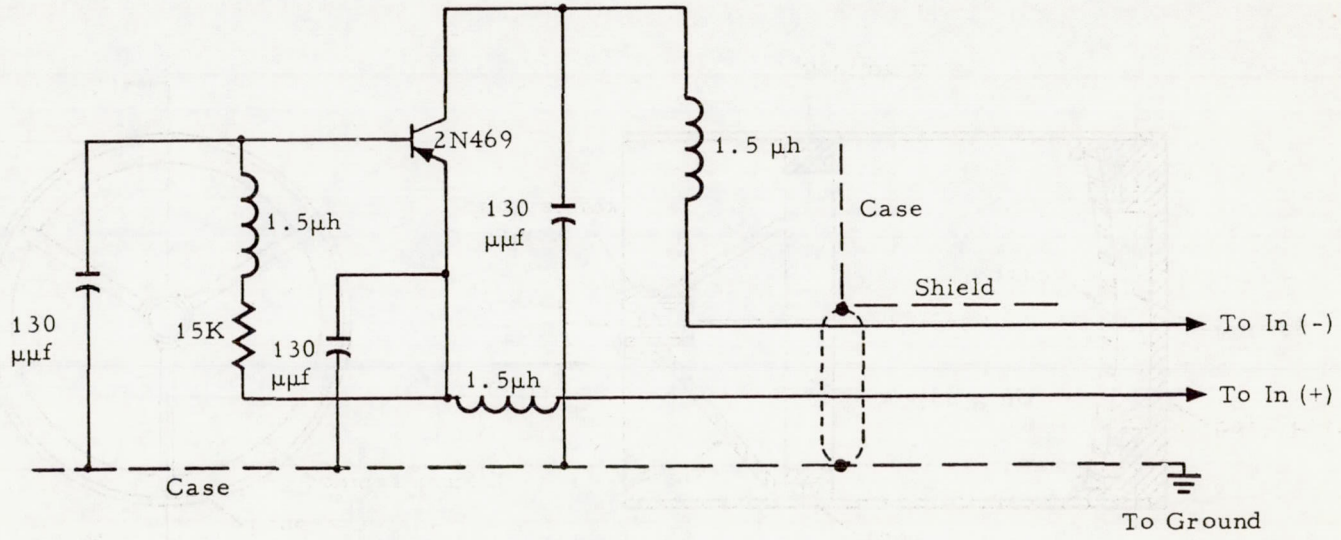

Figure 2-42. Schematic for the Optical Unit.

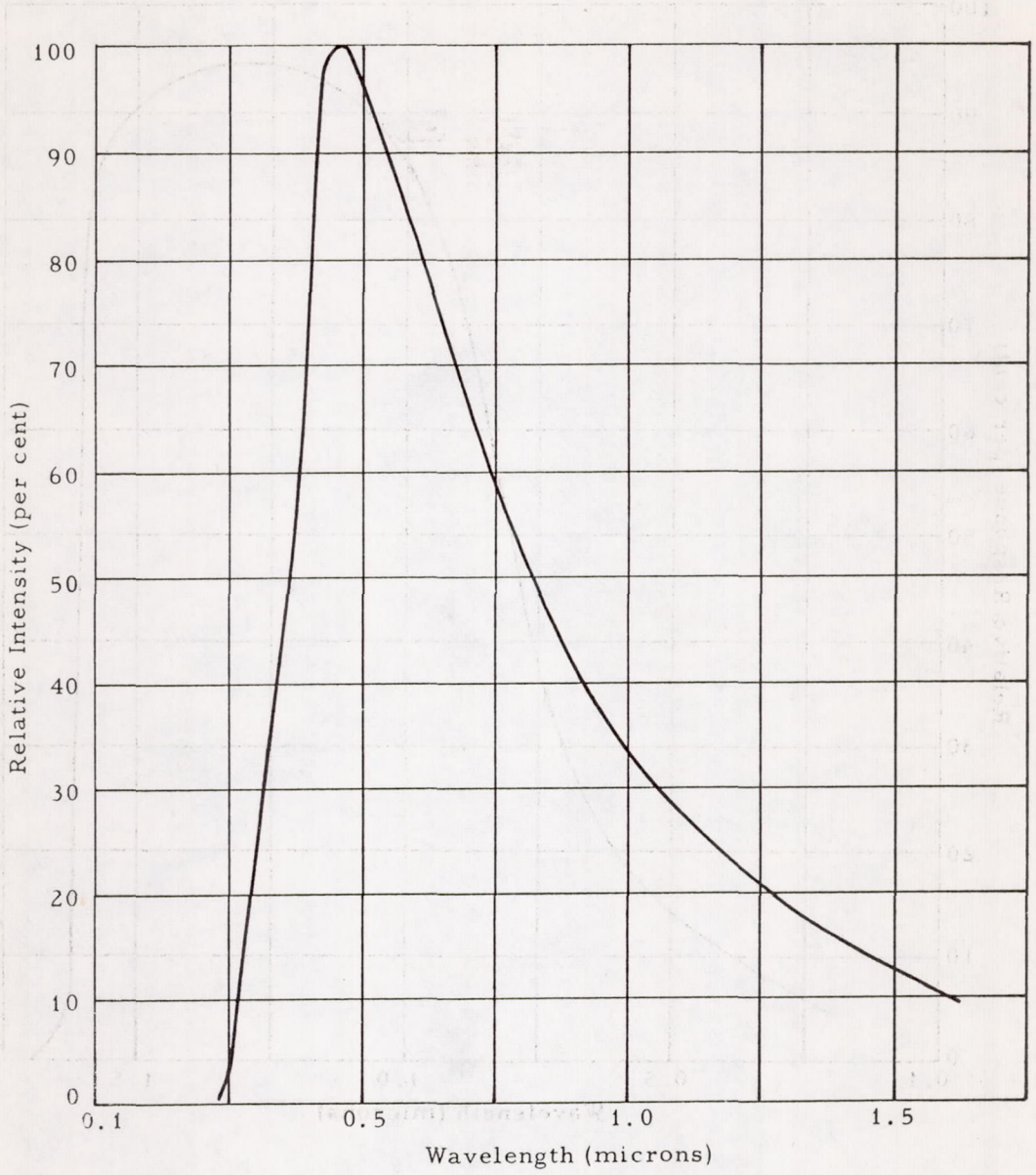

Figure 2-43. Spectrum of Light Reflected from Moon's Surface.

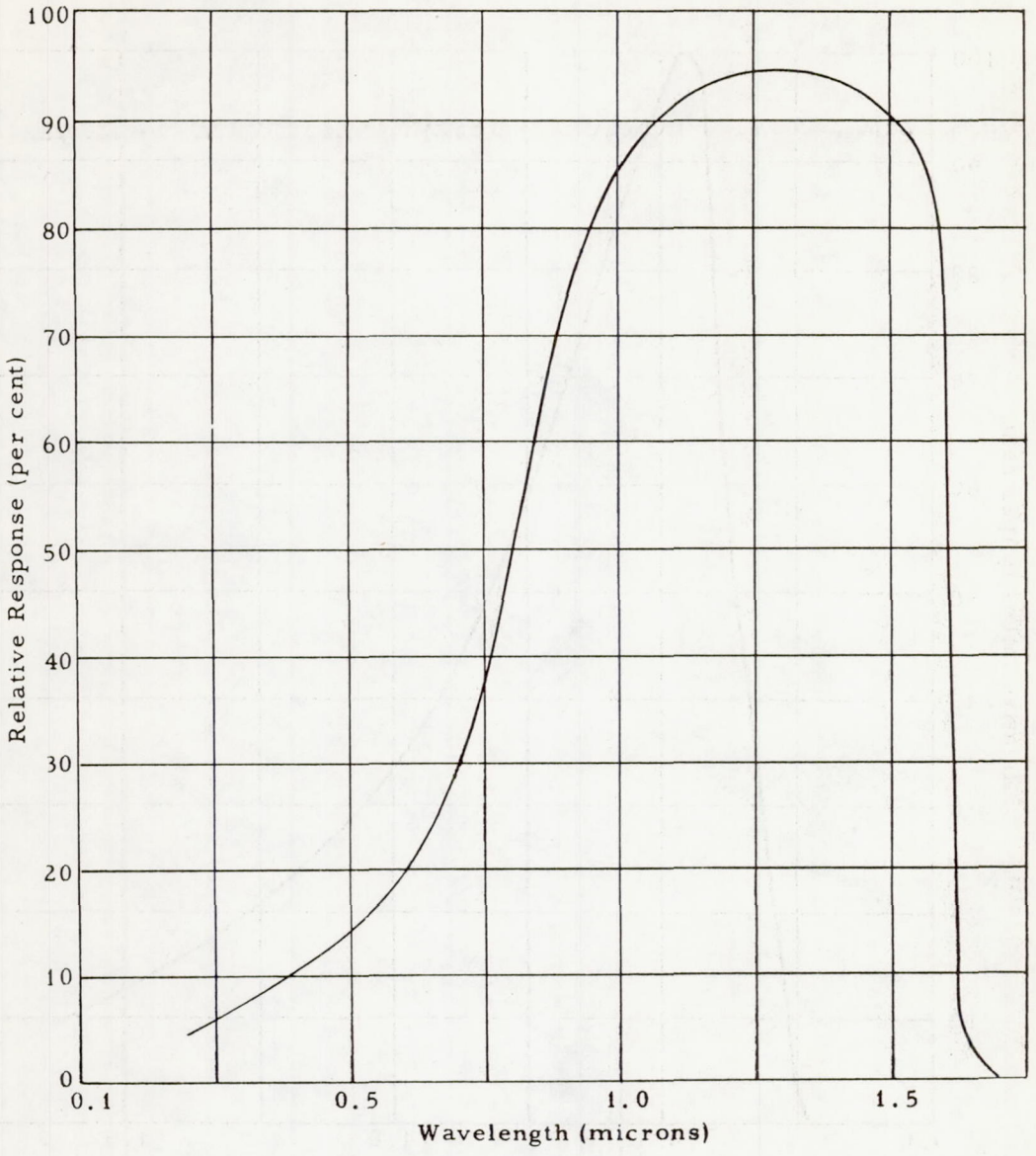

Figure 2-44. 2N469 Phototransistor Response

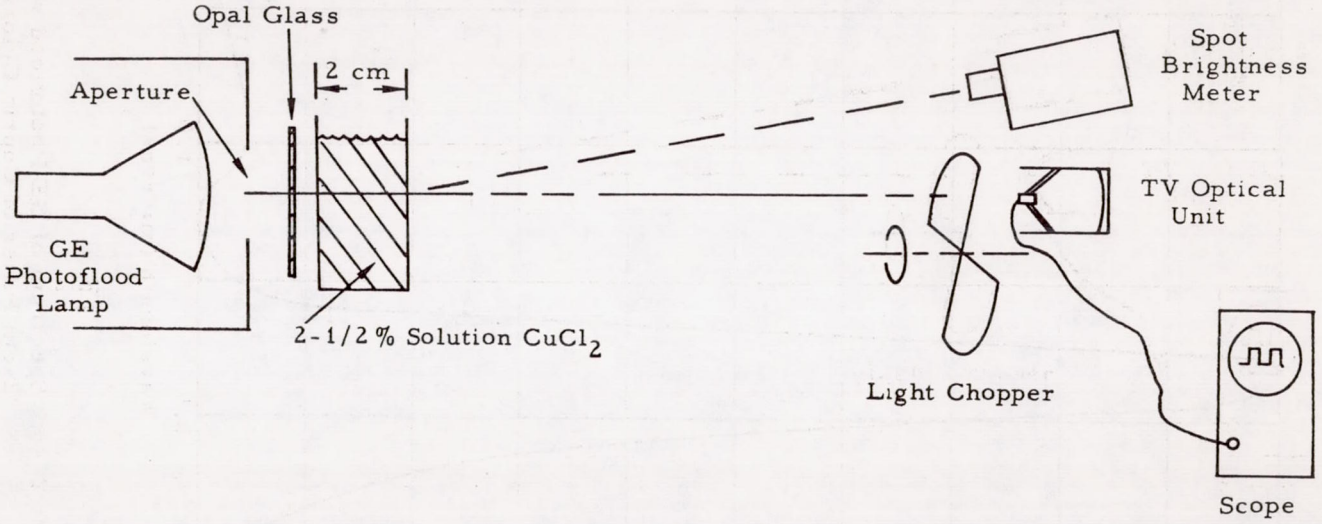

Figure 2-45. Sketch of Optical Unit Calibration Setup.

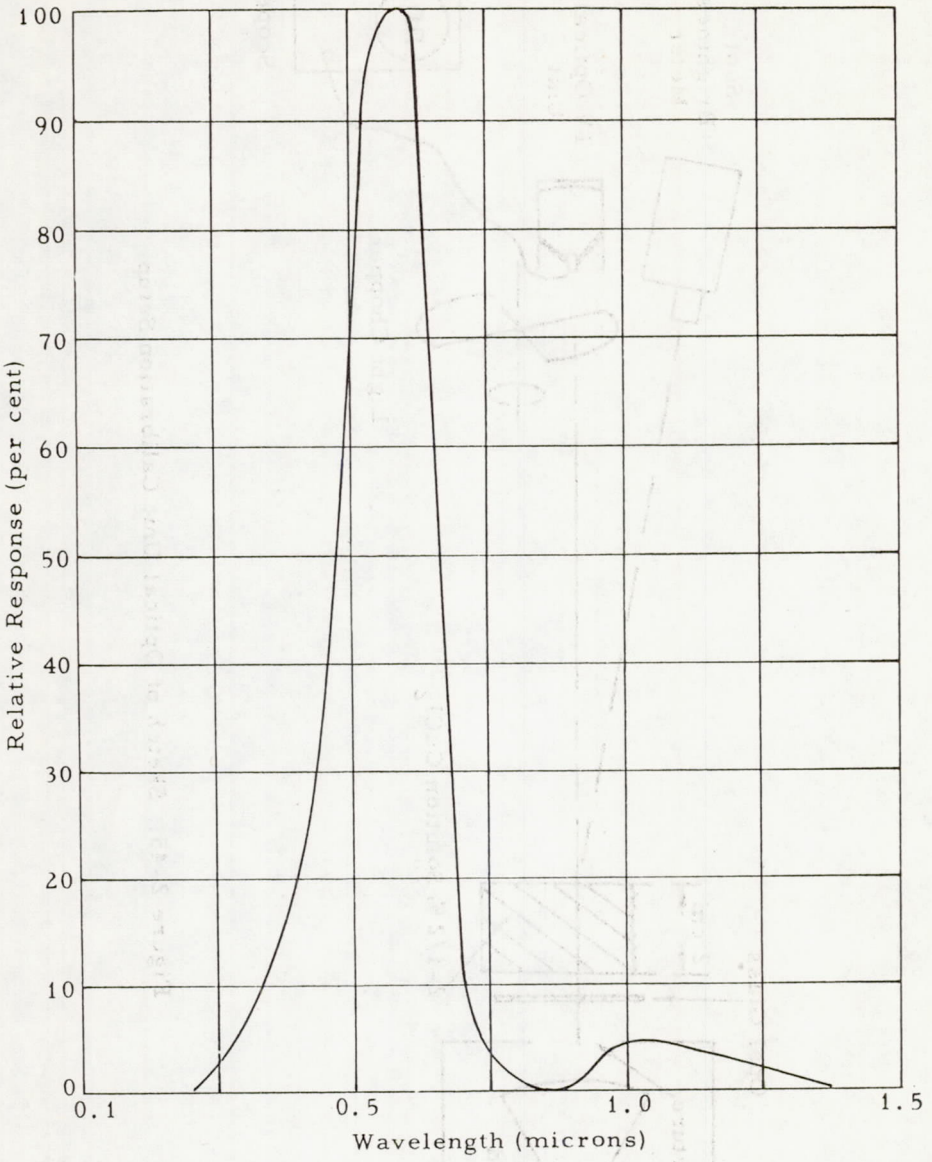

Figure 2-46. Spectrum of GE Photoflood with 2-cm Filter of Cupric Chloride.

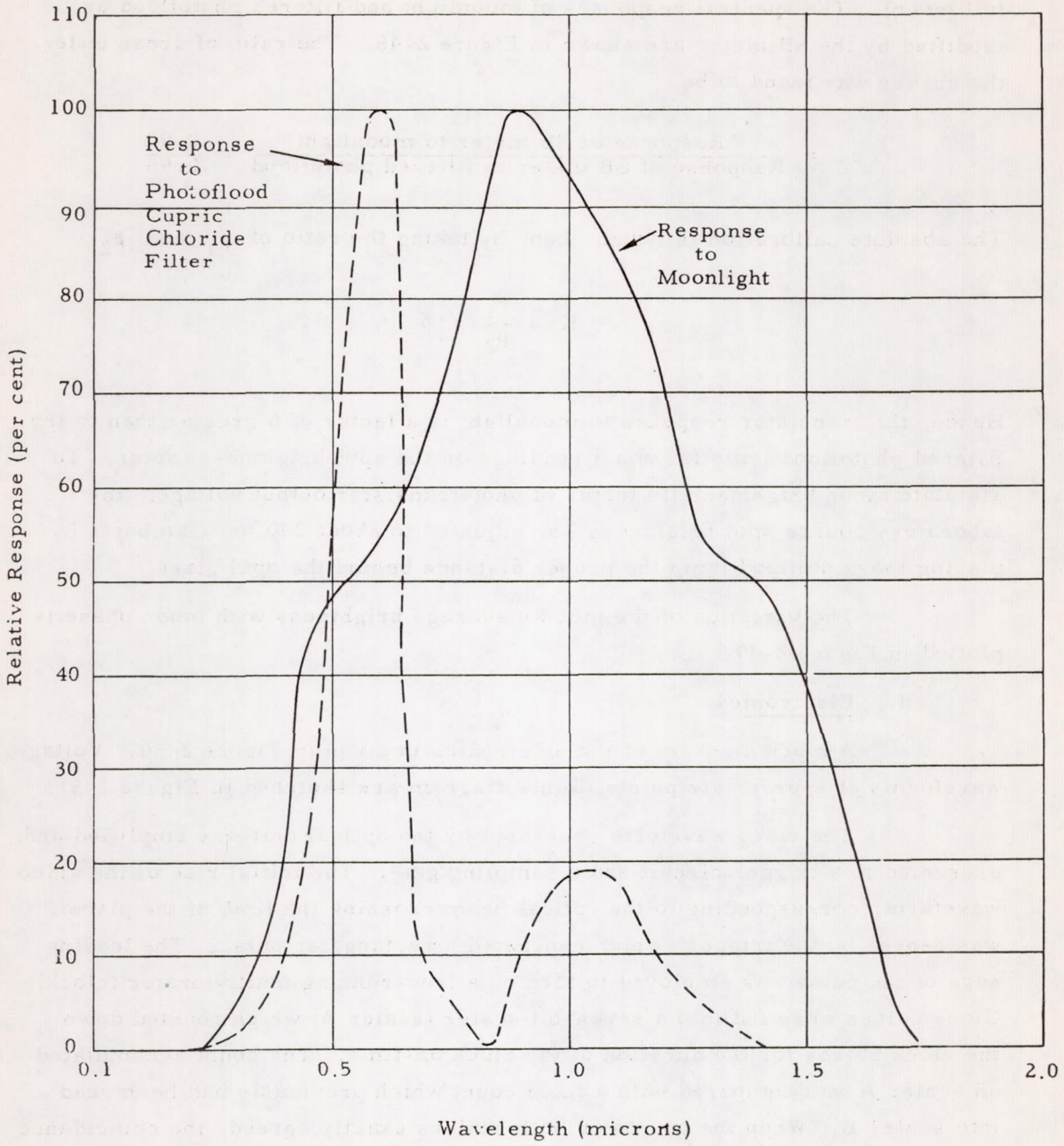

Figure 2-47 Relative Response of a 2N469 Phototransistor to Moonlight and Lab Source

source with the known brightness of the moon (about 1400 foot-lamberts average, full moon). The spectral responses of moonlight and filtered photoflood as modified by the SB meter are shown in Figure 2-48. The ratio of areas under the curves was found to be

$$\rho_2 = \frac{\text{Response of SB meter to moonlight}}{\text{Response of SB meter to filtered photoflood}} = \frac{0.90}{0.95}$$

The absolute calibration is found, then, by taking the ratio of ρ_1 and ρ_2

$$K = \frac{\rho_1}{\rho_2} = 6$$

Hence, the transistor response to moonlight is a factor of 6 greater than to the filtered photoflood lamp for equal readings on the spot brightness meter. To simulate moon brightness (in terms of phototransistor output voltage), the laboratory source spot brightness was adjusted to about 240 foot-lamberts by placing the photoflood lamp the proper distance behind the opal glass.

The variation of the moon's average brightness with moon phase is plotted in Figure 2-49.

d. Electronics

A block diagram of the electronics is given in Figure 2-50. Voltage waveforms at appropriate points in this diagram are sketched in Figure 2-51.

The video waveform generated by the optical unit was amplified and presented to a trigger circuit and a sampling gate. The initial rise of the video waveform, corresponding to the optical beam crossing the limb of the planet, was sensed by the trigger, which generated a rectangular pulse. The leading edge of the pulse was employed to turn on a free-running multivibrator (clock). Clock pulses were fed into a seven-bit scaler (scaler A) which counted down the clock pulses for the duration of the clock on-time. The count accumulated on scaler A was compared with a fixed count which previously had been read into scaler B. When the counts on both scalers exactly agreed, the coincidence circuit generated a pulse, and triggered a pulse generator.

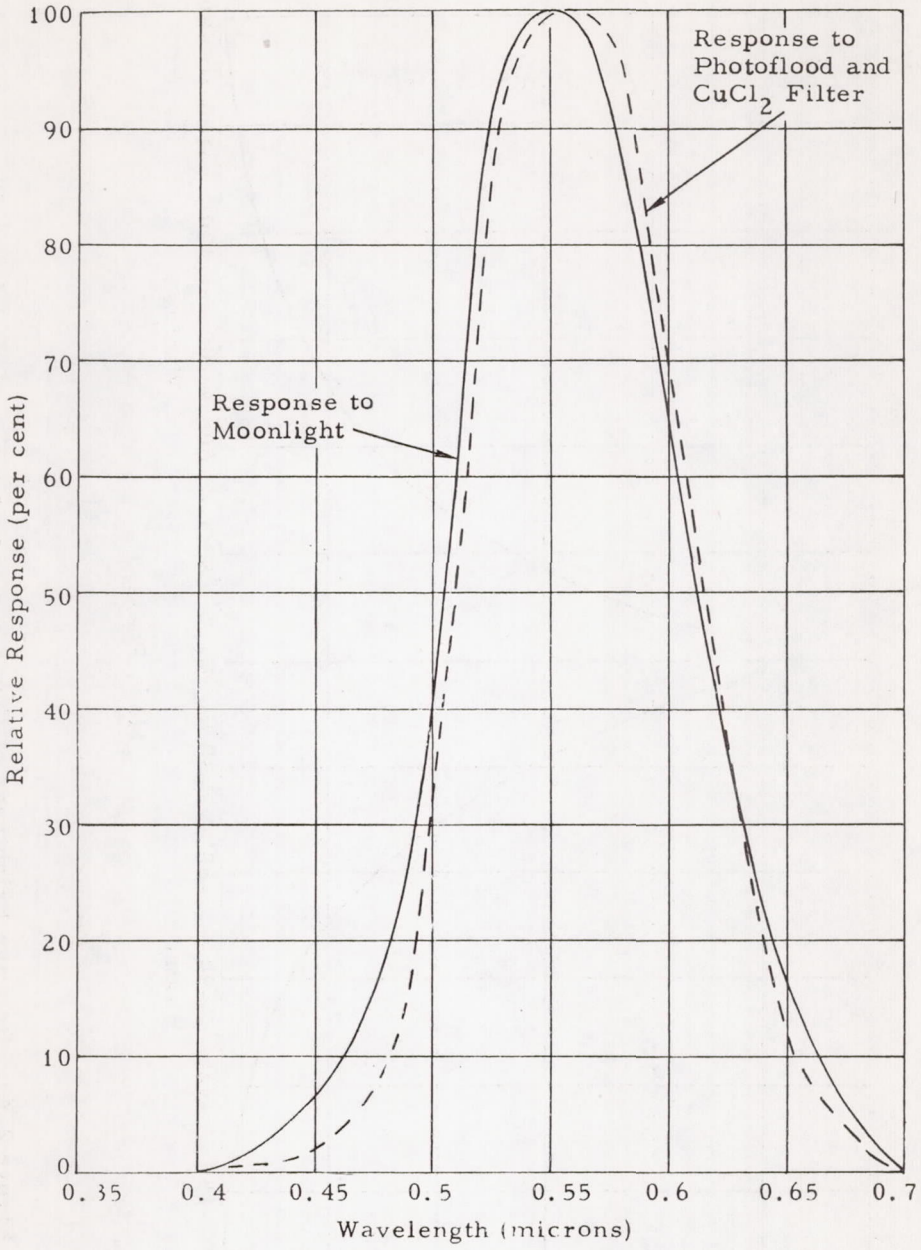

Figure 2-48. Response of Spot Brightness Meter to Moonlight and Lab Source.

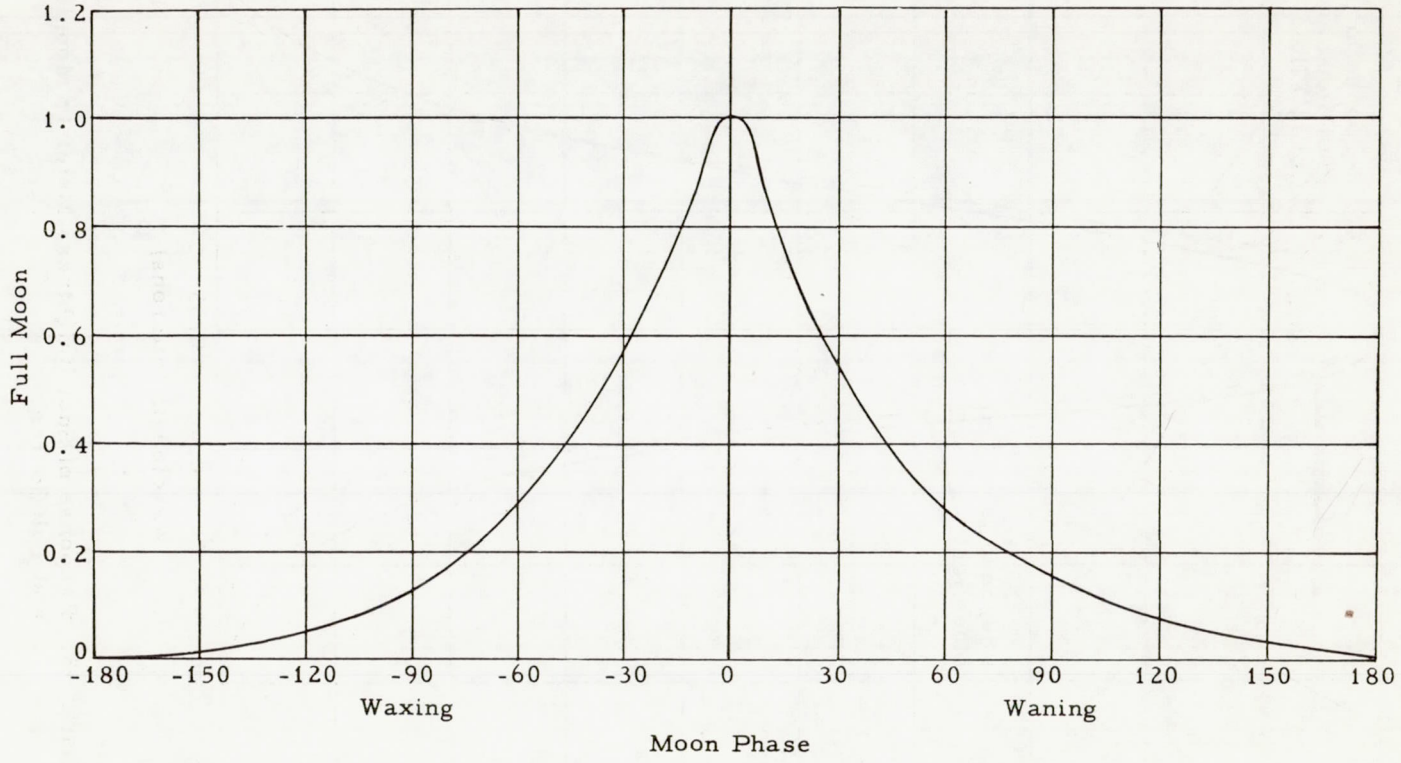

Figure 2-49. Relative Brightness of Lunar Surface as a Function of Lunar Phase.

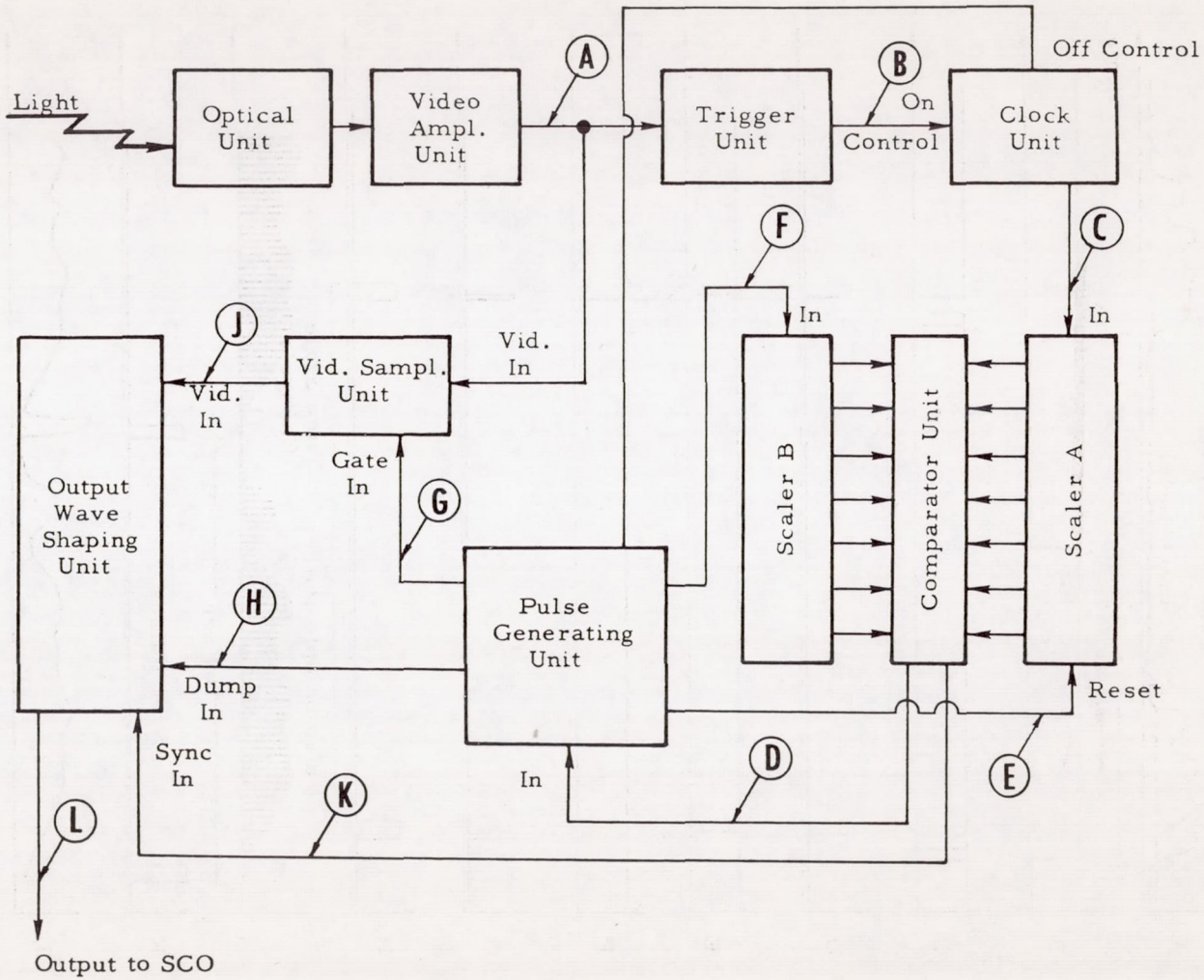

Figure 2-50. Block Diagram of TV System.

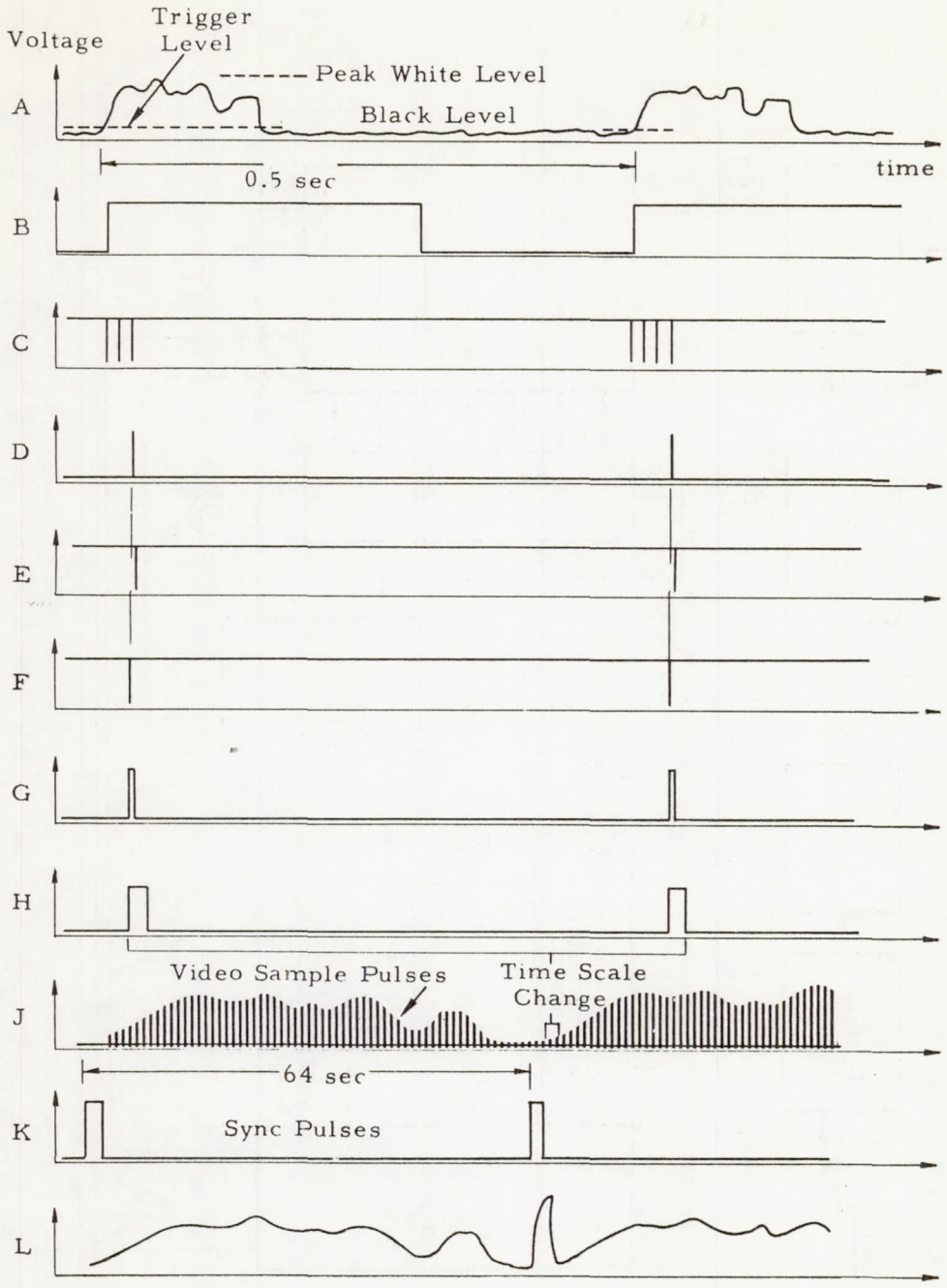

Figure 2-51. Waveforms for TV System.

The pulse generator outputs were used for several purposes. First, they stopped the clock; second, they triggered a one-shot multivibrator which is used to sample the amplitude of the video waveform, and to reset the A scaler; third, they added one additonal count into scaler B; fourth, in the pulse stretcher, it dumps the sample voltage (being held since the sampling of the video waveform during the previous spin cycle) in preparation for reading in the new voltage sample.

With the completion of this sequence, the electronic system awaited the application of another video signal on the next spin revolution. At that time, the operation was repeated, except that counter A required one more clock pulse before coincidence occurred with counter B.

Each half second, sampling pulses of various amplitudes were routed from the sample gate to the output pulse forming unit. The latter device read and held the amplitude information of each pulse until the next sample arrived. The held-voltage level was delivered to the subcarrier oscillator of the telemetry system. At the completion of each line, as determined by a full B scaler, a sync pulse (1-second duration) was added to the output voltage.

A more detailed description of the electrical components of Figure 2-50 follows.

(1) Amplifier

A conventional four stage, capacitor coupled, transistorized amplifier was employed to amplify the video signal. Its gain was adjustable to allow for sensitivity uncertainty of the photosensor. For Pioneer II the gain was approximately 1000. The frequency response was flat within 3 db from 0.1 cps to 2 kc. Roll-off was provided at 2 kc to eliminate high frequency noise.

A d-c restorer was provided at the output of the amplifier to maintain a reference black level independent of video wave shape.

The schematic for the amplifier and d-c restorer is shown in Figure 2-52.

(2) Trigger

A Schmidt trigger and one-shot multivibrator was employed to initiate the clock. A schematic for this block is given in Figure 2-53. The

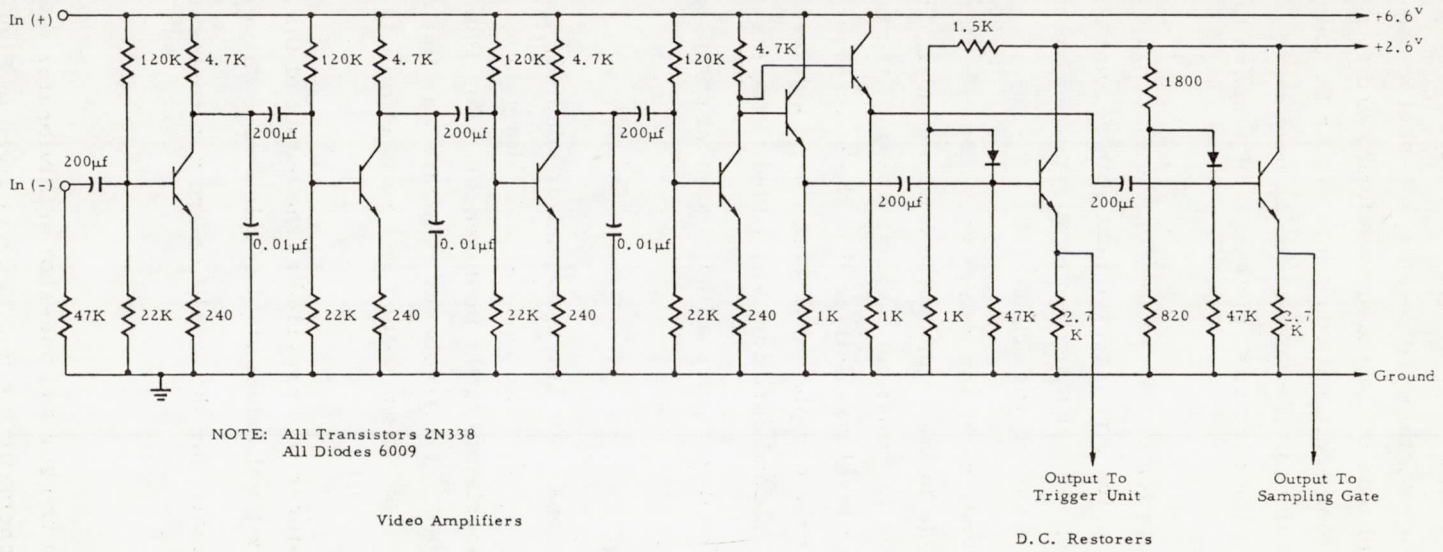

Figure 2-52. Video Amplifier and d-c Restorer Schematic.

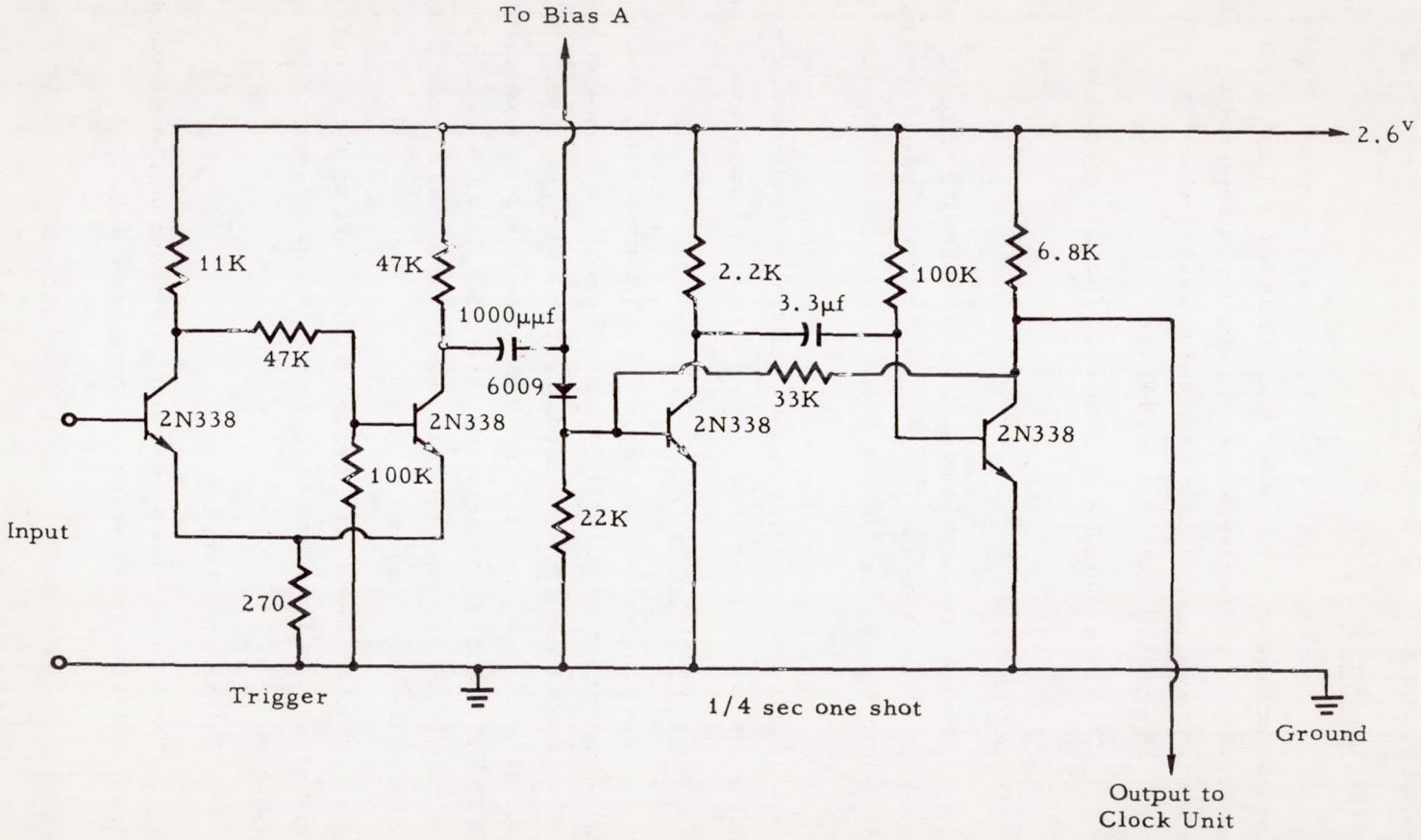

Figure 2-53. Trigger Unit Schematic.

purpose of the one-shot (1/4-second duration) was to prevent clock initiation twice in one spin revolution.

(3) Clock Unit

The clock and clock control circuitry is given in Figure 2-54. The clock was a standard multivibrator using stable "West Cap" capacitors in the feedback branches, and one base resistor which was returned to B plus when clock operation was desired and returned to ground when the clock was to be stopped. The clock frequency was 1440 cps.

The clock control was a standard flip-flop circuit with individual base controls.

(4) Scalers A and B

The scalers were identical, each consisting of seven bistable multivibrators (counters) shown in Figure 2-55. In each scaler, the counter units were wired in series, the output 1 of one counter feeding the input of the next.

The input to the first counter of scaler A was from the clock, and the input to the first counter of the scaler B from the pulse generator.

(5) Comparator Unit

The comparator unit (Figure 2-56) accepted the individual outputs of all counters from both scalers and compared the counts on scalers A and B. When these counts agreed, an output pulse was generated. In addition, a second coincidence pulse on a separate output line was generated during the last two (127th and 128th) counts read into scaler B. This 1-second pulse, marking the completion of a scan line, was fed to the output circuitry where it was mixed with the video signal.

Standard diode coincidence circuits make up the comparator, with emitter followers at the output to lower the driving impedance to the pulse generator unit.

(6) Pulse Generating Unit

The input circuit of the pulse generating unit was a standard Schmidt trigger and was used to shape the comparator pulse.

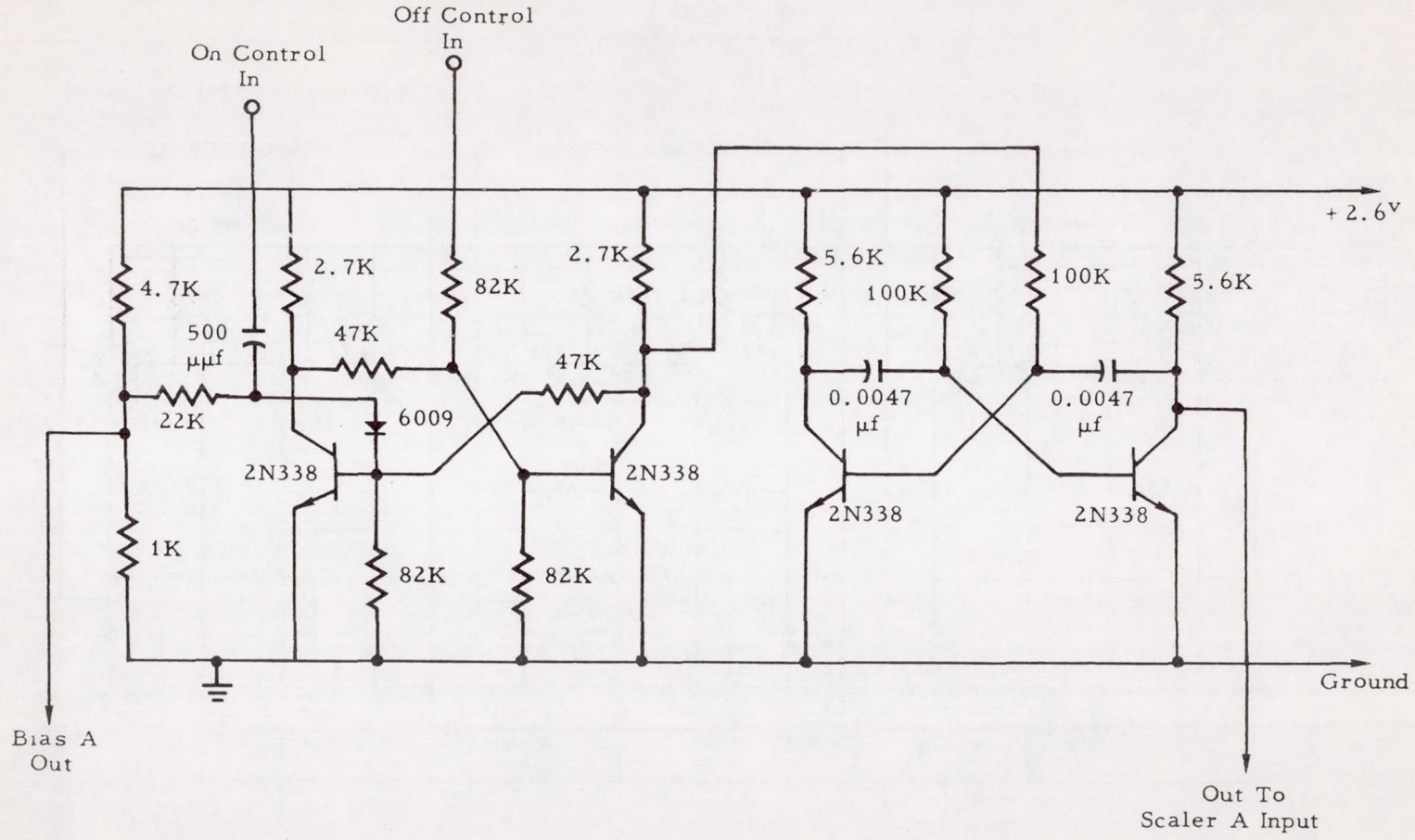

Figure 2-54. Clock Unit Schematic.

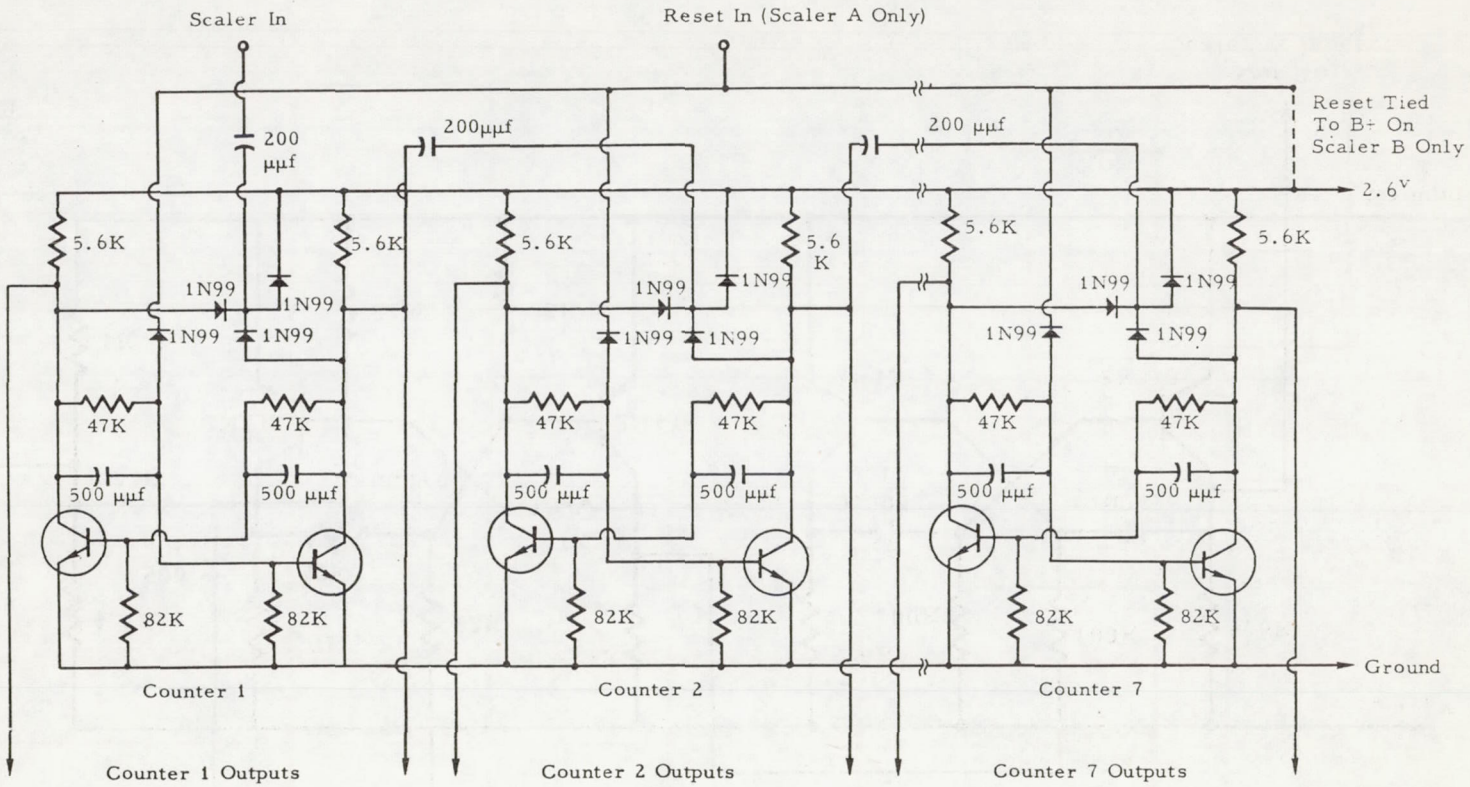

NOTE: All Transistors 2N338

Figure 2-55 - Scaler Schematic.

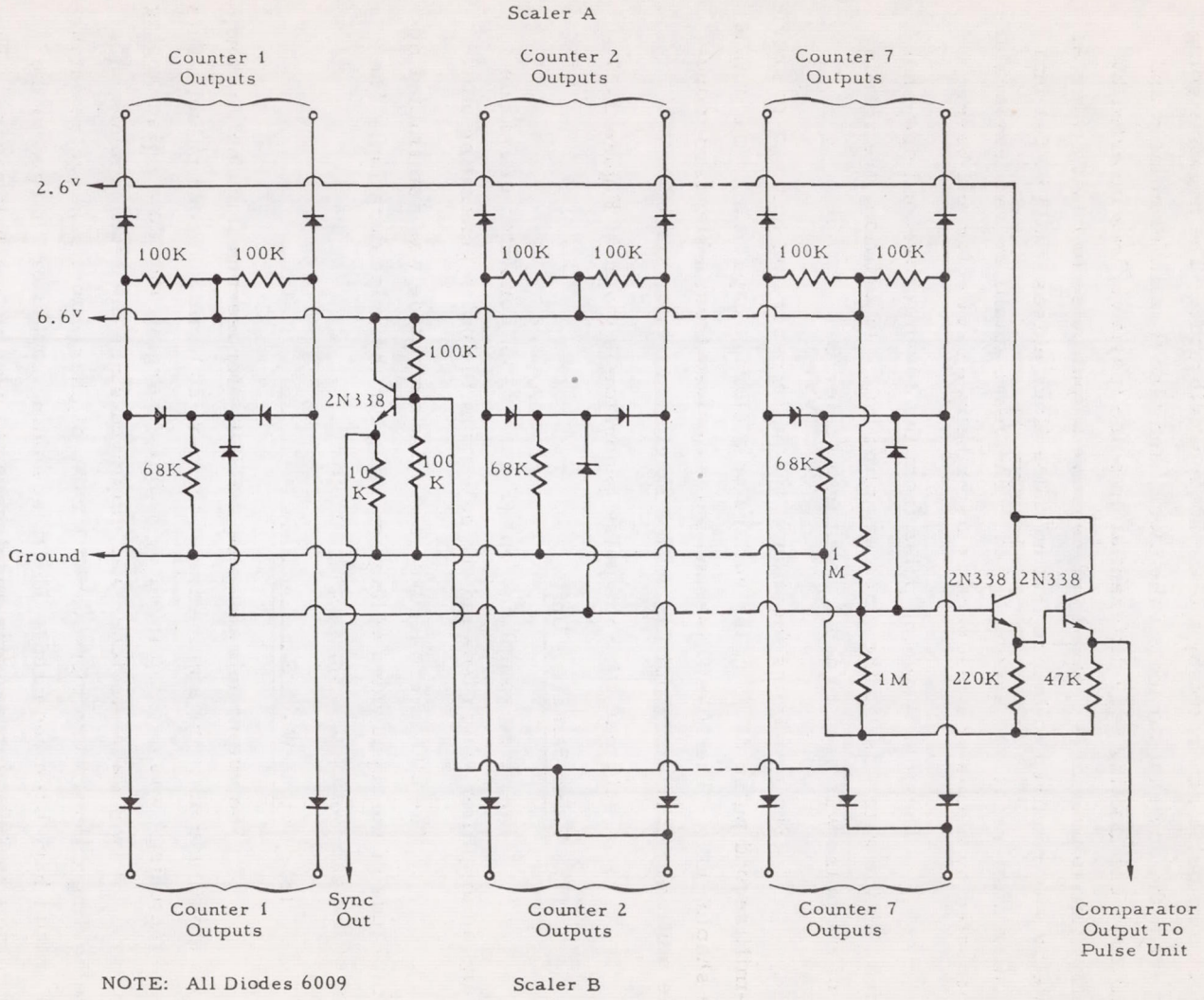

Figure 2-56. Comparator Unit Schematic.

The fast rise of the trigger was employed to initiate a 200-microsecond pulse generated by a one-shot multivibrator. The negative going pulse from the one shot turned off the clock, and also was differentiated and amplified. The trailing edge differentiation pulse (positive) was inverted by the amplifier to provide a delayed and negative output pulse to reset scaler A. The delay was required to insure that no more clock pulses would be fed into the scaler after reset was accomplished. The reset amplifier was temperature compensated by means of a feedback resistor between collector and base.

The positive going pulse from the 200-microsecond one-shot was fed, as the gate was, to the video sampling unit. In addition, the trailing edge of the pulse was used to add a count into scaler B.

The remaining function of the pulse generator unit was to provide a 10-millisecond pulse to dump the voltage on a storage capacitor in the output wave shaping unit. The 10-millisecond pulse derived from a standard mono-stable multivibrator, and amplified with a single transistor stage.

A schematic for the pulse generator is given in Figure 2-57.

(7) Video Sampling Unit

The video sampling unit (Figure 2-58) consisted of a diode gate and an amplifier which isolated the gate from the pulse generating unit.

The 200-microsecond gate pulse amplitude was determined by the amplitude of the input video voltage existing for the pulse duration. The output of the gate was fed to the output circuitry.

(8) Output Wave Shaping Unit

The output unit accepted the 200-microsecond input pulse, and held its amplitude until the application of the next 200-microsecond pulse. This "pulse stretching" was accomplished by rapidly charging and slowly discharging capacitors. A two-stage stretcher was employed since the requirements on a single holding circuit were too severe; a ratio of charge to discharge resistance of 10^5 would have been required. The first holding capacitor charged to the input voltage in 200 microseconds and decayed to zero in one-half second. The second holding capacitor charged, in 10 milliseconds, to the value stored on the first capacitor. This 10-microsecond charge period was preceded by a

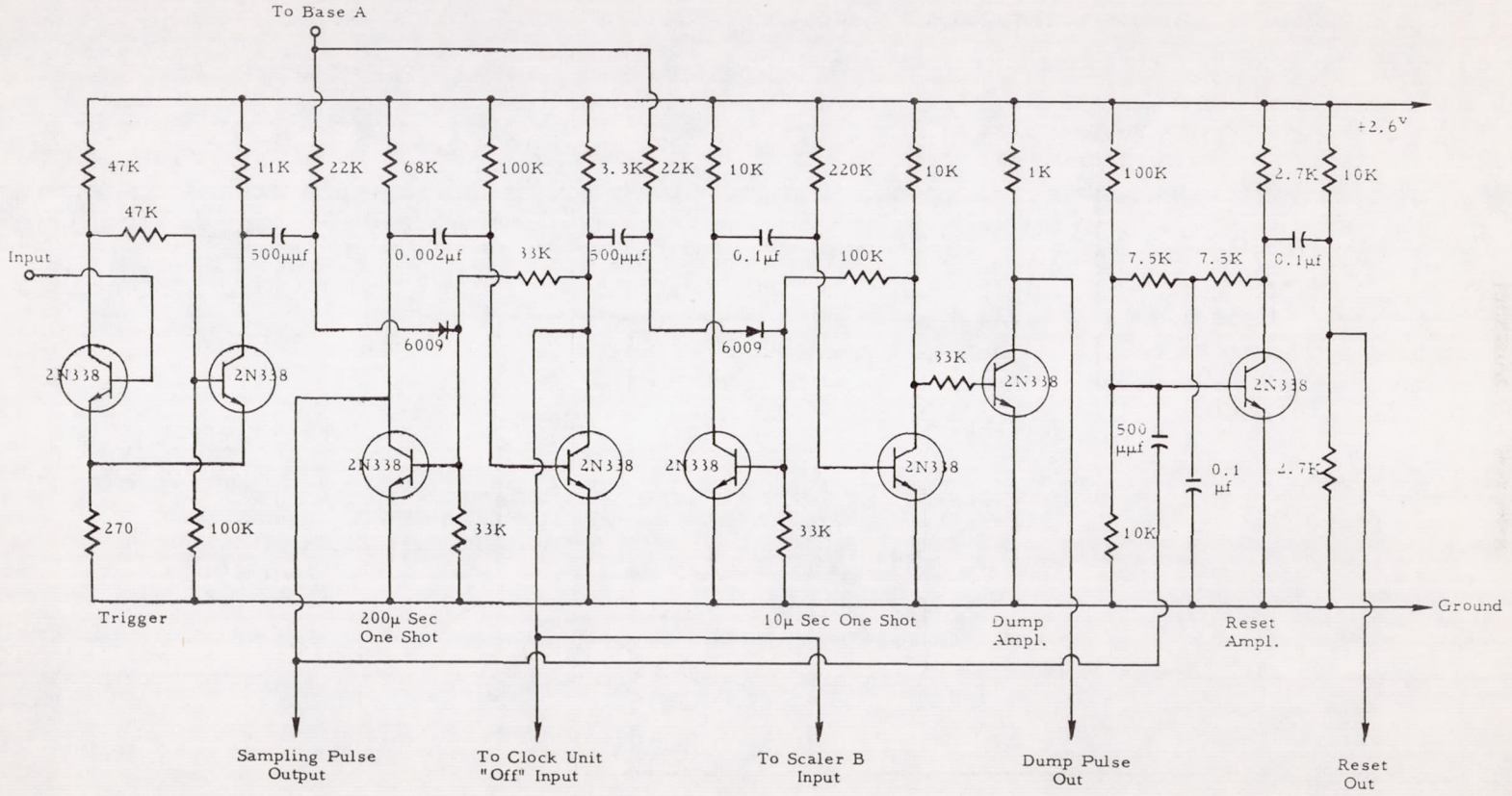

Figure 2-57. Pulse Generating Unit Schematic.

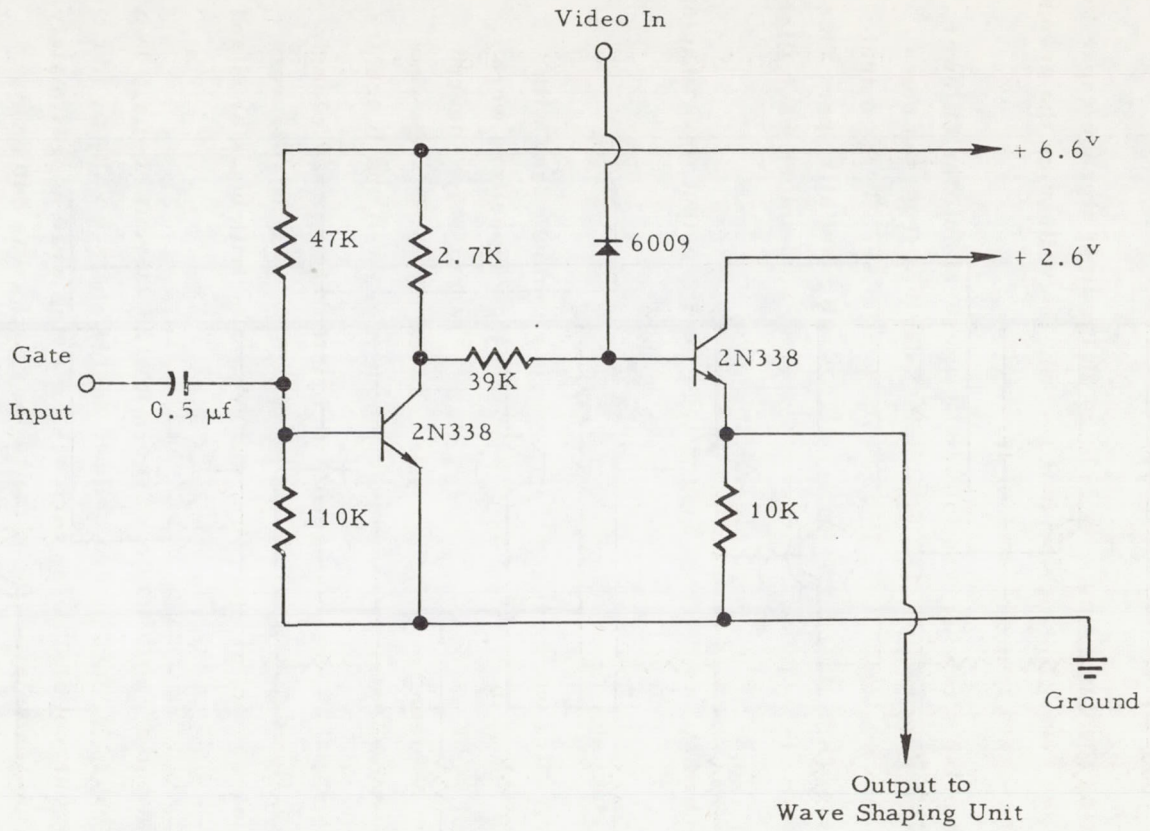

Figure 2-58. Video Sampling Unit Schematic.

10-millisecond discharge period, starting at the beginning of video sampling, during which the voltage previously stored on the second capacitor was dumped. Dumping is accomplished by the 10-millisecond pulse from the pulse generating unit.

During the dump time, the voltage on the first storage capacitor decreased about 10 per cent. During one-half second, the voltage on the second storage capacitor decreased no more than 10 per cent.

The pulse stretcher was followed by several emitter follower stages to reduce output impedance. The sync pulse, derived from the comparator, was added into the input of the final emitter follower. At the output an RC integrating network is provided with a 3-db roll-off point at 1 cps. This frequency characteristic is required to prevent discriminator unlock when flight data are reduced.

A schematic is given in Figure 2-59 for the output wave shaping unit.

e. Construction and Power Supply

The electronics were packaged in a single aluminum can, with removable cover, as shown in Figure 2-60. Feed-through capacitors were employed to bring out input, output, and power leads. Finger stock insured a good r-f connection between can and the cover. Three circuit boards were employed, the top board containing the counter modules of the A and B scalers.

All circuit boards were designed with printed wiring, and coated with epoxy as a precaution against the effects of moisture. The boards were fastened to the can, at nine points, by bolts, and separated with black anodized aluminum spacers.

The flight battery pack employed seven RM12R mercury cells. Two voltages were provided; 2.6 volts by two cells in series and 6.6 volts by five cells in series. The current drains for each series string were approximately 15 milliamperes. Total calculated life of the battery packs was 240 hours.

R-f chokes were placed in each B plus line to eliminate r-f interference.

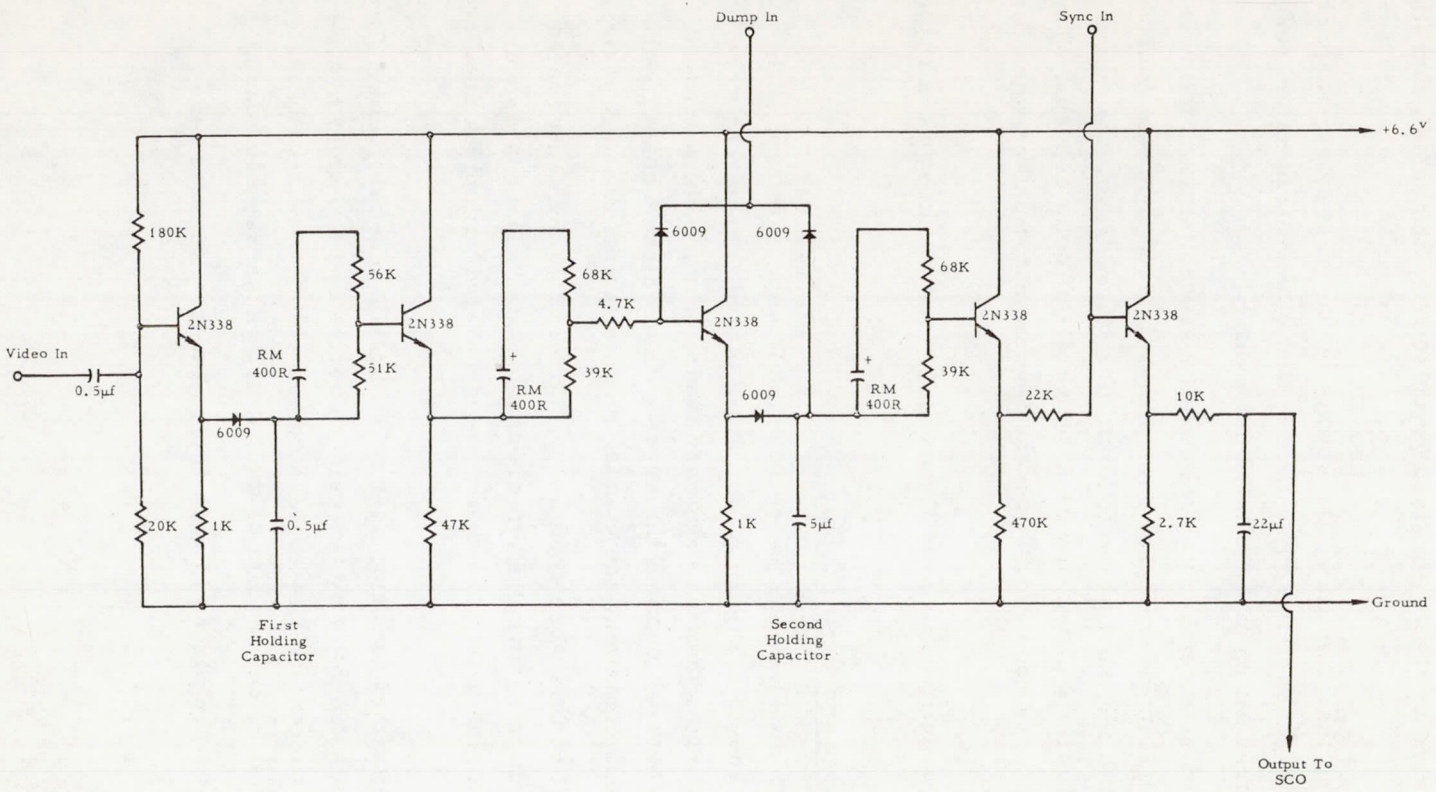

Figure 2-59. Output Wave Shaping Unit Schematic.

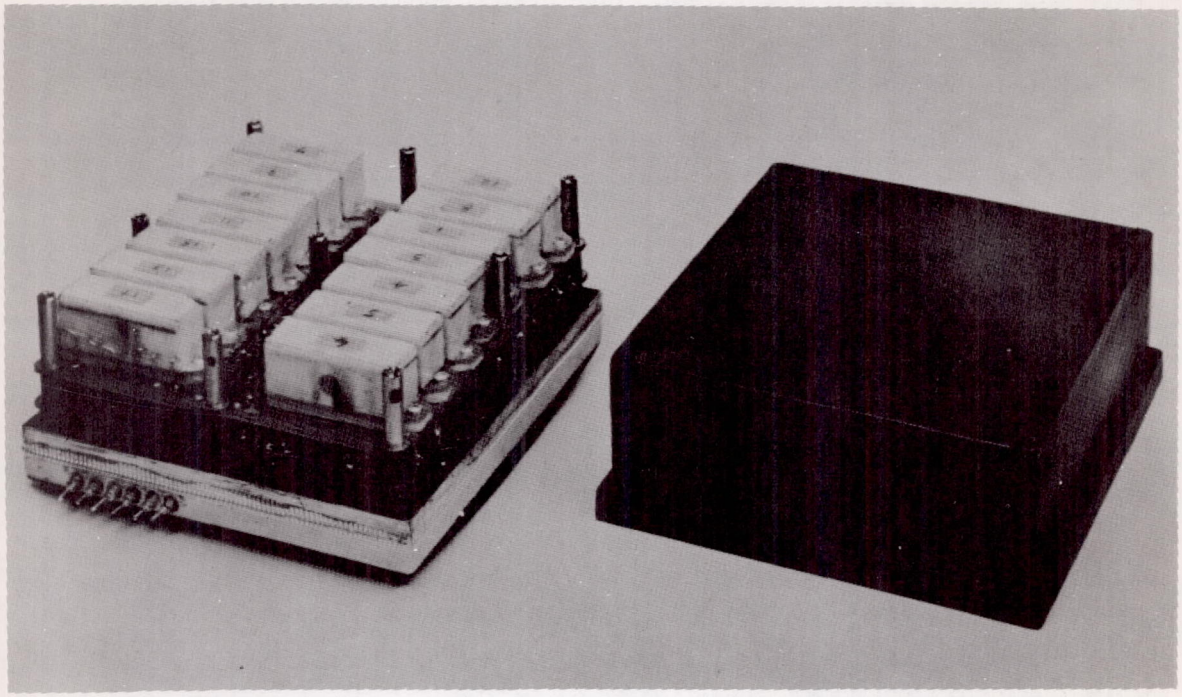

Figure 2-60. Television System Package

f. System Checkout

A test pattern was drawn on a heavy cardboard sheet, 39 inches by 39 inches. It was placed in a vertical frame that allowed motion up and down. A motor, shaft, pulley, and wire arrangement allowed a slow, continuous motion of the test pattern in the vertical direction, simulating vehicle motion along its trajectory.

The optics unit was placed before a rotating mirror thereby providing optical beam scanning across the test image. The mirror revolution rate was 1 rps, in simulation of the 2-rps vehicle spin. A sketch of the test setup is shown in Figure 2-61.

The output of the television electronics was used to intensity modulate the beam of an oscilloscope. The scope sweep was adjusted so that it completed a sweep just prior to the television line completion. The next scope sweep was initiated by the television sync pulse. The scope vertical sweep was provided by a slowly varying d-c voltage from a helipot driven by a 1/16-rpm motor.

At the rate of two elements per second, a 128 by 128 element image of the test pattern required about two hours to be obtained. A scope camera was employed to record the television picture presented on the scope face. The camera was opened at the beginning of the 2-hour interval and left open while the test image was scanned. A 64 by 64 element picture resulting from such a test is shown in Figure 2-62.

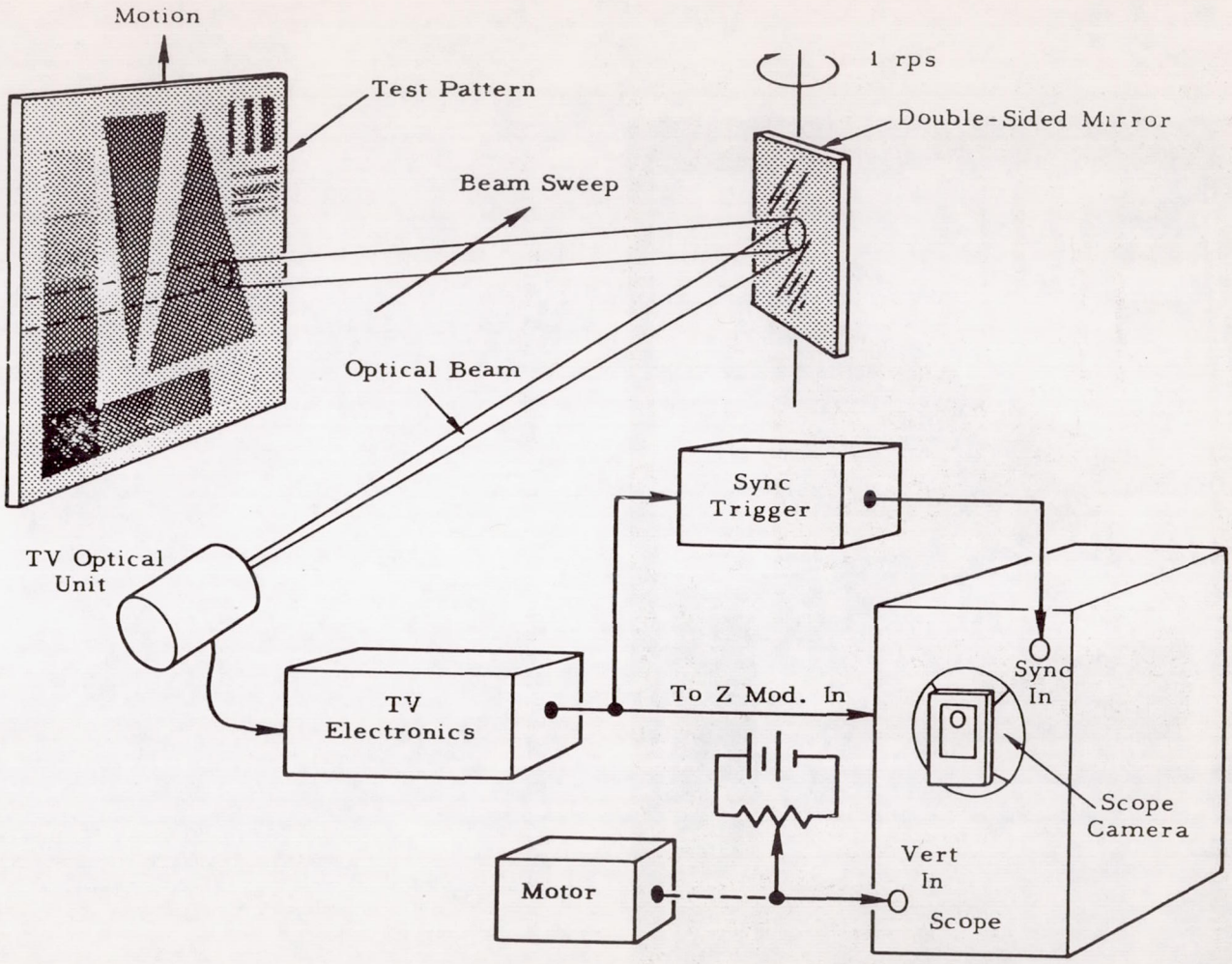

Figure 2-61. TV Test Setup.

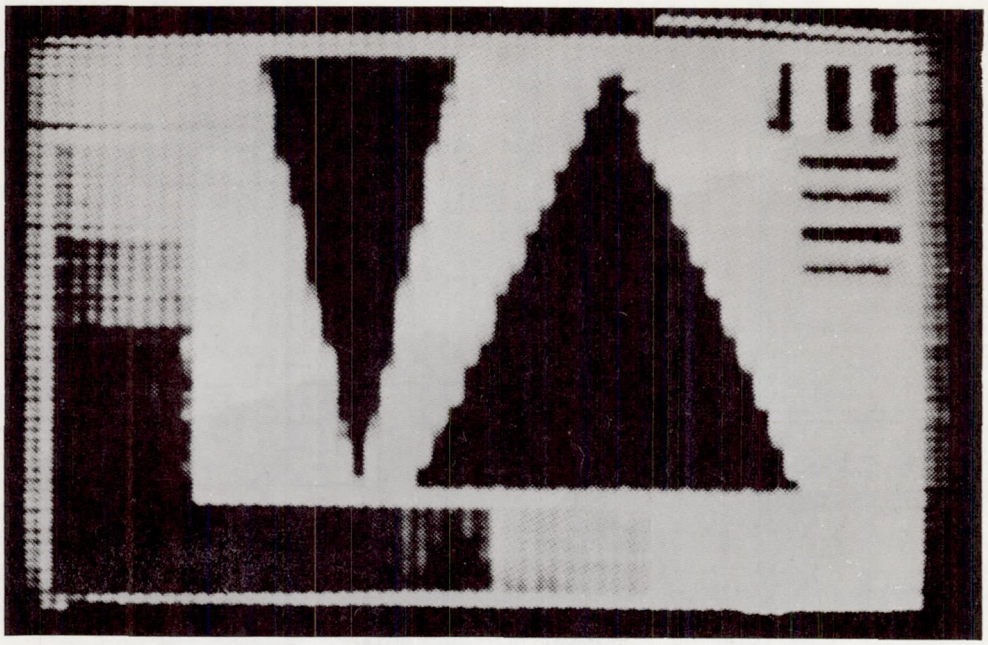

Figure 2-62. 64 x 64 Element STL TV Image of Test Pattern.

2.2.6 NOTS TV System

Able-1 Flights 1 and 2 contained a TV system developed by the Naval Ordinance Test Station, which was to have obtained a rudimentary image of that part of the lunar surface normally unseen by earth observers. A comprehensive report on this system will be issued by the Naval Ordinance Test Station. Only a brief description of the system is presented here.

Figure 2-63 is a block diagram of the system, showing the primary principles of operation. Light is collected on a parabolic reflector and focused on the sensor. As the light intensity varies, this signal is amplified and becomes the modulation for a crystal-controlled amplitude-modulated vacuum tube transmitter.

As a means of conserving weight, several circuits were added to permit system operation only when meaningful data could be transmitted. An enable switch is closed at the time of firing the final stage motor, at which time the rocket-firing conveniently operates the switch mechanism. After this switch closure, the transistorized video amplifier operates continuously. If light pulses are detected, the signal-present sensor, a condenser-charging circuit, will cause a relay to close which will supply filament and B-plus power to the vacuum tube circuitry of the oscillator modulator and power stages of the transmitter. When light pulses cease to be detected, the condenser discharges, the relay falls open, and the battery power is conserved until the next occasion for picture transmission.

The complete final stage is spinning in a circular or elliptical orbit around the moon. The light sensor is alternately looking at black space and light from the sun reflected from the surface of the moon. With each rotation of the payload, a strip of the moon's surface is scanned. As the payload moves in orbit it may take hours to generate a complete frame, depending on the distance of the payload from the moon's surface. The television system operates to amplitude modulate the r-f carrier in a "black level-low power, white level-low power" system, since only the whites and grays contain information, and require a maximum signal at the receiving stations. Approximately 50 watts of carrier power is peak at the white level. The transmitted video information uses only a few kilocycles of bandwidth, a necessary limitation to provide adequate signal at the communication range involved.

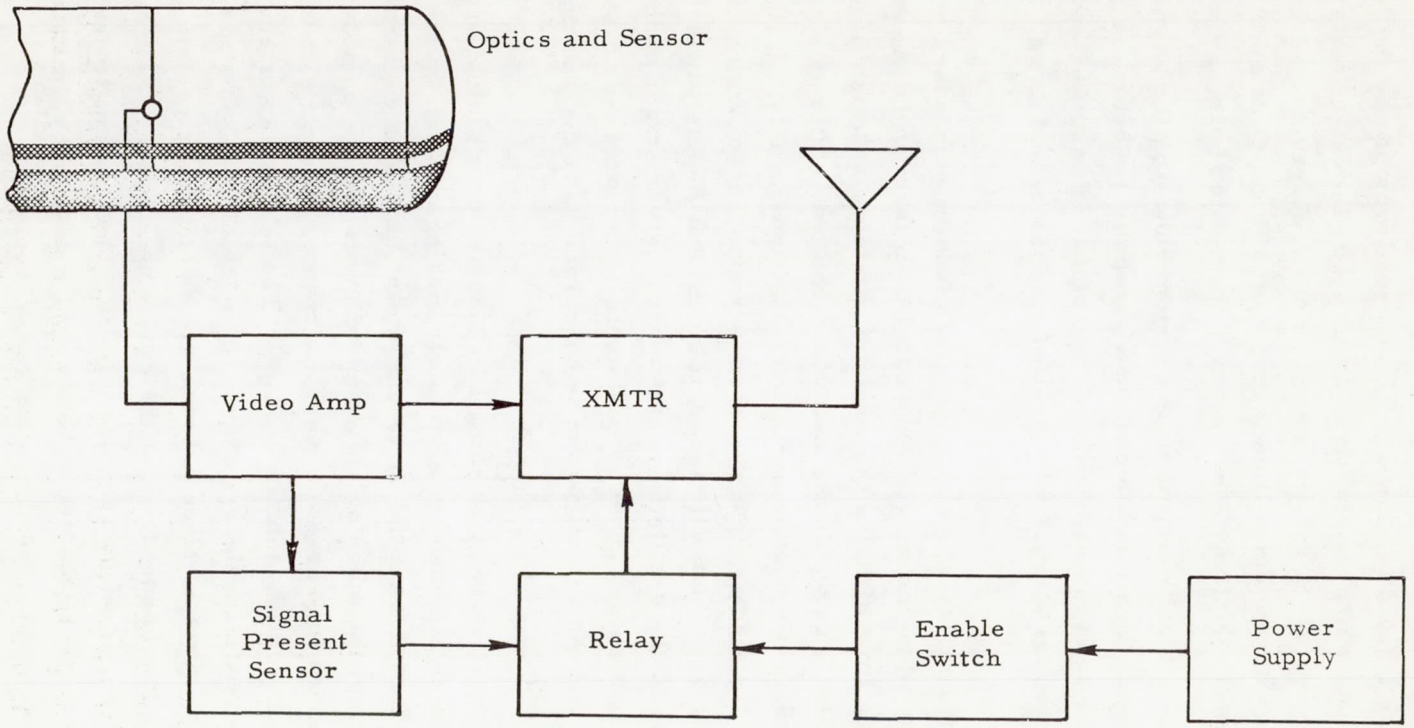

Figure 2-63. NOTS TV System.

2.2.7 Temperature Measurement

Thermometers of two types were included in Pioneers I and II. These instruments were carried so that some estimate of the operating temperatures of the various pieces of equipment within the vehicle could be made. The temperatures recorded by these instruments are those of the elements themselves, and may be at some variance with the temperatures of other components in the package. The possibility of such a discrepency is due to the fact that thermal equilibrium is attained by radiative processes since conductive and corrective processes are not present, the components being separated by insulating materials and a vacuum.

Of the two thermometers, one is a thermistor, the resistance of which controls the frequency of a subcarrier oscillator. The thermistor was mounted on an insulator inside the vehicle. The second is an electronic circuit the output of which, with constant voltage input, varies with temperature. The output of this circuit was used primarily as a calibration voltage for the ionization chamber experiment. This circuit was contained in a metal can. Schematics for subcarrier oscillators, including thermistors, are shown in Figures 2-64, 2-65, 2-66.

The temperature of the thermistor during the flight of Pioneer I is shown in Figure 2-67. The temperature indicated by the ionization chamber calibration was about $50 \pm 10°F$ at 19 minutes after launch and had dropped to a value below $32 \pm 10°F$ after two hours. The low temperature readings of the latter device are based upon an extrapolated calibration and are not reliable. Over the first two hours of the flight the temperatures as measured by these two devices agreed within approximately $10°F$. The values indicated by the ion chamber calibration pulse for later times were not included on the calibration curves, thus requiring extrapolation.

For Pioneer II the temperature history of this flight, as measured by the thermistor, is shown in Figure 2-68 . The temperature, as indicated by the calibration pulse, remained approximately constant at $68 \pm 5°F$ over the first 15 minutes of the flight.

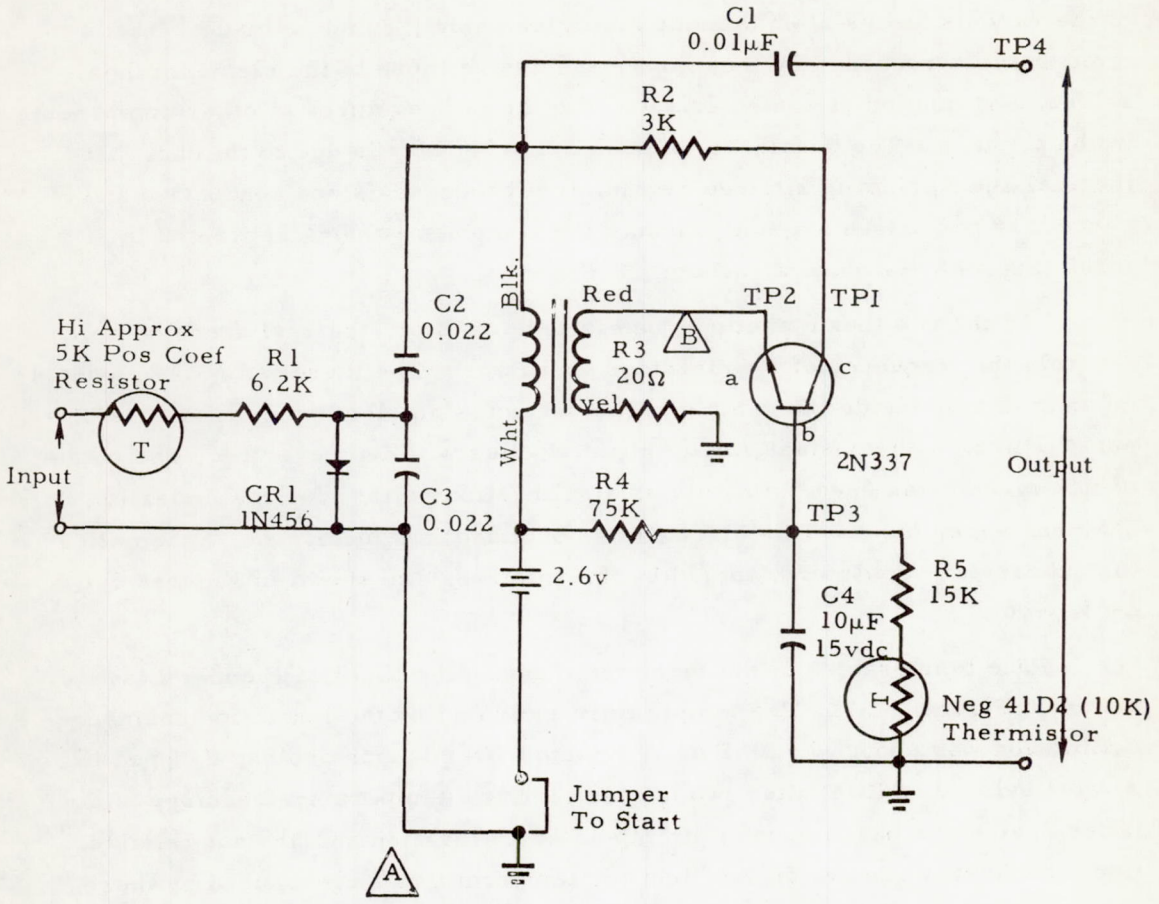

Figure 2-64. Subcarrier Oscillator Band 2

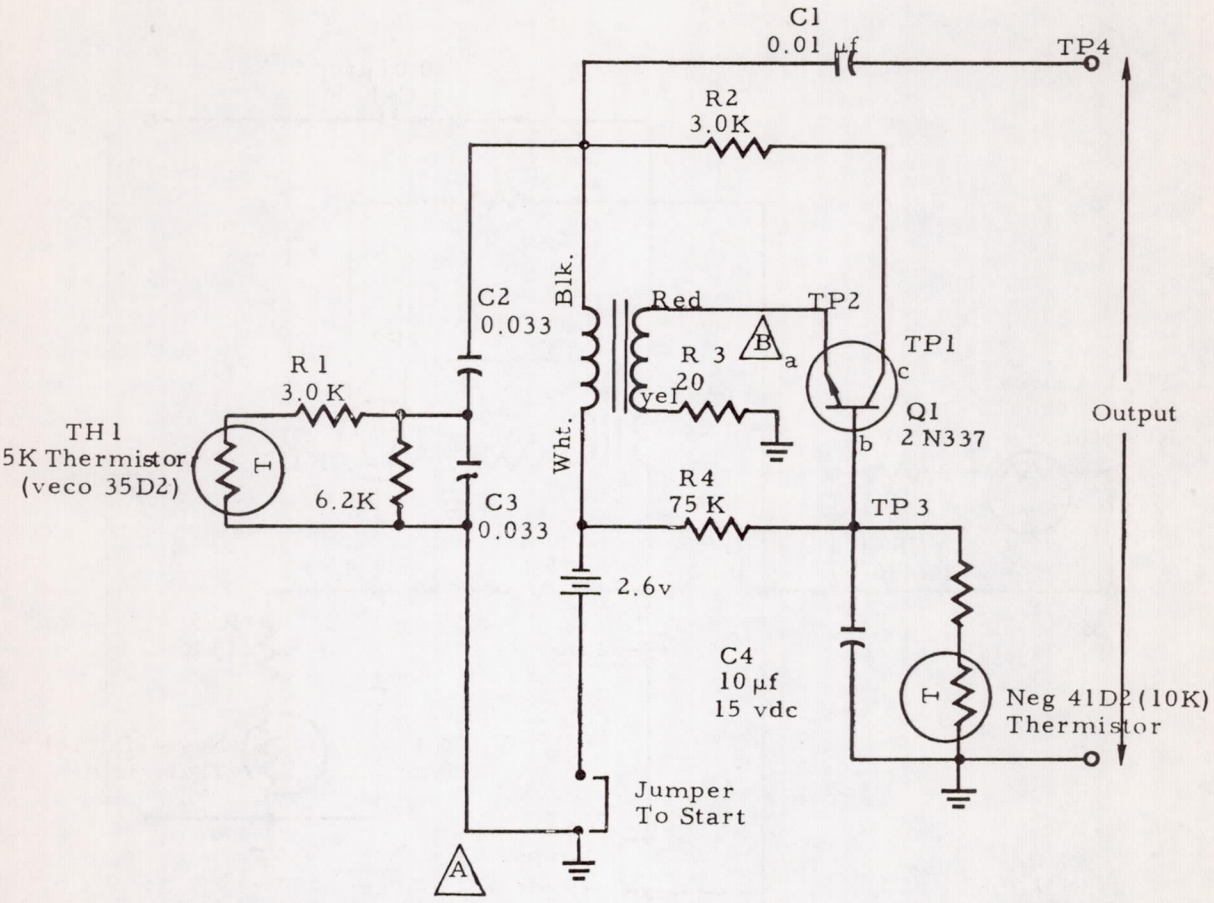

Figure 2-65. Subcarrier Oscillator Band 4.

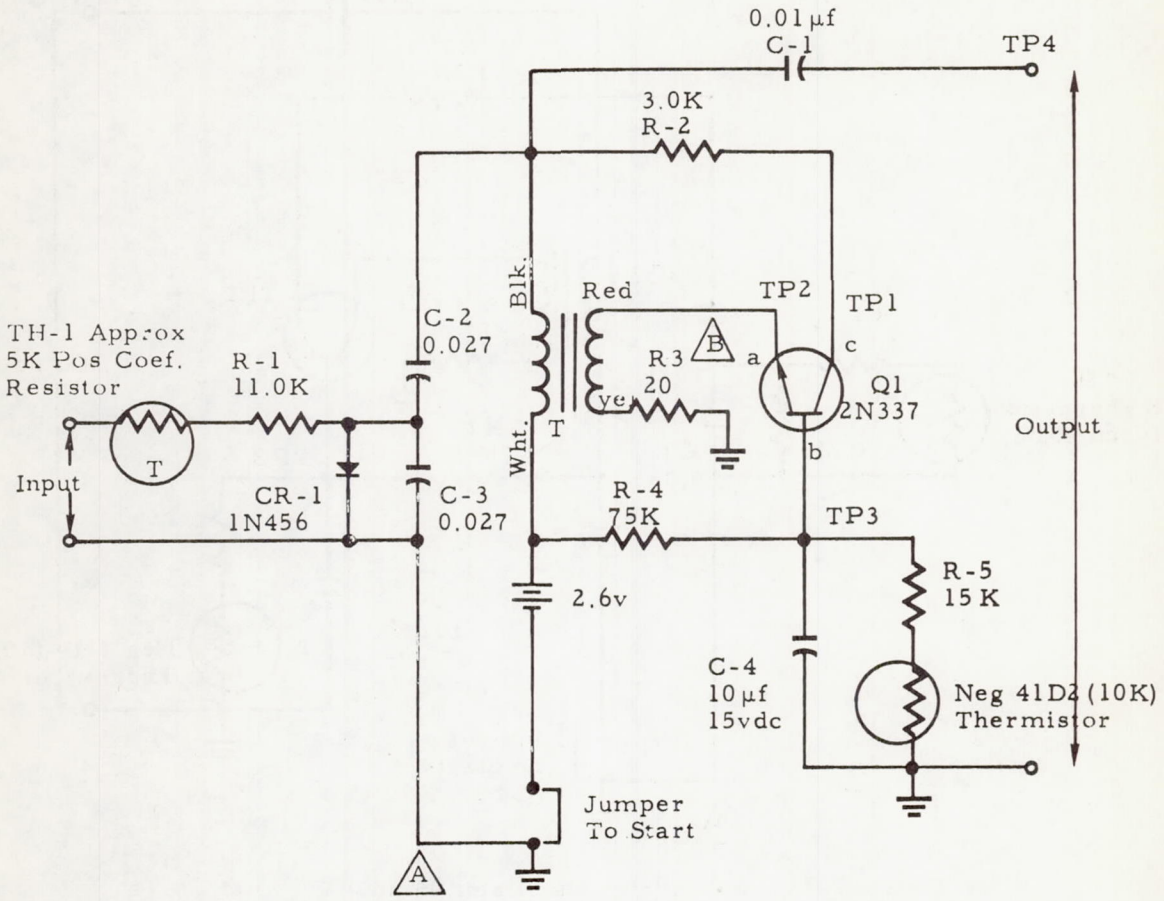

Figure 2-66. Subcarrier Oscillator Band 5.

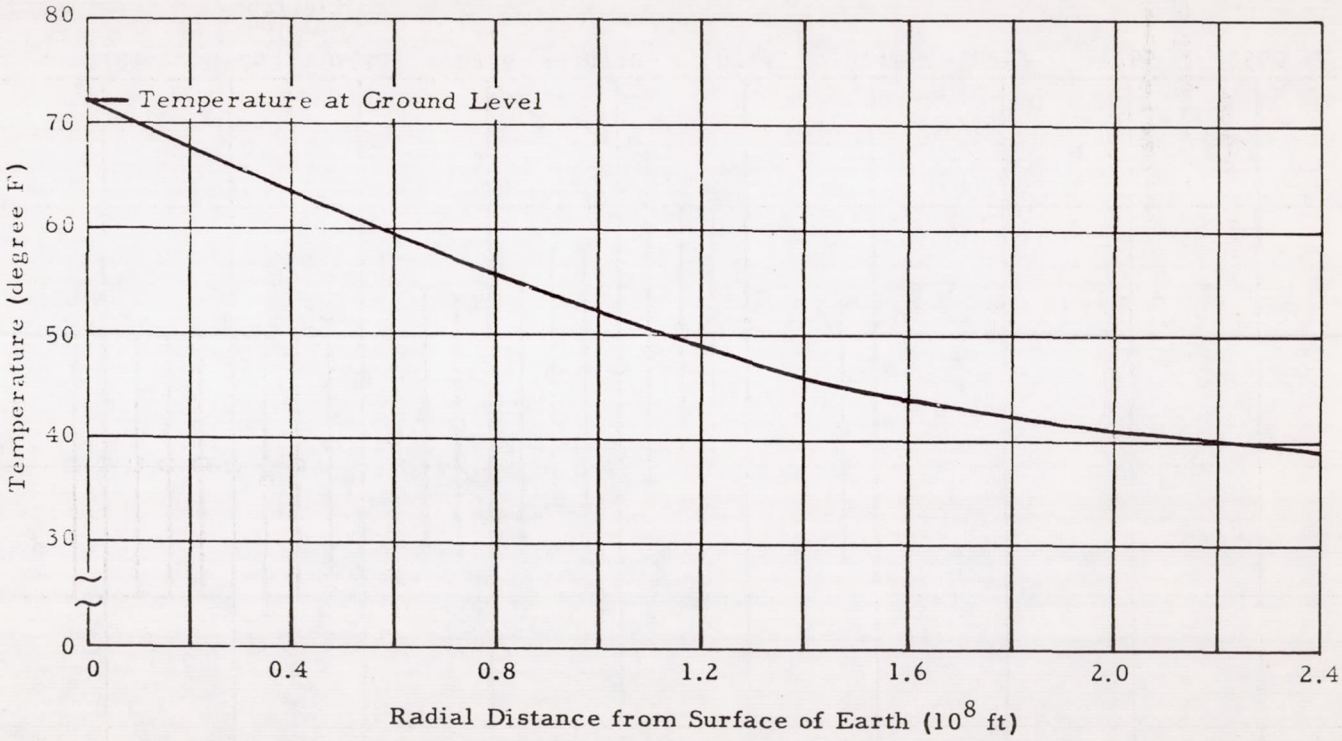

Figure 2-67. Temperature Versus Radial Distance from Earth's Surface for Pioneer 1.

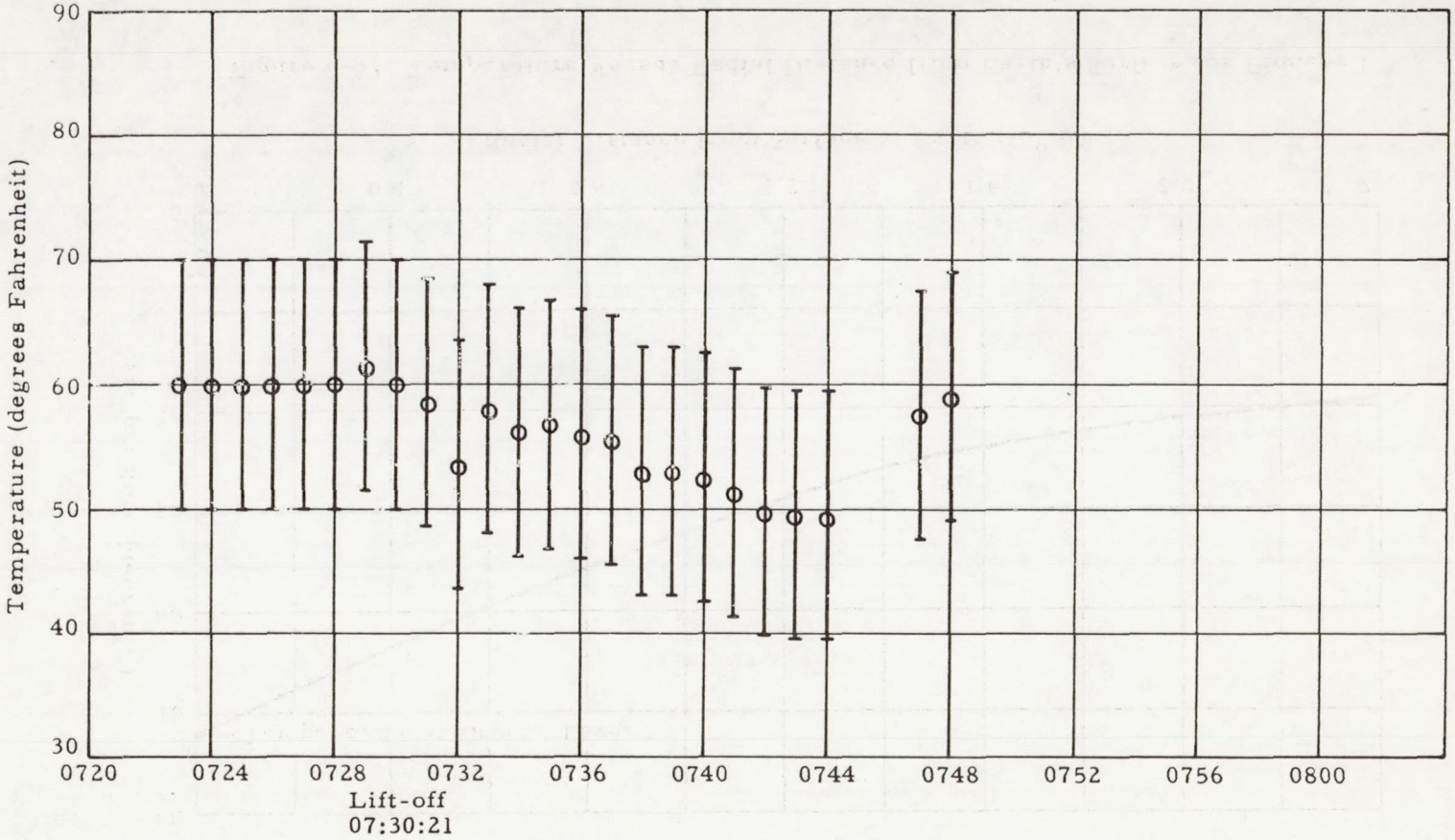

Figure 2-68. Temperature History of Pioneer II.

2.3 Telemetry

2.3.1 Introduction

Range, weight, and equipment considerations yielded a telemetry design which incorporated a signal-to-noise ratio of 10 db over a 10-cps passband. A payload transmitter of 300-mw power using an isotropic antenna was therefore needed to meet the requirements dictated by the system parameters of the ground station receiving equipment (see Section 2.2). The effective signal-to-noise ratio reflects directly into the spectrum of the subcarrier lines so that for a 10-db ratio the power within the side bands, associated with a particular instrument, is functionally dependent on the information passband.

2.3.2 Transmitters

The telemeter in Pioneer I consisted of a wholly transistorized 300-mw r-f generator operating at 108.06 mc. The same oscillator was carried on Pioneer II with the addition of a 100-mw r-f generator operating at 108.09 mc. Both transmitters were phase modulated by a complex subcarrier spectrum applied through a multiplexing amplifier (Figure 2-69) which summed the outputs of the various subcarrier oscillators.

The 300-mw transmitter on Pioneer I (Figure 2-70) served both as telemetry transmitter and the return link of the two-way coherent doppler system (see Section 2.4). Normally telemetry was transmitted, but on command from the ground the crystal control and modulation was removed and the telemetry ceased.

During the first 17 minutes of the Pioneer I launch phase, the coherent doppler was operative, but at T + 17, when the vehicle was at an altitude of 2000 nautical miles, telemetry transmission began. Subsequent interruptions resulted from commands for vernier cluster separation and retrorocket firing and range-rate interrogations (see Figure 2-71).

This telemetry-doppler transmitter included the four parallel transistor-stage output as well as the driver stage and the modulation unit

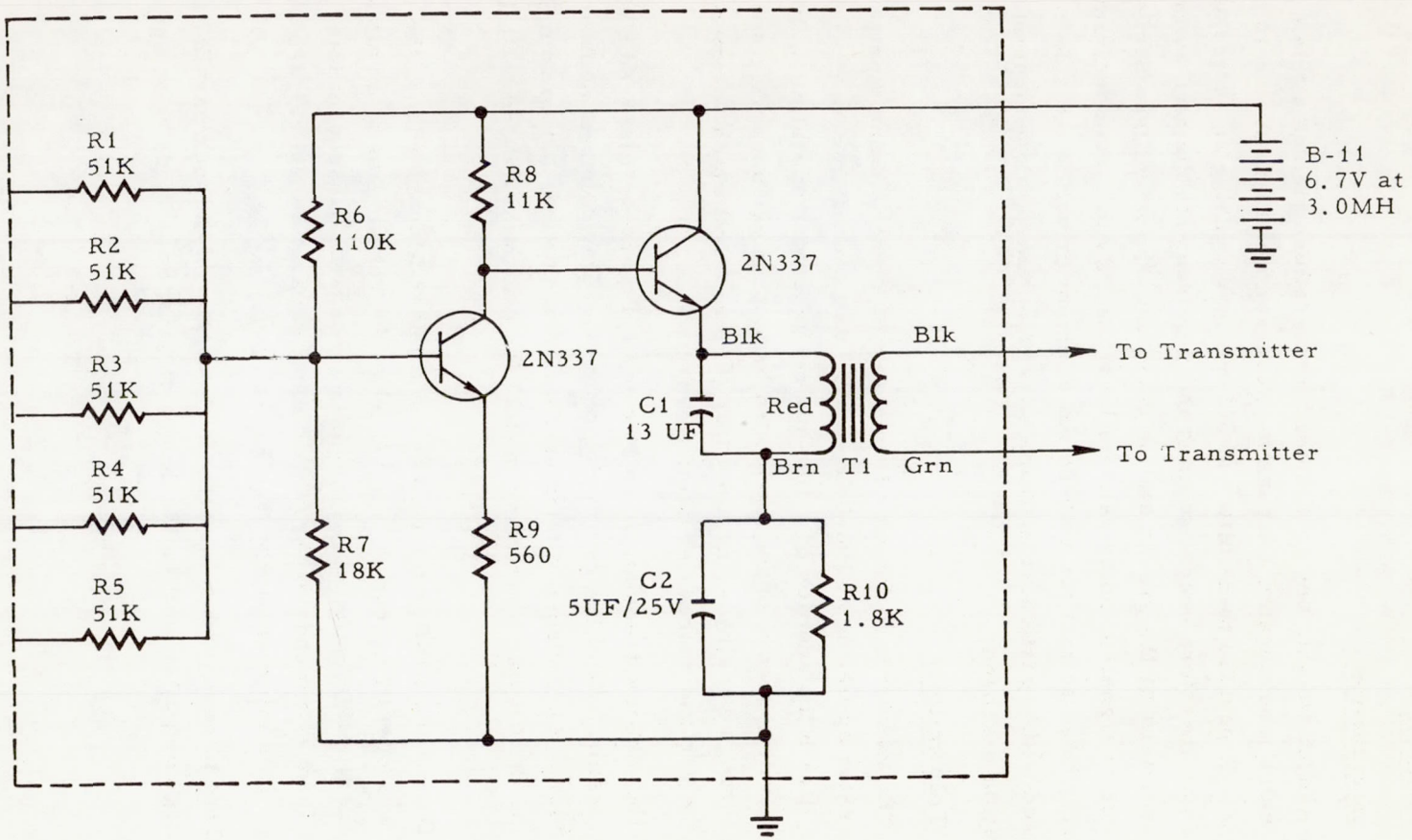

Figure 2-69. Schematic of Multiplex Amplifier.

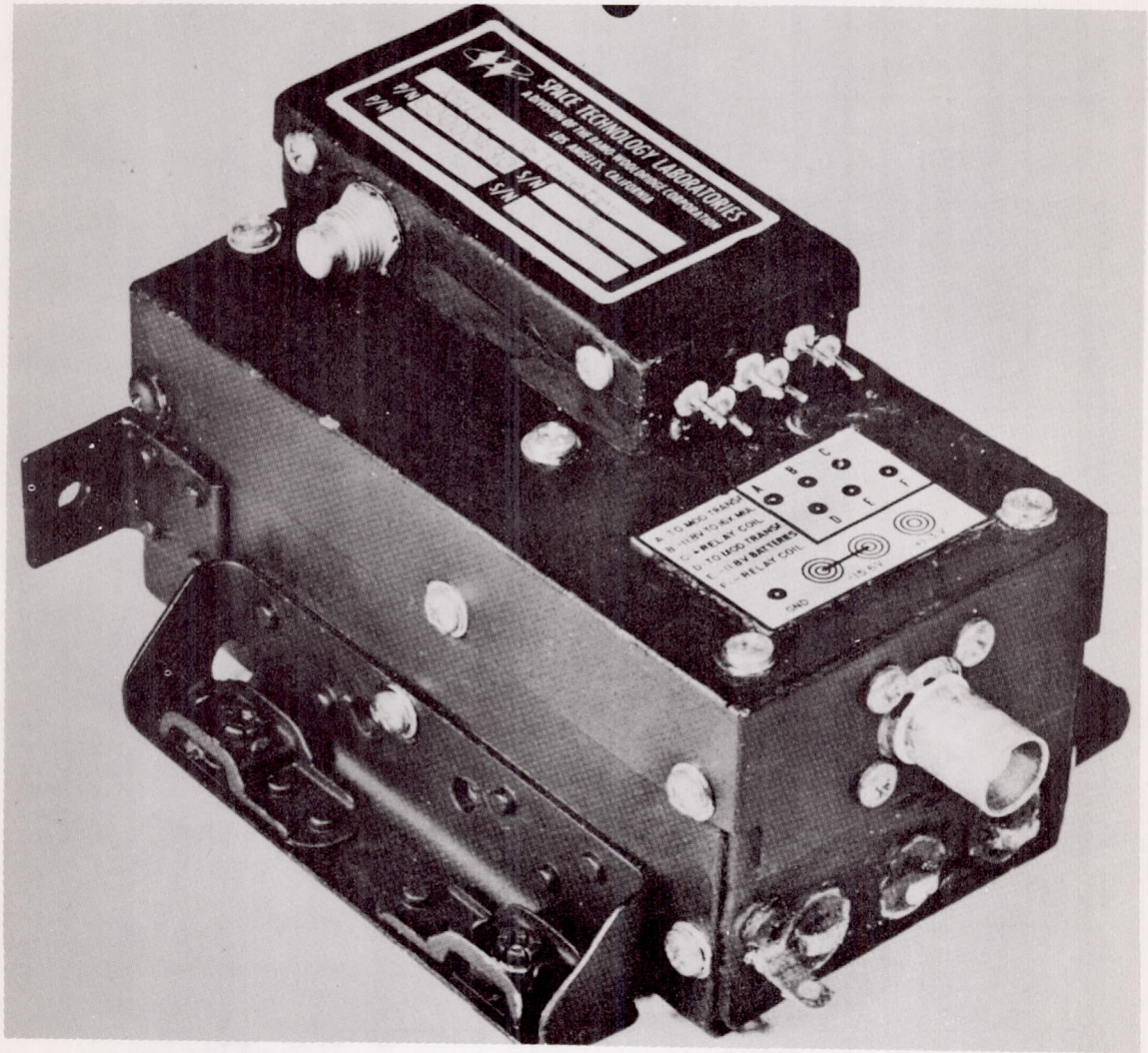

Figure 2-70. Telemetry-Doppler Transmitter.

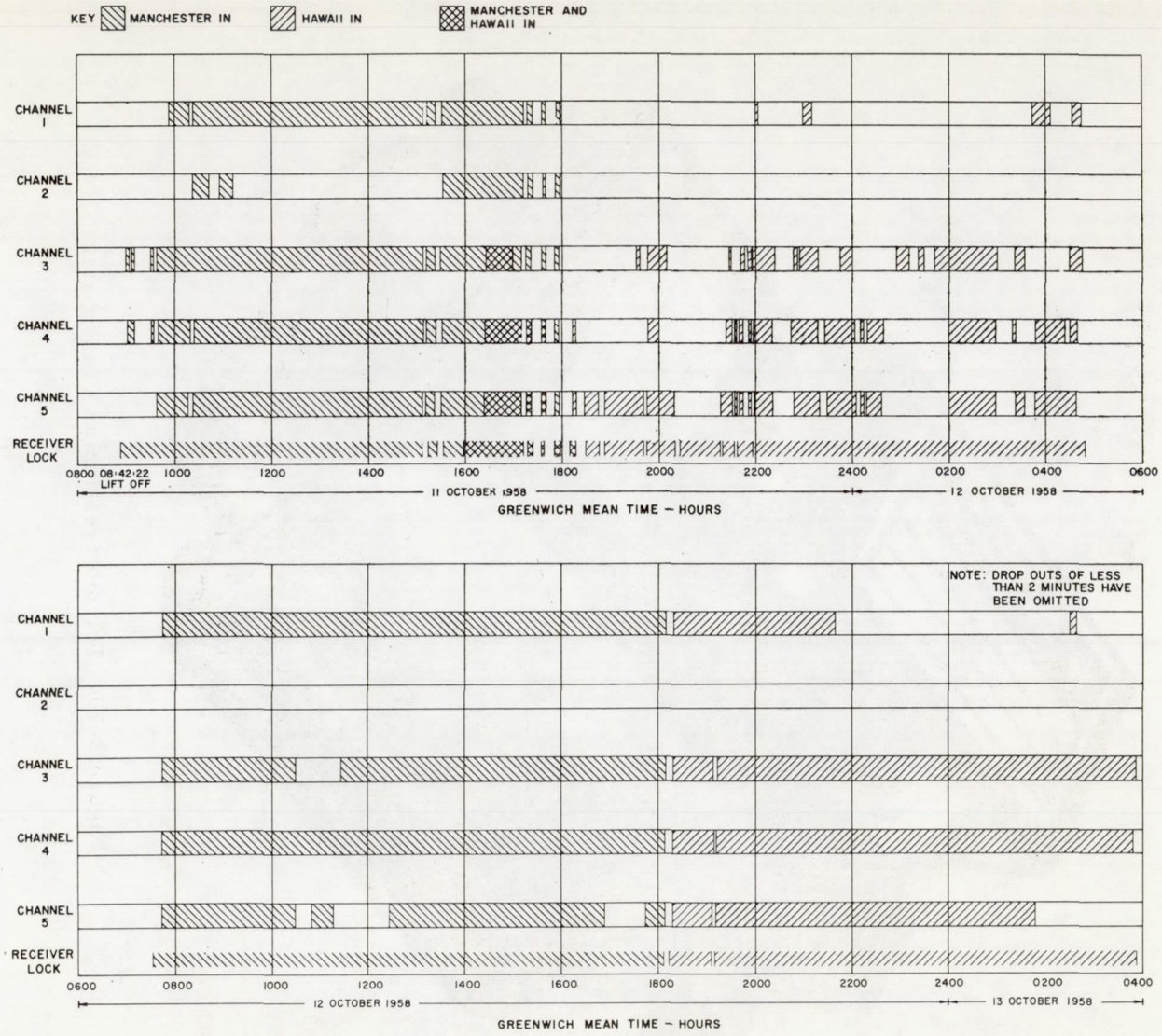

Figure 2-71. Telemetry Reception at Various Stations (Flight 2).

(Figure 2-72). It was a three-stage, crystal-controlled, phase modulated device, with output power 300 mw into 50 ohms, distortion less than 5 per cent, phase jitter less than 0.6 degree, and frequency stability better than 2 parts in 10^7. Before each flight the transmitters were shake-tested at 30 cps and 2000 cps and heat-tested from $10^{\circ}F$ to $105^{\circ}F$.

For Pioneer II the 100-mw telemetry transmitter was included to supply telemetry data during doppler interruptions. This transmitter was to supply continuous telemetry during its battery lifetime of 100 hours. The same subcarrier complex was transmitted on both the 100 and the 300-mw units. The 100-mw transmitter consisted of a phase-modulated oscillator operating at 54 mc, a frequency doubler, and a final power amplifier stage (Figure 2-73). Total input power versus output power gave an over-all efficiency of approximately 40 per cent.

The oscillator was of the grounded base type, using a Philco 2N500 transistor. Crystal control was obtained by inserting a series resonant crystal into the feedback loop, with phase modulation varying the collector voltage. The doubler stage used a WE 45015 transistor in the grounded emitter and delivered approximately 20 mw with an input of 100 mw. The final r-f amplifier employed a WE 45015 in the grounded collector with power output coupled to the antenna through a capacitive-impedence divider network.

2.3.3 Subcarrier Oscillators

Each of the experiments on Pioneer I was fed to the input of a subcarrier oscillator. The five subcarrier oscillators carried in Pioneer I corresponded to the first five RDB standard channels beginning with 400 cps and ending at 1300 cps center frequency (see Figure 2-74). Guard band specifications for the RDB standards were observed. Channel 1 contained ion chamber information, Channel 2 magnetometer data, Channel 3 temperature data, and Channels 4 and 5 micrometeorite data. The output of each of the subcarriers was an audio tone whose frequency was dependent upon the input signal and therefore upon the physical information. The subcarrier spectrum was then summed into the multiplexing amplifier so that a composite was obtained which was used to

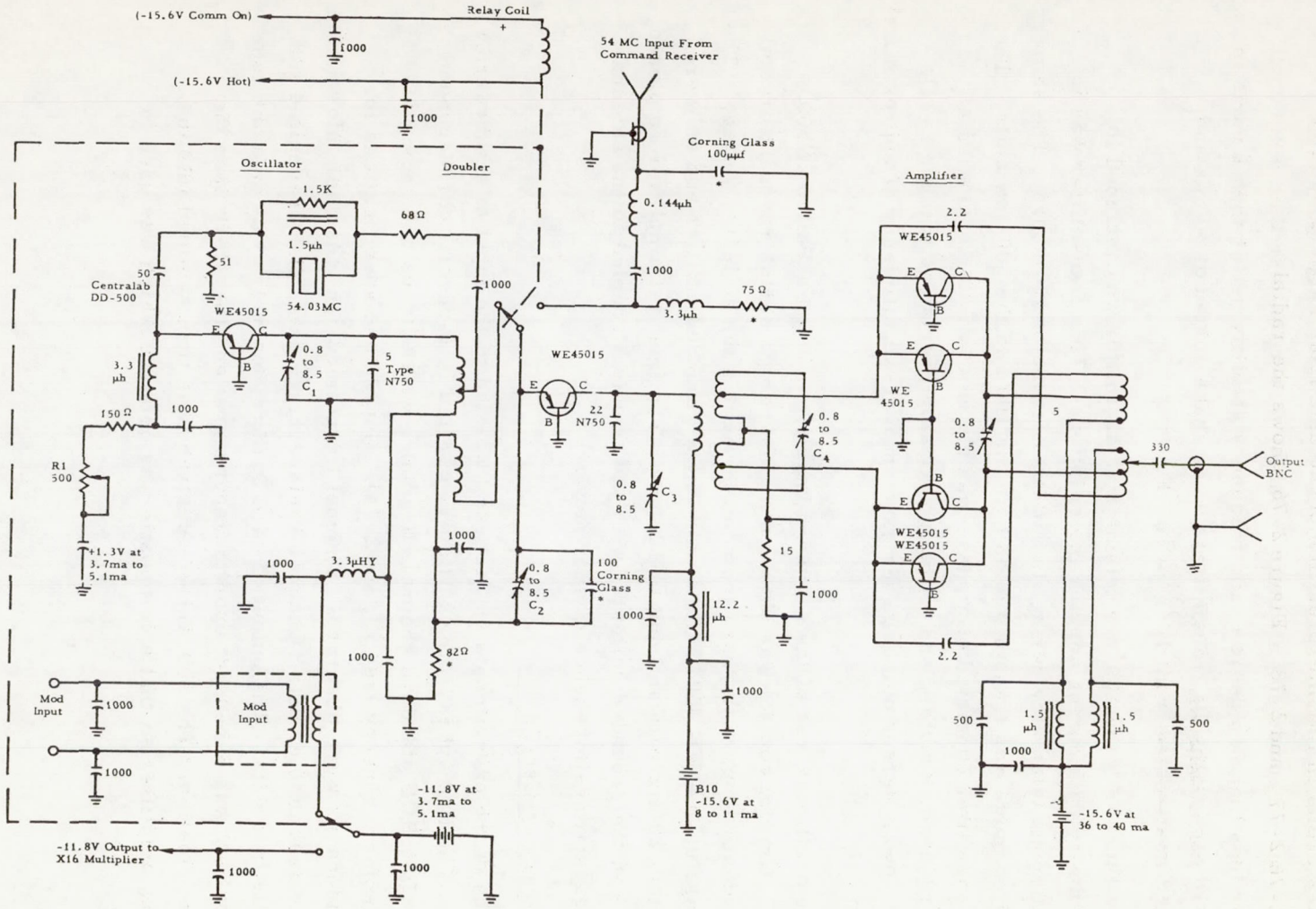

Figure 2-72. Schematic of 300-mw Transmitter.

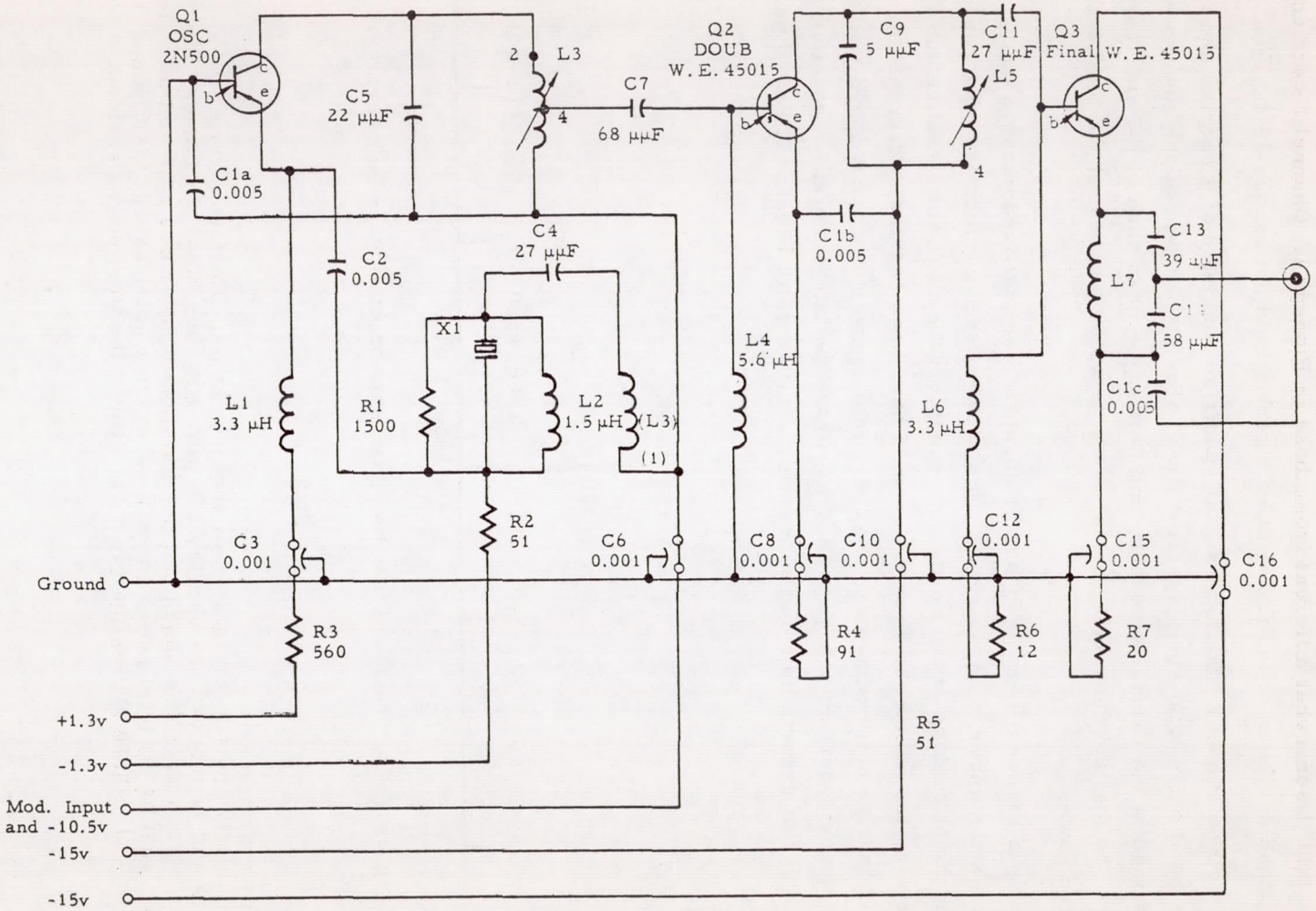

Figure 2-73. Schematic of 100-mw Transmitter.

modulate the transmitter. Design criteria indicated that the rms value of the phase deviation of the transmitter signal should not exceed 30 degrees.

For Pioneer I the total signal spectrum consisted of a carrier and five side-band pairs totaling 11 spectral lines. Eighty per cent of the power was contained in the carrier frequency and four per cent in each of the side-band pairs, so that the subcarrier complex contained 20 per cent of the total transmitted power.

In Pioneer II, six subcarrier channels were utilized because of the increased number of experiments. Since the effective information passband from the Microlock receiver is 4 kc, considerably more than the five subcarriers, the number in Pioneer I, could have been carried. With the addition of subcarrier discriminators, however, more power was apportioned to the subcarrier spectrum. A greater rms phase deviation therefore resulted and the order of experiments and subcarrier oscillators in Pioneer II had to be

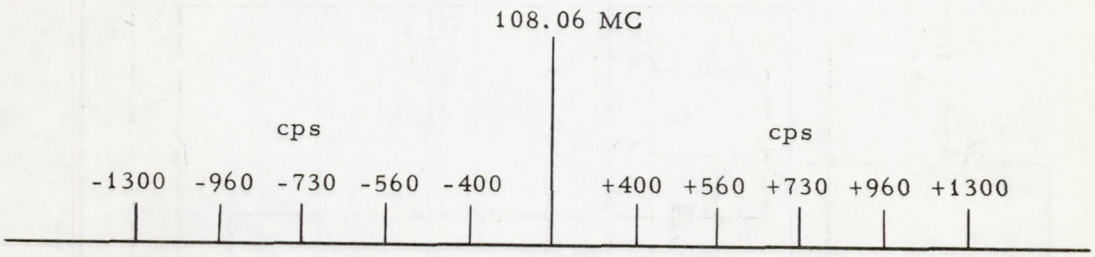

Figure 2-74. Total r-f Spectrum as Seen for Stationary Subcarriers.*

*The relative power levels are not shown to scale. Each subcarrier pair contained 12 mw and the carrier 240 mw, a 4:1 division. In Pioneer II a sixth subcarrier was added and the division of power was adjusted to yield 3 per cent of the total power in each subcarrier pair, except for Channel 3 (STL-TV), where approximately 8 per cent of the total power resided.

somewhat different from those in Pioneer I. Channel 1 carried ion chamber information. Channel 2 carried the magnetometer data. Channel 3 carried the STL television signal. Channel 4 consisted of two multiplexed pieces of information: the micrometeorite total count rate and temperature data. (The two-level micrometeorite momentum spectrometer was abandoned for this flight because of the lack of telemetry capacity within the six subcarriers.) Channel 5 carried the signal rate on the triple-coincidence proportional counter telescope, and Channel 6 the triples rate which was multiplexed with the AGC voltage from the magnetometer amplifier. The AGC voltage was transmitted to increase the range over which the magnetometer could be read, since the AGC signal was a more slowly varying function than the 2-cps tone.

Each subcarrier oscillator is basically a Hartley oscillator (Figure 2-75), employing a variable resistor in shunt with one of the frequency determining capacitors for frequency modulation. The oscillator employed the six lowest standard IRIG channels, namely 400, 560, 730, 960, 1300, and 1700 cps. A thermistor was used for temperature measurements with a suitable resistive network to control the frequency of oscillation. The oscillator was modulated for analog measurements by employing the nonlinear characteristic of a semiconductor diode. This provided variable resistance and hence control of the oscillation frequency.

The oscillator required a current of approximately 140 microamperes at 2.7 vdc. The two RM 625 mercury cells provide approximately 75 days of operation. Temperature compensation is provided by the use of a thermistor in the amplifier bias network. A positive temperature coefficient resistor of Balco wire was used to cancel the effects of temperature on the modulating diode. Temperature drift was limited to 5 per cent of bandwidth maximum for variations of $32^{\circ}F$ to $150^{\circ}F$.

The nominal sensitivity was 0 to 150 microamperes input current for full bandwidth deviation, but each experiment was matched to its subcarrier. Calibration, deviation, and temperature effects were also determined for each set of experiment oscillators.

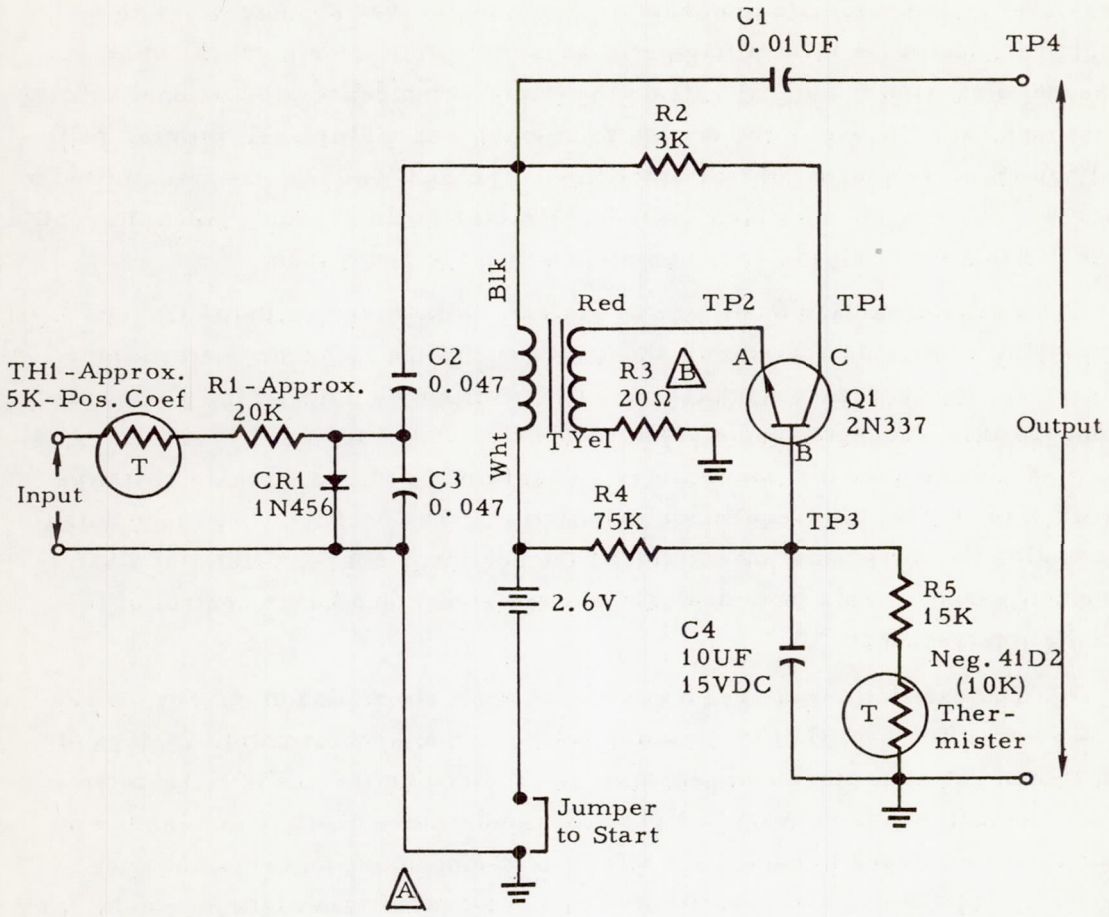

Figure 2-75. Subcarrier Oscillator Band 2.

The outputs of the subcarriers contained approximately 8 per cent of predominately second harmonic distortion. Since phase modulation was employed, and also since the amount of radiated power available for the subcarriers was limited, low pass filters were used.

A multiplexer was designed to sum resistively the outputs of the subcarrier oscillators and to amplify the resultant composite wave form to a level capable of modulating the crystal controlled transmitter. The summing network performed two functions: (1) it provided a linear summing circuit and (2) by proper selection of the resistor value it set the r-f deviation schedule. The composite signal was amplified and the output transformer coupled. Modulation for the transmitter took the form of superimposing the audio signal on the oscillator supply battery.

Final adjustment of the telemetry system and study of the subcarrier oscillators took place at AFMTC. The final check of the system was made with the fourth-stage payload mounted in place. Each of the experiments, in turn, was activated--the magnetometer by a bar magnet, the micrometeorite by striking the diaphragm, and the radiation experiments by means of a Cobalt 60 source. In addition to preparations, final calibration of the sensors for the third flight took place at AFMTC in the payload laboratory.

2.3.4 Data Collection for Flight 2

The telemetry on Flight 2 was designed to function over all flight intervals except for doppler breaks and lock time from the various stations. During the first 17 minutes of this flight, the doppler lock removed the subcarrier modulation from the transmitter. At T + 17 telemetry was activated and signals were received at Manchester. Due to the deviation in the flight path of the vehicle, the antenna tracked on a side lobe for the first hour. Estimates of the side lobe degradation vary from 30 to 40 db. The result was loss of lock for a good portion of the first hour's flight. However, sufficient lock time occurred to enable radiation measurements to be made on the descending side of the intensity curve. Magnetometer data were irregular, apparently because of a faulty subcarrier oscillator, since there was a loss of the spectrum lines in Channel 2 while the tape was being played.

Several quantities useful in the interpretation of the data from Flight 2 are shown in Figures 2-76, 2-77, and 2-78. Figure 2-76 shows the radial distance from the center of the earth plotted as a function of the time after lift-off. Figure 2-77 shows the inertial velocity as a function of the time after lift-off. Figure 2-78 shows the locus of the vehicle in geographical coordinates, with the corresponding radial distance indicated at a number of points on the locus.

2.3.5 Data Collection for Flight 3

The principal receiving sites for this flight were Manchester, ABAMA-Hold (located at AFMTC), NRL (AFMTC), and Radiation, Inc. at Malabar, Florida. Manchester data were limited to short segments as the result of the low apparent altitude of the vehicle as seen by Manchester. This look-angle problem resulted in serious multipath problems and consequent excessive fading and loss of receiver lock. The data have been exhaustively checked for receiver lock, and it is believed that all regions of lock have been demodulated. Some further work on the tapes is being done, especially to check Channel 6, the proportional radiation counter singles rate.

For this flight Figure 2-79 gives the radial distance from the center of the earth to the vehicle plotted as a function of the time after lift-off. Figure 2-80 shows the inertial velocity of the vehicle as a function of the time after lift-off.

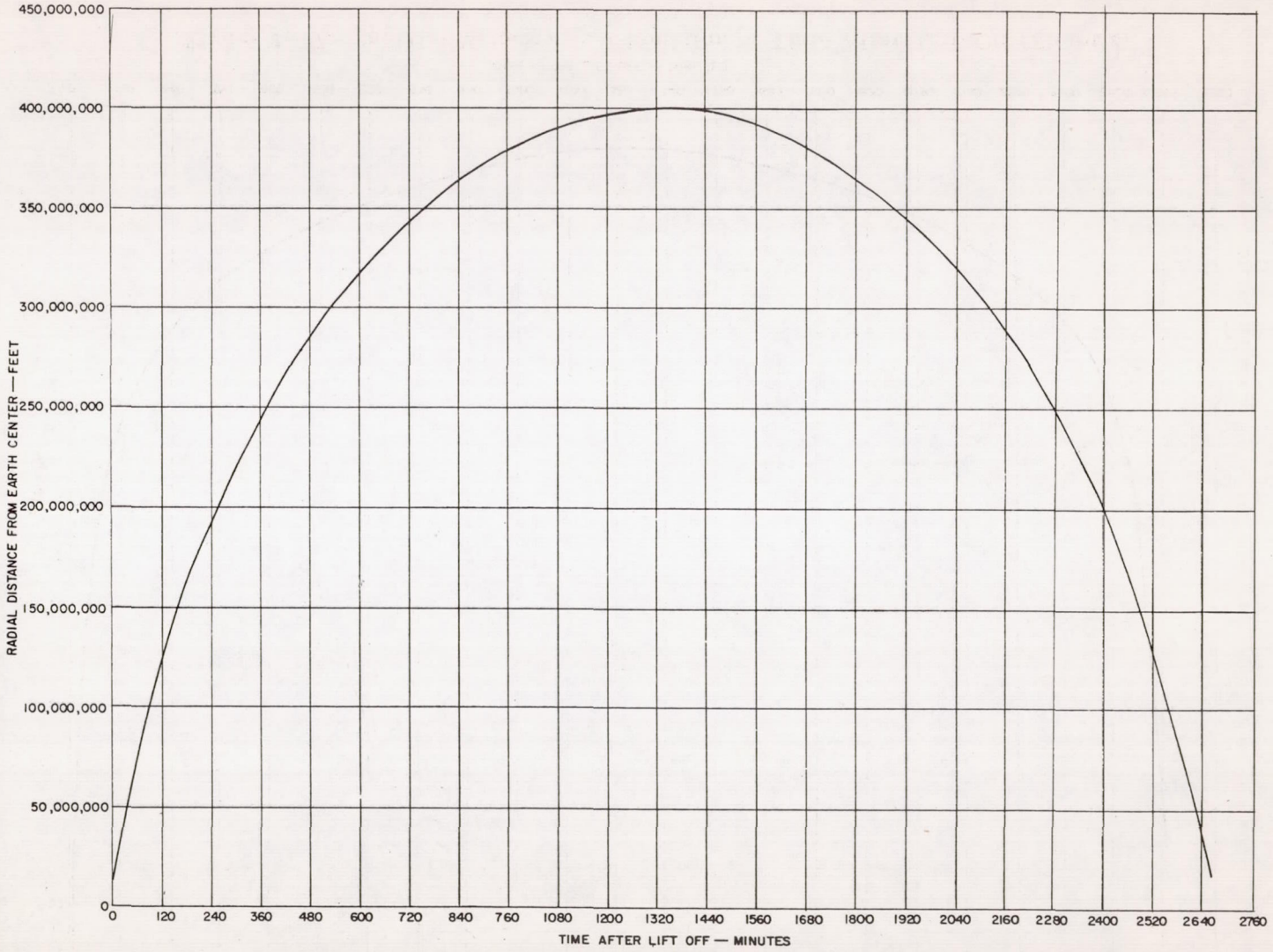

Figure 2-76. Radial Distance from Center of Earth as a Function of Time After Lift-Off (Flight 2).

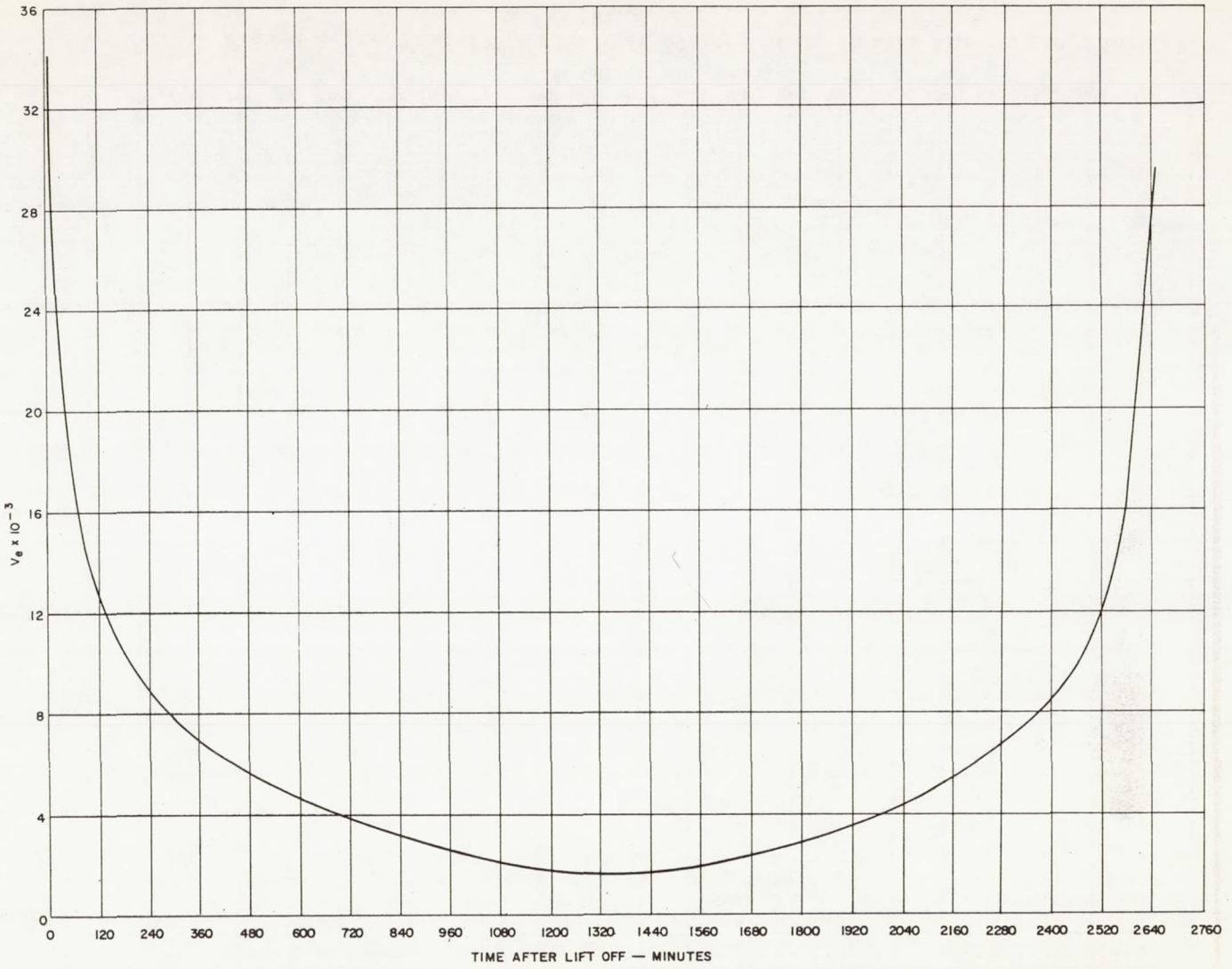

Figure 2-77. Inertial Velocity as a Function of Time After Lift-Off (Flight 2).

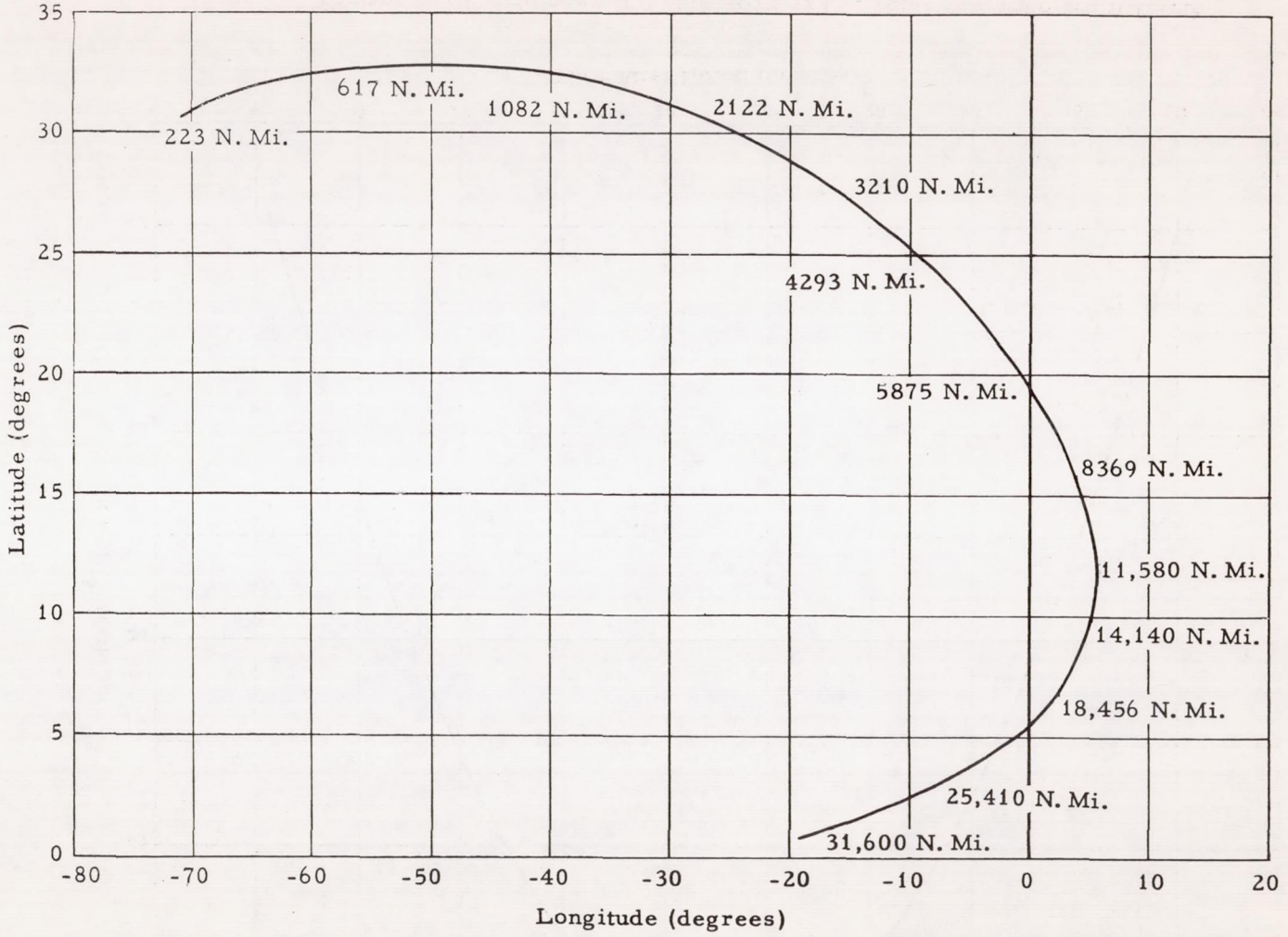

Figure 2-78. Pioneer I Trajectory No. 61 Longitude as a Function of Latitude for First Four Hours of Flight.

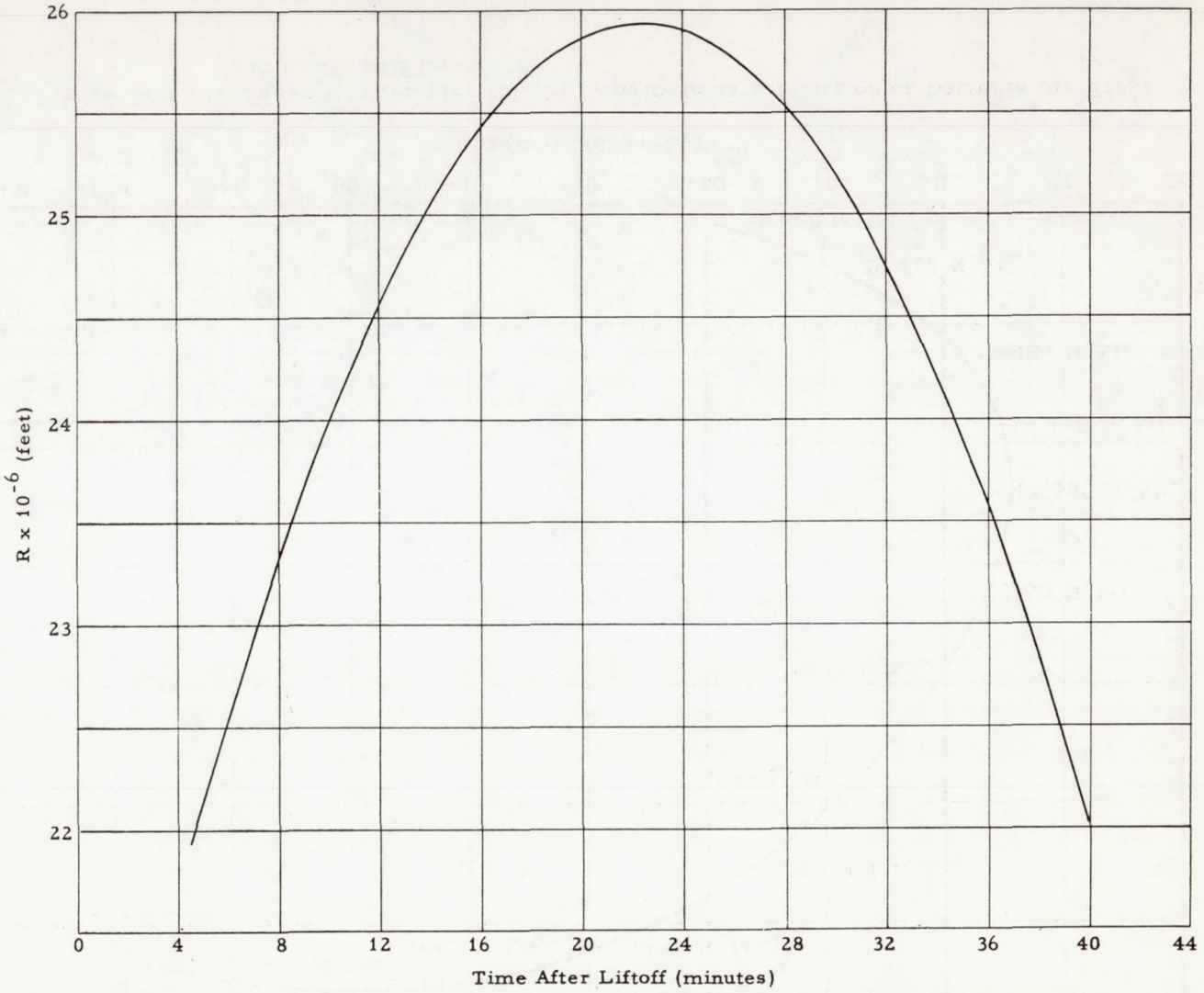

Figure 2-79. Pioneer II Trajectory T4 Radial Distance from Earth Center as a Function of Time after Lift-off.

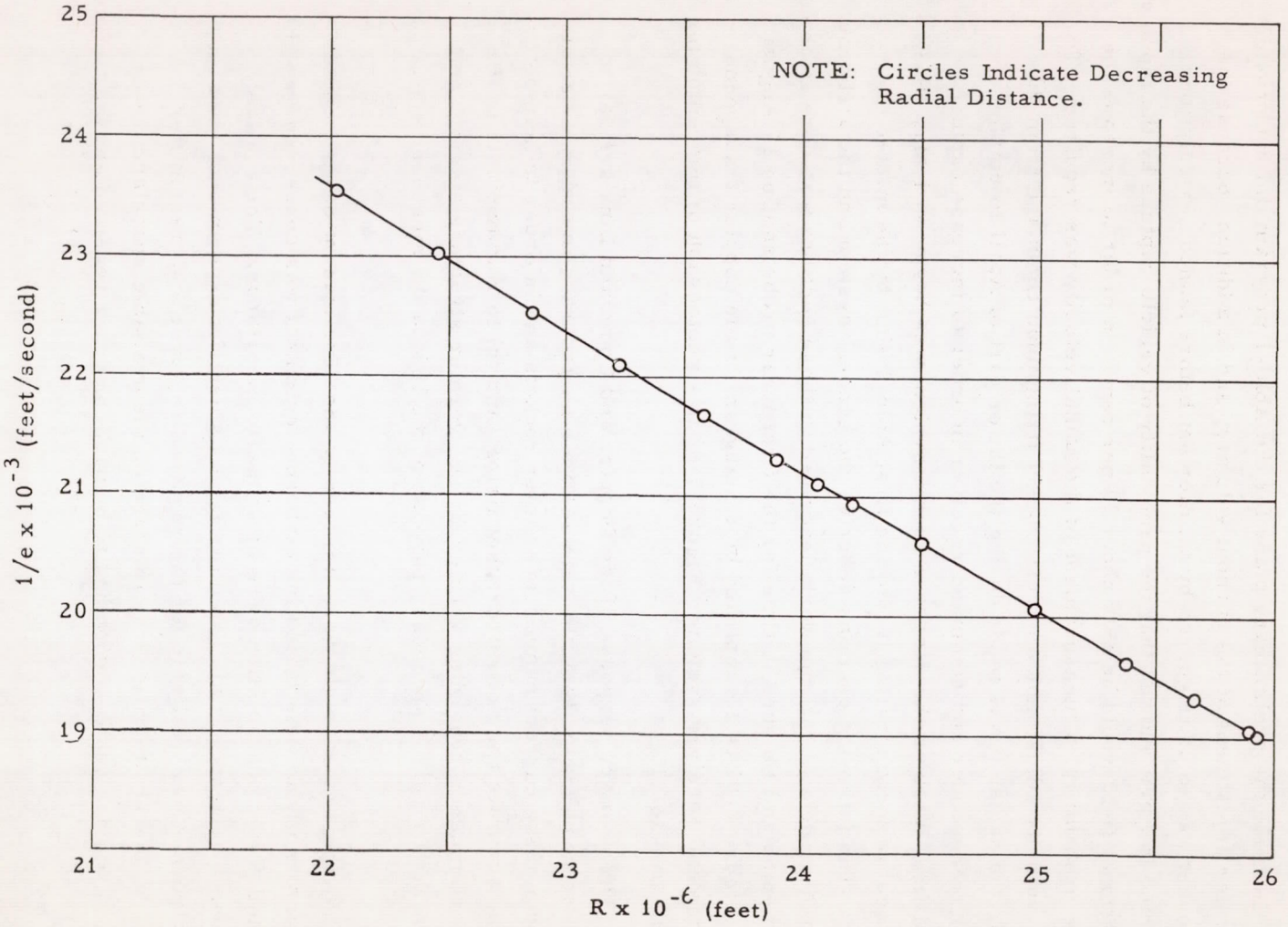

Figure 2-80. Pioneer II Trajectory T4 Inertial Velocity as a Function of Radial Distance from Earth Center.

2.4 Command/Doppler System

2.4.1 Introduction

Because the preliminary plans for the Able-1 program did not provide for vernier adjustment of the burnout velocity; and in addition, because the retrorocket was to be triggered by a timer set before launch, calculations performed in April showed that the probability of vehicle capture by the moon's gravitational field would be only about 30 per cent. In order to increase the capture probability, a measurement of the radial velocity was required. To permit velocity adjustment and retrorocket firing upon command from the ground, the decision was made during the latter part of April to employ a doppler transponder and command receiver in order to increase capture probability. Work on the design of such a system was begun on 1 May 1958, with a goal of incorporating it into the first Able-1 shot by the middle of August. The following sections describe the general system and the airborne equipment in detail. All the work described in these sections was done in about three months and finished in time for the first lunar probe shot on 17 August 1958. Figure 2-81 is a simplified block diagram of the doppler transponder and command receiver system. Figure 2-82 is a photograph of the completed airborne package.

The primary purposes of the Doppler and Command Link are (a) to determine radial velocity of the vehicle to a high accuracy in order to permit the firing of the correct number of vernier rockets and in order to help determine the accurate time of retrorocket firing, and (b) to communicate to the vehicle commands regarding vernier firing, vernier structure staging, and retrorocket firing. A secondary purpose of the link is the measurement of range.

Various constraints were imposed on the development of the Doppler and Command Link. As far as the airborne equipment was concerned, weight, size, and power consumption were of primary importance. The available electronics payload was allocated to various scientific experiments, and less than 10 pounds was available for the required receiver and transmitter. A similar stringent limitation was imposed on the available space and power. A simple antenna configuration had to be used, both for received and transmitted

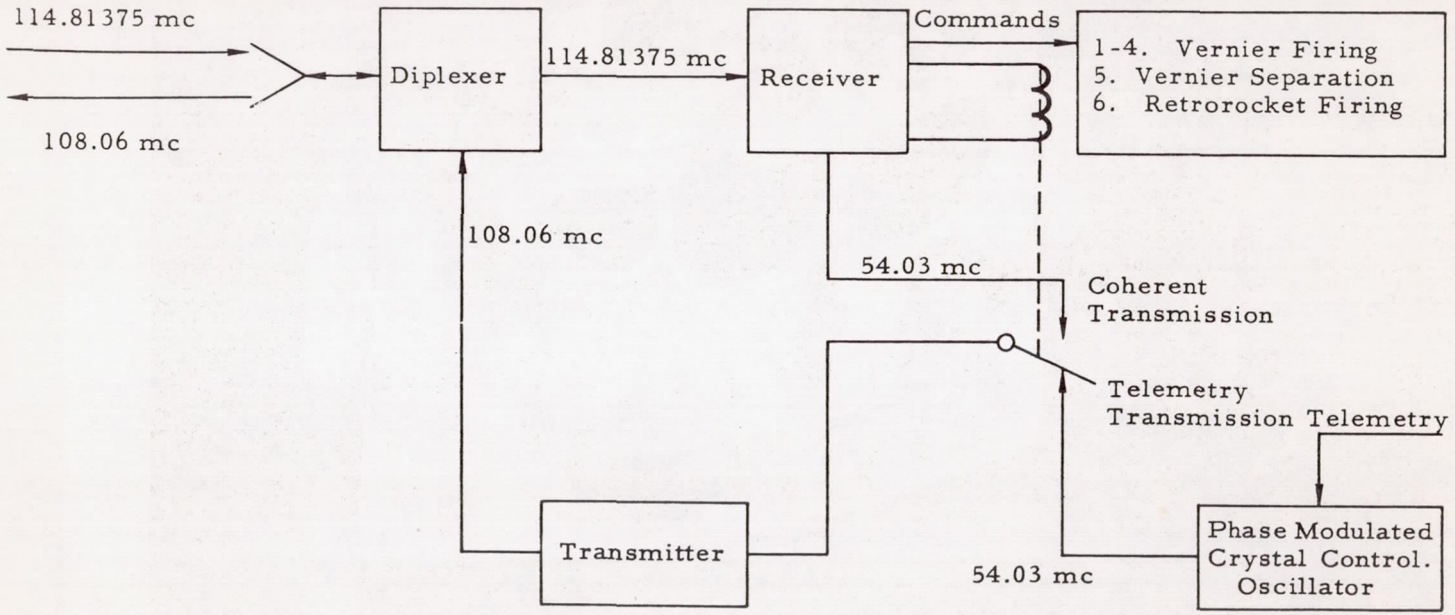

Figure 2-81. Simplified Block Diagram, Doppler Transponder and Command Receiver.

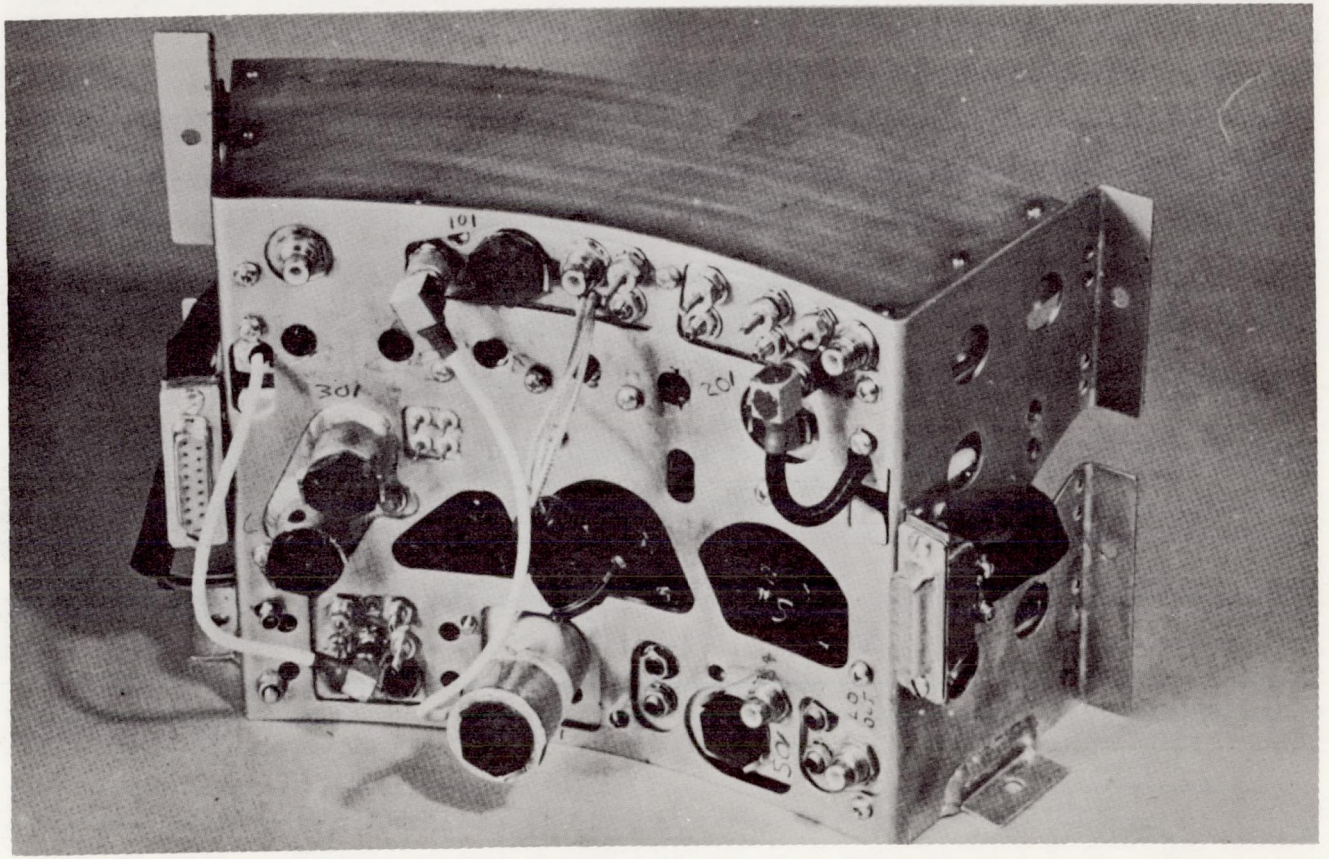

Figure 2-82. Doppler and Command Receiver.

signals. By far the most stringent limitation, however, was the available time, since only three and one-half months lay between the initiation of design and development work on the Doppler and Command Link and the first launch date. This time limitation made it mandatory to use as many existing and available components and proven techniques as feasible. Since some of the ground equipment was already either in existence or on order, including microlock receivers and a large receiving antenna, the system was designed to simplify the airborne package which had to be designed, breadboarded, and manufactured within an extremely short time. A powerful ground transmitter, which could be purchased and installed within a short time, was one of the items which permitted some simplification of the airborne equipment.

A detailed discussion on the choice of the basic parameters for the ground and airborne portions of the Doppler and Command Link will be given in the following pages. The circuit aspects of the airborne subsystem are described in Appendix A.

2.4.2 Basic System Considerations

This section is devoted to a description of the basic considerations which determined the system configuration.

a. Antennas

The characteristics of the antennas on the payload package are determined largely by the fact that the vehicle is spin stabilized. This circumstance, together with the wide range of aspect angles over which the system must function, implies that the payload antenna must be very nearly isotropic. To avoid amplitude and phase modulation of the signal received by the ground tracking station, the polarization characteristics of this antenna must be symmetrical about the spin axis. The antenna chosen was a simple axial dipole. Weight limitations on the payload package required that the same antenna be used for both transmission and receiption. For reception at the primary ground station in Hawaii the Air Force made available a fully steerable 60-foot parabolic dish with a gain of about 24-db at 108 megacycles per second. Because of the relatively high power levels employed for the ground transmitter and because of the very high sensitivity of the microlock receiver,

it was not feasible to employ this dish for transmission also. Instead, a helix of approximately 14-db axial gain was employed for transmission. Both transmitting and receiving ground antennas are circularly polarized. The antennas used for transmission and reception at AFMTC are 14-db helices identical to the transmitting helix at the Hawaii station. Note that the use of a linearly polarized airborne antenna and circularly polarized ground antennas implies a 3-db polarization loss.

b. Transmitter Powers

The power of the ground transmitter in Hawaii is 5 kilowatts. Here the choice of transmitter size was dictated by the fact that the 5-kilowatt transmitter was the largest transmitter readily obtainable on a very short time schedule. The power of the ground transmitter at AFMTC is about 250 watts, which is adequate for the ranges at which its use is required. Considerations of size, weight, and power required that the power of the airborne transmitter should not exceed one watt, and considerably smaller powers were highly desirable. The transmitter developed is a completely transistorized unit which has an output power of between 300 and 500 milliwatts (adjustable); 400 milliwatts is specified for normal operation.

c. Operating Frequencies

The choice of operating frequencies for the system was a compromise between and among a number of factors. Ionospheric effects and the rapid increase in galactic noise with decrease in frequency made it desirable to employ as high a frequency as possible. Size limitations on the payload antenna imposed a further lower bound on the frequencies which could be used. The upper limit on the usable frequencies was set by the requirement that the airborne portion of the system must be completely transistorized. This constraint, together with the available development time, placed an upper limit of slightly in excess of 100 megacycles per second on the band of usable frequencies. Once these decisions had been made, the decision to employ the IGY frequency of 108 megacycles per second for the air-to-ground transmission was almost immediate. This choice of frequency had the additional advantage that existing minitrack and microlock stations could be used to provide additional trajectory

data, at least during the early portion of the flight. The basis for the choice of the ground-to-air frequency will be given in the course of the discussion of the method used to generate a coherent frequency offset.

d. Receiver Type

The choice of the receiver type to be employed was governed entirely by the very great ranges at which the system is required to operate. At a range of 240,000 miles and with the available transmitter powers and antenna gains, the signal power at the airborne receiver is about -110 dbm and that at the ground receiver is approximately -139 dbm.* These estimates suppose a 3-db polarization loss and incidental line and mismatch loss of 2 db. Successful operation at these signal levels required use of receivers with extremely narrow effective bandwidths. Whereas a suitable receiver was available for the ground stations in the form of the receivers employed by the microlock tracking system, no receiver existed which could be modified or adapted for use in the airborne subsystem. Accordingly, it was necessary for STL to undertake development of an extremely sensitive transistorized and ruggedized receiver for incorporation in the payload package. Bandwidth requirements were such that the operation of this receiver could not depend on the long-term stability of a stable reference oscillator. Even had suitably stable oscillators been available, the one-way doppler shift of something in excess of three and one-half kilocycles per second would have precluded their use for this application. The only receiver type which could meet the requirements thus imposed on the airborne equipment was the phase-locked receiver with an equivalent noise bandwidth of a few hundred cycles per second.

e. Coherent Frequency Offset Technique

One of the primary requirements on the airborne subsystem was that it should be capable of functioning as a coherent doppler transponder. For the sake of transmitter-receiver isolation it was essential to provide a method of coherent frequency offsetting or conversion. The method employed for the generation of this coherent frequency offset is illustrated in Figure 2-83. It will be seen from this figure that the output of a voltage-controlled oscillator (VCO)

*The figures quoted are appropriate for the primary ground station in Hawaii.

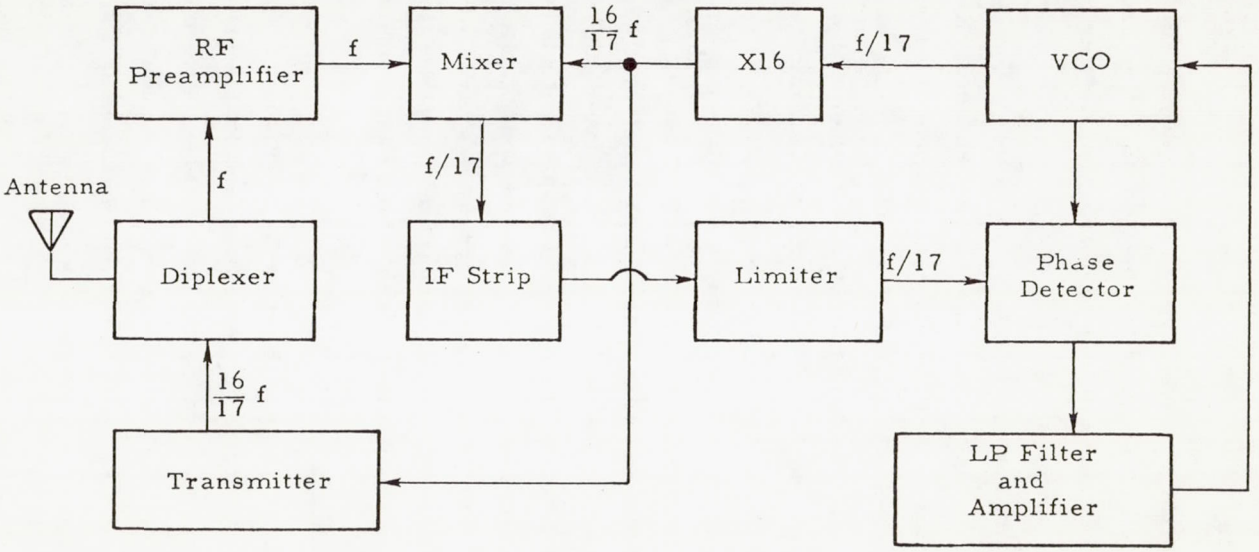

Figure 2-83.. Basic Airborne Phase-Locked Loop and Transponder.

at the intermediate frequency is multiplied by a factor of 16 to obtain the local oscillator signal. The frequency of the voltage-controlled oscillator is controlled by means of an error signal generated by phase detecting the output of the IF strip with respect to the signal from the VCO. Because of the stringent requirement for elimination of sidebands separated from the local oscillator frequency by odd multiples of the intermediate frequency, it was desirable to choose a multiplicative factor which could be realized by a succession of frequency doublers with considerable filtering at the output of each stage. As shown in Figure 2-83, the local oscillator signal is then amplified and transmitted to the ground system. The particular factor of 16 was selected because it permitted a sufficiently great separation between transmitted and received frequencies to allow construction of a diplexer to effect satisfactory transmitter-receiver isolation while, at the same time, the resulting frequency separation was sufficiently small to allow transmitter and receiver to operate efficiently with a single antenna. The specification placed on the diplexer called for at least 30 db isolation between the two channels.

With the configuration illustrated, the local oscillator could be operated either above or below the frequency of the signal received from the ground station. Since no frequency assignment was available in a suitable band below the IGY frequency, it was necessary that the frequency of the ground-to-air signal lie above the frequency of the signal transmitted from air-to-ground. With this requirement on the ground-to-air frequency, the operation of the receiver is such that the frequency of the signal retransmitted by the transponder is precisely $16/17^{ths}$ of that received. Thus, a 108-megacycle per second signal radiated from air-to-ground corresponds to a ground-to-air frequency of 114.75 megacycles per second and to an intermediate frequency of 6.75 megacycles per second. (Actually, the exact frequencies assigned are 108.06000 megacycles per second for the air-to-ground link and 114.81375 megacycles per second for the ground-to-air link.)

The use of the limiter shown at the output of the IF strip has three important implications. In the first place, since the d-c gain of a phase-locked loop is proportional to the amplitude of the signal component of the input to the phase detector, it can be shown that inclusion of a limiter causes the loop to

function in such a way that, as the input signal-to-noise ratio falls, the loop bandwidth is automatically narrowed so as to trade off the dynamic performance of the loop for the narrower noise bandwidth desirable for the case of very low input signal-to-noise ratios. This limiter action has been discussed in considerable detail by Rechtin and Jaffe* in a paper published several years ago. The second implication of the use of a limiter in the IF strip is that, so long as adequate gain is employed, there is no necessity for the use of an automatic gain control. This observation permits considerable simplification in the implementation of the receiver. The third implication of the limiter pertains to the command feature of the receiver and will be discussed at the appropriate point.

f. Doppler Data Extraction

In order to extract the doppler data at the ground station it was necessary, in essence, to generate a reference signal at $16/17^{ths}$ the frequency of the transmitted signal and to beat this signal against the signal received by the microlock receivers. In practice, a considerably more complicated data extraction system was employed than would be indicated by the preceding sentence. This more complex system was chosen in order to avoid generation of a spurious 108-megacycle per second signal which might either saturate the extremely sensitive microlock receiver or cause it to lock onto a signal generated in the data extraction circuitry. The nearest frequency to 108 megacycles per second produced in the doppler data extraction equipment differs from this critical frequency by the frequency of the second IF of the microlock receiver (455 kilocycles per second). To minimize quantization errors, the output of the data extraction circuit is 16 times the doppler frequency rather than the doppler frequency itself.

g. Commands

Commands are encoded onto the ground-to-air signal by phase modulating the transmission with audio frequency tones whose frequencies are considerably higher than the bandwidth of the phase-locked loop. These tones are recovered at the output of the loop phase detector. To provide an additional

*Jaffe, R, and R. Rechtin, "Design and Performance of Phase-Lock Circuits Capable of Near-Optimum Performance over a Wide Range of Input Signals and Noise Levels," IRE Transactions on Information Theory (PGIT), Vol. IT-1, No. 1 (March 1955), pp. 66-76.

measure of protection against interference and noice, the well-known device of employing a coincidence of multiple tones is employed. In the present case a coincidence of two tones is required for the execution of any one command. Provision is made for a total of four tone channels, with tone frequencies of 2000, 2500, 3000, and 3500 cycles per second. The lowest frequency tone was chosen to be 2000 cycles per second because it lay well outside of the loop bandwidth and because below this frequency the sizes and weights of the audio filters required tended to become excessive. A 500-cycle per second separation was allowed between the frequencies of the audio tones to assure that the audio filters employed would have sufficient rejection of tones from adjacent channels. The bandwidths of the audio tone filters were specified as 50 cycles per second. Narrower bandwidths would have been desirable, but it was not feasible to obtain the necessary filters commercially on such short notice. The detected outputs of the tone filters are further filtered by low-pass filters with relatively long time constants. These filters serve to remove the fluctuation noise in the detected output of the tone filters. However, even in the absence of signal there will in general be a d-c component in this output caused by the noise beating with itself in the detector. This d-c output level will be proportional to the square root of the total noise power passed by the tone filter and hence directly to the square root of the filter noise bandwidth. This is the primary reason why it would be desirable to have filter bandwidths considerably narrower than the 50 cycles per second specified, even though the rejection of these filters is more than adequate to reject tones from adjacent tone channels.

The phase deviation is approximately 0.65 radians for each tone. This choice of modulation index places approximately 15 per cent of the total transmitted power in each of the tone channels for the tones which are transmitted. At the same time, negligible power appears in the form of intermodulation products or at harmonics of the tone frequency transmitted. Avoidance of intermodulation products is of particular importance since it is apparent that third order intermodulation between some of the tone frequencies chosen could produce a spurious third tone from the transmission of a tone pair, and this tone could in turn make coincidence with each of the other tones transmitted to give a total of three commands, of which two are spurious. In the present system, the intermodulation of tones can arise not only from the

inherent nonlinearity of the phase modulation process, but also from the action of the limiter employed in the receiver. Only by holding the phase modulation index low is it possible to effect a satisfactory suppression of such inter-modulation products.

The limiter shown in Figure 2-83 plays an important role in connection with the command function of the receiver. It can be shown that the action of this limiter causes the output amplitudes of both the carrier and tone components of the signal to vary with the input signal-to-noise ratio in such a way that auxiliary circuitry can be employed to decide whether the signal-to-noise ratio is sufficiently high to warrant acceptance of a command as valid. The principal of operation of these decision-making circuits will be explained in Section 2.4.3.

h. Bandwidth Considerations

The noise bandwidth of the microlock receivers in the ground system is approximately 20 cycles per second. With this bandwidth and with a total noise input (galactic noise plus receiver noise) equivalent to that produced by a receiver with a 6-db noise figure, these receivers will maintain lock down to a signal level of -150 dbm. Since the power received from the 400 milliwatt airborne transmitter will be about -139 dbm when the payload package is in the neighborhood of the moon,* the transmitted power should prove adequate and, in fact, should provide a margin of approximately 10 db over and above the power required by the microlock receivers to maintain marginal lock.

Mention has been made previously of the fact that the bandwidth requirements on the airborne receiver are of the order of a few hundred cycles per second. Actually, any bandwidth in excess of 100 cycles per second not exceeding approximately 500 cycles per second should prove satisfactory. The minimum bandwidth figure is the result of the dynamic tracking characteristics of the loop and the requirement that the loop should be able to track during the powered flight phase of operation. The 500-cycle per second figure is an expression of the system requirement for a very narrow effective bandwidth in order to be able to operate at very great ranges at low input signal levels. The noise bandwidth of the receiver as presently designed is approximately 150 cycles

*As previously, this figure is appropriate for the primary tracking station at Hawaii.

per second at a signal level of -130 dbm. With this bandwidth and with a total noise input equivalent to that produced by a receiver with a 10-db noise figure, analysis indicated that the receiver should be capable of locking onto the received signal down to signal levels of between -130 dbm and -140 dbm. A design objective of -130 dbm was chosen for lock-on and command channel operation, while operation at -120 dbm was regarded as an acceptable performance level. Since the received signal power in the neighborhood of the moon should be about -110 dbm, these figures correspond to a desired operating margin of 20 db, with a 10-db margin required.

The bandwidth of the airborne IF strip should, of course, be as narrow as possible consistent with other system requirements. In the present case, the minimum IF bandwidth which can be employed is determined by the fact that the IF strip must be capable of passing the command tones on the signal received from the ground. Since the maximum tone frequency is 3500 cycles per second, the IF bandwidth must be at least 7 kilocycles per second in order to pass both sidebands of this tone. In addition, some margin must be allowed for shifts in the IF center frequency and also for the effect of doppler shift in the received signal. Since the loop operates in such a way that the IF offset produced by the doppler shift is precisely $1/17^{th}$ of the doppler shift in the input signal, the maximum IF offset produced by a radial velocity of 35,000 feet per second is less than 250 cycles per second. A 10-kilocycle per second IF bandwidth was chosen as a reasonable compromise because it allows adequate margin for both center frequency shift and doppler effect while, at the same time, it is not substantially wider than is necessary to accommodate the command tones.

2.4.3 Auxiliary Features

In order that the airborne equipment may operate unattended, the system contains a number of auxiliary decision-making features which are of some interest. These features, togehter with the ranging subsystem, are described in this section.

a. Acquisition Sweep Circuit

Since the rapid pull-in range of the phase-locked loop in the airborne receiver is very considerably less than the uncertainty in the frequency of the

received signal, it is necessary to provide the loop with an auxiliary acquisition circuit. This circuit functions as follows. When the loop is not locked, an auxiliary circuit causes the frequency of the voltage-controlled oscillator to sweep. The output of the voltage-controlled oscillator is phase-shifted by 90 degrees and the IF output is phase-detected with respect to the resulting reference signal. The output of this phase detector is then smoothed and serves as the input to a threshold detector which, when triggered, stops the acquisition sweep. The operation of the signal-present circuit is illustrated in Figure 2-84. When the loop sweeps past the frequency of the signal, a bias voltage is generated which effectively counteracts the sweep voltage. After a delay of a fraction of a second, this d-c bias voltage passes the low-pass filter and hence serves to trigger the threshold circuit and thus to disconnect the sweep circuit. The period of the acquisition sweep is set at between 6 and 10 seconds and the threshold level is set just high enough so that excessive false triggering by noise does not occur. It should be observed that occasional stopping of the sweep by noise is not serious inasmuch as the loop will not lock in the absence of the signal and hence, after a brief lockout period, the sweeping action will be resumed. The lower limit of a 100-cycle per second loop bandwidth permits a reasonable sweep time. Inasmuch as the sweep time varies inversely as the square of the loop bandwidth, substantially narrower loop bandwidths, even if they permitted satisfactory loop dynamic tracking performance, would result in inordinately long sweep times. Since the loop bandwidth could indeed be made considerably smaller for the extreme ranges and low accelerations which are encountered during the latter part of the trajectory, the constraint on acquisition sweep time is actually the factor which imposes a lower limit on loop bandwidth for these ranges.

b. Gated Command Circuitry

Since the time during which the airborne system will actually receive signals from the ground transmitter is very small relative to the length of the time over which the receiver must operate, it is necessary to provide the command channels with additional protection against false triggering by noise, over and above that provided by their coincidence and threshold circuitry. For this purpose the signal-present circuitry discussed in the preceding paragraph

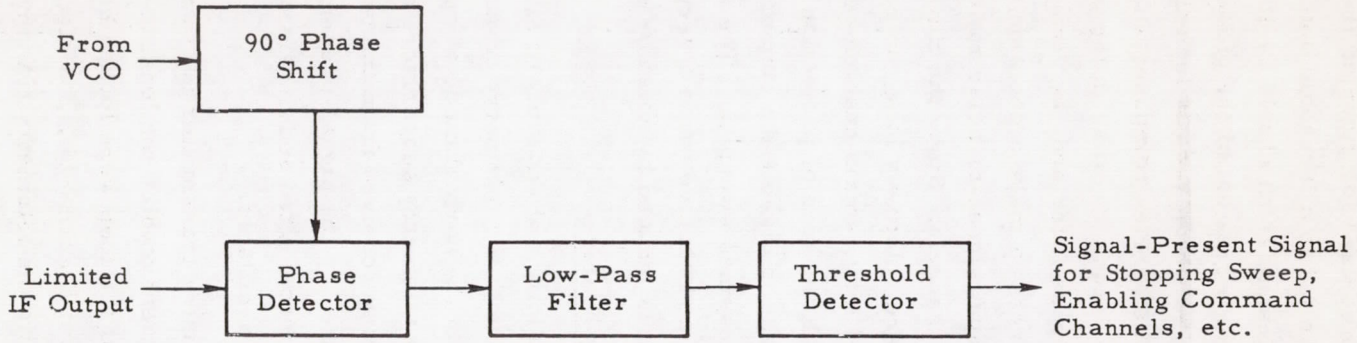

Figure 2-84. Simplified Functional Diagram Illustrating Operation of Signal-Present Channel.

and illustrated in Figure 2-84 is employed, but with a somewhat longer time constant in the low-pass filter than is used for stopping the acquisition sweep. The output of this low-pass filter is fed to a threshold detector which, when triggered, enables the command channels. It should be observed that for this function no envelope detection of the signal out of the phase detector occurs. Advantage is taken of the fact that, when the loop is locked, the output of the quadrature phase detector due to the carrier component of the signal will take the form of a d-c bias level. Low frequency noise in the phase detector output is effectively removed by the low-pass filter and, by virture of the action of the limiter, the threshold detector serves to make a decision that, first, the loop is locked, and, second, that the input signal-to-noise ratio is sufficiently high to warrant enabling the command channels. Since the time constants in the command-channel-enable circuit are relatively long, unless additional circuitry is employed, the command channel may remain enabled even after the loop has unlocked. To provide an additional measure of protection against interfering signals and noise, provision is made to disable the command channels immediately whenever the acquisition circuit resumes sweeping. The combination of features here described provides the command receiver with a very substantial margin of protection against false commands induced by noise or spurious signals.

c. Transmitter Switching Feature

In the interest of simplicity and economy of size, weight, and power, the same transmitter is employed both for telemetry transmission and for transponding the doppler signal. In the normal mode of operation a quartz-controlled exciter is modulated by telemetry subcarriers and fed into the transmitter whenever a signal is not being received from the ground transmitter. When the loop is locked, as indicated by the signal-present signal, the exciter with its telemetry modulation is disconnected and the transmitter is connected to the output of the receiver local oscillator.

The fact that the telemetry transmitter is normally on and is nominally transmitting on the frequency which the local oscillator would have if the system were receiving and if the loop were locked has rather interesting implications. As may be seen from Figure 2-83 , if a signal from the ground transmitter enters the antenna while the telemetry transmitter is in operation,

it can beat in the mixer with the leakage signal from this transmitter through the diplexer and hence generate a signal which will pas the IF strip. There is therefore a possibility that the loop will lock the frequency of the voltage-controlled oscillator to the frequency of this spurious signal in the IF output. When the signal-present signal disconnects the telemetry channel and connects the output of the local oscillator to the transmitter, the spurious signal will, of course, vanish. In this case, however, the loop will unlock and resume its search mode until it once again locks upon a suitable signal. In order to preclude the possibility that the loop will always lock to the spurious signal generated as was indicated, the telemetry lockout circuit is provided with a hold feature. The action of this hold is to keep the telemetry channel disconnected from the transmitter for a period of approximately 10 seconds after the cessation of the signal-present signal from the stop-sweep circuit. In this way the receiver has an opportunity to lock onto the correct signal and hence to lock out the telemetry channel for the remainder of the period during which a signal is received from the ground station. Should the loop lock onto the signal generated by mixing the input from the ground station with the proper local oscillator signal, the action of the hold circuit is, of course, unnecessary.

d. Ranging Subsystem

Provision has been made to measure range approximately by frequency modulating the signal transmitted from the ground with a sinusoidal waveform. The period of this waveform will be approximately one-half second and the peak frequency deviation about 2.4 cycles per second. Range is measured by comparing the transmitted waveform with the control voltage to the voltage-controlled oscillator in the ground-based Microlock receiver. Relatively long averaging times can be used for this comparison. When the output signal-to-noise ratio of this ground-based Microlock receiver is 10 db, the root-mean-square range error caused by noise, when the range is measured from a one-minute sample, is estimated to be approximately one millisecond. In practice, the real limitations on the ranging accuracy of this system will be due to errors in the measurement and calibration of system delays. These errors are presently estimated to be somewhere between 3 and 5 milliseconds.

2.5 Antennas

The antenna system for Pioneer I and II included both an electric and a magnetic dipole. The magnetic dipole was used for the NOTS television system which operated on 108.09 mc at a peak power of 50 watts. This system will be discussed later. The electric dipole was used for the 108.06 mc STL telemetry transmitter. The pattern of this dipole was adjusted to be as closely omni-directional as possible.

The antenna systems for the payload as developed by the STL Antenna Laboratory are capable of transmitting signals to the tracking stations at 108.06 mc and at 108.09 mc and also of receiving command signals at 114.813 mc. Since the vehicle was spin stabilized, a radiation pattern symmetric about the geometric spin axis was desired, at the same time allowing a system loss of only 2 db. However, the small disparity between two transmitting frequencies prevented sufficient isolation between them without a 3 db loss in power. A more practical approach to the problem led to the development of a magnetic and an electric dipole. Figure 2-85 shows the payload and antennas. The electric dipole system was used to transmit the 108.06 mc signal and because of its broader bandwidth to receive the 114.813 mc command signal.

Inthe electric dipole system, two stubs comprise half of the dipole antenna. These are driven against the fourth stage retrorocket which acts as the second half of the dipole. The stubs are diametrically opposite each other and protrude through the fiberglass payload shell at an angle of approximately 14.5 degrees with respect to the spin axis. Figures 2-85 and 2-87 show the stubs and the transmission lines. The two stubs are fed in phase against the retrorocket case while the transmission line and a tuning stub are employed to match the antenna system to the transmitter and receiver. The transmitter is isolated from the receiver by a diplexer which gives greater than 40 db rejection and 0.5 db insertion loss. The diplexers were designed and manufactured by the C.A. Rypinski Company.

The magnetic system is comprised of a loop antenna employing folded tripole techniques for correcting impedance match. This system transmitted

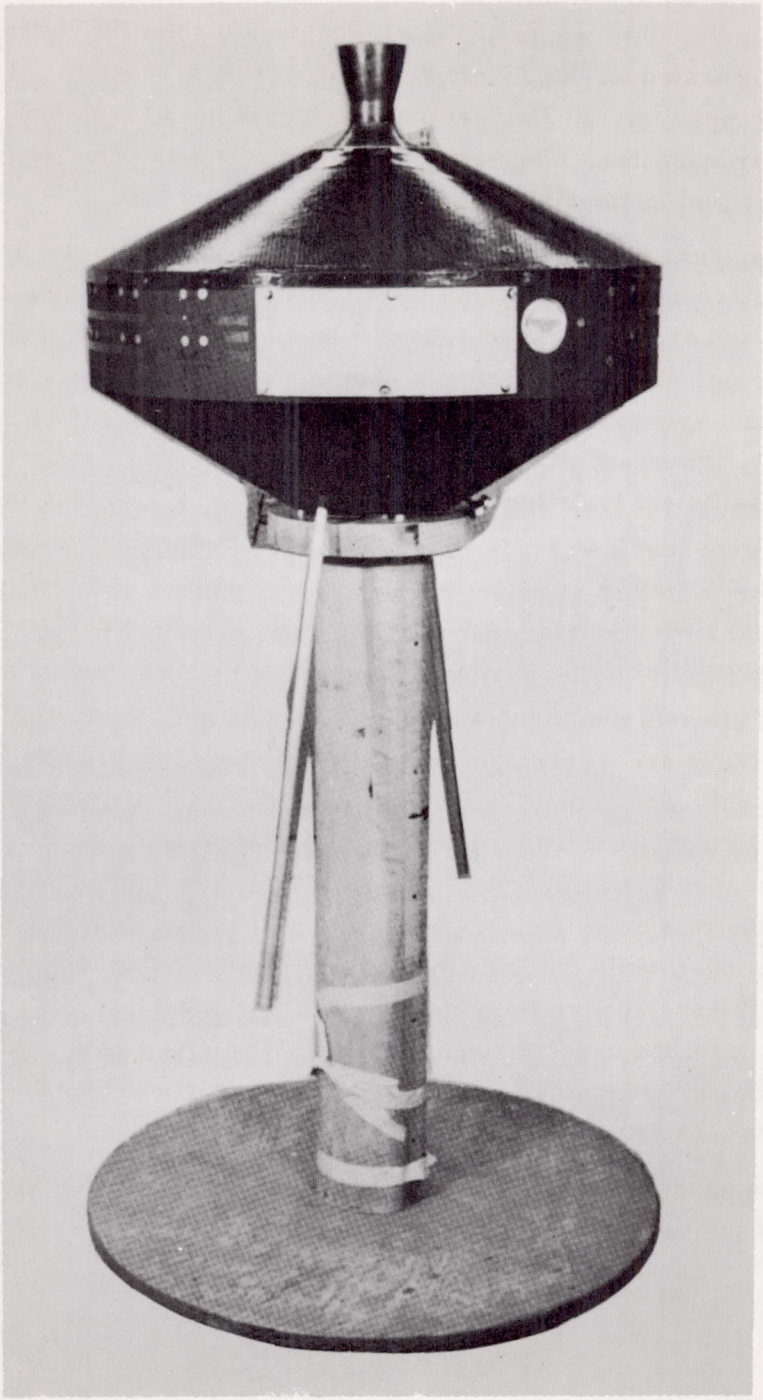

Figure 2-85. Payload Showing Stub Antennas.

the NOTS television signal of 108.09 mc. Figure 2-85 shows the copper foil loop element glued in place.

The loop, 2-1/4 inches in over-all and made from a 0.005 inch thick copper sheet, was developed to transmit the relatively high power of 50 watts from the NOTS television signal. It is placed within the payload shell approximately 3-1/2 inches from the retrorocket opening and is tuned by varying the capacitive gap diametrically opposite the feed point.

From an electrical point of view, the loop antenna is the counterpart of the electric dipole. Its resultant radiation pattern is identical to that of the dipole except for its cross polarization. High Q's are inherent in this type of loop and critical tuning is necessary to obtain the optimum impedance match. Temperature stability was tested by subjecting the payload to temperatures up to 140°F with no detuning of the loop evidenced beyond the amount specified. Coupling between the loop and payload wiring was minimized by a spider-type ground plane as shown in Figure 2-87. The ground plane, composed of eight equally spaced 3/8 inch OD aluminum tubes, originates at the inner periphery of the payload ledge and terminates on a ring situated around the retrorocket at the center of gravity of the payload. There was greater than 25 db isolation between the two radiated signals.

Final tuning of the stub and loop antennas was completed at the STL Antenna Laboratory after placement of payload components and associated wiring was finalized. In order to stabilize temperature during flight within the payload, dispersion of the sun's heat was accomplished by painting the payload exterior. Since the paint configuration is a function of the orientation of the Able-1 vehicle with respect to the sun, it was necessary to have a new paint configuration for each flight day with at least two payloads ready tuned for each flight. The tunings for each payload used are compared in the following table.

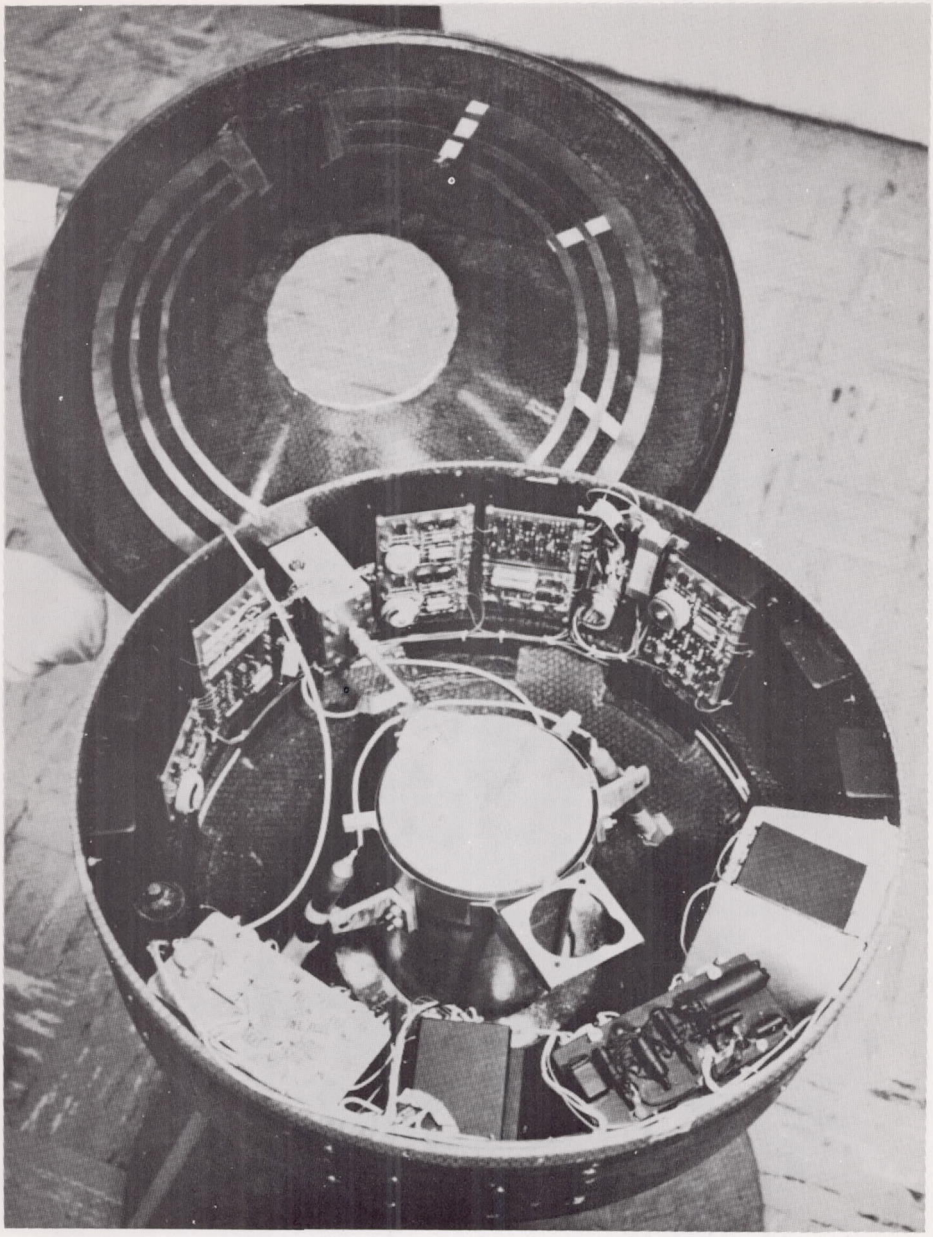

Figure 2-86. Payload Package Showing Magnetic Dipole on Inside Top Cover.

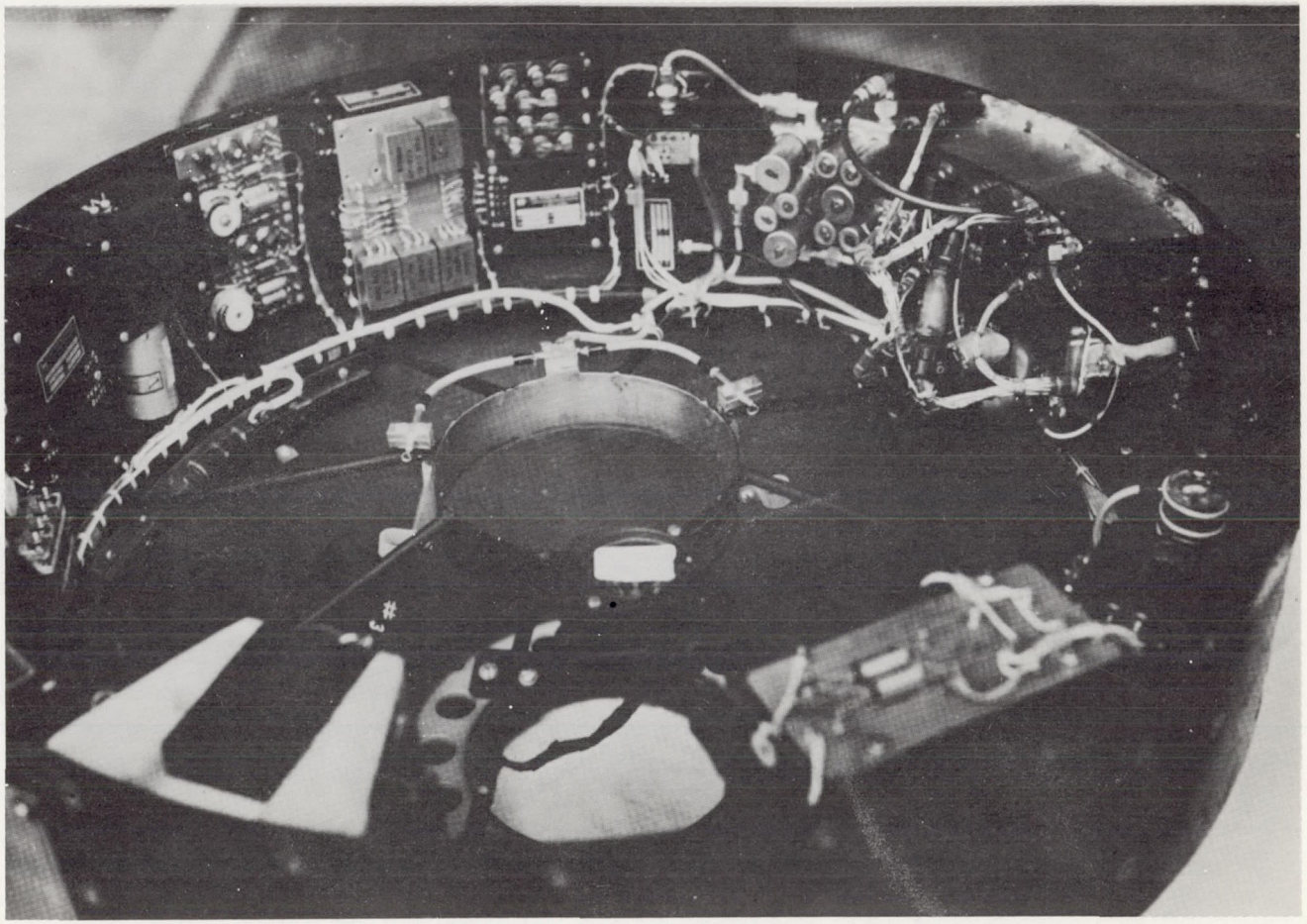

Figure 2-87. Payload Package Showing Stub Antenna Mounting and Wiring.

Table 2-9. Characteristics of the Airborne Antenna.

STUB ANTENNA DATA (Transmitter and Receiver

Serial Number	Use	Payload Diameter (inches)	Radiation Pattern Circularity (db)		Frequency (mc)		VSWR (50 ohm line)		Impedance (ohms)		Phase Angle (deg)	
			Trans.	Recvr.	Trans.	Recvr.	Trans.	Recvr.	Trans.	Recvr.	Trans.	Recvr.
1	Backup model	22	0.25	0.25	108.06	114.8	1.35	1.66	38.5*	38.5*	-90	-24
2	August Flight Payload	29	0.5	0.5	108.06	114.8	1.18	1.78	50*	28*	+10	+ 3
3	August Flight Standby-Returned to STL	29			108.06	114.8	1.50	1.83	33***	81***	0	-20
4	October Flight Payload	29	1	1	108.06	114.8	1.33	1.68	38.3***	81.8***	-7.5	+9.2
3A	October Flight Standby-Rework of Payload No. 3	29	0.1	0.1	108.06	114.8	1.15	1.42	50.5***	68.4***	- 8	-11
5	November Standby	29			108.06	114.8	1.1	1.55	47.5***	51***	+ 5	+24
6	November Flight Payload	29μ			108.06	114.8	1.2	1.56	43***	78***	- 6	- 2

LOOP ANTENNA DATA (Transmitter)

Serial Number	Use	Payload Diameter (inches)	Radiation Pattern Circularity (db)	Frequency (mc)	Isolation Between Antennas at Operational Frequencies (db)	Color	VSWR (50 line)	Impedance (ohms) **	Phase Angle (deg)
1	Backup model	22	1.11	108.09	>25		1.72	79	+17
2	August Flight Payload	29	0.5	108.09	>30	No. 1 hat black	1.64	63	-24
						No. 2 hat green	1.58	50	-25
3	August Flight Standby-Returned to STL	29	——	108.09	>30	No. 1 hat green	1.28	64	-40
						No. 2 hat black	1.15	57	- 2
4	October Flight Payload	29	1	108.09	>30		1.46	36.5	-9.5
3A	October Flight Standby-Rework Payload No. 3	29	——	108.09	>36		1.09	47.1	+3.7
5	November Standby	29	0.1	108.09	——		1.13	53.4	-6.5
6	November	29μ	0.1	108.09	——		1.32	58	+13

* Stub Impedance measurements were taken at the input to the feed line.
** Loop Impedance measurements were taken at the input to the feed line.
*** Stub Impedance measurement taken at output and input of transmitter and receiver, respectively.

2.6 Power Supply

In the Able-1 payload, three different dc power supplies were used. Mercury batteries, used for all of the STL electronic equipment, were selected because of their favorable shelf life, watt hours per pound ratio, and their ability to work in a vacuum. The NOTS TV used the Yardney Silver Cell Type battery which gives higher delivery rates of current for short periods of time. STL also selected the Goulton nickel-cadium storage battery for the rocket ignition circuit because of its ability to deliver current in a hermetically sealed container and still remain under a specified weight allowance.

STL also decided that each electrical component should carry its own power supply so that the failure of one power supply would not jeopardize the operation of other electrical equipment. Approximately 16 separate power packs were used to supply power to such equipment as the command receiver, ion chamber, cosmic ray telescope, etc.

The power supplies were broken down into separate units and mounted along the circumference of the payload for equal weight distribution. Each unit was insulated for protection from environmental changes and electrical interference and was rigidly mounted to eliminate vibration.

Except for the mercury batteries that failed to close the command circuit relays on the payload of Missile 130 because of the adverse environmental conditions encountered, the power supply on all the lunar probes operated satisfactorily and verified design specifications. The electrical output of the mercury batteries was almost doubled in order to insure current capability under adverse environmental conditions, such as those experienced in the payload of Missile 130.

During the year, STL investigated the possibility of payload failure which might be caused by the rupture of individual batteries in the payload. However, tests indicated the method of insulation and the manner in which the batteries were isolated and mounted prohibited any possible rupture. Much time was spent by STL, too, in determining configurations which would permit batteries to provide maximum watt hours with minimum weight.

APPENDIX A

DESCRIPTION OF THE AIRBORNE COMMAND DOPPLER (Section 2.4)

A. General

Shown in Figure 2A-1 is a simplified block diagram of the doppler transponder and command receiver system. The frequency of transmission to the ground stations is 108.06 megacycles per second and is employed both for the coherent transmission necessary for the extraction of doppler data, and for transmission of certain telemetry information. The telemetry subcarrier oscillators phase modulate the transmitter crystal controlled oscillator. The frequency of reception, 17/16 that of the transmitter, is 114.81375 megacycles per second.

The receiver must receive the transmitted ground frequency, operate on it to produce a phase-coherent offset and transmit this offset frequency to a ground Microlock receiver installation where doppler data extraction is performed. Also, the airborne receiver must demodulate and decode the phase-modulated command information from the received signal and transfer the proper command information to the guidance circuitry. When not being interrogated for command or doppler purposes, the system is continuously transmitting telemetry data.

Because of the extensive circuitry required along with constraints on size, weight and power consumption, it was necessary that the receiver-transmitter combination be entirely transistorized.

B. Transmitter

The ability of the ground Microlock receiver system to acquire a signal depends upon the nature of the signal. The principle factors affecting acquisition are receiver signal-to-noise ratio and phase stability of the signal source.

The required signal-to-noise ratio at the ground station prescribed an airborne transmitter power of 400 milliwatts and the requirement on phase stability dictated an airbone transmitter phase jitter of 10° rms or less. Other requirements include: weight less than 1 pound (exclusive of batteries), over-

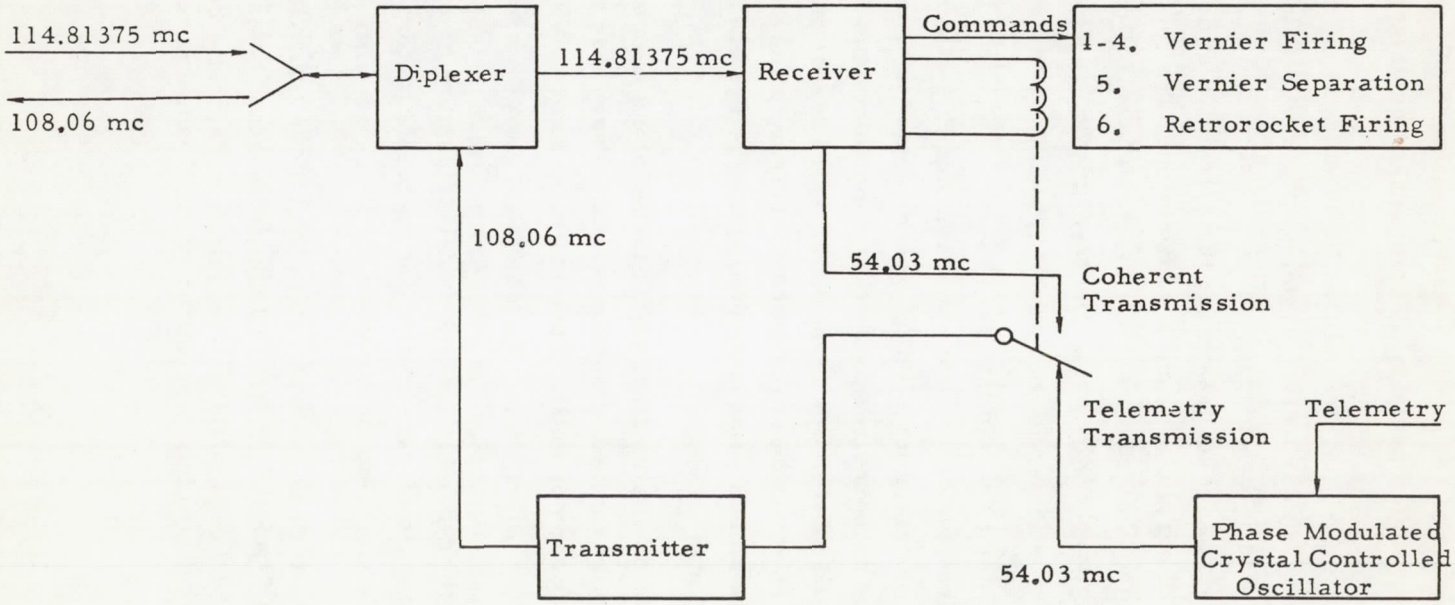

Figure 2A-1. Simplified Block Diagram, Doppler Transponder and Command Receiver.

all efficiency of 50 percent or better because of the requirement of 120 hours of operation on 2 pounds of batteries, size less than 20 cubic inches, missile and vacuum environment, frequency accuracy within 0.002 percent, and frequency stability within 5 parts in 10^7 per degree centrigrade over the temperature range 10° C to 32°C.

For transmitting telemetry information, the requirement was a phase modulation capability of an average of 0.8 radians which would be effective in transferring 30 percent of the transmitted power into the sidebands. This degree of modulation thus provides for 70 percent of the power to be in the carrier which ensures sufficient signal strength for secure microlock receiver operation.

For this small a phase deviation, the sideband power is, for all practical purposes, entirely that of the fundamental of the modulating frequency; the power in the second harmonic sidebands being approximately 1 percent of the total.

Shown in Figure 2A-2 is a block diagram of the telemetry and doppler transmitter. The oscillator is a crystal controlled two-terminal device with a series mode crystal between collector and emitter. The oscillator is specially compensated for frequency stability and phase modulation capabilities. A simplified oscillator schematic is shown in Figure 2A-3 .

Resistor R_1 is a swamping resistor for transistor input impedance variations. Capacitor C_1's negative temperature coefficient compensates for frequency drift with temperature. Resistor R_2 is required in order to make possible the required phase-deviation; this phase deviation being accomplished by varying the collector supply voltage and thus its shunt capacitance. The coil shunting the crystal tunes out the crystal parallel capacitance at 54.03 megacycles per second.

The doubler is conventional grounded-base and drives a neutralized stage of four transistors in push-pull parallel. Four transistors are required in the final stage so that the collector dissipation would remain within allowed limits over the expected temperature extremes. The table below summarizes the final performance characteristics.

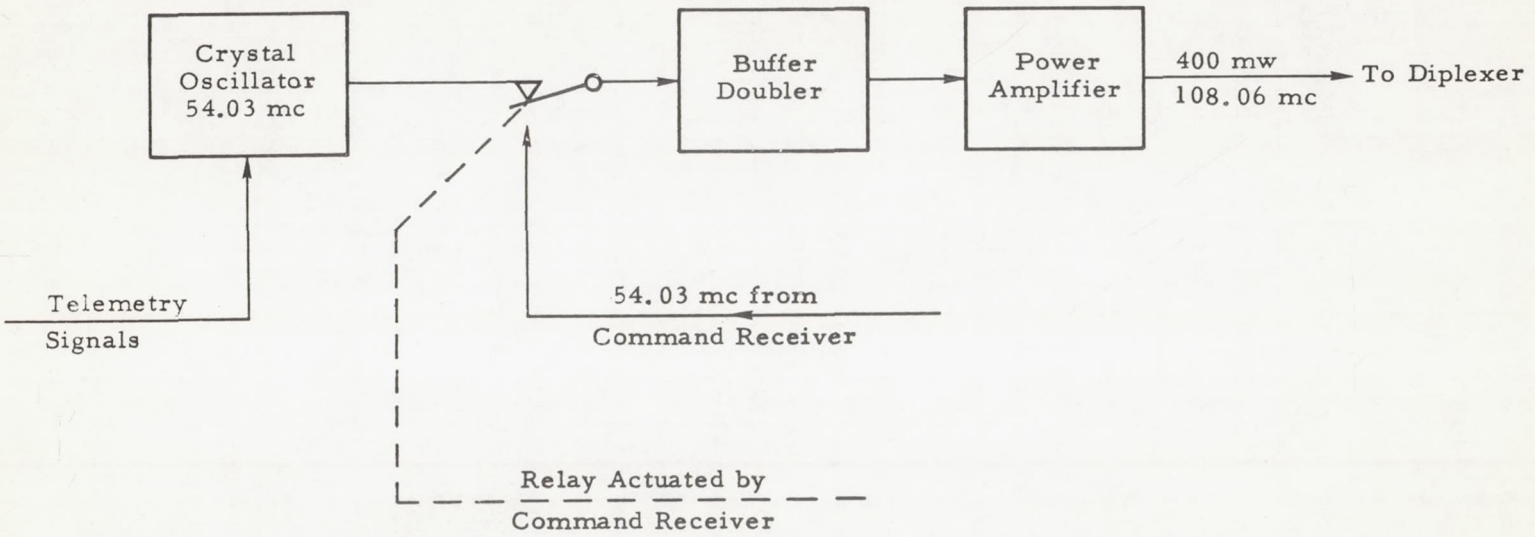

Figure 2A-2. Block Diagram, Telemetry and Doppler Transmitter.

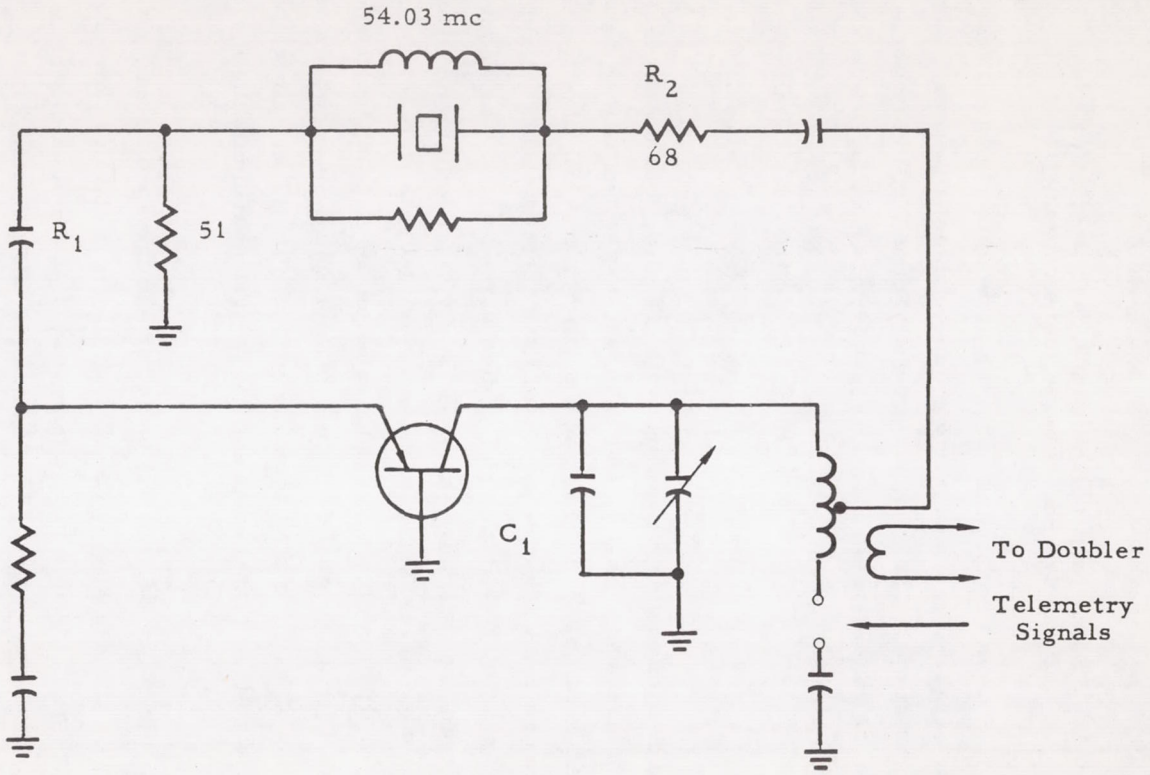

Figure 2A-3. Simplified Schematic, Transmitter Oscillator.

Frequency Stability	2 Parts in $10^7/^oC$
Power Output	400 Milliwatts
Over-all Efficiency	53 Per cent
Weight	14 Ounces

Table 2A-1. Some final performance characteristics, telemetry and doppler transmitter.

Possible improvements consist of reducing size and weight and increasing the power output capabilities by employing more sophisticated methods of heat-sinking the transistors. The final stage easily produced more than 1 watt of output power at room temperature. Figures 2A-4 and 2A-5 are views of the completed transmitter.

C. Receiver

1. General

The ground transmitter power and antenna gain, space attentuation at 240,000 miles, polarization losses, and unknown losses and safety factor all added up to a required goal for threshold sensitivity of -130 dbm for the airborne command receiver. The frequency of the received signals undergoes a maximum doppler shift up to about -4100 cycles per second. The receiver must be capable of tracking this shift, as well as any expected transmitter instabilities. It was also necessary that the receiver be able to track frequency ramps in the order of 1000 cycles per second/second for acquisition purposes. Allocated volume was 100 cubic inches; 5 inches high and 2-3/4 inches deep with an average width of 7-1/4 inches on a 27-inch radius. Total power consumption was limited to less than 1 watt and the weight goal including batteries was 5 pounds.

To obtain the required sensitivity and tracking capabilities, a narrow-band phase-locked system was employed. Shown in Figure 2A-6 is the command receiver block diagram. This is a single conversion phase-lock design with the IF amplifier operating at about 6.75 megacycles per second.

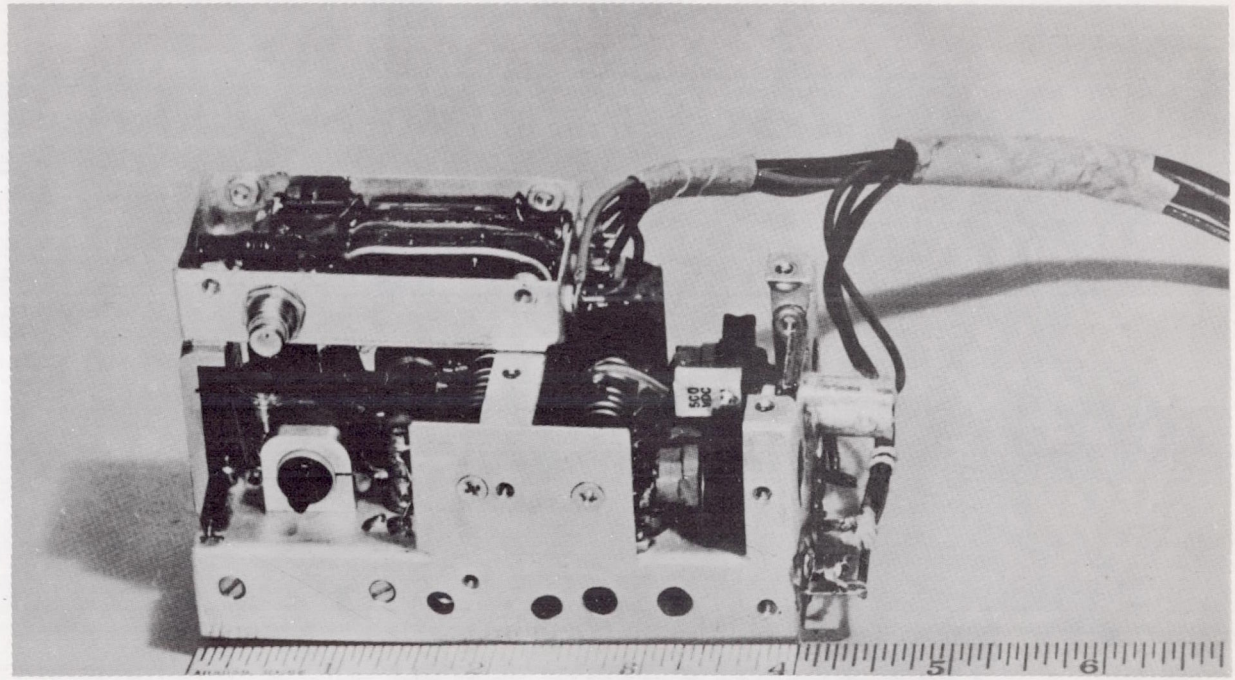

Figure 2A-4. Telemetry - Doppler Transmitter, Cover Removed.

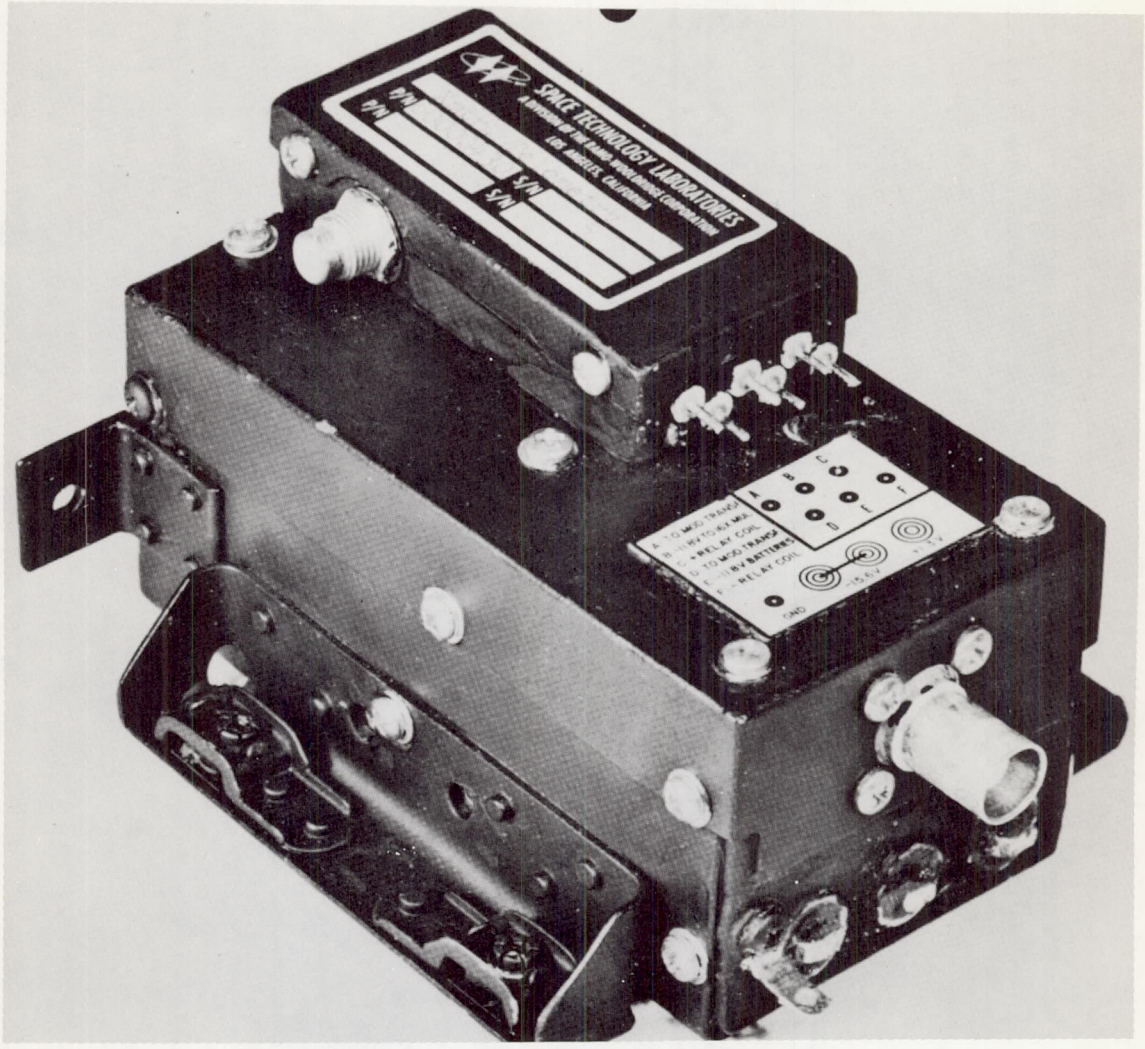

Figure 2A-5. Telemetry - Doppler Transmitter.

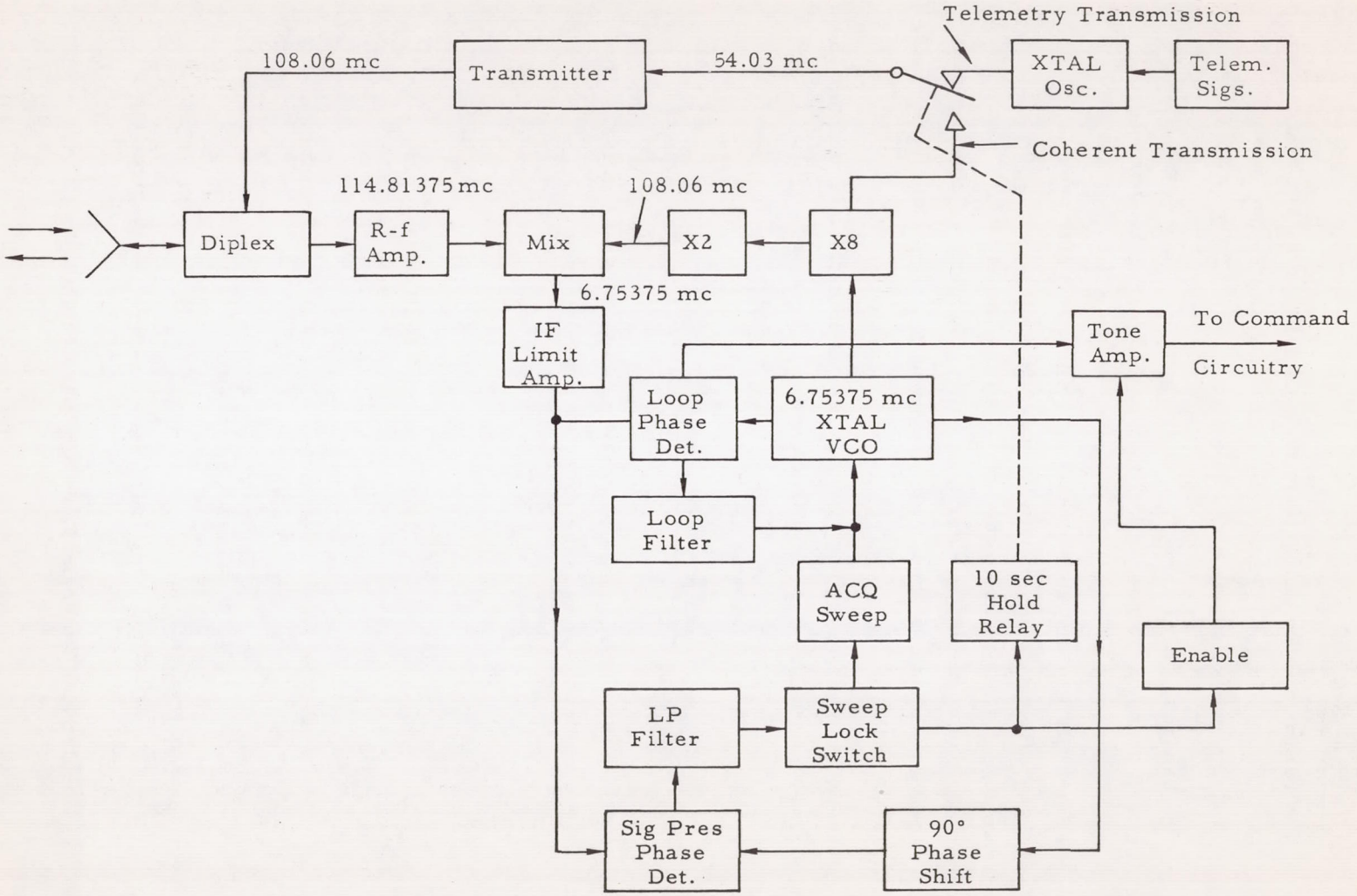

Figure 2A-6. Block Diagram, Doppler Transponder and Command Receiver.

2. RF and IF Section

The receiver noise characteristic is established by two stages of r-f amplication, operating at approximately 115 megacycles per second. The r-f amplifier has a gain of 20 decibles and a typical noise figure of 8.0.

The bandpass characteristic was synthesized with a crystal lattice filter at the IF frequency. The crystal filter was 10 kilocycles per second wide at the 6 decibles points with a shape factor of about 4. In order to achieve the desirable limiting action referred to in a previous paper,* it was necessary that sufficient receiver gain be provided so that the ratio of the rms noise voltage at the limiter to the voltage at the limiter which just produces limiting is somewhat greater than unity. A factor of 2 was chosen and the following calculations show that a receiver gain of 102 decibles ahead of the limiter is required.

Using germanium diodes, one can limit symmetrically at about 150 millivolts rms at a 10,000-ohm impedance level. Therefore,

$$P_{limiting} = 2.25 \times 10^{-6} \text{ watts}$$

Setting $$\frac{\text{noise power at limiter}}{P_{limiting}} = 2$$

one may calculate the receiver gain required prior to the last limiter. The available noise power referred to the receiver input is given by

$$N_A = (NF)\ K\ T\ B$$

where

$$NF = 8 \text{ db}$$

$$T = 300^{\circ} K$$

$$B = 10,000$$

$$K = 1.37 \times 10^{-23},$$

and $$N_A = 26.2 \times 10^{-17} \text{ watts}$$

Therefore, the required gain is,

$$\text{Gain} = 10 \log \frac{4.5 \times 10^{-6}}{26.2 \times 10^{-17}} = 102 \text{ decibles}$$

*"Two-Way Doppler and Command Link for Space Flight", by H. A. Samulon and R. E. Graves.

To approach a 0 decible dynamic range in amplitude, it was necessary to use more than one stage of limiting, and therefore distributed limiting, consisting of back to back diodes in the first four IF stages, was employed.

Each r-f amplifier stage provides 10 decibles gain for a total of 20 decibles and this along with an active mixer gain of 15 decibles and four stages of IF gain of 20 decibles per stage provides 105 decibles of gain to the last limiter stage. Two further stages of IF gain are employed in order to ensure a constant power output to the phase detectors of about 1 milliwatt. All IF stages are of the neutralized common-emitter configuration, achieving the required gain with the minimum number of stages.

3. Phase-Locked Loop

Shown in Figure 2A-7 is a detailed block diagram of the phase-locked loop. When ϕ_i is zero (no imput to the receiver) the VCO is being swept in frequency. The input to the phase detector is then changing in frequency over the range of frequencies to be expected when the receiver is interrogated by the ground transmitter. Thus the loop will make acquisition of the transmitted signal despite the frequency uncertainty due to drift and doppler shift.

Loop parameters were chosen on a basis which would yield a satisfactory compromise of such performance characteristics as:

1. Acquisition Threshold
2. Acquisition Time (sweep speed)
3. Loop Bandwidth
4. Phase Jitter (solidity of loop lock)
5. Loop Stability
6. Tracking Rate
7. Frequency Range

In view of the limited time available for system design, a simple quadrature loop using a double time constant lead-lag network for filtering was chosen. The system characteristic equation then has the familiar form

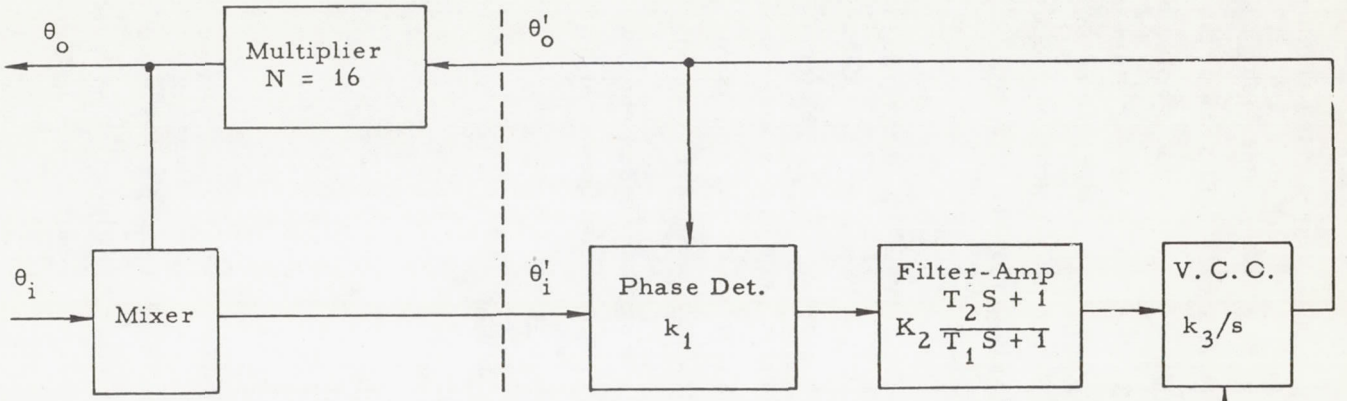

$$1.\quad K_1 G(S) = \frac{k_1 k_2 k_3}{S} \cdot \frac{T_2 S + 1}{T_1 S + 1}$$

$$2.\quad \frac{\theta_o}{\theta_i}(S) = \frac{(N+1) K_1 G(S)}{1 + (N+1) K_1 G(S)}$$

Figure 2A-7. Diagram, Phase-Locked Loop.

$$S^2 + 2 W_n S + W_n^2 \qquad (1)$$

where

$$= \text{damping ratio}$$

$$W_n = \text{undamped resonant frequency}$$

Denoting the forward transfer function of the phase detector, filter-amplifier, VCO combination by $K_1 G(S)$, the closed loop transfer-function, $\frac{\phi o}{\phi i}$ (S), is given by equation (2) of Figure 2A-7. In other words, the effect of the multiplier-mixer loop is to increase the gain constant of the simple closed loop (to the right of the dotted line in Figure 2A-7) by the factor (N+1). In Figure

k_1 = phase detector scale factor, volts/radian

k_2 = amplifier gain

k_3 = VCO sensitivity, radians/second/volt

and

$$K_1 = k_1 k_2 k_3 \text{ radians/second/radian} \qquad (2)$$

Upon substitution and clearing of fractions, the complete closed loop transfer function is given by

$$\frac{\phi o}{\phi i}(S) = K \frac{T_2}{T_1} \times \frac{S + 1/T_2}{S^2 + \frac{1 + KT_2}{T_1} S + \frac{K}{T_1}}, \qquad (3)$$

where

$$K = (N+1) K_1$$

and where it can be seen that the transfer function of the loop is completely determined by the parameters K, T_1 and T_2. Also

$$W_n^2 = \frac{K}{T_1} \qquad (4)$$

$$2\zeta W_n = \frac{1 + KT_2}{T_1} \tag{5}$$

and if $KT_2 \gg 1$,

$$\zeta = \frac{W_n T_2}{2} \tag{6}$$

The determination of the loop gain constant, K, was based on static phase error at maximum doppler frequency offset and the limiting characteristic of the IF amplifier.

The design of the loop is such that the loop gain varies as a function of the received signal strength. As the loop gain decreases (due to falling signal strength), the loop bandwidth decreases. Hence, the loop automatically compensates for decreasing signal strength. The measured limiter characteristic showed that from full limiting to design threshold (-130 dbm), the gain varied by a factor of about 5 to 1.

Allowing a 5^o phase error (representing solid lock) at the maximum doppler offset of 4100 cps, the required gain with minimum expected received signal power is

$$K = \frac{4100}{5} = 820 \text{ cps/degree} \tag{7}$$

$$= 300{,}000 \text{ radians/second/radian}$$

Because of uncertainties in the expected minimum received signal power, gain constants in various portions of the receiver, and ground transmitter instabilities, a rather large safety factor was assigned to this gain constant. Accordingly, it was established that the loop gain should be approximately 1.5×10^6 radians/second/radian at a received power of -130 dbm (design threshold), the maximum gain for strong signals would be then approximately 7.5×10^6 radians/second/radian.

For a given gain constant and damping ratio, the integration time constant determines loop noise bandwidth and tracking rate capability. A value of 80 seconds was established as follows:

It was desired that the loop be able to track a frequency ramp of approximately 1000 cps/second, corresponding to the acquisition sweep rate established by operational considerations. At the same time, the loop bandwidth for signals near the design threshold of -130 dbm must be kept less than about 150 cps in order that phase-lock be maintained.

The ramp following error is given by

$$\phi_e = \frac{A}{W_n^2} = \frac{A}{K/T_1} \tag{8}$$

where

ϕ_e = following error, radians

A = ramp rate, radians/second/second

W_n = undamped loop resonant frequency

T_1 = integration time constant

The noise bandwidth is given by*

$$B = \frac{4\zeta^2 - 4\zeta\frac{W_n}{K} + \left[\frac{W_n}{K}\right]^2 + 1}{2\zeta} \cdot \chi W_n \text{ radians/second} \tag{9}$$

which for $\zeta = 0.5$ and K large reduces to

$$B = 2\chi W_n \text{ radians/second} \tag{10}$$

Using equations (8) and (10) it was found that $T_1 = 80$ seconds was a satisfactory compromise, for then $\phi_e = 18^\circ$ (representing good lock) and B = 141 cps.

For a given loop gain and integration time constant, the lead time constant establishes loop stability and transient behavior. This is conveniently expressed in terms of the damping ratio from equation (6). As the loop gain is increased for given values of lead and lag time constants, the damping ratio

* Gruen, W. J., "Theory of AFC Synchronization," Proc. IRE Vol. 41, No. 8 (August 1953) P 1046.

increases. In view of this, a minimum damping ratio of $\zeta = 0.5$ was selected for minimum gain conditions. The required lead time constant is then given by (from equation (6))

$$T_2 = \frac{2}{W_n} = 7.2 \times 10^{-3} \text{ seconds}$$

where

$$= 0.5$$

$$W_n = 141 \text{ radians/second}$$

For maximum loop gain, corresponding to strong signals, the damping ratio increases to about 1.2.

4. Filter - Amplifier (Loop Filter)

The parameters

$$K = 1.5 \times 10^6$$

$$T_1 = 80$$

$$T_2 = 7.2 \times 10^{-3}$$

were implemented by means of a direct-coupled operational amplifier, where $k_2 = K/k_1 k_3$ was set at a value of 40 for the amplifier gain; k_1 and k_2 having been determined in advance by practical considerations. Figure 2A-8 is a simplified schematic of the loop filter-amplifier.

5. Acquisition Sweep Circuit

During the search mode, when the receiver is not locked on a received signal, a sweep voltage must be superimposed on the output of the filter-amplifier to the VCO. As shown by the block diagram of Figure 2A-9 the switching for the sweep is initiated by a Schmidt trigger circuit that samples the output of the loop amplifier. This arrangement makes the sweep range of control voltage to the VCO independent of any offset voltage or thermal drift of the loop phase detector or loop amplifier. A small charging current

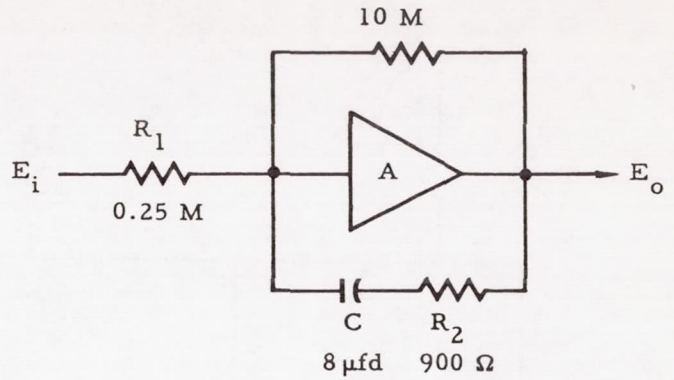

$$A = 500$$
$$k_2 = 10/0.25 = 40$$
$$T_1 = K_2 R_1 C = 80$$
$$T_2 = R_2 C = 7.2 \times 10^{-3}$$

Figure 2A-8. Simplified Schematic, Filter Amplifier.

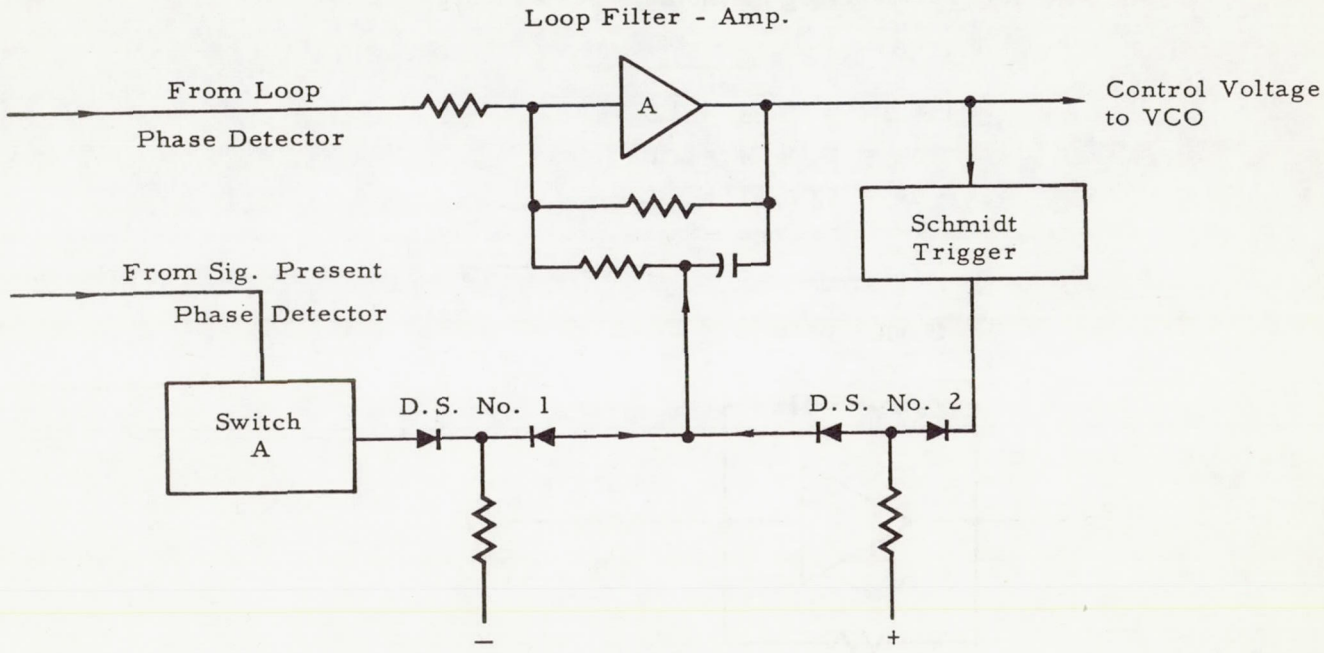

Figure 2A-9. Simplified Schematic, Acquisition Circuit.

is continually supplied to the loop-filter integrating capacitor through diode switch No. 1 as long as no received signal is present. This small current increases the voltage to the VCO in a linear saw-tooth fashion thus creating the frequency search for an input signal on which to lock. When this output voltage reaches the upper triggering level of the Schmidt circuit, diode switch No. 2 is opened and a large charging current swamps the charging current from diode switch No. 1 (in the opposite direction) and a rapid return of the loop filter-amplifier to the lower Schmidt triggering level then disconnects diode switch No. 2. This allows the slow saw-tooth sweep to again cause searching due to the charging current through diode switch No. 1. When acquisition is made, the signal present detector activates switch A which removes the charging current through diode switch No. 1.

6. Signal Present Circuit (Reference Figure)

By shifting the IF output 90^{o} in phase and phase detecting this shifted signal with respect to the VCO output, a d-c voltage is the result which is directly proportional to received signal amplitude. This voltage, after filtering and switching, supplies commands to stop the acquisition sweep, enable the command circuit, and control the doppler-telemetry transmitter relay. These functions are accomplished using standard transistor switching circuits.

7. Phase Detector

The phase detector is of conventional configuration. However, the balance requirements were rather stringent and caused some design difficulty. It was required that unbalance should not exceed about 0.15 volts d-c at the loop phase detector output. Otherwise, the acquisition sweep rate would be seriously altered (either increased or decreased depending on the polarity of the phase detector unbalance voltage). With a VCO reference drive signal of about 15 volts peak-to-peak into the phase detector the requirement is for a balance to within about 1 per cent.

To ensure good balance, matched load resistors and matched diode pairs were employed along with a balance adjustment in the form of a small slug in the signal transformer. This slug acted to adjust the coupling

coefficient between primary and each secondary half so as to obtain balanced conditions. With a value for k_2 of 40, and knowing k_3 (a value of 1800 radians/second/volt was employed for VCO sensitivity), the phase detector sensitivity at minimum operating signal may be determined from

$$k_1 = \frac{K}{17 k_2 k_3}$$

as approximately 1.2 volts/radian which was easily achievable.

8. Voltage Controlled Oscillator

Deviation of the crystal controlled reference oscillator was accomplished by the use of a voltage-variable capacitor (trade name "Varicap") effectively shunting the crystal. Since only a small amount of capacity change was required to effect the 300 cycles per second per volt deviation, high linearity could be achieved over this range, i.e., 1 per cent. A standard tuned-collector tuned-base type of oscillator was used with the crystal in the collector circuit. Temperature compensation was employed in the base tank circuit by means of a positive temperature coefficient capacitor with a resulting temperature stability of two parts in 10^6 per degree centigrade.

9. Frequency Multiplier

One of the major problems encountered in implementing the command receiver was the prevention of "feed-around" and "feed-through" of the VCO frequency and harmonics thereof which caused undesired phase detector outputs and, thus, unwanted offsets and false lock-on. The offsets either slowed or increased the sweep speed (as explained previously) such that proper acquisition was marginal or impossible. False lock-on would also prevent acquisition of the true signal. Small offsets were not sufficient to actuate the signal present phase detector but yielded enough output from the loop phase detector to affect the charging and discharging of the integrating capacitor in the loop filter-amplifier.

The multiplier (times 16) offered a direct path for the VCO -IF frequency of 6.75 megacycles per second and its various harmonics. Especially troublesome were the 15th and 17th harmonics since they could beat

with the 16th or with the transmitter output to form the IF frequency. Of course any pickup of the VCO output by the IF amplifier would cause a self-lock.

This problem was overcome by the use of efficient shielding and isolation and by some very special precautions in the design and layout of the frequency multiplier. Special precautions were quite necessary since, because of the high gain r-f, mixer and IF combination, undesired signals were required to be in the order of 130 db below a milliwatt. The two main criteria, then, upon which the multiplier design was based are, (1) attenuation cannot be achieved without some reasonable space separation, and (2) all odd harmonics, including the fundamental, of 6.75 megacycles per second must be reduced to very low levels near the front end of the frequency multiplier.

With point one in mind, it was decided to employ double tuned transformer stages in order to achieve as much filtering as possible throughout the entire frequency multiplier. Also, the well known fact that waveguide beyond cutoff provides 27.3-db attenuation for each increment of length equal to width was made use of in the layout.

In line with point two, it was decided to perform the first doubling by use of a push-push doubler since such a doubler ideally eliminates the fundamental and generates no odd harmonic components. Several advantages were incurred by the performance of this doubling passively (i.e., by the use of semiconductor diodes in a full-wave rectifier circuit): (1) the power supplies are not contaminated by undesired frequency components, (2) diodes are available in matched pairs for better circuit balance, (3) unbalance due to thermal effects is minimized, and (4) circuitry is simpler. The passive push-push doubler was followed by a neutralized 13.5 megacycle per second pass-band crystal filter, and then by a buffer amplifier for additional isolation and filering of undesired frequency components.

10. Command Circuitry

The command frequencies (2000, 2500, 3000 and 3500 cps), phase-modulated onto the ground transmission, are taken from the receiver loop phase-detector before narrowing banding and applied to the command circuitry for filtering, detection, and decoding. Commands are initiated by tone pairs

channeled to appropriate switching circuits. Two tones are required to initiate a given command in order that the probability of producing false commands is reduced.

Figure 2A-10 shows a block diagram of the command circuitry. Decoding is done by a simple transistor AND circuit which closes a relay if sufficient voltage is present from each of two channels after filtering and detection. The bandpass filters employed have a 3-db bandwidth of approximately 75 cps and the attenuation at 400 cps either side of center frequency (adjacent channel) is in excess of 40 db. Filters with narrower bandwidths were desired, but because of limited development time it was not possible to obtain them.

11. Final Performance Characteristics

Laboratory tests of the completed receiver show a signal lock-on capability of about -130 dbm. Commands could be transmitted and correctly decoded at this level consistently.

Acquisition time was a maximum of 7.5 seconds, which included time for sweeping the expected frequency range plus a guard band at either end. Referred to r-f, the total sweep covered was approximately 7.5 kilocycles per second, corresponding to a sweep ramp of 1000 cycles per second per second.

The total power consumption when acquired was 267.2 milliwatts and when sweeping 215.4 milliwatts, an amazingly low power drain considering that, when last counted, there were 62 transistors in the receiver alone. The battery weight for the receiver, based on 120 hours of operation for the cells of highest drain, came to 1.46 pounds.

The weight of the receiver, including batteries, came to 5.7 pounds, (slightly higher than the goal) and the total volume came to 90 cubic inches.

Figures 2A-11, 2A-12, 2A-13, 2A-14, and 2A-15 are views of the completed receiver and receiver units.

12. Improvement Possibilities

Laboratory optimization of the loop parameters K, T_1, and T_2 would enable the receiver to acquire at even lower signal levels in the order of

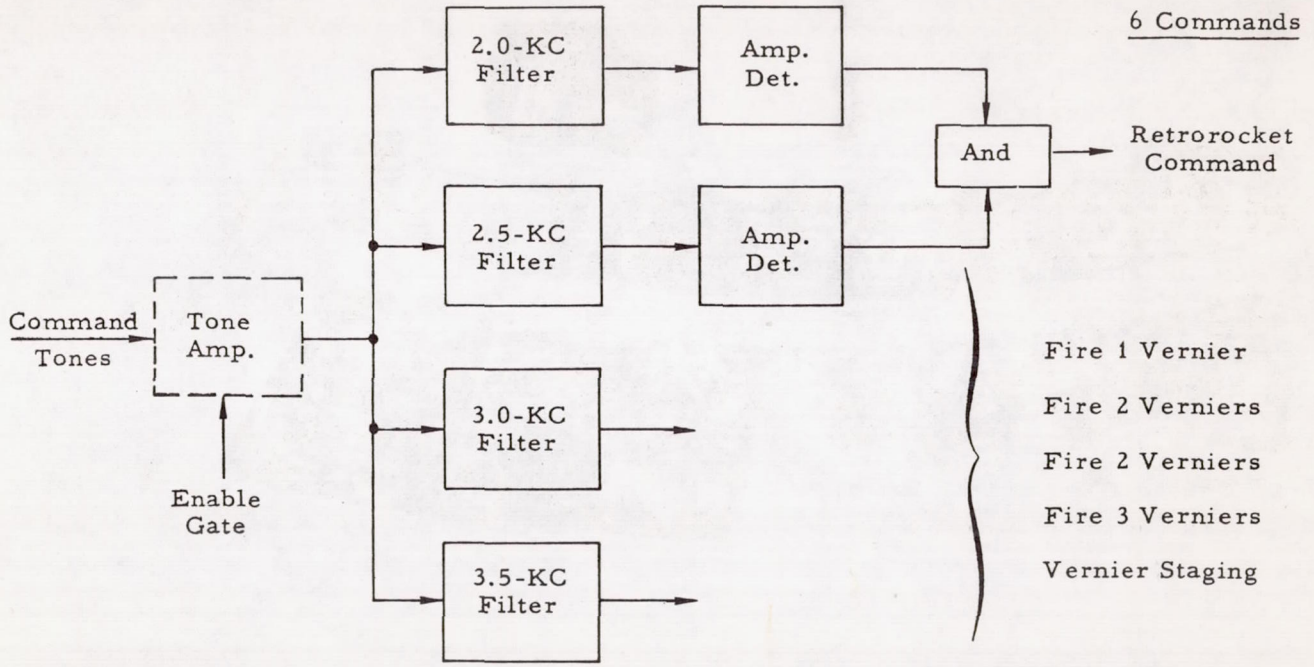

Figure 2A-10. Block Diagram, Command Circuitry.

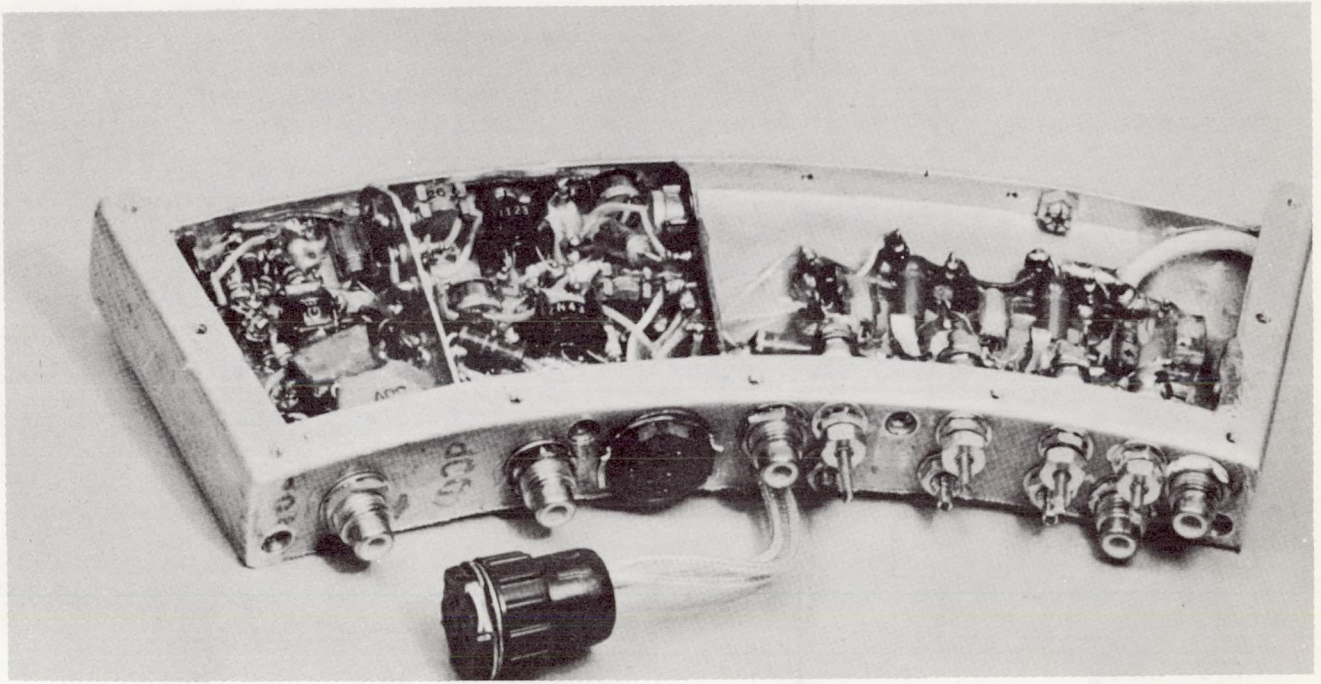

Figure 2A-11. RF and Acquisition Unit.

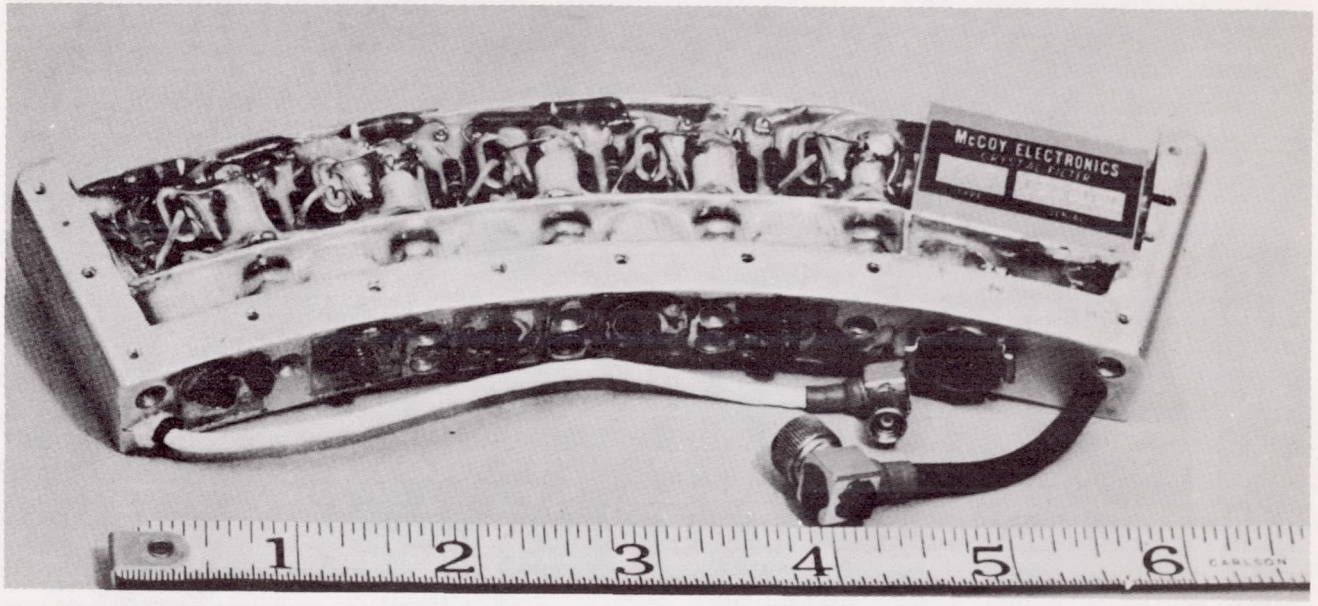

Figure 2A-12. IF Unit.

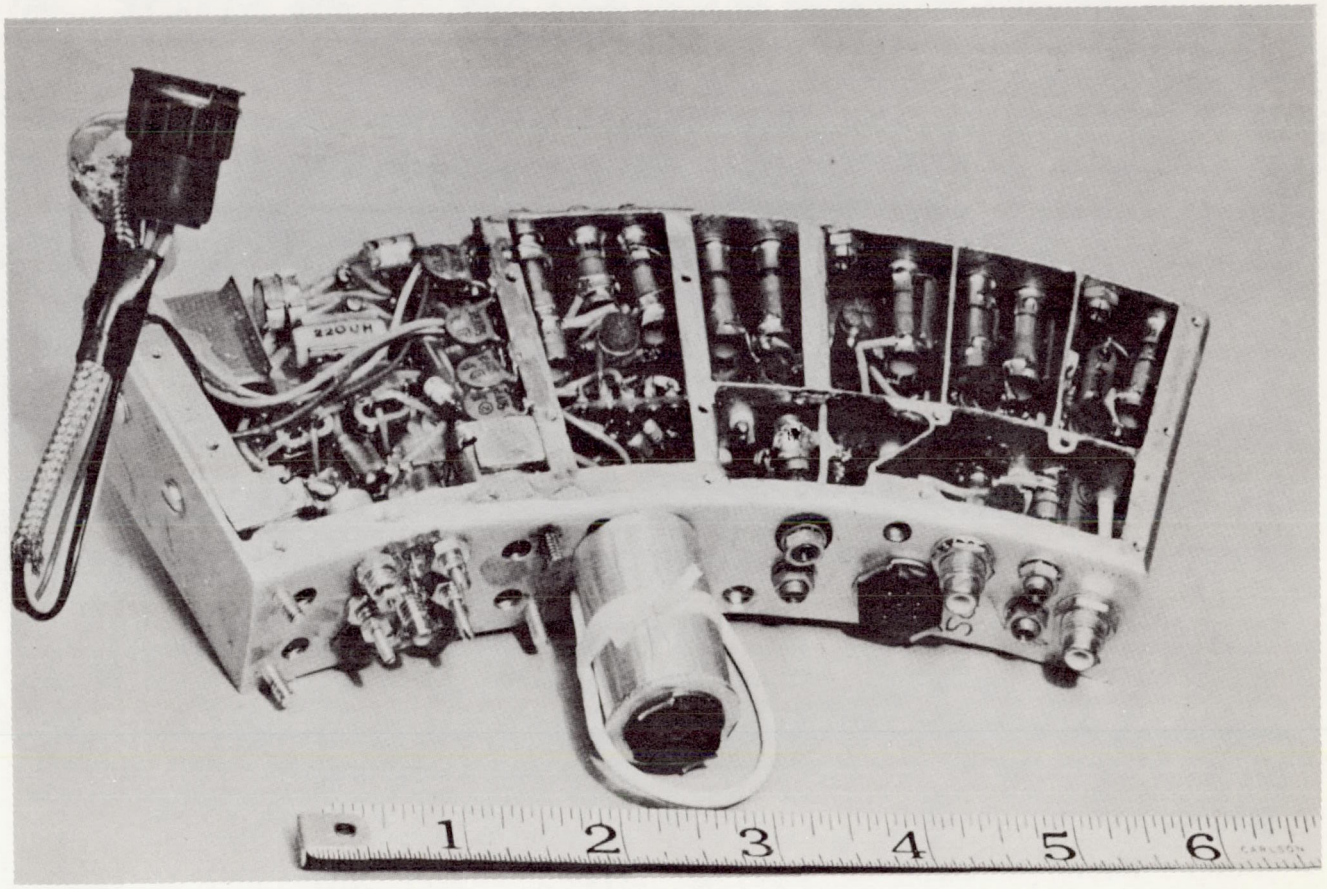

Figure 2A-13. Phase Detector, VCO Multiplier Unit.

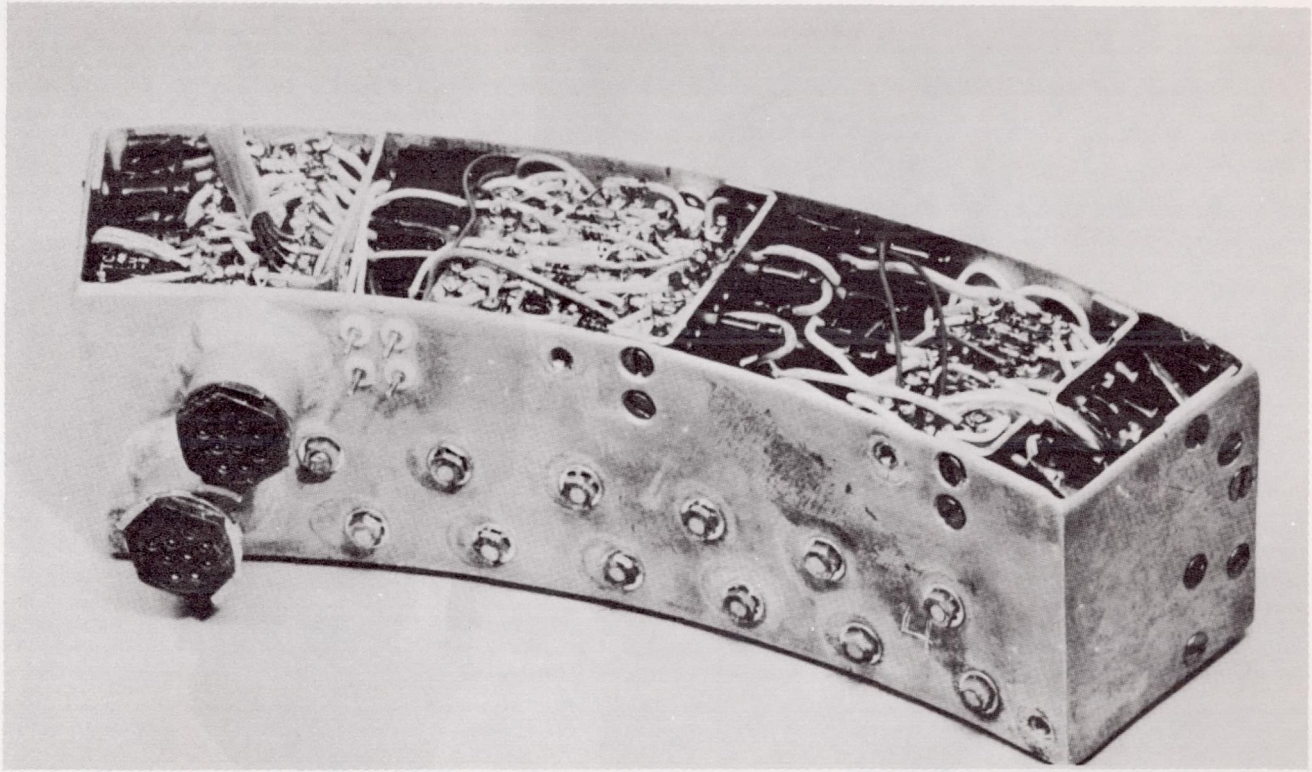

Figure 2A-14. Command Decoding Unit.

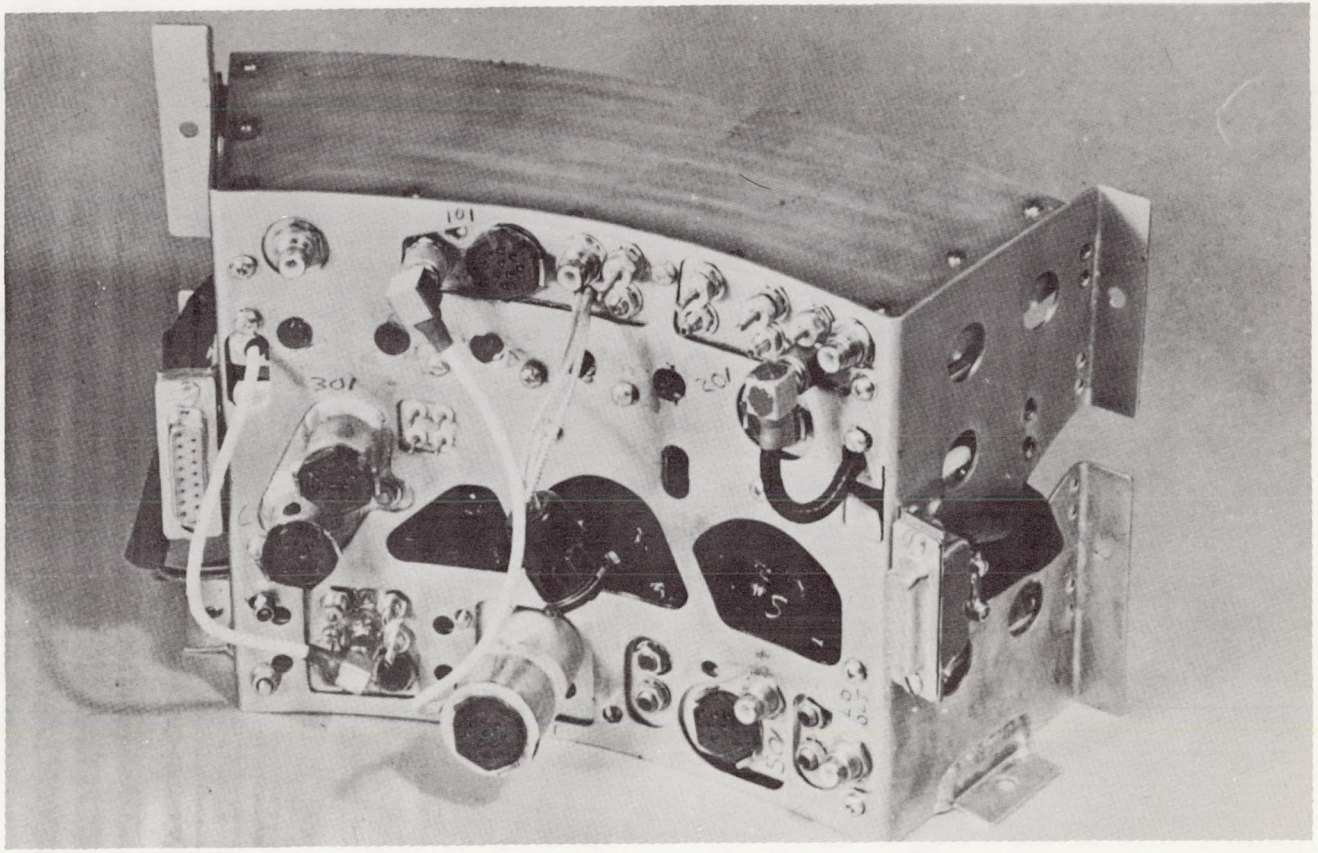

Figure 2A-15. Doppler and Command Receiver.

-145 dbm. Better harmonic filtering and increased shielding and isolation would be necessary in order to achieve this greater sensitivity.

Repackaging of the receiver could result in reduced volume and weight, as would more efficient use of battery power.

Tone filters of narrower bandwidth with less insertion loss (such as active filters) would improve system performance by requiring less amplification and by giving greater protection to the command decoder. The improvement in signal-to-noise ratio would increase command sensitivity by allowing a lower switching threshold; this improvement being necessary also if the receiver threshold sensitivity is increased.